Rapid sample introduction through interfacing flow injection analysis (FIA) to an ICP emission spectrometer

by

Phillip Lyle Kempster

Submitted in partial fulfilment of the requirements for the degree Doctor of Science (analytical chemistry), in the Faculty of Science, to the University of Pretoria, Pretoria.

Date of submission: January 1988

Vinnige monsteropname deur koppeling van vloei-inspuitanalise (VIA) aan 'n IGP emissie spektrometer

deur

Phillip Lyle Kempster

Voorgelê ter vervulling van 'n deel van die vereistes vir die graad Doktor in Wis- en Natuurkunde (analitiese chemie), in die Fakulteit Wis- en Natuurkunde, aan die Universiteit van Pretoria, Pretoria.

Datum van voorlegging: Januarie 1988

CONTENTS

CONTENTS

CONTENTS

ACKNOWLEDGEMENTS

I wish to express my gratitude to my promoter, Professor J.F. van Staden of the University of Pretoria, and to my co-promoter, Dr. H.R. van Vliet of the Hydrological Research Institute for their leadership, advice and encouragement in this study.

In particular I wish to thank Mr. R.G. Geiling and Mr. H.W. Schönberger, of the glass-blowing section at the Council for Scientific and Industrial Research for their construction of the spray chambers and modified concentric nebulizer. Without their skill this work would not have been possible.

Further I am indebted to Mr. I. Schoonraad of the Hydrological Research Institute for constructing the electronic timer with which the flow injection valve and sampler were operated. My thanks also go to Mrs. D. Portsmouth, Miss Y. Cronjé and Miss V. Govender, the technical staff in the trace metal laboratory, for their dedicated assistance in the preparation of the many standards. Mrs. A. Kolbe is thanked for her patience, care and effort in the preparation of the figures.

Thanks must also go to my father for his help in proof-reading the manuscript. I am also very grateful to Mrs. C. Edwards for her mammoth effort in the typing of the document.

Finally, my appreciation is extended to the Department of Water Affairs for the use of their facilities, and for giving permission for undertaking the D.Sc study project.

ABSTRACT

Rapid sample introduction when using flow injection analysis (FIA) as a sample introduction method to an inductively coupled plasma (ICP) emission spectrometer necessitates that the problem of the large dead volume of the typical spray chamber used in the nebulization and sample transport system of an ICP source be dealt with. The long equilibration times of conventional ICP spray chambers tend to cause poor wash-out with carry-over between sample peaks. A literature survey indicated that a simple reduction of spray chamber volume, without modification of the basic design was associated with poor spray chamber performance and appearance of volatilization type interferences. A promising avenue identified in the literature study to designing a small, yet effective spray chamber was to incorporate centrifugal principles in the spray chamber design. Of a variety of reduced volume spray chambers designed and evaluated, one which made use of a tangential aerosol outlet proved to have desirable characteristics for use in an FIA-ICP interface. The outlet placement was important for the success of the centrifugal approach. This mini-volume spray chamber had a volume of one-tenth that of the commercial chamber, thereby providing more rapid equilibration times with an aerosol displacement time of less than 1 s. The mini-chamber conditioned the aerosol effectively, and showed less volatilization interference than the large commercial chamber. The small volume chamber, when used with FIA sample introduction allowed excellent peak resolution to be obtained at sample injection rates as fast as 320 per hour when determining boron. Using a 300 microlitre injected sample volume, carry-over from a 25 $mg.\ell^{-1}$ boron standard to a 2,5 $mg.\ell^{-1}$ boron standard following immediately thereafter was 3% for the mini-chamber as compared to 15% carry-over for the conventional spray chamber. A further advantage of the small chamber was that dispersion ratios close to unity were obtained, so that

little sensitivity loss occurred through using the FIA sample introduction mode. The relationship between FIA peak height and concentration was linear, which made calibration a relatively simple procedure. The FIA-ICP method was also evaluated for the determination of calcium, magnesium, manganese and strontium.

OPSOMMING

Vinnige monsteropname, is moontlik wanneer vloei-inspuitanalise (VIA) gebruik word as 'n monster-toedieningsmetode vir 'n induktief gekoppelde plasma (IGP) emissie spektrometer. Die groot dooie-volume van tipiese sproeikamers wat gebruik word in die verstuiwing- en monster-transportsisteme van 'n IGP bron is egter die belangrikste struikelblok ten opstige van die suksesvolle koppeling van VIA met IGP. Die lang ewewig-bereikingstye van konvensionele IGP sproeikamers neig om swak uitwas tot gevolg te hê en dit lei tot oormatige oordrag tussen monsterpieke. 'n Literatuuroorsig het getoon dat 'n eenvoudige verkleining van sproeikamer volume, sonder wysiging van die basiese ontwerp, gepaard gaan met swak sproeikamer eienskappe en die ontstaan van vervlugtingstipe interferensies. 'n Belowende rigting wat uit die literatuur geïdentifiseer is vir die ontwerp van 'n klein maar nogtans effektiewe sproeikamer, is die inbouing van sentrifugale beginsels in die sproeikamer- ontwerp. Uit 'n verskeidenheid van sproeikamers wat ontwerp en geëvalueer is, het een die verlangde kenmerke gehad vir 'n suksesvolle VIA-IGP koppeling. Die tangensiale aerosol uitlaat het onder andere 'n waardevolle en belangrike bydrae gelewer tot die sukses van die tipe sproeikamer. Die mini-volume sproeikamer se volume was een-tiende van die van 'n kommersiele kamer. Daardeur is vinniger ewewigbereikingstye daargestel met 'n aerosol verplasingstyd van minder as 1 s. Die mini-kamer het die aerosol doeltreffend gekondisioneer, en het minder vervlugtingsinterferensie getoon as die groot kommersiele kamer. Met VIA monstertoediening het die klein volumekamer 'n uitstekende piekresolusie tot gevolg gehad in die bepaling van boor teen 'n monsteranalisetempo van so hoog as 320 per uur. Met 300 mikroliter monster, is die oordrag vir 'n 25 $mg.\ell^{-1}$ boor standaard gevolg deur 'n 2,5 $mg.\ell^{-1}$ boor standaard 3% vir die mini-kamer in

vergelyking met 15% vir die konvensionele sproeikamer. 'n Verdere voordeel van die kleinkamer was dat dispersie-verhoudings van nagenoeg een bereik is. Dus het min sensitiwiteitsverlies plaasgevind as 'n gevolg van die VIA monster toedieningswyse. Die verband tussen VIA-piekhoogte en konsentrasie is lineêr, met die gevolg dat kalibrasie relatief eenvoudig is. Die VIA-IGP metode is ook geëvalueer vir die bepaling van kalsium, magnesium, mangaan en stronsium.

SYMBOLS

δ	-	differential; dispersion number.
Δ	-	difference.
ε_n	-	transport efficiency.
ζ	-	stop distance of an aerosol particle or droplet.
η	-	nebulization efficiency; viscosity.
κ	-	an integral multiple of standard deviation.
λ	-	wavelength.
μ	-	coefficient of viscosity; micro-(as a prefix).
ν	-	kinematic viscosity.
π	-	ratio of circumference to diameter of a circle ca., 3,14159.
ρ	-	density.
σ	-	standard deviation; gas density; surface tension.
σ_t	-	peak standard deviation in time units.
σ_v	-	peak standard deviation in volume units.
σ^2	-	overall peak variance.
σ_d^2	-	peak variance contribution of detector.
σ_f^2	-	peak variance contribution due to flow through lines of manifold.
σ_i^2	-	peak variance contribution due to sample injection.
ϕ	-	volume fraction.

a	-	radius (or r = radius).
A	-	absorbance; Cunningham slip correction.
A_m	-	absorbance for steady state condition.
b	-	slope term of a linear regression equation.
B	-	particle mobility.
c	-	centi-(as a prefix).
C	-	concentration.
C°	-	original analyte concentration in the sample aliquot at the instant of injection.
C^{max}	-	the analyte concentration at the maximum of the peak as recorded by the detector.
$^\circ C$	-	degrees centigrade (measure of temperature).
d	-	diameter.
d_c	-	cutoff diameter, characteristic of spray chamber design.
d_{min}	-	minimum particle diameter trapped by a cyclone separator.
d_o	-	diameter of aerosol droplet before desolvation; mean droplet diameter.
d_x	-	diameter of a dry aerosol particle.
D	-	dispersion, dispersion ratio; diffusion coefficient.
D_a	-	axial dispersion coefficient.
D_m	-	molecular diffusion coefficient.
e	-	base of natural logarithms, ca., 2,71828.
f	-	correction factor.
F	-	axial flow speed.
F_c	-	carrier flow rate.
g	-	gravitational acceleration; gram.
H	-	length of a cyclone chamber; peak height.
$\overline{H}$	-	mean peak height.
i	-	intercept term of a linear regression equation.

k	-	proportionality constant; kilo - (as a prefix).
K	-	Kelvin (unit of temperature).
K_n	-	Knudsen number, the ratio of the mean free path of a particle in a gas to the particles radius.
ℓ	-	litre; radius of curvature of stream flow lines.
ln	-	logarithm to base e.
L	-	length.
m	-	mass; milli-(as a prefix); metre.
mℓ	-	millilitre.
mol	-	mole.
M	-	mass of analyte.
n	-	number.
P	-	fractional penetration of particles of diameter d through a tube of length L.
Pa	-	pascal.
q	-	flow rate.
Q	-	volumetric flow rate.
Q_e	-	mass of analyte entering plasma.
Q_g	-	volume flow of gas.
Q_ℓ	-	volume flow of liquid.
Q_u	-	mass of analyte aspirated by the nebulizer.
r	-	radius (or a = radius); linear correlation coefficient.
r(x,y)	-	linear correlation coefficient between x and y.
R	-	radial distance from axis of a cyclone.
R_1	-	radius of inner tube of a cyclone.
R_2	-	radius of outer tube of a cyclone.
R_c	-	radius of spray chamber for 50% cutoff of droplets of diameter d_c.
R_e	-	Reynolds number.

s	-	second (unit of time); number of spiral turns in a cyclone.
S_{max}	-	maximum sampling rate.
S_{tk}	-	Stokes number.
t	-	time; t-statistic for comparison of means.
t_d	-	aerosol displacement time.
t_r	-	residence time of aerosol in spray chamber.
$t_{x\%}$	-	wash-out time to x% of initial signal at t=o.
t^{in}	-	wash-in time.
t^{out}	-	wash-out time.
Δt	-	baseline-to-baseline time of peak.
$\overline{T}$	-	mean residence time.
u	-	sample uptake rate.
U	-	mean speed of flow.
v	-	volume.
V	-	velocity difference; tangential velocity; volume; volt.
V_e	-	volume of liquid in aerosol form leaving the spray chamber for the atomizer.
V_i	-	volume of sample injected.
V_o	-	initial velocity.
V_s	-	terminal settling velocity.
V_u	-	volume of liquid aspirated by the nebulizer.
w	-	peak width.
w_k	-	full width of FIA signal peak at the kth proportion of maximum peak height.
W	-	width of inlet tube of a cyclone separator; watt (unit of power).
X	-	distance from centre of sample zone.

ABBREVIATIONS

AAS	-	atomic absorption spectrometry.
A.I.R.	-	aerosol ionic redistribution.
ARL	-	Applied Research Laboratories.
ca.	-	circa (= about).
CON	-	conical.
CDA	-	controlled dispersion analysis.
DB	-	double barrel.
DCP	-	direct current plasma.
DIN	-	direct injection nebulization.
EIE	-	easily ionizable element.
FI	-	flow injection.
FIA	-	flow injection analysis.
FSD	-	full scale deflection.
HPLC	-	high performance liquid chromatography.
ICP	-	inductively coupled plasma.
i.d.	-	internal diameter.
max	-	maximum.
min	-	minute; minimum (as a subscript).
N & T	-	Nukiyama and Tanasawa.
o.d.	-	outer diameter.
RAO	-	right angle outlet.
rf	-	radio frequency.
RFA	-	rapid flow analysis.
RSD	-	relative standard deviation.
TI	-	tangential inlet.
TO1	-	tangential outlet type 1 (where the outer side of the aerosol exit tube is tangential to the spray chamber body).
TO2	-	tangential outlet type 2 (where the axis of the aerosol exit tube is tangential to the spray chamber body).
TO3	-	tangential outlet type 3 (where the inner side of the aerosol exit tube is tangential to the spray chamber body).
viz.	-	videlicet (= namely).

CHAPTER 1: INTRODUCTION

1.1 The analytical problem

Inductively coupled plasma (ICP) emission spectrometry is an established technique for the determination of trace metals in aqueous solution. Conventionally, this technique makes use of the presentation of discrete samples at a sampling rate of around 30 samples per hour, at least 5 mℓ sample volume being required for analysis (Kempster, 1986). As a conventional ICP source typically has an argon consumption rate of 10 to 15 $\ell.min^{-1}$ (Kempster, 1986; Montaser *et al*, 1986), the relatively slow sampling rate has cost implications, and an increase in sample presentation rate would be desirable. Montaser and co-workers cite the cost implications of the high argon consumption rate as an important factor militating against wider use of the ICP emission spectroscopic method, apart from the capital cost of ICP emission spectrometers.

The flow injection analysis (FIA) technique has been successfully used in combination with atomic absorption spectrometry (AAS) to achieve rapid flow analysis (RFA), as shown for example, by Basson and Van Staden (1980) and others (Tyson, 1983). As AAS has sample nebulization, with passage of the aerosol through a spray chamber, in common with the ICP emission spectrometric technique, the FIA method therefore has potential for achieving RFA likewise with the ICP technique.

Direct coupling of a flow injection valve to the nebulizer of an ICP, without modification of the spray chamber does not, however, lead to dramatic improvement in the sampling rate (Jacintho *et al*, 1981; Zagatto *et al*, 1983), as might be expected from the experience of others with the FIA-AAS combination (Tyson, 1983). This is due to the long wash-out time and memory effects in ICP spray chambers (Dale and Buchanan, 1986).

The analytical problem is therefore the design of a reduced volume spray chamber for an ICP emission spectrometer, to thereby reduce the wash-out time, and thus make possible the achievement of RFA, by interfacing FIA as a sample introduction technique, to the ICP method. In the terminology of FIA theory, the contribution of the spray chamber to peak broadening i.e., axial dispersion, must be reduced to increase the sampling rate.

The reduction of spray chamber volume is, in itself, an analytical challenge. Reduction in aerosol residence time should be achieved without a degradation in the ability of the spray chamber to remove large aerosol droplets (Browner and Boorn, 1984a and 1984b), with consequent detrimental effects on the analytical characteristics of the plasma.

The aim of this work is therefore to design a suitable reduced volume spray chamber, for use in coupling the FIA technique to an ICP emission spectrometer, to achieve RFA.

The goal of rapid flow analysis is particularly needed where many hundreds of samples must be analyzed for a single element by ICP emission spectrometry for environmental purposes. The application of the FIA technique to increase sampling rates is particularly relevant to methods used for the determination of pollutants in water (Valcarcel and Luque de Castro, 1987). A case in point is the determination of boron in surface waters, where the slow analytical rate of conventional discrete sample introduction to the ICP emission spectrometer results in a considerable argon consumption, and associated expense. The use of an FIA-ICP combination for this purpose has the potential of reducing the cost of boron determinations. Such cost reduction is also applicable for other elements.

1.2 Scope of this thesis

The scope of this thesis encompasses the following:

(i) An overview of the relevant literature, with particular reference to FIA-AAS, HPLC-ICP and FIA-ICP interfacing, as well as nebulization and spray chamber theory. The use of cyclone theory (Davies 1952a; Fuks, 1955) presents a promising avenue in the design of small volume spray chambers (Gustavsson, 1984b). The literature overview revealed that spray chamber dead volume is a critical problem hindering RFA when interfacing FIA to ICP.

(ii) The design of reduced volume spray chambers, based on centrifugal droplet removal, as well as the aerosol flow reversal principle of the conventional Scott spray chamber (Fuks, 1955; Scott et al, 1974).

(iii) The evaluation of spray chambers for drainage, nebulization efficiency, and memory effect in terms of wash-in and wash-out times, as well as precision, sensitivity and detection limits. Spray chambers were also evaluated for the occurrence of volatilization type interference of aluminium and phosphate on calcium, and interference of sodium on calcium, as a test for easily ionizable element (EIE) interference.

(iv) The behaviour of selected spray chambers for use with FIA-ICP interfacing for boron analysis, and the establishment of the conditions necessary for rapid sample introduction.

(v) The analytical characteristics of the FIA-ICP interface for the determination of calcium.

(vi) The potential of the FIA-ICP interface for the RFA determination of magnesium, manganese and strontium.

(vii) The thesis is concluded with a discussion on the achievement of RFA by FIA-ICP interfacing, through the design of an efficient reduced volume spray chamber.

CHAPTER 2: LITERATURE SURVEY

2.1 Introduction

This literature survey is directed towards gleaning those facts and concepts, as discussed by other researchers, which will be of value in studying the central theme of this thesis, viz the interfacing of FIA to ICP so as to achieve rapid flow analysis (RFA).

The subjects covered in this overview of the literature are as follows:

(i) The history and development of the FIA technique.

(ii) The use of FIA in conjunction with AAS, a technique which shares sample nebulization as the means of sample introduction to the spectroscopic source, in common with ICP emission spectrometry.

(iii) The interfacing of the chromatographic and ICP techniques, the former method having facets in common with FIA.

(iv) The literature on the interfacing of FIA with ICP, naturally of particular relevance to this study.

(v) The subject of pneumatic nebulization i.e., the production of the primary aerosol.

(vi) Spray chamber theory and aerosol conditioning processes.

(vii) Cyclone theory, being particularly relevant to the design of effective spray chambers of small dead volume.

The overview of the literature is concluded with a synopsis of the present status of the art of interfacing FIA to ICP, the experience of others in the past providing direction pointers for promising avenues of advance.

2.2 Flow injection analysis (FIA)

Flow injection analysis (FIA) may be defined as, "an automated or semi-automated analytical process consisting of the insertion of sequential discrete sample solutions into an unsegmented continuously flowing liquid stream with subsequent detection of the analyte" (Stewart, 1981). A concept which should be added to this definition is that the injected sample, which forms a well-defined plug or zone, is subjected to physical as well as on occasion chemical processes, during transport between the point of injection and the detector (Van Staden, 1987).

As early as 1953 Lindsay had used the principle of FIA in the colorimetric measurement of hypochlorite for process control (Lindsay, 1981). In 1958 Spackman and co-workers employed the concept of a continuously flowing, non-segmented reagent stream for amino acid analysis, and indicated the need for precise and reproducible pumping of sample and reagent flows (Spackman *et al*, 1958). A year earlier *viz* 1957, the concept of air-segmented continuous flow-analysis had been described for use in the analysis of blood serum samples for urea nitrogen (Skeggs, 1957). Blaedel and Hicks (1962) used unsegmented sample and reagent streams in studying enzyme catalyzed reactions, using a differential filter photometer as detector.

In the early seventies, a number of pioneering workers started investigating flow injection principles. For example, Mottola (1981) in his review of the history of FIA mentions Pungor and co-workers in Hungary, who experimented with the use of FIA in electrochemistry; Franz and Hare who described a manifold for the colorimetric determination of silica; and Bergmeyer and Hagen (1972) who used FIA with a closed-loop manifold for the enzymatic determination of glucose and achieved a sampling rate of around 60 per hour. Pungor and co-workers used an on-line mixing cell

between the point of manual sample injection and the voltammetric detector to improve the reproducibility of the peak-area measurements (Nagy et al, 1970). The beneficial effects on sensitivity of using small diameter tubing for the flow lines in FIA manifolds was shown by Gerding et al (1972) who investigated the spectrophotometric determination of peptides. A very slow pumping rate of 1 mℓ per hour, and Teflon tubing of only 0,3 mm i.d was used.

The use of sample insertion into an unsegmented flowing liquid stream took a leap forward in 1975 when Ruzicka and Hansen in Denmark coined the term, flow injection analysis. An advantage of FIA over air-segmented continuous flow analysis based on Skeggs (1957) work, is that in FIA the carrier reagent stream flows more regularly than in the case of air-segmented streams, as water unlike air is not compressible (Ruzicka and Hansen, 1975). A series of papers on FIA by Ruzicka and Hansen followed (Stewart, 1981). The usefulness of FIA in achieving the automation of colorimetric methods, and at the same time increasing the analytical rate to as much as 120 samples per hour was shown by Stewart and co-workers in America (Stewart et al, 1976). These researchers emphasized the need to minimize the volumes of the flow lines and detector cell in achieving rapid flow analysis.

By 1979, the three principles on which flow injection analysis is based had been clearly formulated viz., (i) injection of a sample aliquot into a non-segmented carrier stream, (ii) reproducible timing of sample injection and (iii) controlled dispersion of the analyte in the passage of the sample aliquot from the point of injection to the detector (Hansen and Ruzicka, 1979).

The dispersion, or dispersion ratio, D of the analyte in the sample is defined as (Ruzicka, 1981);

$$D = \left(\frac{C^{o}}{C^{max}} \right) \qquad \ldots \quad (1)$$

where C^{o} = the original analyte concentration in the sample aliquot at the instant of injection,

and C^{max} = the analyte concentration at the maximum of the peak as recorded by the detector.

The degree of dispersion may be classified as limited, medium or large (Ruzicka and Hansen, 1978). The application of these three degrees of dispersion being as follows:

In limited dispersion, with $1 \leq D \leq 3$ (Tyson and Idris, 1981), the injected sample volume is sufficiently large in relation to the carrier stream so that $C^{max} \geq C^{o}/3$. The achievement of limited dispersion requires that the time lapse, and thus the length of tubing, between the injection point and detector be as short as possible (Ruzicka and Hansen, 1978). Limited dispersion is used where the original sample composition is sought e.g., in pH measurement (Ruzicka, 1981). Limited dispersion is the flow injection analogue of discrete nebulization (Tyson and Idris, 1981). Most applications of FIA with AAS employ limited dispersion (Tyson et al, 1983b).

In medium dispersion, D lies in the range 3 to 10* (Tyson and Idris, 1981). Medium dispersion values are frequently used in colorimetry, where several reagents must be mixed with the sample aliquot (Ruzicka, 1981).

In large (Ruzicka, 1981), or high (Tyson and Idris, 1981) dispersion, D is greater than 10. High dispersion is useful where the analyte concentration lies above the analytical range of the detector, and the sample requires dilution prior to analysis (Ruzicka, 1981). The use of a

---

* A figure of 15 is also sometimes used (Valcarcel and Luque de Castro, 1987).

manifold with a high dispersion ratio is also useful in the evaluation of the effect of potential interferants on the analyte signal (Tyson *et al*, 1985).

Christian and Ruzicka (1987) have suggested the use of the term reduced dispersion (D < 1), where FIA manifolds are used for on-line preconcentration of analyte.

In discussing the theory of the dispersion process which occurs in the time interval between injection of sample and subsequent measurement of the analyte concentration in the detector, Ruzicka *et al* (1977) showed the importance of the Gaussian approximation for describing the shape of the peak of the dispersed analyte at the detector. The concentration gradient C, in an axial direction, within the sample zone may be approximated as;

$$C = \frac{M}{2a^2.\pi}\left(\frac{1}{\sqrt{\pi.\delta.L^2}} \cdot e^{[-(L-X)^2/(L^2.4\delta)]}\right) \quad \ldots \quad (2)$$

where C = concentration of analyte at distance X from the centre of the sample zone,
M = mass of analyte at injection point at time t=0,
a = radius of tube,
δ = dispersion number
and L = tube length.

The dimensionless dispersion number δ is given by;

$$\delta = (D_a.t)/(L^2) \quad \ldots \quad (3)$$

where D_a = axial dispersion coefficient, $cm^2.s^{-1}$,
t = time, s,
and L = tube length, cm.

As the axial flow speed F, is given by L/t, equation 3 may also be given as (Ruzicka and Hansen, 1978);

$$\delta = (D_a)/(F.L) \quad \ldots \quad (4)$$

In reality the concentration peaks observed show an asymmetry, with tailing on the wash-out side of the peak due for instance to abrupt changes in internal diameter at connection points in the manifold, or to dead volumes in the system or the time constants of the electronic measuring circuitry (Tijssen, 1980). Yet, when the length of the flow line is at least one hundred times greater than the diameter of the tubing, the degree of asymmetry is usually small (Taylor, 1954).

The maximum sampling rate in FIA is governed by the degree of peak broadening, as well as by the acceptable extent of overlap between adjacent sample peaks. Ruzicka and Hansen (1981) give the following formula for the maximum sampling rate, S_{max} in samples per hour;

$$S_{max} = (60.Q)/(\kappa.\sigma_v) \quad \ldots \quad (5)$$

where Q = the volume flow rate, $m\ell.min^{-1}$,

σ_v = the peak standard deviation in volume units, $m\ell$,

and κ = the number of standard deviation units chosen for acceptable resolution, κ normally being chosen as 4.

S_{max} may alternatively be given as;

$$S_{max} = 3600/(\kappa.\sigma_t) \quad \ldots \quad (6)$$

where σ_t = the peak standard deviation given in time units, s,

and κ = as defined for equation 5.

The overall observed peak variance σ^2, is the sum of the variances contributed by the broadening processes occurring during sample injection, flow through the flow lines of the manifold, and occurring within the detector (Reijn et al, 1980; Ruzicka and Hansen, 1981);

$$\sigma^2 = \sigma_i^2 + \sigma_f^2 + \sigma_d^2 \qquad \ldots \quad (7)$$

where σ^2 = overall observed peak variance,

σ_i^2 = peak variance due to the injector,

σ_f^2 = peak variance arising from flow through lines of manifold,

and σ_d^2 = peak variance contribution of detector.

The variance in equation 7 being expressed either in volume or time units. From equation 6 it is immediately obvious that for high sampling rates, the experimental conditions should be such that the peak standard deviation σ should be small. According to the Taylor-Aris model, σ is given by;

$$\sigma_t = [\bar{T}.a^2/(24\ D_m)]^{1/2} \qquad \ldots \quad (8)$$

where σ_t = peak standard deviation, given in time units,

$\bar{T}$ = mean residence time, in seconds,

a = radius of flow line, cm,

and D_m = the molecular diffusion coefficient, $cm^2.s^{-1}$.

The analagous expression for σ in volume units is;

$$\sigma_v = [\pi.a^4.\ L\ Q/(24D_m)]^{1/2} \quad \ldots \quad (9)$$

where σ_v = the peak standard deviation, given in volume units,

L = flow line length,

Q = volume flow rate

and D_m = the molecular diffusion coefficient.

From equation 9 it follows that narrow peak width necessitates flow lines with small inner diameter, shorter length and slower pumping rate (Ruzicka amd Hansen, 1981). While flow line diameter is readily reduced, a constraint is though, the avoidance of back pressure of greater than 1 bar in FIA. Detector volume and its contribution to peak broadening is not so readily reduced (Reijn et al, 1983).

Instead of assuming axial dispersion to be the most important cause of peak broadening, Vanderslice and co-workers assumed that radial rather than axial dispersion contributes most significantly to peak broadening in FIA (Ranger, 1981; Vanderslice et al, 1981; Vanderslice et al, 1984). Assuming that convection and diffusion contributed to peak broadening, Vanderslice et al (1984) expressed baseline-to-baseline time Δt, as;

$$\Delta t = \left(\frac{35,4.r^2 f}{D^{0,36}} \left(\frac{L}{q} \right)^{0,64} \right) \quad \ldots \quad (10)$$

where r = radius of tubing, cm,

f = correction factor, between 0,5 and 1,0 which accounts for recorder sensitivity,

D = the diffusion coefficient, $cm^2.s^{-1}$,

L = length of tubing, cm,

and q = flow rate, $m\ell.min^{-1}$.

Equation 10, also implies that reducing tube diameter and tube length leads to narrower peaks. The occurrence of radial dispersion also results in non-symmetry of observed peaks (Vanderslice et al, 1981). Gomez-Nieto et al (1985) showed experimentally that a shortcoming of equation 10, which limits its practical application, is that the correction factor f is influenced by the values of L, q and r.

In summary, apart from isolated instances of the use of sample injection into unsegmented flow streams for analytical purposes prior to 1970, the major development of the FIA technique to automate wet chemical and especially spectrophotometric determinations took place in the seventies.

The FIA technique also proved of value for use in conjunction with potentiometric methods. It was only in 1979, however that the FIA technique was applied to AAS measurement (Ruzicka and Hansen, 1980; Zagatto et al, 1979). The FIA technique allowed more rapid analysis of many samples; the miniaturization of manifolds and flow through cells, with narrower peaks, together with the concepts of controlled dispersion with measurement of analyte concentration at non-steady state conditions contributing to this achievement. The early eighties saw the use of FIA in conjunction with AAS (Tyson, 1983) while interest in employing FIA as a sample introduction technique for ICP emission spectrometry emerged after Greenfield's article in 1981 on the potential marriage of the FIA and ICP techniques (Greenfield, 1981). A central difficulty in reaching the latter goal is that of decreasing the peak broadening effect of the spray chamber, as is discussed later. The great attraction of the FIA method is that the absence of air segmentation means that the carrier liquid flow stream may be pumped with greater regularity than is possible using segmented continuous flow analysis.

2.3 Flow injection analysis in combination with atomic absorption spectrometry

The year 1979 saw the use of flow injection analysis as a means of sample introduction in atomic absorption spectrometry, the combination of the two techniques providing a means of increasing sampling rate as well as reducing the volume of sample consumed (Wolf and Stewart, 1979; Yoza et al, 1979; Zagatto et al, 1979). Wolf and Stewart (1979) used FIA as a means of sample introduction to an AAS instrument for the determination of copper and zinc, a 25 to 300 µℓ sample volume being injected into a carrier stream which was pumped to the nebulizer. Already at this early stage, these workers mentioned the potential FIA had as a sample introduction technique for other spectroscopic methods using nebulization. The injection of not only the sample into the carrier stream, but the injection of reagents as well, may serve as a means of reducing reagent consumption. Zagatto et al (1979), for example, made use of a double proportional injector (Bergamin F^{o} et al, 1978) to inject a lanthanum solution and sample into two separate carrier streams, which were then merged prior to atomic absorption spectrometric determination of calcium and magnesium. Zagatto et al (1979) achieved a sampling rate of 300 per hour with a relative standard deviation of 1% or better, for a 150 mg,ℓ^{-1} Ca standard. The potential of the FIA technique in achieving rapid sample throughput for water analysis by AAS was shown by Basson and Van Staden (1980) who used FIA to determine magnesium and calcium in water, at a sampling rate of 128 per hour. Fukamachi and Ishibashi (1980) showed that the FIA-AAS combination was also capable of handling organic solvents. Fukamachi and Ishibashi injected the aqueous sample into a carrier stream of n-butyl acetate, which served to increase the sensitivity of the AAS measurement for a number of metals. Renoe et al (1981) used FIA to subsample the eluate from a liquid

chromatograph for introduction into a carrier stream fed to an AAS nebulizer for the determination of calcium and magnesium.

Tyson (1981) showed that the combined effect of nebulizer and spray chamber dead volume, together with instrument response in an FIA-AAS combination could be considered in terms of a hypothetical mixing chamber of volume V, with exponential increase in concentration occurring as the dispersed sample passes into the detector, until peak maximum is reached, followed by exponential decrease in concentration as the concentration decreases back to the baseline value. Tyson (1981) described the concentration response versus time, where a step change in concentration from C_1 to C_2 occurred prior to the mixing chamber, as follows:

$$C = C_2 - (C_2 - C_1).\ e^{(-ut/V)} \qquad \ldots \quad (11)$$

Where C = concentration readout of AAS,
t = time following step change in concentration from C_1 to C_2,
u = sample uptake rate
and V = volume of hypothetical mixing tank.

If $C_1 = 0$ then equation 11 reduces to:

$$C = C_2.\ (1 - e^{(-ut/V)}) \qquad \ldots \quad (12)$$

While if $C_2 = 0$ then equation 11 reduces to:

$$C = C_1.e^{(-ut/V)} \quad \ldots \quad (13)$$

Assuming concentration is a linear function of absorbance A, the volume V of the hypothetical mixing tank is given by (Tyson, 1981; Tyson and Idris, 1981);

$$V = ut/(\ln[A_m/(A_m-A)]) \quad \ldots \quad (14)$$

where A = absorbance at time t,
and A_m = absorbance for steady state signal.

The relationship between dispersion D, and the volume of sample injected V_i, is given by (Tyson and Idris, 1981);

$$D = [\ 1 - e^{(-V_i/V)}]^{-1} \quad \ldots \quad (15)$$

where V_i = volume of sample injected,
and V = volume of hypothetical mixing chamber.

As the dispersion D, can be experimentally obtained from the ratio of the initial concentration at the point of injection to the peak concentration recorded by the detector, equation 15 may be used for calculating V, where the injection volume V_i is known.

An advantage of the intermittent introduction of dispersed samples, as against continuous aspiration enables FIA to be used to introduce samples with a high dissolved solids content into an AAS nebulizer without clogging occurring. Thus Rocks et al (1982a) were able to determine copper and zinc in serum, without prior precipitation of the serum proteins, as normally required for AAS analysis. This property of FIA, to increase the ability of the AAS transport system to handle high dissolved solids samples,

was also used by Zhou et al (1983), in analyzing for metals in steel digests, with a total metal concentration of 8% (m/m). Zagatto et al (1986) made use of a high dispersion manifold when determining chromium in steels. Flow injection has made possible the introduction of samples which would cause severe problems by conventional nebulization (Tyson, 1985). Total dissolved salt concentrations as high as 32% (m/v) may be handled with the FIA-AAS technique, using suitable dispersion (Tyson, 1984a). The use of a flow injection manifold to achieve on-line dilution of samples, in parallel with a direct aspiration line was described by Ramsey and Thompson (1982). A four-port valve was used to shunt sample either directly to the AAS nebulizer, or through the dilution manifold to the atomic absorption instrument.

The advantage of the FIA technique of reduced sample volume consumed for analysis is particularly valuable in clinical applications, where the quantity of sample available for analysis is often limited. Examples of the application of the FIA technique as a means of sample introduction for AAS for the analysis of clinical samples are, for instance, the determination of copper and zinc in serum (Rocks et al, 1982a), the determination of iron in serum (Rocks et al, 1983a), the determination of zinc in serum (Attiyat and Christian, 1984; Simonsen et al, 1986), the determination of lithium in serum (Rocks et al, 1982b), and the determination of copper, zinc and iron in saliva (Burguera et al, 1986). Burguera et al (1983) used manual sample injection into a carrier stream, without a peristaltic pump, for the determination of calcium and magnesium in serum, and reported RSD values of 0,9 to 5,9 %. Better precision is possible, however, and the use of a positive pressure pump is advisable to control the rate of flow of the carrier stream in the use of FIA as a sample introduction technique for AAS (Rocks et al. 1983b, Rocks et al, 1984). Rocks and co-workers described a variant of

FIA in 1985, where no sample volume is wasted in filling flow lines to a sample loop (Sherwood et al, 1985). In their procedure, termed controlled dispersion analysis (CDA), no injection valve is used, and a controlled volume of sample is instead aspirated into the carrier flowline using a microprocessor controlled stepper motor. Simonsen et al (1986) used a microprocessor controlled three-way valve, using sample aspiration without a positive pressure pump, for the determination of zinc in serum. An interesting aspect of Simonsen and co-workers method is the use of peak area calibration, as a means of avoiding the difficulty of peak height variation, consequent to viscosity induced changes in aspiration rate.

Tyson et al (1983a) described the application of the standard additions method to the FIA-AAS combination, where the sample is aspirated as the carrier stream, and the calibration standards injected with an injection valve into the carrier stream. A plot of deviation in concentration is then made against the concentration of the standards. The concentration of analyte in the sample is then given by the point where zero deviation occurs. An advantage of the FIA standard additions method described by Tyson is that the concentration of analyte in the sample is given by interpolation, rather than by extrapolation as is the case with the conventional standard additions procedure (Tyson and Idris, 1984). Tyson et al (1983b) point out that in applying FIA-AAS to the analysis of real samples, these should where possible be injected in triplicate so as to obtain an estimate of analytical precision with each sample. The actual numbers of determinations per hour in FIA-AAS is then in effect three times less than the samples per hour figures often quoted in the literature. A practical point of importance in using FIA with AAS, emphasized by Brown and Ruzicka (1984) is that the forced liquid flow to the nebulizer should be as pulse free as possible.

When reviewing the applications of FIA in AAS analysis Tyson (1983) indicated that the majority of applications had used single-line manifolds as a means of sample introduction for the AAS method, and that potential existed for the use of the FIA technique in calibration procedures. Tyson and Appleton (1985) demonstrated how a calibration could be established using a single high concentration standard with a mixing chamber, and employing equation 12 to establish the concentration time response. The use of a variable dispersion flow injection manifold with six parallel dispersion lines, providing dispersion coefficients from 5,9 to 38,8 was described by Tyson et al (1986) as a means of single standard calibration, as well as dilution for off-range samples in FIA-AAS determinations.

The possibility of determining concentration from peak width was shown by Tyson (1984a and 1984b), the basis for the procedure being the exponential shape of the recorded peaks. While peak width calibration may be used to extend the calibration concentration range of AAS by about one order of magnitude (Tyson 1984b), the difficulty of accurately measuring peak width reduces the precision of measurement. This detracts from its practical application (Bysouth and Tyson, 1986). The procedure may have value, however, in determining dilution factors for samples which are over-range by conventional peak height or peak area calibration. An interesting application of FIA in evaluating the effect of potential interfering substances on analyte signal in AAS was described by Tyson et al (1985), where a solution of the potential interferant is injected into a water carrier stream, mixed with the analyte stream and then fed to the AAS instrument. Changes in absorbance may then provide information on the sign and degree of interference. A null measurement procedure for FIA-AAS use, where a stock standard solution is automatically diluted until its absorbance matches that of

the sample, was described by Bysouth and Tyson (1987). A source of error in this method arises from flow pulsations in the peristaltic pumps used in the iterative dilution manifold.

Another application of the FIA technique, used in conjunction with AAS, is the automation of sample pretreatment procedures, such as ion-exchange pre-concentration (Olsen et al, 1983), preconcentration by complexation and liquid/liquid extraction (Nord and Karlberg, 1981), or hydride formation (Astrom, 1982). Olsen et al (1983) used a manifold with a micro-column containing 25 mg Chelex-100 resin to preconcentrate cadmium, lead, copper and zinc from sea water.

Difficulties were experienced with resin swelling and column compaction due to the pronounced volume changes of Chelex-100 resin on conversion between the ammonium and hydrogen ion forms. Fang, Xu and Zhang (1984) experimented with ion-exchange preconcentration of nickel, copper, lead and cadmium from sea water, using a chelating resin with salicylic acid functional groups (resin 122). Poor recovery of cadmium and nickel was found for sea water, with problems of breakthrough. A difficulty of using on-line resin columns in FIA-AAS is that the occurrence of back-pressure limits the length of the resin columns. Fang, Ruzicka and Hansen (1984) developed a FIA-AAS procedure for ion-exchange preconcentration of copper, zinc, lead and cadmium from sea water, using Chelex-100 resin with its iminodiacetate functional group, as previously attempted by Olsen et al (1983). Fang and co-workers were able to minimize the swelling and concentration changes of the Chelex-100 resin by limiting the contact time of the resin with ammonium acetate to less than 50 s, for a 0,5 $mol.\ell^{-1}$ ammonium acetate solution at a flow rate of 6 $m\ell.min^{-1}$. An additional precaution, to

avoid excessive resin swelling, of washing the resin in the ammonium form first with 2 mol.ℓ^{-1} nitric acid and then only with water was also mentioned. Fang, Ruzicka and Hansen (1984) reported recoveries for copper, zinc, lead and cadmium from sea water of 99%, 92%, 95% and 93% respectively. Fang and co-workers noted that samples containing high concentrations of iron and aluminium present a greater difficulty for ion-exchange preconcentration procedures than sea water. Malamas and co-workers described an FIA-AAS method for the determination of traces of copper in tap water, using an on-line column containing 8-quinolinol immobilized on porous glass to effect sample enrichment (Malamas et al, 1984).

A FIA-AAS hydride generation method for the determination of bismuth was described by Astrom (1982), who injected a 700 µℓ sample into a dilute hydrochloric acid carrier stream, with which was merged a stream containing sodium borohydride followed by a nitrogen gas stream. The mixture passed through a miniaturized gas-liquid separator, with the gas phase being led to an electrically heated quartz tube of the AAS instrument. Cobalt, nickel and copper interfered. Chan (1985) described a FIA-AAS hydride method for the determination of selenium, where 1,10-phenanthroline was used to reduce the interference of copper and nickel on the generation of the selenium hydride.

On-line sample pretreatment in FIA-AAS may also employ filtration. Martinez-Jimenez et al (1987), for example, described the use of an on-line filter for removal of silver chloride in the indirect determination of chloride. A drawback of the procedure was the necessity to wash the filter after every 150 to 200 samples.

The FIA-AAS method may also be used with organic solvents as carrier stream, provided the solvent is compatible with aspiration into the flame without extinguishing occurring. Taylor and Trevaskis (1986) described a method for the determination of lead in gasoline, where a gasoline sample pretreated with iodine, a cationic detergent and diluted with methyl isobutyl ketone (MIBK) is injected into the acetone carrier stream and aspirated into an air-acetylene flame. Sampling rates of up to 240 per hour were achieved.

The FIA technique lends itself to sample pretreatment chemistry for reactions reaching near completion within a few seconds Lynch et al (1984) used a flow-injection manifold, with a flow through cell spectrophotometer in line with an AAS instrument, for the speciation of chromium and iron in water and mineral process solutions. The AAS measurement provided total Fe and Cr readings; while 1,10-phenanthroline was used to form a coloured complex with Fe(II), and 1,5-diphenylcarbazide was used to form a complex with Cr(VI), for spectrophotometric measurement; the Fe(III) and Cr(III) concentrations being given by subtraction of the spectrophotometric concentration from the AAS concentration for each element. Another sequential flow-injection method was described by Alonso et al (1986) for the potentiometric determination of calcium, followed by AAS determination of magnesium, with sampling rates of up to 90 per hour being reported.

It is notable that in the FIA-AAS literature, the commercial nebulizer/spray chamber combinations of AAS instruments have been used without modification, with efforts to minimize dead volumes being directed at the FIA manifold per se (Astrom, 1982; Chan, 1985; Tyson, 1985). The latter because good sensitivity and detection limits is favoured by limited dispersion. If the injected sample volume is small compared to the volume of the hypothetical mixing chamber equivalent to the manifold, then high

dispersion values result. When V_i = V (equation 15) then D = 1,58. Harnly and Beecher (1985) decreased the wash-out time in a FIA-AAS combination by using a two valve, three pump system, and using a forced flow of 10 mℓ.min^{-1} to wash the nebulizer/spray chamber of the AAS between sample plugs. The first valve was used in the conventional manner, with one pump propelling the carrier stream, at a flow rate of 1,6 mℓ.min^{-1} to the nebulizer. The second pump was employed to fill the sample loop of the first valve, the sample plug being introduced into the carrier stream when the valve was switched. The carrier stream then passed through a second valve which, when switched, allowed a wash liquid to be pumped to the nebulizer at the much faster flow rate of 10 mℓ.min^{-1}. In this way memory effects between samples were reduced. Harnly and Beecher used their manifold to analyze for potassium, magnesium, sodium and zinc in urine.

In summary flow injection analysis has been successfully used as a means of sample introduction to an AAS instrument to increase the sample handling rate while at the same time reducing the sample volume required for analysis. The intermittent injection of a sample into a carrier stream has enabled samples with high total dissolved solids, such as sea water, to be analyzed without clogging of the nebulizer. The FIA technique has also made possible the automation of sample pretreatment procedures such as addition of releasing agents such as lanthanum (Tyson, 1985), as well as more complex manipulations such as hydride generation (Astrom 1982; Chan, 1985), or on-line ion-exchange preconcentration (Fang, Ruzicka and Hansen, 1984). The wash-out time of an AAS spray chamber is sufficiently short not to require reduction of spray chamber volume. This has made the interfacing of FIA to AAS a relatively simple procedure in contrast to the interfacing of FIA to ICP, where longer wash-out times present a problem (Tyson, 1985). The potential of using

the FIA technique for single standard calibration of an AAS instrument was shown by Tyson and Appleton (1985), the employment of mixing chamber theory, and the concept of the detector and manifold as a hypothetical mixing chamber providing a useful adjunct to optimizing flow systems (Tyson, 1981; Tyson and Idris, 1981).

2.4. Interfacing chromatographic and inductively coupled plasma techniques

The literature on the interfacing of chromatographic apparatus to ICP sources is instructive regarding the use of the FIA technique as a means of sample introduction, because of facets investigated by chromatographic researchers which are common to the interfacing of FIA to ICP. Indeed, as Ranger (1981) has pointed out, FIA may be considered as a hybrid of segmented flow analysis and high pressure liquid chromatography (HPLC).

The coupling of the outlet of a gas chromatograph to a plasma source is relatively simple, as no nebulizer or spray chamber is required (Sommer and Ohls, 1979; Uden et al, 1978; Windsor and Denton, 1979). Windsor and Denton (1979) modified the ICP torch design by reducing the diameter of the sample introduction tube to 0,1 mm to reduce dead volume.

Fraley et al (1979) and Gast et al (1979) experimented with the coupling of an HPLC outlet to the nebulizer uptake tube of an ICP source. Neither of these two groups of researchers made any attempt to decrease the spray chamber dead volume, although Fraley et al (1979) mentioned that the dead volume of the interface is crucial, and that a minimal length of Teflon capillary tubing, still allowing flexibility, should be used. Later, Fraley et al (1981) utilized an HPLC-ICP combination for the separation and determination of metal chelates. The problem of plasma instability was described, where methanol was present in the eluant, whereas where pure xylene was used, no such instability was encountered. Morita and Uehiro (1981) used HPLC with an ICP detector for the analysis of phosphates. No changes were made to the commercial nebulizer/spray chamber, the outlet of the liquid chromatograph merely being coupled to the sample uptake tube of the pneumatic nebulizer using a 130 mm length of Teflon capillary tubing.

An important advance was made in 1981 when Hausler and Taylor (1981a and 1981b) in America, addressed the problem of spray chamber dead volume, and identified the need to reduce spray chamber volume so as to minimize peak broadening when using an ICP emission spectrometer as a detector for liquid chromatography. These workers chose a 9 mℓ volume conical spray chamber with a glass bead spoiler, after finding that the use of even smaller volume interfaces between the nebulizer and torch such as a glass "Tee" or Swageloc "Tee" led to drainage problems, with solvent eventually rising into the aerosol (inner) tube of the torch. Hausler and Taylor also noted that cooling the spray chamber, using a water jacket improved detection limits by an order of magnitude, presumably as a result of decreased evaporation of the toluene solvent (Hausler and Taylor, 1981a).

Krull and co-workers (Bushee et al, 1982; Krull et al, 1982; Krull et al, 1983) in experimenting with ICP or direct current plasma (DCP) as a detector for HPLC, found poor detection limits, due in part to interface hardware dead volumes. McCarthy et al (1983) who interfaced an HPLC to an ICP pneumatic nebulizer, using 0,25 mm i.d., Teflon tubing, also reported inadequate limits of detection, in the speciation of arsenic and selenium. Browner and co-workers (Whaley et al, 1982) noted that in interfacing a liquid chromatograph with an ICP source, the dilution effects in both the liquid transport portion of the interface as well as in the aerosol transport portion of the hardware need to be considered.

Caruso and co-workers (Nisamaneepong et al, 1984) also reported relatively poor detection limits when interfacing HPLC to an ICP pneumatic nebulizer by the simple process of using a short length of Teflon capillary tubing, without reducing spray chamber dead volume. Following identification of the relatively large volume of commercial

spray chambers as one reason for poor sensitivity (Ibrahim et al, 1984), Caruso and co-workers experimented with small volume spray chambers with a glass-frit nebulizer for use in HPLC-ICP analysis (Ibrahim, Nisamaneepong and Caruso, 1985), the volume of chambers tried being about two orders of magnitude smaller than that of a conventional Scott spray chamber. Problems of inadequate drainage with foam formation were experienced, however, and Caruso and co-workers settled on a larger spray chamber, of around 7 mℓ capacity, with their glass-frit nebulizer when determining alkyllead compounds by HPLC-ICP (Ibrahim, Nisamaneepong, Haas and Caruso, 1985). The glass-frit nebulizer only proved successful for the nebulization of organic solvents, and severe clogging was observed when attempts were made to aspirate dilute aqueous inorganic salt solutions.

Jinno et al (1985) when studying the problem of interfacing a liquid chromatograph to an ICP source as detector, investigated the use of a no-spray chamber approach, i.e., the direct injection of the nebulized aerosol from a cross-flow nebulizer into the plasma, using a liquid flow rate of 4 to 16 $\mu\ell . min^{-1}$. Poor signal reproducibility was reported, with collection of droplets on the inner surface of the sample introduction tube. Partial desolvation improved the precision. Jinno et al (1985) in summarizing the dilema of a spray chamber with a stable reproducible signal but a large dead volume with memory effects, as against using no spray chamber with consequent problems of instability and poor precision stated "... the spray chamber has a basic function in the nebulization processes; that is, it is the effective remover of sample aerosol droplets whose sizes are unsuitable diameters to be introduced into the plasma. Then, however, it unfortunately produces a mixing effect". Jinno et al (1985) also experimented with a small volume spray chamber of 62 mℓ capacity, and found better

sensitivity than when using a larger, 124 mℓ capacity, spray chamber. A promising avenue in the no-spray chamber approach of interfacing HPLC to ICP is that of LaFreniere and co-workers, who designed a microconcentric nebulizer (Lawrence et al, 1984) for direct injection of solvent into the plasma. At the optimum flow rate of around 120 $\mu\ell.min^{-1}$ organic solvents may be introduced without causing plasma instability (LaFreniere, 1986; LaFreniere et al, 1987).

Faske et al (1985) in discussing the problems of HPLC-ICP and FIA-ICP interfacing mention that there are three probable factors which have contributed to the slow acceptance of microlitre sample introduction devices interfaced to ICP emission spectrometers. These factors are: (i) The difficulty of manipulating microlitre volumes with problems of precision and accuracy, (ii) the relatively large dead volume of many injection systems and (iii) poor precision associated with discrete, manual injection of microlitre samples. To the dead volume of the sample injection and manipulation hardware, must be added the dead volume of the spray chamber, which is a significant source of peak broadening in liquid chromatography-ICP interfacing (McLeod et al, 1985; Gardiner et al, 1987).

In summary, the researchers who have interfaced HPLC to ICP have shown that the relatively large volume of commercial spray chambers is a source of peak broadening and leads to poor sensitivity and detection limits. Sensitivity can be improved, and the memory effect reduced, by using spray chambers with reduced volumes. Attempts to do without the spray chamber altogether* were not promising, and plasma

---

* An exception, where the no-spray chamber approach has shown promise, is the work of LaFreniere et al (1987), who successfully interfaced HPLC to ICP for the analysis of oil-based materials using a microconcentric nebulizer.

instability was encountered. Use of very small chambers, of only a few millilitre capacity was also not successful. The spray chamber must apparently be of sufficient volume to function adequately.

2.5 Flow injection analysis - inductively coupled plasma interfacing for aqueous solution analysis

Greenfield and Smith (1972) in the United Kingdom showed that the analysis of small aliquots of solutions of between 1 and 25 µℓ by ICP emission spectrometry was feasible. These authors described the use of either a Drummond microcapillary or a Hamilton micro-syringe for dispensing a measured volume of the sample solution to the sample uptake tube of a cross flow nebulizer of an ICP source. Manual sample introduction is, however, subject to non-reproducibility with a consequent detrimental effect on precision. The feasibility of analyzing manually dispensed discrete microlitre sample aliquots by ICP emission spectrometry was also shown by Kniseley et al (1973) in America, by Broekaert and Leis (1979) and Broekaert et al (1980) in Germany and by Uchida et al (1981) in Japan. Uchida and co-workers aspirated sample volumes of 100 µℓ or less, using yttrium as an internal standard. The importance of minimizing air-aspiration between samples and blanks, through rapid transfer of the sample uptake capillary between blank and sample solutions, was emphasized, if nebulizer blockage by salt deposition for example was to be avoided (Uchida et al, 1981). Greenfield (1981) discussed the potential of the marriage of the FIA and ICP techniques, indicating the promise which the use of controlled injection, usually with the use of a rotary-type valve, would have on the practical application of the combination. In the application of an FIA-ICP combination to the analysis of calcium in Portland cement (Greenfield, 1983) the value of the injection of a high total dissolved solids sample into a carrier stream, with the subsequent dispersion of the sample, was shown. This was that the nebulizer showed less tendency to blockage by salt deposition than with continuous aspiration of the sample solution (Baginski and Meinhard, 1984; Cobbold, 1986). As Greenfield did not reduce the dead volume of the spray

chamber, relatively low sampling frequencies were achieved viz 90 per hour, using 233 µℓ sample volume. A RSD value of 1,6% was reported for a 40 $mg.\ell^{-1}$ calcium standard. Peak height measurements were recorded in micro-amperes, directly from the photomultiplier tube of a Baird Plasma Spectrovac ICP spectrometer. Detailed information on the exact operating conditions was unfortunately not given (Greenfield, 1983). Greenfield also showed that the use of flow injection as a means of sample introduction had promise for the determination of other elements apart from calcium in solution. Apart from the advantage of FIA in increasing the tolerance of ICP pneumatic nebulizers to high salt concentrations, an additional advantage is that sample dispersion in the manifold, which reduces the salt concentration nebulized, will lessen any aerosol ionic redistribution (A.I.R.) interference (Borowiec et al, 1980).

Jacintho, Zagatto and co-workers in Brazil, (Jacintho et al, 1981; Zagatto et al, 1983) investigated the use of FIA for sample introduction into an ICP system. For a manifold with medium dispersion, a sampling rate of 100 samples per hour was achieved. These workers emphasized that an advantage of the use of the FIA technique of injecting the sample into an unsegmented carrier stream, is that the absence of air bubbles implies no disturbance to the steady state of the plasma. In discrete aspiration of samples, by contrast, an air-plug is aspirated into the plasma, and interferes with the steady state of the source.

It is not merely the introduction of an air-plug which disturbs the steady state of the plasma, but the interruption of the aspiration of water which affects plasma temperature. Tang and Trassy (1986) showed that the hydrogen produced by dissociation of water in the plasma plays an important role in the transfer of heat from the annular plasma to the axial analyte channel, and thus in

the intensity of the analyte emission signal from an ICP source. As the FIA technique employs an unsegmented flow of liquid to the detector, in this case the plasma, greater stability of source temperature and consequently invariance of analyte signal may be expected.

As shown by Kempster (1986) change in the temperature of an ICP source affecting analyte emission intensity occurs also when a change in the liquid uptake rate of as little as 10% occurs. The emphasis on controlled and reproducible liquid flow rates in the ICP technique can therefore be expected to lead to greater stability of plasma temperature.

Ito et al (1982) in Japan experimented with the introduction of 40 µℓ samples into the sample line of the nebulizer of an ICP instrument by manually injecting a sample aliquot into an injector-tee placed just prior to the nebulizer. An Argon stream was used to flush the injected sample aliquot into the nebulizer and spray chamber, while the sample line was flushed with water between injections. Their technique presents thus something of a combination of segmented and flow injection continuous flow methods. A particularly significant aspect of this paper was the use of a small volume conical spray chamber of 35 mℓ capacity instead of a conventional Scott-type ICP spray chamber with a capacity of around 220 mℓ (Scott et al, 1974).

By reduction of the dead volume, Ito and co-workers were able to achieve an analyte signal of 67% of steady state, using a sample volume of only 40 µℓ.

The desirability of a small spray chamber volume in achieving sensitivity in FIA analysis was recognized by the Japanese workers (Ito et al, 1982). The implications of a small spray chamber volume were not discussed by Ito and co-workers, however, and their major concern was with achieving reproducibility of the manual sample injection.

In Australia, Alexander and co-workers (Alexander et al, 1982) investigated the use of a manual FI technique with ICP emission spectrometry, using a Gilson peristaltic pump to pump a carrier stream of deionized water at a flow rate of 7,5 mℓ. min^{-1} to a Babington type nebulizer; and injecting sample volumes of between 10 and 300 µℓ into the carrier stream with the aid of a micro-syringe and a conventional liquid chromatographic septum injector valve. These workers placed the injector point prior to the peristaltic pump, as they found that the flow rate disturbance caused when the injection point was close to the nebulizer resulted in plasma instability. While injecting the sample just prior to the nebulizer might allow sampling rates as fast as 600 per hour, the plasma instability encountered rendered this attempt to achieve rapid sample introduction impractical. Such instability not only occurs with sudden changes in liquid flow rate, but may also occur when the nature or pressure of a gas flowing to the analyte channel of the plasma changes. This is a primary difficulty encountered when interfacing hydride generators to an ICP source (Browner 1983). While the Australian workers (Alexander et al, 1982) showed the potential that FIA-ICP interfacing has for RFA (rapid flow analysis), they did experience difficulty in attaining sufficient sensitivity. For a 300 µℓ injected sample volume, deterioration in the detection limit was as great as fourfold for the Ba 233,5 nm analytical line, and eightfold for the Cr 267,7 nm line, compared to continuous nebulization. Poor results for iron were also reported, which Alexander et al (1982) attributed to Fe contamination from the syringe needle used.

The decided advantage of using a flow injection valve instead of manual syringe injection when interfacing FIA to ICP spectrometry was shown by McLeod, Worsfold and Cox (McLeod et al, 1984), who experimented with the determination of metals in serum using a simple manifold of

a Gilson Minipuls peristaltic pump and a flow injection valve to introduce a 100 µℓ sample to the nebulizer and commercial spray chamber of an ICP spectrometer. The Rheodyne rotary type flow injection valve was placed as close as possible to the nebulizer. No difficulty with plasma stability was encountered. For the 100 µℓ sample aliquot, the dispersion was 2,1 i.e., sensitivity was approximately 50% of that achieved by continuous nebulization. As the presumably large dead volume of the commercial spray chamber was not modified, long equilibration times, in excess of 10 s for reaching steady state, were reported.

Other workers who addressed the problem of FIA-ICP interfacing for aqueous solution analysis during 1984 were Browner and Boorn (1984b), Israel and Barnes (1984), Lawrence et al (1984) and Liversage et al (1984).

Browner and Boorn (1984b) identified the slow wash-out of typical ICP spray chambers as a problem in the achievement of rapid flow analysis when interfacing FIA to ICP. The slow wash-out occurs because of the much smaller aerosol gas flow rate of around 1 $\ell.min^{-1}$ in the ICP method, as against around 18 $\ell.min^{-1}$ in the AAS method. The typical $t_{1\%}$ values, i.e. wash-out time to 1% of the initial signal are 25 s for the ICP method and 1 s for the AAS method.

Israel and Barnes (1984) showed that the standard addition method of calibration, similar to that described for FIA-AAS (Tyson et al, 1983a) could also be used for the FIA-ICP combination. Israel and Barnes also point out, however, that the Tyson et al (1983a) standard additions approach may be unnecessary in ICP, where large linear dynamic ranges occur, unless matrix interferences are expected.

Lawrence, Rice and Fassel (Lawrence et al, 1984) in the United States attempted to solve the problem of the large dead volume of the spray chamber by removing the spray chamber altogether and designing a microconcentric nebulizer for direct injection nebulization (DIN), where the aerosol from the nebulizer tip is sprayed directly into the inner aerosol tube of an ICP torch. A major drawback of this approach is, however, the high velocity of the nebulizing gas of around 120 $m.s^{-1}$ as opposed to 20 $m.s^{-1}$ with conventional nebulization. This results in a sixfold decrease in the residence time of the analyte in the axial channel of the plasma. This, in association with the approximately tenfold increase in water loading to the plasma with a sample uptake rate of 200 $\mu\ell.min^{-1}$ using DIN, is expected to result in volatilization interference phenomena. Lawrence et al (1984) reported detection limits inferior to those achieved with conventional nebulization. The deleterious effect of an increased water loading to the plasma on analytical characteristics was discussed by Browner and Boorn (1984b). Merely doubling the water loading can cause a 100-fold reduction in the analytical signal for certain ion-lines.

The Canadian workers (Liversage et al, 1984) experimented with the use of FIA for application of the hydride generation method for arsenic determination using ICP emission spectrometry. Hydrogen tends to extinguish the plasma. By using the FIA technique to only intermittently introduce the sodium borohydride reagent and acidified sample into a distilled water carrier stream Liversage and co-workers were able to maintain the plasma at 1,5 kW radiofrequency (rf) power input. At 1,3 kW, however, plasma instability was observed. This experiment of the Canadian workers is a good example of how the FIA principle of intermittent injection into a carrier stream may be used to minimize the deleterious effects of some substances on the plasma.

The year 1985 saw further work by McLeod and co-workers in the United Kingdom (Cox et al, 1985; McLeod et al, 1985) on the use of the FIA-ICP combination for the analysis of aqueous solutions. Cox et al (1985) used an FIA manifold with an activated alumina column to separate Cr(III) and Cr(VI), the chromium being determined by ICP emission spectrometry. The manifold consisted of a peristaltic pump, a rotary injection valve, and a micro-column of activated alumina with an internal volume of 44 µℓ. A practical problem was the poor elution of Cr(VI) from the column after adsorption at alkaline pH. McLeod et al (1985) used a similar manifold with an activated alumina column for the separation of iron interferant from phosphorus, in the analysis of phosphorus in steels.

Hartenstein, Ruzicka and Christian (1985) described a FIA manifold, with a miniature Chelex 100 ion-exchange column, used in the reversed flow-mode, for the on-line preconcentration and elution of trace metals into an ICP source, a sampling rate of 30 per hour being achieved. Detection limits were superior to those obtained by conventional direct aspiration. Hartenstein, Christian and Ruzicka (1985), who described the application of a Chelex 100 iminodiacetic acid resin column for preconcentration on a FIA manifold, prior to ICP analysis, found that only labile forms of the metals were recovered, and suggested that while this was a drawback where total metal concentrations were sought, it might be useful in speciation studies.

Browner and co-workers in the United States (Faske et al, 1985) interfaced FIA to ICP, using a conventional pneumatic nebulizer system with a Scott spray chamber. The rf incident power to the plasma was between 1 and 1,25 kW. The signals were recorded by measuring the photomultiplier signal output directly with a picoammeter. The sampling rate was not given. Samples were injected using a syringe

loading sample injector. Peak height measurements were found to be linear over several orders of magnitude, and precision was 2,3% RSD for a 4 $mg.\ell^{-1}$ Fe solution, using a 50 µℓ injected sample volume. Injections were performed in triplicate.

LaFreniere and co-workers (LaFreniere et al, 1985) in further investigation of DIN by means of a microconcentric nebulizer (Lawrence et al, 1984) showed that the water loading of the plasma in the FIA-DIN-ICP combination resulted in volatilization type interferences, with a depression of calcium atomic line and ion-line emission at an Al to Ca molar ratio of 10 to 1. A phosphate on calcium interference was also present. A sodium on calcium interference was also observed, with enhancement of Ca(I) 422,7 nm emission, and depression of Ca(II) 393,4 nm emission. The occurrence of matrix interferences where sample is directly introduced into the plasma by means of a DIN microconcentric nebulizer is not unexpectedly associated with a decrease in excitation temperature by as much as 990 K at an observation height of 14 mm, when compared to conventional pneumatic nebulization (LaFreniere, 1986). The excellent detection limits, comparable to those achieved by continuous conventional nebulization are somewhat marred by the presence of volatilization type interferences, for the FIA-DIN-ICP combination. Nevertheless, the use of a direct injection nebulizer holds great promise as an interface between HPLC and ICP for the elemental speciation of oil-based materials, particularly as organic solvents may be introduced into the ICP by DIN without causing plasma instability (LaFreniere et al, 1987).

As the spray chamber serves an essential function of removing large droplets, which are incompletely vaporized during the residence time in the plasma (Browner and Boorn, 1984b) it is not unexpected that LaFreniere et al (1985)

found volatilization interferences when introducing a pneumatically nebulized aerosol without the large droplet filtering function of a spray chamber.

In 1986 a similar manifold described by Cox and co-workers the year previously (Cox et al, 1985) was used for the preconcentration and determination of Cr(III) in human urine, the concentration step being effected on an acid-alumina column (Cox and McLeod, 1986). The suitability of an acid-alumina column for preconcentration of other oxyanions apart from Cr(VI), such as arsenate, phosphate and molybdate was investigated using the manifold of Cox et al (1985) by Cook et al (1986). Some difficulty was experienced with desorption of the oxyanions in the short contact time for elution required for FIA-ICP use. In discussing the use of on-line ion-exchange preconcentration for use with the FIA-ICP technique, Fang et al (1986) state that knowledge of the kinetic aspects of such processes is not yet at the point where it can be applied in routine analysis on the complex matrices typical of environmental samples. These workers also point out the FIA-ICP combination has an important advantage in ameliorating the detrimental effects of high dissolved salts concentration in the ICP technique through dispersion of the sample.

In 1987 Granchi and co-workers described the use of FIA-ICP for the determination of wear-metals in oils, using xylene as carrier, at a flow rate of 1 $m\ell.min^{-1}$. Peak baseline-to-baseline width was 55s. Signals were integrated over an 80s interval (Granchi et al, 1987).

In summary, the primary problem in the achievement of the rapid flow analysis of aqueous solutions by interfacing the FIA with the ICP technique lies in the large dead volume of conventional ICP spray chambers and the consequent long equilibration times and prolonged wash-out times. The dead

volume problem of the spray chamber has been recognized by many workers who have experimented with FIA-ICP interfacing e.g., Alexander et al (1982); Browner and Boorn (1984b); Cox et al (1985); LaFreniere et al (1985); Lawrence et al (1984); McLeod et al (1984); McLeod et al (1985); and Tyson (1985).

The two directions of resolving this spray chamber dead volume problem have been firstly that of Lawrence et al (1984) and LaFreniere et al (1985) of removing the spray chamber and using DIN to directly introduce the sample aerosol into the plasma. This approach is unfortunately subject to volatilization type interferences. The second approach typified by the work of Ito et al (1982) is to reduce the volume of the chamber without removing the spray chamber. This latter approach has also been used by a number of the workers who have experimented with interfacing HPLC with ICP, as discussed in section 2.4 (Hausler and Taylor, 1981a; Hausler and Taylor, 1981b; Ibrahim, Nisamaneepong and Caruso, 1985; Ibrahim, Nisamaneepong, Haas and Caruso, 1985; Jinno et al, 1985; Nisamaneepong et al, 1985).

It is not only necessary to reduce the volume of the spray chamber to improve wash-out times, but the dead volume in the nebulizer may also be reduced in the case of the dead-space where the sample uptake tube is attached to a conventional Meinhard concentric glass nebulizer. Ramsey et al (1983) reduced the Meinhard nebulizer clean-out time from 17 s to approximately 9 s by cementing a platinum-iridium capillary inside the nebulizer uptake tube. In FIA-ICP interfacing, however, the central problem is the long wash-out time of the spray chamber (Tyson, 1985). By comparison with the spray chamber residence time, the transit time of the sample through the plasma itself is negligible (Duursma et al, 1981).

2.6 Sample nebulization

The goal of sample nebulization, and subsequent passage of the aerosol through a spray chamber is, "...the reproducible transfer of a representative portion of sample material to the atomizer cell, with high efficiency and with no adverse interference effects." (Browner and Boorn, 1984a). Of the quantity of sample aspirated, only a small portion actually reaches the atomizer cell. There are two ways in which this fraction has been expressed *viz*.,

(a) As the nebulization efficiency η, defined as (Gustavsson, 1984a):

$$\eta = \frac{V_e}{V_u} \times 100\% \qquad \ldots \quad (16)$$

Where V_e = volume of liquid, in aerosol form, which leaves the spray chamber for the atomizer,
and V_u = volume of liquid aspirated by the nebulizer in the same time period.

(b) As the transport efficiency ε_n, defined as (Smith and Browner, 1982):

$$\varepsilon_n = \frac{Q_e}{Q_u} \times 100\% \qquad \ldots \quad (17)$$

Where Q_e = mass of analyte entering the flame or plasma,
and Q_u = mass of analyte aspirated by the nebulizer during the same time period.

The symbol ε_n has been used in the literature for the nebulization efficiency (Armstrong Lowe, 1975; Browner *et al*, 1982). If no aerosol ionic redistribution (A.I.R.) and/or evaporation occurs, i.e., that the composition of

the aerosol droplets leaving the spray chamber is the same as the bulk composition of the liquid aspirated, then $n = \varepsilon_n$ (Gustavsson, 1984c).

Typical values for the nebulization efficiency for pneumatic nebulization using cross-flow or concentric nebulizers are 1 to 3% in the case of ICP emission spectrometry and 5 to 7% in the case of the AAS method (Browner and Boorn, 1984a; Gustavsson, 1984c; Gustavsson, 1986; Smith and Browner, 1982). As such a small portion of the aspirated sample reaches the source in the case of the ICP technique, accurate measurement of nebulization or transport efficiency is difficult. Direct measurement of the quantity of aerosol leaving the spray chamber, using a cascade impactor, was employed by Smith and Browner (1982), who contended that indirect measuring techniques through measurement of the volume passing to waste give inaccurate values. Gustavsson (1984c) on the other hand maintained that the indirect method was capable of as good accuracy as the direct method, where uptake and waste volumes were determined by weighing rather than volumetrically. Indirect measurement of transport efficiency nevertheless tends to give ε_n values which are 50 to 130% higher than those measured directly, due probably largely to droplet evaporation, although collision between droplets may also play a role (Gustavsson, 1986).

Pneumatic nebulizers are normally employed to nebulize the sample in ICP emission spectrometry (Michaud-Poussel and Mermet, 1986). Typically, these are either of the cross-flow type, with the sample liquid and nebulizing gas capillaries placed at an angle to one another (Fujishiro *et al*, 1984; Kniseley *et al*, 1974; Kranz, 1972; Valente and Schrenk, 1970) or of the concentric type, with the sample liquid uptake capillary co-axial with the nebulizing gas capillary (Baginski and Meinhard, 1984). Fujishiro *et al* (1984) reported that while the cross-flow design provides

higher nebulization efficiency than the concentric nebulizer, the former was plagued with difficulties of capillary alignment and inadequate long-term stability. Use of a fixed cross-flow design circumvents the latter difficulty (Maessen et al, 1984; Novak et al, 1980). Nebulization efficiency is influenced by the spray chamber employed. Maessen et al (1984) found higher nebulization efficiency for the concentric nebulizers than for a cross-flow nebulizer when using a 113 mℓ capacity spray chamber.

Other nebulizer designs which have been described for use with ICP emission spectrometry are: (i) The Babington type, where the sample flows through a groove across the nebulizing gas capillary (Wolcott and Sobel, 1982), or over a hemisphere with an orifice (Gabarino and Taylor, 1980). (ii) The ultrasonic type, which has a nebulization efficiency around 11%, tending to result in plasma instability unless the aerosol is desolvated (Olson et al, 1977). (iii) The glass frit type, for which a nebulization efficiency as high as 94% has been reported, but which unfortunately has extremely long equilibration times of as much as 4 min, as well as a $t_{0,1\%}$ Cu value of 10 min, i.e., an unacceptably long memory (Layman and Lichte, 1982; Nisamaneepong et al, 1985). Where a glass frit nebulizer is used with AAS, the memory effect is considerably less pronounced than with ICP spectrometry, due to the greater gas flow rates through an AAS spray chamber (Niemczyk and Espinosa, 1987). (iv) The Hildebrand platinum grid-type nebulizer, where the sample flows over the grid past the nebulizing gas stream, with nebulization occurring as a result of shearing from the wetted grid. The Hildebrand grid nebulizer is useful for the introduction of organic solvents into the ICP source (Brotherton et al, 1987). (v) The microconcentric type, which is essentially a modified concentric pneumatic nebulizer with an additional capillary carrying an auxiliary gas placed around the nebulizer

(LaFreniere et al, 1985; Lawrence et al, 1984). (vi) The thermospray type, where the liquid uptake capillary is heated electrically, either indirectly (Blakley and Vestal, 1983) or directly (Vestal and Fergusson, 1985), so as to produce a vaporized sample at the tip of the capillary tube. Elgersma et al (1986) experimented with a thermospray nebulizer, with a fused silica capillary, in conjunction with a Scott-type spray chamber for ICP emission spectrometric detection, and found comparable detection limits to conventional pneumatic nebulization. A major drawback was, however, the contamination of sample with boron, iron and other metals from the heated capillary tubing, as well as clogging at temperatures above 205°C. Thermospray type nebulizers are also prone to matrix effects e.g., Vermeiren et al (1987) observed a mean analyte signal depression of 13% in the presence of 1 $g.\ell^{-1}$ sodium chloride, when using a directly heated thermospray nebulizer and desolvation assembly for sample introduction to an ICP source. An interchangeable insert probe was designed by Unger et al (1987) to replace clogged thermospray probes used in liquid chromatography/mass spectrometry interfacing.

Michaud-Poussel and Mermet (1986), who compared the characteristics of nebulizers used in ICP emission spectrometry, found that the Meinhard-concentric and cross-flow type nebulizers had similar analytical performance. Frit nebulizers showed unacceptable memory, with $t_{1\%}$ wash-out values as much as 25 min. The ultrasonic nebulizer gave the best detection limits, but was most difficult to operate on a routine basis.

An advantage of the concentric pneumatic nebulizer emphasized by Gustavsson (1984a) was its so-called self-stabilizing property i.e., the relative insensitivity of transport efficiency to slight temperature change. This applies only, however, for free sample uptake, where the

tendency to decreased efficiency of nebulization at higher temperatures is counteracted by decreased liquid viscosity with increase in sample uptake rate.

An important empirical equation giving the mean droplet diameter produced by a concentric pneumatic nebulizer is the Nukiyama and Tanasawa (N & T) equation (Gustavsson, 1983). This equation was formulated by Nukiyama and Tanasawa while studying carburettor theory. The measure chosen to express mean droplet diameter d_o, was that for the volume to area relationship, the equation being;

$$d_o = \frac{585 \cdot \sqrt{\sigma}}{V \cdot \sqrt{\rho}} + 597 \cdot \left(\frac{\mu}{\sqrt{\sigma \cdot \rho}} \right)^{0.45} \cdot \left(\frac{10^3 \cdot Q_\ell}{Q_g} \right)^{1.5} \quad \ldots \quad (18)$$

where d_o = mean droplet diameter, for the volume to area ratio, μm,

σ = surface tension of the liquid, $dyn.cm^{-1}$,

V = velocity difference, $m.s^{-1}$ between the nebulizing gas velocity V_g and the liquid gas velocity V_ℓ,

ρ = density of the liquid, $g.cm^{-3}$,

μ = coefficient of viscosity of the liquid, $dyn.s.cm^{-2}$,

Q_ℓ = volume flow of liquid,

and Q_g = volume flow of the gas.

While the N & T equation is strictly only valid where the nebulizing gas is air, only a negligible error occurs for argon (Gustavsson, 1983). Using a value of $1{,}002 \times 10^{-2}$ poise ($dyn.s.cm^{-2}$) for the viscosity of water at 20°C; together with a value of 72,75 $dyn.cm^{-1}$ for the surface tension of water at 20°C, and a value for the density of water at 20°C of 0,9982 $g.cm^{-3}$ (Weast, 1980), and substituting in equation 18 we get:

$$d_o = \frac{4994}{V} + 28{,}68 \left(\frac{10^3 . Q_\ell}{Q_g} \right)^{1{,}5} \quad \ldots \quad (19)$$

This is the form of the N & T equation given by Skogerboe and Freeland (1985b), except that they give the numerical proportionality constants as 5000 and 28,6 respectively for the 1st and 2nd terms of equation 19 and not 4994 and 28,68 as above. Skogerboe and Freeland (1985b) experimentally evaluated the applicability of the N & T equation for estimating droplet diameter in the case of a cross-flow nebulizer using a cascade impactor, and found that the equation is an adequate model. This is a not unexpected finding in view of the similarity of analytical characteristics of the cross-flow and concentric pneumatic nebulizers (Michaud-Poussel and Mermet, 1986).

As an example of the application of equation 19, if we take typical ICP emission spectrometric values for Q_ℓ of 1,3 $m\ell.min^{-1}$ and for Q_g of 1360 $m\ell.min^{-1}$ at atmospheric pressure, and taking the radius of the nebulizing gas and sample capillaries as 0,5 mm, a value for the velocity difference V of $1{,}72 \times 10^3 m.s^{-1}$ is obtained. By substitution in equation 19 the following results*:

---

* The N & T equation is not dimensionally balanced. In the absence of any other adequate theoretical model to predict mean droplet size diameters for pneumatic nebulization, it is necessary to employ the N & T equation.

$$d_o = 2,9 + 26,8\ \mu m \qquad \ldots \quad (20)$$

i.e., $d_o = 29,7\ \mu m$

Note that the 2nd term of the N & T equation is of greater importance than the 1st term. If the 2nd term in equation 19 is qualitatively inspected, it can be seen that an increase in the sample uptake rate increases the mean droplet diameter; while an increase in the nebulizing gas flow decreases the mean droplet diameter. As the spray chamber has a characteristic cutoff diameter d_c, with $d_c \ll d_o$ for ICP spray chambers, only a small fraction of the nebulized aerosol reaches the plasma. Typical values for d_c are 3 to 5 μm for the ICP technique (Gustavsson, 1983). The practical implication of the N & T equation in effects of flow rate changes on nebulization efficiency, is that the efficiency increases at lower sample uptake rates; as a decrease in d_o shifts the droplet size distribution to smaller values, with a greater fraction of the distribution then being within the cutoff diameter limit. Novak and Browner (1980) have demonstrated this relationship experimentally. These two workers have also expressed the N & T equation in quasi-S.I. units as:

$$d_o = \frac{1850.\sqrt{\sigma}}{V} + 4661.\left(\frac{\eta}{\sqrt{\sigma.\rho}}\right)^{0.45}.\left(\frac{10^3.Q_\ell}{Q_g}\right)^{1.5} \qquad \ldots \quad (21)$$

Where d_o = droplet diameter μm, Sauter median,

σ = liquid surface tension, $N.m^{-2}$,

V = velocity difference, $m.s^{-1}$ between the nebulizing gas velocity and liquid velocity,

η = liquid viscosity, $N.s.m^{-2}$,

ρ = liquid density, $kg.m^{-3}$,

Q_ℓ = volume flow rate of liquid, $m\ell.s^{-1}$,

and Q_g = volume flow rate of gas, $m\ell.s^{-1}$.

Novak and Browner (1980) have omitted the square root of the liquid density from the denominator of the 1st term, i.e., assuming the aqueous solution aspirated to have unit density. One wonders why they do not also omit ρ from the 2nd term by way of uniformity!

In summary, the mean droplet size produced by a concentric or cross-flow pneumatic nebulizer is given by the Nukiyama and Tanasawa equation (18). This is the primary droplet size i.e., at the point of nebulization. Only a small fraction of the aerosol droplets produced are carried into the plasma, the rest passing to waste. The efficiency of the nebulizer-spray chamber combination, expressed as nebulization efficiency η where the volumes of sample atomized and aspirated are measured; or as transport efficiency ε_n where the mass of analyte is used, serves as an indicator of the efficacy of the nebulization process. Sample droplets larger than the cutoff diameter of the spray chamber pass to waste. In the next section the effect of the spray chamber on the aerosol produced by the nebulizer will be addressed.

2.7 The spray chamber and conditioning of the aerosol

"The fundamental limitation of all pneumatic nebulizers of conventional design is that they produce aerosols with a wide drop size range" (Browner and Boorn, 1984b). The introduction of large droplets into the flame, in the case of the AAS technique, or into the plasma, in the case of the ICP technique is analytically undesirable, because of incomplete atomization and the associated interference effects. A spray chamber must be used to condition the aerosol and remove large droplets (Cresser and Browner, 1980; Farino and Browner, 1984; Kranz, 1972).

The processes involving production and conditioning of the aerosol are classified into: (i) A primary aerosol generation step, resulting in a polydisperse droplet distribution, (ii) a secondary process of impaction, with the aerosol assuming a secondary drop size distribution, and (iii) a tertiary stage, resulting in the tertiary or preatomization drop size distribution (Browner et al, 1982). These stages are not rigidly separated from one another, and the secondary impaction process may be less evident in spray chambers lacking an impact bead. Impaction is also not limited to the secondary stage, but also occurs in the tertiary stage. The tertiary stage involves in addition turbulent and centrifugal processes, gravitational settling and evaporation (Browner and Boorn, 1984a; Browner et al, 1982; Skogerboe and Freeland, 1985b).

Impact beads, typically used in AAS spray chambers firstly remove large droplets from the aerosol stream by impaction, and secondly cause further fragmentation of droplets, thus shifting the droplet distribution to smaller values (Cresser and Browner, 1980). The Scott-type spray chamber often used in ICP spectrometry has no impact bead (Scott et al, 1974).

The gravitational settling of particles is an important process in the removal of large droplets from the aerosol. If buoyancy is ignored, which is a reasonable approach as the density of aqueous aerosol particles is much greater than the density of the nebulizing argon gas, then the terminal settling velocity is given by (Butcher and Charlson, 1972);

$$V_s = \frac{2r^2 \rho g}{9\eta} \qquad \ldots \quad (22)$$

where r = radius of aerosol droplet,
ρ = density of aerosol droplet,
g = gravitational acceleration,
and η = viscosity of the gas.

The terminal velocity is reached in a time interval much shorter than the residence time in the spray chamber of the aerosol for the large droplets which must be removed e.g., a 50 μm diameter droplet reaches terminal velocity in 8 ms (Browner et al, 1982). Gravitational settling is only capable of removing droplets whose radius is greater than the mean free path length in the gas. Droplets with a radius smaller than the mean free path length are kept in suspension by Brownian motion. The mean free path is around 0,07 μm for air at standard temperature and pressure@ (Butcher and Charlson, 1972). The mean free path for argon at 750 mm Hg pressure and at 20°C is 0,099 μm (Weast, 1980). The importance of the gravitational settling process in removing large droplets can be seen by substituting values for the variables in equation 22: Take, for example, a droplet of 10 μm radius.

@ Temperature of 0°C (273K) and pressure of 760 mm mercury (Sisler et al, 1949).

Using values for ρ for water of 1 $g.cm^{-3}$; 980 $cm.s^{-2}$ for g; and $221{,}7 \times 10^{-6}$ $g.s^{-1}.cm^{-1}$ for η of argon (Weast, 1980), a terminal velocity V_s of 9,8 $mm.s^{-1}$ is obtained.

The residence time for a Scott chamber of the order of 10 s (Scott et al, 1974) allows more than adequate time for a 10 µm radius droplet to traverse the diameter of the spray chamber of 45 mm. The cutoff diameter d_c, for gravitational settling may be obtained by equating the product of the terminal settling velocity and the residence time of aerosol in the chamber to the radius of the spray chamber (Browner et al, 1982);

$$R_c = V_s \cdot t_r \qquad \ldots \quad (23)$$

where R_c = radius of spray chamber for 50 % removal of droplets with the diameter d_c (cutoff diameter),

V_s = terminal settling velocity of droplets of diameter d_c,

and t_r = residence time of aerosol in the spray chamber.

Of the other large droplet removal processes in the spray chamber, impaction against the far wall of the chamber, as well as turbulent losses contribute to the production of the tertiary aerosol (Browner et al, 1982; Gustavsson, 1984b; Skogerboe and Freeland, 1985a; Skogerboe and Freeland, 1985b). Gustavsson (1984b) believes that inertial impaction is probably the main large droplet removal process in ICP spray chambers. One of the problems of describing aerosol processes in a nebulizer/spray chamber combination is that one is faced with a transition from turbulent to laminar flow. The gas flow at the

nebulizer is highly turbulent with a Reynolds number[@] around 15000, while for the spray chamber *per se* the Reynolds number is around 83, i.e., laminar flow, for the typical ICP chamber (Browner *et al*, 1982). Skogerboe and Freeland (1985a) have shown that the liquid flow at the nebulizer capillary orifice is also characterized by turbulence. Browner *et al* (1982) give the following formula to describe the fractional penetration P, of particles of diameter d, through a tube of fixed diameter as a consequence of turbulent flow losses:

$$P = e^{(-kd^4 L/Q)} \qquad \ldots \quad (24)$$

Where P = the fractional penetration of particles of diameter d through the tube length L,

d = diameter of particles of aerosol,

Q = volumetric flow rate,

and k = constant, whose value is determined by the degree of turbulence.

@ The Reynolds number R_e is given by $R_e = 2rU/\nu$, where r is the radius of the tube through which a fluid is flowing, U is the mean speed of flow, and ν is kinematic viscosity (Taylor, 1954). As the volume flow rate Q is given by $Q = \pi r^2 U$, an alternative equation for the Reynolds number is $R_e = 2Q/\pi r\nu$. For water at 20°C, with a kinematic viscosity of 0,01 $cm^2.s^{-1}$ (Weast, 1980), this reduces to 63,7Q/r or 127Q/d, which is the form quoted by Ruzicka *et al* (1977). For argon, with a kinematic viscosity of 0,13 $cm^2.s^{-1}$ at 20°C (Weast, 1980), R_e is given by 10Q/d; volume flow rate Q being expressed in $cm^3.s^{-1}$ and tube diameter d in cm. Turbulent flow occurs with $R_e \geq 2000$, and laminar flow when $R_e < 1000$. For $1000 \leq R_e < 2000$ a transition occurs between laminar and turbulent flow, termed incipient turbulence (Ruzicka *et al*, 1977).

The impaction of aerosol particles against a solid surface may be described by the dimensionless Stokes number S_{tk}, which is a measure of a particle's ability to follow the gas stream around an object (Browner et al, 1982). The Stokes number is approximately given by (Butcher and Charlson, 1972);

$$S_{tk} \simeq \frac{\zeta}{\ell} \qquad \ldots (25)$$

where ζ = the stop distance of the particle,

and ℓ = the radius of curvature of the flow streamlines.

The stop distance ζ, is given by;

$$\zeta = V_0 . Bm \qquad \ldots (26)$$

where V_0 = initial velocity of the aerosol before meeting the object,

B = the particle mobility,

and m = the mass of the aerosol particles.

The particle mobility B, is given by (Butcher and Charlson, 1972);

$$B = \frac{1}{6 \pi \eta r} \qquad \ldots (27)$$

where η = viscosity of the gas,

and r = radius of the aerosol droplet.

Combining equations 25 and 27, and expressing mass as the product of volume and density, the following expression for the Stokes number is readily derived;

$$S_{tk} \simeq \frac{2 V_o \rho r^2}{9 \ell \eta} \qquad \ldots \quad (28)$$

where V_o = initial velocity,

ρ = density of aerosol droplet,

r = radius of aerosol droplet,

ℓ = radius of curvature of the stream flowlines,

and η = viscosity of the gas.

For small particles, whose radius approaches the mean free path in the gas, the mobility B is greater than that given by equation 27, being given by;

$$B = \frac{1 + A.K_n}{6 \pi \eta r} \qquad \ldots \quad (29)$$

where K_n is the ratio of the mean free path to the particle radius, and is called the Knudsen number; and A is a proportionality constant, called the Cunningham slip correction, and has a value from 0,82 to 0,9 for aqueous aerosol droplets (Butcher and Charlson, 1972).

Evaporation of aerosol droplets decreases the diameter of the droplets, thus shifting the size distribution to smaller values. A greater number of droplets then fall within the cutoff diameter of the given spray chamber, and the transport efficiency is increased (Skogerboe and Olson, 1978). The evaporation process may be accelerated through the application of external heat, the aerosol then being desolvated. Marinov (1984a, 1984b, 1984c) for example, used desolvation to dry the aerosol from a cross-flow nebulizer when analyzing blood serum by emission spectrometry. A disadvantage of Marinov's approach was the large dead volume, in excess of 1ℓ, of the desolvation and condenser chamber. Gustavsson (1987), overcame the problem of the long retention time associated with a desolvation chamber, by introducing an auxiliary gas flow. The desolvated aerosol was then subsampled, using a venturi jet separator, based on the Bernoulli principle, for reducing the gas flow rate to a level suitable for introduction into an ICP source. The decrease in particle diameter on desolvation is given by (Browner and Boorn, 1984a);

$$d_x = d_o \cdot \left(\frac{C.10^6}{\rho} \right)^{1/3} \qquad \ldots \quad (30)$$

where d_x = diameter of the dry aerosol particle,

d_o = diameter of aerosol droplet before desolvation,

C = salt concentration in aerosol droplet prior to desolvation, $\mu g.m\ell^{-1}$,

and ρ = density of the dry aerosol particle, $g.m\ell^{-1}$.

Centrifugal losses also play a role in the removal of large droplets in a spray chamber (Browner *et al*, 1982; Gustavsson, 1984b; Skogerboe and Freeland, 1985b).

Intentional use of cyclone principles in applying centrifugal droplet removal to aerosols in AAS or ICP spray chambers is a promising concept for designing new types of spray chambers. Gustavsson (1984b) states that the paucity of experimentation along this line probably arises from the mediocre selectivity of the droplet size separation process in coventional dust separators based on cyclone principles, where large droplets may bypass the cyclone and reach the aerosol outlet tube. Cyclone principles will be addressed in Section 2.8.

While the typical Scott type ICP spray chamber, with a volume in excess of 100 mℓ is an effective remover of large droplets, with a median tertiary droplet size less than 5 μm (Gustavsson, 1983; Routh, 1986), the long residence time of around 10 s for the original 220 mℓ Scott design (Scott et al, 1974), or 6 s for a 140 mℓ modified Scott design at 1,4 $ℓ.min^{-1}$ nebulizer gas flow rate (Schutyser and Jansens, 1979) is a problem in the use of FIA with the ICP technique. In the AAS technique, with its typically at least ten-fold greater gas flow rates through the spray chamber, this problem does not arise (Browner and Boorn, 1984b; Malloy et al, 1980).

Recently there has been a trend towards the use of reduced volume spray-chambers in ICP emission spectrometry in order to reduce the memory effect and shorten equilibration times (Dale and Buchanan, 1986; Luffer and Salin, 1986; Routh, 1986; Vieira et al, 1986; Brotherton et al, 1987). Applied Research Laboratories (ARL) has for instance produced a 25 mℓ spray chamber, of a baffled Teflon design, which provided a median droplet diameter for the tertiary aerosol of less than 5 μm (Routh, 1986). A 50 mℓ conical spray chamber manufactured by ARL has an equilibration time, to reach 95% of the steady state signal, of 9 s at a gas flow rate of $1ℓ.min^{-1}$ (Dale and Buchanan, 1986). A cooled,

conical mini-Pyrex chamber of approximately 18mℓ capacity with a bead spoiler, for reducing wash-out time when introducing organic solvents into an ICP source, was described by Brotherton et al (1987). A novel approach to reducing spray chamber volume was described by Luffer and Salin (1986). They used a variable volume cylindrical spray chamber, consisting of a glass cylinder with an inner piston to adjust spray chamber volume. A glass frit was used at the piston face to drain away the liquid waste. Volumes as small as 8 mℓ were investigated.

Luffer and Salin (1986) reported poor precision for the small volume spray chamber and identified the condensation of droplets in the aerosol outlet tube from the chamber as a major source of noise. The long-term precision of the reduced volume spray chamber, in particular, was inferior to that of a conventional Scott chamber. In reducing the volume of the spray chamber, ensuring efficient drainage of the excess liquid to waste is essential (Routh, 1986). Drainage problems may be severe in spray chambers of only a few millilitres capacity (Ibrahim, Nisamaneepong and Caruso, 1985; Jinno et al, 1985). Pressure changes consequent to irregular drainage may contribute to deterioration in detection limits (Zhuang and Barnes, 1985). Schutyser and Jansens (1979) solved the problem of droplet formation at the tip of the inner tube in a Scott-type spray chamber by placing a thin glass rod across the gap between the inner and outer tubes to provide a path for the liquid to flow to waste. A similar approach was used to avoid drop collection at the nebulizer tip. Vieira et al (1986) found that by modifying the teflon connector and inserting the nebulizer deeper into the spray chamber, that the problem of droplet collection on the nebulizer tip was solved. These workers also described a ca., 60 mℓ capacity cyclone spray chamber, which had slightly better precision than a conventional Scott chamber.

In summary, the spray chamber serves the important function of removing large droplets, which would give rise to volatilization type interferences, and the tertiary median droplet diameter of the aerosol as it leaves an ICP spray chamber is around 3 to 5 μm (Routh, 1986). As surfactants have little effect on the droplet distribution for droplet diameters less than 2,5 μm, the typical ICP transport system is relatively insensitive to changes in sensitivity caused by surfactants (Farino and Browner, 1984). While ions such as sodium do cause changes in droplet distribution within the cutoff diameter of spray chambers, the transport efficiency is little affected (Skogerboe and Freeland, 1985c).

A serious disadvantage of ICP spray chambers is the large dead volume, which in association with the relatively low nebulizing gas flow rate in ICP emission spectrometry of around $1\ell.min^{-1}$, causes long equilibration and wash-out times, often in excess of 10 s (Dale and Buchanan, 1986). To successfully interface FIA to ICP, to achieve RFA (rapid flow analysis), the volume of the spray chamber must be reduced. This, however, should be achieved without loss of the large droplet exclusion characteristics of the spray chamber. A promising manner of reaching this goal is by using cyclone principles to effect centrifugal removal of droplets (Gustavsson, 1984b; Vieira et al, 1986), and is addressed in the following section.

2.8 Centrifugal processes and cyclone theory

The incorporation of cyclone processes, to effect centrifugal removal of large droplets, is an idea which merits inclusion in spray chamber design (Gustavsson, 1984b). Centrifugal processes become important where the spray chamber design is such that a centrifugal motion is imparted to the aerosol (Browner et al, 1982).

A difficulty in the incorporation of centrifugal principles in spray chamber design is the uncertainty existing in the theoretical treatment of the centrifugal aerosol processes. Davies (1952a) in discussing the processes occurring in cyclone dust separators, assumes that the tangential velocity V is inversely proportional to the radial distance R i.e., VR = constant. Fitton (1952) and Fuks (1955) on the other hand, make a more general assumption viz.,

$$VR^n = k \qquad \ldots \quad (31)$$

where V = tangential velocity,
R = radial distance from axis of cyclone,
n = number between +0,5 and +1,0,
and k = constant.

In the approach used by Davies (1952a), the exponent n of R in equation 31 is 1,0. In a cyclone dust separator, the dust-laden gas enters the cyclone chamber, which is cylindrical in the upper portion with a tapered cone at the lower end, at a tangent. The gas assumes a spiral motion, with the dust particles collecting at the base, and the dust-free gas exiting along the axis of the chamber (Fig. 2-1). The maximum time interval δt, for a particle to traverse the space between R_1, the radius of the inner tube, and R_2 the radius of the outer tube, is given by (Davies, 1952a);

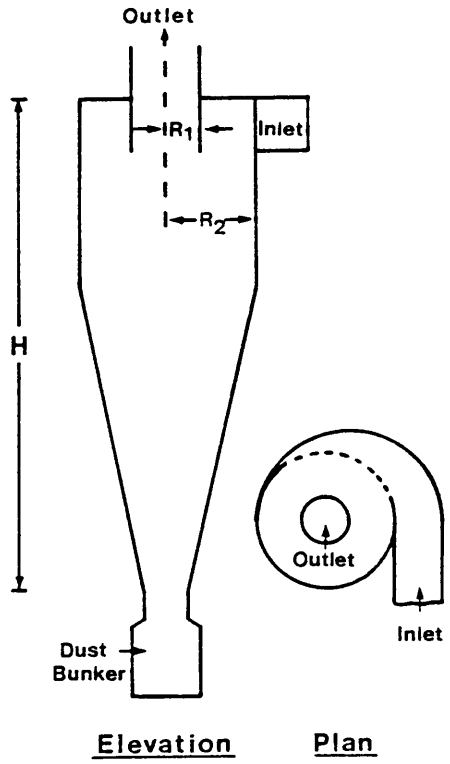

Fig. 2-1: Cyclone dust separator (Davies, 1952a), showing the close proximity of the inlet and outlet orifices.

$$\delta t = \left(\frac{9\,\eta \,.\,(R_2^4 - R_1^4)}{8\,d_{min}^2 .(\rho - \sigma) V_o^2 R_2^2} \right) \qquad \ldots \quad (32)$$

where η = viscosity of the gas,

R_2 = radius of outer tube (body of cyclone),

R_1 = radius of inner tube (exit from cyclone),

d_{min} = minimum particle diameter trapped by the cyclone,

ρ = density of dust particle,

σ = density of the gas,

and V_o = tangential velocity of gas at inlet to the cyclone.

In deriving equation 32 Davies (1952a) assumes that the tangential component of particle velocity is equal to the gas velocity. By making the additional assumption that the time of descent of the gas to the base of the cyclone is also given by δt, and that $\delta t = H/V_o$, Davies (1952a) derived the following formula for d_{min};

$$d_{min} = \left(\frac{9\eta R_2}{8(\rho-\sigma) V_o H/R_2} \cdot \left(1 - \left(\frac{R_1}{R_2} \right)^4 \right) \right)^{1/2} \ldots (33)$$

where η, R_1, R_2, ρ, σ and V_o are as described for equation 32;

H = length of cyclone chamber (cyclindical portion plus cone),

and d_{min} the particle diameter above which the collection efficiency is 100%.

An inspection of equation 33 shows that to achieve small values of d_{min}, the outer radius R_2 should be small, the length of the cyclone H large, and the ratio of the inner tube radius R_1 to the outer tube radius R_2 close to unity.

Davies (1952a) points out that in practice R_1 cannot approach R_2 too closely, as interference then occurs with the gas flow.

Instead of assuming that $\delta t = H/V_0$, Bosanquet assumed $\delta t = \pi(R_1 + R_2)/V_0$, the numerator representing a type of mean circumference for the cyclone. Using Bosanquet's assumption equation 33 becomes (Davies, 1952b);

$$d_{min} = \left(\frac{9\eta R_2}{8(\rho-\sigma)\, V_o \cdot \pi(R_1 + R_2)/R_2} \cdot \left(1 - \left(\frac{R_1}{R_2} \right)^4 \right) \right)^{1/2} \quad \ldots \quad (34)$$

where the variables are as given for equations 32 and 33.

Fuks (1955) carried Bosanquet's approach further, pointing out that the effective periphery of the cyclone is given by $2\pi R$, where R lies somewhere between R_1 and R_2, and not necessarily being given by the mean $(R_1 + R_2)/2$ as Bosanquet had assumed.

For the special case of a cyclone with dimensions such that the inlet width W is equal to the distance between the outer and inner tubes, Fuks gives the following formula for the smallest diameter particles which fully precipitate in a cyclone (Fuks, 1955);

$$d_{min} = 6. \left(\frac{0.3\, \ln(R_2/R_1)\eta R_2}{\pi V_o \rho S} \right)^{1/2} \quad \ldots \quad (35)$$

where R_2 = radius of outer tube,

R_1 = radius of inner tube,

η = viscosity of gas,

V_0 = inlet velocity of gas,

ρ = particle density,

and s = number of spiral turns in cyclone, usually assumed to be between 1 and 3.

Further $W = R_2 - R_1$, where W is the width of the inlet tube.

Fuks (1955) further states that where the cyclone dimensions are such that $W \neq R_2 - R_1$, then V_0 should be multiplied by the ratio $W/(R_2 - R_1)$. Equation 35 then becomes:

$$d_{min} = 6. \left(\frac{0.3 \ln(R_2/R_1) \eta R_2}{\pi V_0 \rho s W/(R_2 - R_1)} \right)^{1/2} \quad .... \quad (36)$$

While equations 35 and 36 at first sight differ from 33 and 34, an examination of equation 36 will show that it leads to similar conclusions to those of Davies (1952a) as regards minimizing d_{min} i.e., that d_{min} tends to zero as the ratio R_2/R_1 approaches unity; and that the cyclone effectiveness increases as the cyclone diameter decreases. The approach of Fuks (1955) differs from the approach of Davies (1952a) in that Fuks considers inlet width W and the number of spiral turns s as important variables, whereas Davies considers cyclone length as important.

Despite the fact that equations 33 to 36 indicate efficient removal of particles when R_1/R_2 approached unity, in practice no decrease in d_{min} is observed when the ratio R_1/R_2 exceeds 0,5 (Davies, 1952b). Fuks (1955), makes a similar observation, noting that cyclone dust separators are usually designed such that the ratio R_1/R_2 is 0,5 to 0,75; and that the difference in radii equals the width of the inlet tube.

The achievement of spiral flow, to effect centrifugal removal of aerosol particles, may also be reached through tangential removal of the gas from a chamber instead of a tangential inlet. Fitton (1952) mentions the "Dunlab tube" type cyclone, with parallel walls, where a portion of the gas flow, carrying the separated particles to waste, is bled off tangentially.

Luffer and Salin (1986) in experimenting with small volume cyclindrical spray chambers, made the observation that when the concentric glass nebulizer was placed at a low angle with respect to the base of the chamber, that shorter wash-out times were observed. These workers attributed this to the probable production of a cyclone effect in the spray chamber. Nevertheless coarse droplets bypassed the chamber and deposited in the aerosol outlet tube from the chamber. The incomplete exclusion of large aerosol particles is also a problem with conventional cyclone separators such as shown in Fig. 2-1, where some of the aerosol may bypass the cyclone by moving directly from the inlet tube to the outlet tube. Ebdon and Cave (1982) experimented with a 500 mℓ volume cyclone type spray chamber for ICP spectrometric use. The chamber was similar in shape to an inverted Erlenmeyer flask, with the outlet to the plasma affixed to the wide base, and the pneumatic nebulizer inlet placed tangentially near the base. Problems were experienced with large droplets bypassing the cyclone, and droplet collection in the inner aerosol introduction tube of the ICP torch led to spitting, with poor precision. A similar 750 mℓ volume cyclone spray chamber was described by Thelin (1981).

Dale and Buchanan (1986) studied the behaviour of large volume cyclone-type spray chambers of 250 and 500 mℓ, constructed from Erlenmeyer flasks, for use in ICP emission spectrometry. Equilibration times to 95 % of the steady state signal were 19 s and 25 s respectively, while $t_{0,1\%}$

wash-out times were 52 s and 110 s respectively. The problem of part of the aerosol circumventing the cyclone was also experienced, this being considered the explanation for the long wash-out times. Vieira et al (1986) who described a 60 mℓ capacity cyclone spray chamber solved the circumvention problem by extending the axial aerosol exit tube deep into the cyclone, with the opening near the apex of the cone.

Mitchell et al (1987) described the use of a cyclone chamber 210 mm in length and 55 mm outside diameter, which was used to remove large dust particles; the cyclone chamber being interfaced between a Laser ablation cell and a DCP source, thereby reducing signal instability in the determination of copper in solid samples.

In summary, the use of cyclone principles in effecting centrifugal removal of droplets from the aerosol is a promising means of achieving small cutoff diameters with reduced volume spray chambers. A disadvantage of the conventional cyclone design, as used in dust separators (Fig. 2-1) or of the conical inverted Erlenmeyer flask design (Ebdon and Cave, 1982; Thelin, 1981), is that a portion of the aerosol bypasses the cyclone and moves directly from the inlet tube to the outlet tube of the chamber. This problem needs consideration in designing a spray chamber, for use in ICP emission spectrometry, which makes use of centrifugal droplet removal processes. Cyclonic movement of the aerosol in a spray chamber may be induced either through tangential introduction of gas to the chamber, or through tangential removal of gas from the chamber.

2.9 Present status of FIA-ICP interfacing and conclusions

As indicated by Greenfield (1981) the marriage of the FIA and ICP techniques has the potential of increasing the sampling rate, while at the same time decreasing the volume required for analysis, as well as increasing the tolerance of ICP pneumatic nebulizers towards high salt concentrations. The successful interfacing of FIA to the AAS method, following the pioneering work of Wolf and Stewart (1979), Yoza et al (1979) and Zagatto et al (1979), prompted a number of other workers to apply the FIA-AAS combination (Basson and Van Staden, 1980; Rocks et al 1982a and 1982b; Tyson, 1983) for increasing the sampling rate in AAS determinations. The interfacing of FIA to ICP, to effect rapid sample analysis was not so readily achieved and a number of workers who experimented with the possibility recognized the dead volume of the typical ICP spray chamber as the underlying cause of the poor sensitivity and broad peaks (Alexander et al, 1982; Cox et al, 1985; LaFreniere et al, 1985; Lawrence et al, 1984; McLeod et al, 1984; McLeod, et al, 1985). The reason for the existence of this problem is that the typical ICP spray chamber has a residence time of as much as 10 s. This is because the aerosol (inner) gas flow is an order of magnitude smaller than with AAS where the residence time is less than one second (Browner and Boorn, 1984b; Malloy et al, 1980; Scott et al, 1974).

The approach of Jinno et al (1985) of removing the spray chamber altogether was not successful, as drainage problems occurred, together with water overloading of the ICP. LaFreniere et al (1985) and Lawrence et al (1984) also took the approach of removing the spray chamber, but redesigned the nebulizer to decrease the water loading to the torch. Yet this approach too, had the problem of volatilization interferences and a decreased residence time of the analyte

in the axial channel of the plasma. The use of direct injection nebulization, however, holds great promise in the interfacing of HPLC to ICP for the introduction of organic solvents into the ICP in the analysis of oil-based materials (LaFreniere et al, 1987).

A hint as to the most promising direction to take in reducing spray chamber residence time, so as to make the use of FIA sample introduction feasible, was provided by the work of Ito et al (1982) who used a 35 mℓ miniaturized spray chamber and obtained good sensitivity using 40 μℓ samples.

An ICP pneumatic nebulizer typically produces a mean droplet size of around 30 μm, as calculated from the Nukiyama and Tanasawa equation (Gustavsson, 1983). Only small droplets pass through the spray chamber, characteristic cutoff diameters being around 3 to 5 μm (Routh, 1986). The reduction in spray chamber volume should not be done at the expense of losing the large droplet exclusion characteristics of a spray chamber, as this will lead to volatilization type interferences, as well as poor precision and sensitivity to matrix effects.

The application of gravitational settling processes (Browner et al, 1982; Scott et al 1974) led to the relatively large volume ICP spray chambers in the first instance, and reduction of chamber size will allow less time for gravitational settling. Gustavsson (1984b) stated that a promising manner of achieving effective large droplet removal from aerosols in small volume spray chambers was the use of centrifugal principles, as decreasing the radius of the spray chamber in the case of spiral motion, tends to increase the effectiveness of the centrifugal removal of large droplets (Davies 1952a and 1952b; Fuks, 1955).

ICP spray chamber design to date using centrifugal droplet removal processes has been somewhat disappointing, due to the basing of design on the so-called cyclone dust separators (Fig. 2-1). Cyclone separators suffer from the problem that the spray chamber inlet and outlet are physically close to one another, with no solid obstruction preventing part of the primary aerosol from passing directly to the outlet and thus not being subjected to the centrifugal droplet removal process. This bypass problem leads to poor precision and the physical deposition of large aerosol droplets in the uptake tube to the torch (Ebdon and Cave, 1982; Luffer and Salin, 1986). To successfully apply centrifugal principles in ICP spray chamber design would necessitate that the aerosol bypass problem be solved by, for example, extending the axial exit tube towards the apex of the cone (Vieira et al, 1986).

Another factor militating against the reduction in spray chamber volume is that of inefficient drainage in small volume spray chambers (Routh, 1986). It is only where very small chambers of only a few millilitres capacity are used that the drainage problem becomes severe, however (Ibrahim, Nisamaneepong and Caruso, 1985; Jinno et al, 1985). With spray chamber volumes of around 25 mℓ adequate drainage is achievable (Routh, 1986). Reduction of spray chamber volume from the approximately 220 mℓ capacity of the Scott chamber (Scott et al, 1974), to one-tenth of this capacity would be quite adequate for reducing aerosol residence time sufficiently to make RFA by interfacing FIA to ICP possible. There is at present a trend towards smaller spray chambers for ICP emission spectrometry. For instance, the recent commercial availability of ICP spray chambers of 25 mℓ capacity (Routh, 1986). Such miniaturized chambers remain to be evaluated for analytical characteristics, however. Zhuang and Barnes (1985) pointed out than an important aspect of the drainage of excess

liquid from the spray chamber is that it should be uniform, as pressure changes consequent to irregular drainage will detrimentally affect precision. The need to reduce spray chamber volume to reduce peak broadening was clearly recognized by those workers who have used ICP as a detector for HPLC (Hausler and Taylor, 1981a; Ibrahim, Nisamaneepong, Haas and Caruso, 1985; Jinno et al, 1985).

Much effort was spent by the workers who experimented with FIA-AAS interfacing in the development of special calibration methods such as standard additions, single point calibration with a mixing chamber, and peak width calibration (Tyson 1984b; Tyson and Appleton, 1985; Tyson et al, 1983a). These procedures are of somewhat less interest in ICP emission spectrometry due to the large linear dynamic range of the ICP technique and its relative freedom from matrix type interferences (Israel and Barnes, 1984). The procedure described by Tyson et al (1986) of using FIA to investigate potential interferences by injecting solutions of suspected interferants into a carrier stream of the analyte is, however, of applicability to the ICP method.

In conclusion, the potential marriage of the FIA and ICP techniques (Greenfield, 1981) is definitely feasible as the work, for example, of Alexander et al (1982), Ito et al (1982) and Faske et al (1985) has shown. The achievement of high analytical rates i.e., rapid flow analysis, will however, require a reduction of spray chamber volume in order to reduce peak broadening within the chamber. This reduction should be effected without jeopardizing the large droplet removal capability of the spray chamber. A promising manner of achieving this is that of using cyclone principles (Gustavsson, 1984b), such as used in dust separators (Davies 1952a and 1952b; Fuks, 1955). The problem of part of the aerosol bypassing the cyclone as

experienced by other researchers (Ebdon and Cave, 1982, Luffer and Salin, 1986) should, however, be avoided. The reduced volume spray chamber should have adequate drainage, and should not give rise to volatilization type interferences through inadequate removal of droplets larger than 10 μm.

CHAPTER 3: SPRAY CHAMBER DESIGNS

3.1 Introduction

This chapter provides a description of the reduced volume spray chambers which were constructed for use on an Applied Research Laboratories (ARL) 34000 ICP spectrometer*. Two basic design approaches were tried i.e., firstly the double-barrel cylindrical type chamber, using the flow reversal principle of the Scott design (Scott et al, 1974); and secondly, the conical type chamber, based on the Davies design (Davies, 1952a). The principle of centrifugal removal of aerosol droplets was also incorporated into the double-barrel Scott-like chambers through the introduction of a modification in the manner of attachment of the aerosol outlet tube. In a number of the reduced volume spray chambers constructed the aerosol tube was attached tangentially to the body of the chamber rather than at right angles as in the conventional Scott design (Scott et al, 1974). The flow-reversal principle, as well as centrifugal aerosol motion was thereby incorporated into a number of the designs, the aim being to ensure adequate large droplet removal in the small volume spray chambers.

In addition to the constructed small volume spray chambers, a modified concentric glass nebulizer was also constructed for use with these chambers, as difficulty was experienced in attaching the Meinhard concentric glass nebulizer of the ARL 34000 ICP spectrometer to the small volume spray chambers with available fittings. The construction of a modified nebulizer also allowed the opportunity of reducing the dead volume of the uptake tube.

---

* A description of the low power ARL 34000 ICP spectrometer, and the operating conditions, is given in Kempster (1986).

A suitable water trap was also constructed for use with the reduced volume spray chambers, a design being used which allowed the water level in the trap to be physically close to the base of the spray chamber, in the interests of reducing dead volume in the drainage outlet tube.

The spray chamber designs were evaluated with respect to aerosol displacement time, and expected aerosol particle exclusion diameter in the case of the designs incorporating centrifugal principles. Nebulization efficiency was determined using an indirect method.

3.2 Spray chamber designs

The spray chamber designs tested are shown in Figure 3-1 to 3-9. For the purposes of discussion, these chambers are numbered from 1 to 9. The volumes given for the chambers includes that of the aerosol outlet tube, but excludes that of the waste drainage tube.

It was initially intended that the reduced volume spray chambers be constructed from a non-boron containing glass, but the lack of suitable starting materials and fittings to the glassblower did not allow this, and all the reduced volume spray chambers were constructed from boro-silicate glass.

3.2.1 Chamber No. 1 (Fig. 3-1)

This 110 mℓ modified Scott-type spray chamber is the existing commercial spray chamber on the ARL 34000 ICP spectrometer used in this study. This chamber differs from the Scott design (Scott *et al*, 1974) firstly in having a smaller volume than the ca., 220 mℓ of the Scott design, and secondly, in the presence of three holes in the inner cylinder, near the nebulizer inlet, which allowed free flow

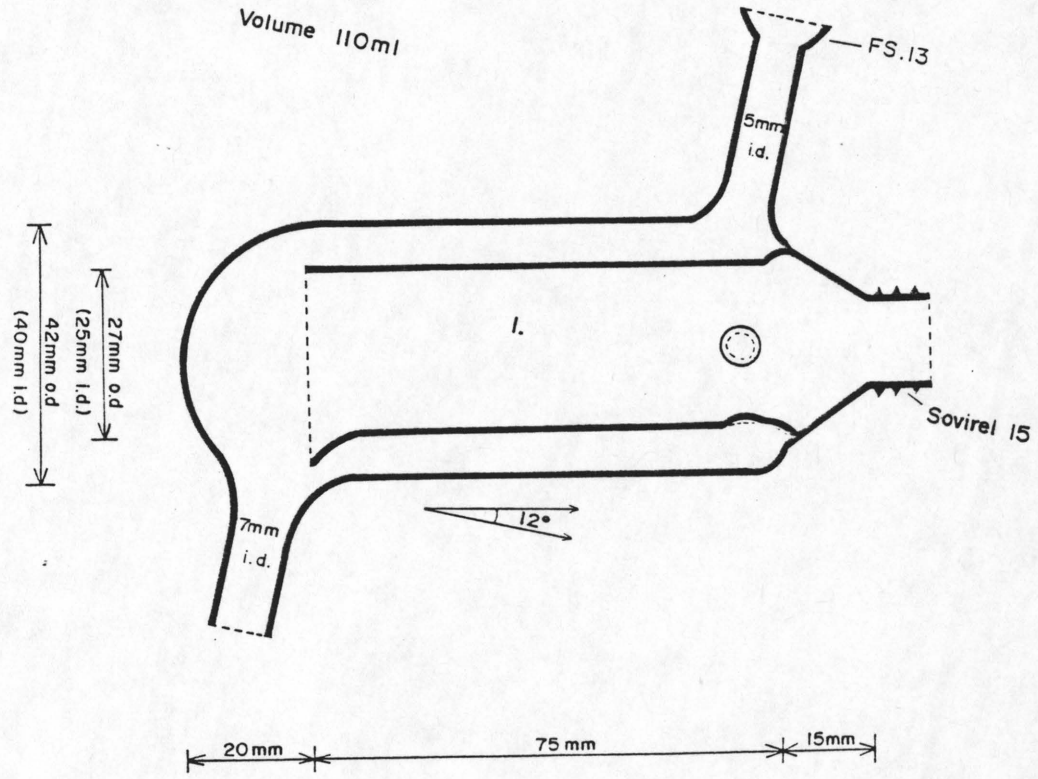

Fig. 3-1: Spray chamber No. 1, the commercial 110 mℓ chamber used on the ARL 34000 ICP spectrometer.

of aerosol between the inner and outer cylinders. These holes were omitted in all reduced volume designs constructed, as they may allow some large droplets of the primary aerosol to pass directly to the aerosol outlet tube. A further criticism of chamber No. 1 was that the lip of the inner cylinder was not close enough to the glass wall of the outer cylinder to prevent large drop formation and collection on the lip, with possible disturbance to the regular flow of the aerosol.

3.2.2 Chamber No. 2 (Fig. 3-2)

Chamber No. 2 is a 24 mℓ double-barrel type chamber, with the aerosol exit tube attached tangentially to the spray chamber body, so that the outer side of the exit tube is tangential to the spray chamber body. For purposes of further discussion, this manner of attachment is termed tangential outlet 1 (TO1). This attachment was also used in chambers Nos. 3, 5 and 6, and is shown schematically in the end-on view in Fig. 3-5. Like chamber No. 1, an inclination of 12° to the horizontal was used when constructing chamber No. 2 (Fig. 3-2). At this rather gentle inclination, however, a layer of liquid collected on the lower portion of the inner cylinder, despite the lip being almost in contact with the outer cylinder. Adequate drainage was obtained when this chamber was inclined at 30° to the horizontal, which was used in all further experiments with chamber No. 2. The ball-and-socket connection between the aerosol exit tube of the spray chambers and the inner tube of the ICP torch fortunately allowed considerable leeway in positioning of the chambers.

3.2.3 Chamber No. 3 (Fig. 3-3)

Chamber No. 3 is a 15 mℓ double-barrel type, with the aerosol exit tube attached tangentially (type TO1) analagous to that used for chamber No. 2. To assist

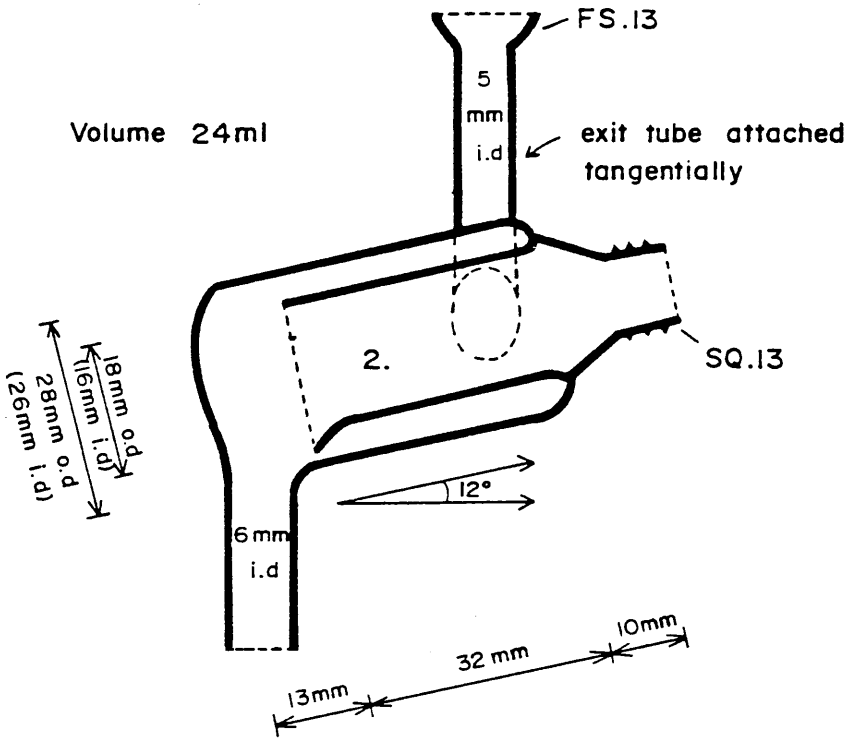

Fig. 3-2: Spray chamber No. 2, a 24 mℓ double-barrel design with a tangential aerosol exit tube.

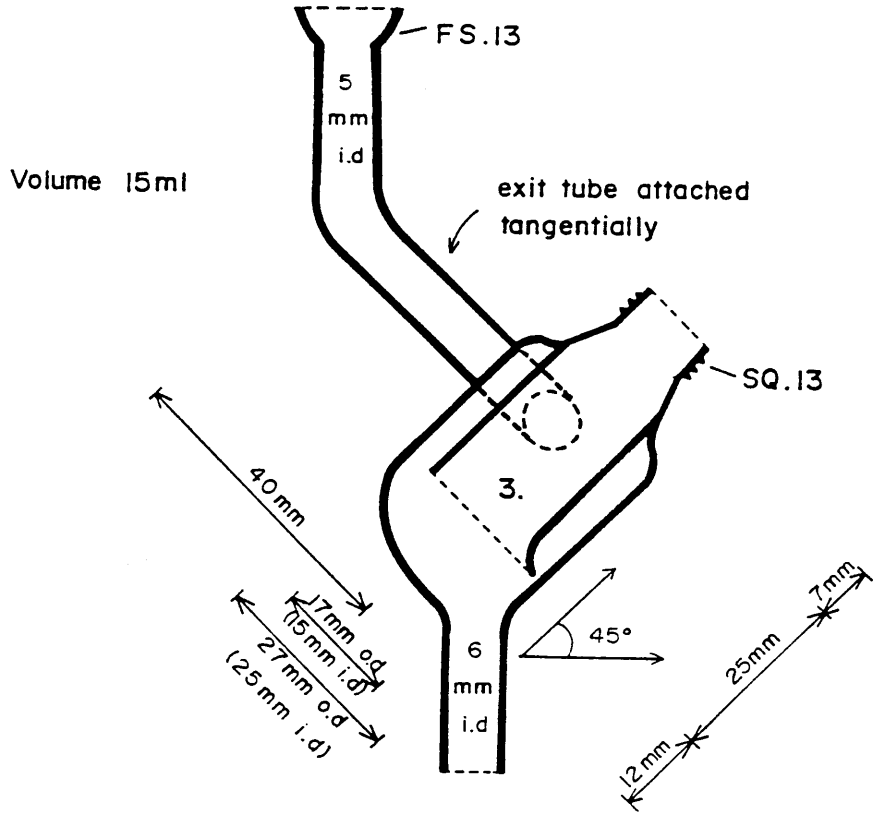

Fig. 3-3: Spray chamber No. 3, a 15 mℓ double-barrel design with a tangential aerosol exit tube.

drainage of liquid from the inner cylinder, the spray chamber body was inclined at 45° to the horizontal (Fig. 3-3). In practice, however, an inclination of the body of the chamber of 30° to the horizontal was found to be just as suitable. The latter orientation had the advantage that the outlet tube was then 15° off the vertical, which appeared to result in better drainage within the outlet tube, with less tendency to liquid plug formation. A 30° inclination of the spray chamber body was used in all further tests. In operation, the collection of large droplets was visible in the distal* portion of the chamber, a distinct ring being observed around the middle of the outer cylinder. No large droplet collection was observed in the aerosol exit tube.

3.2.4 Chamber No. 4 (Fig. 3-4)

Chamber No. 4 was identical in shape to chamber No. 3 in all respects but one, and that is that whereas chamber No. 3 had a tangentially attached aerosol exit tube, the attachment of this tube was a conventional right-angle connection in the case of chamber No.4 (Fig. 3-4). As was the case with chamber No. 3, better drainage from the waste drainage tube was observed with the spray chamber body inclined to 30° to the horizontal.

During operation of chamber No. 4, visible collection of large droplets in the aerosol exit tube occurred, this collection of visible droplets extended past the elbow in the aerosol exit tube.

---

* rounded end of chamber i.e., the end opposite the nebulizer inlet.

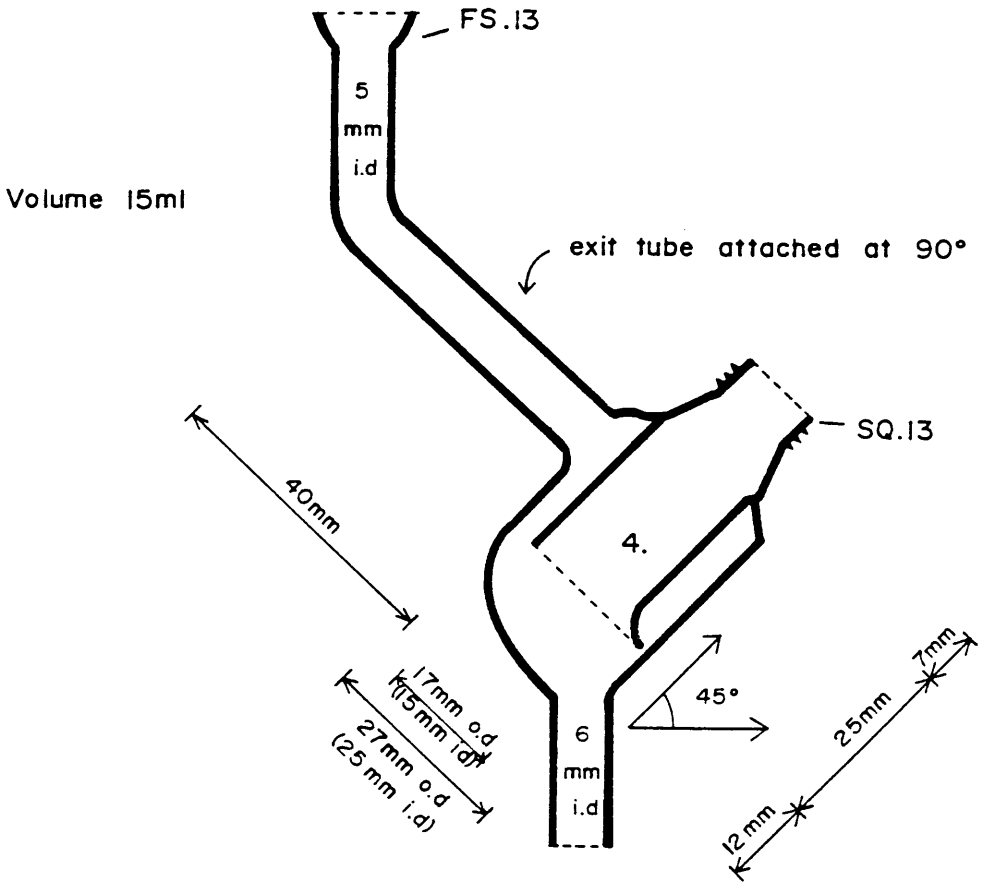

Fig. 3-4: Spray chamber No. 4, a 15 mℓ double-barrel design with conventional attachment of the aerosol exit tube.

3.2.5 Chamber No. 5 (Fig. 3-5)

Chamber No. 5 was an 11 mℓ double-barrel design with a TOI type tangential outlet (Fig. 3-5), and was similar in shape to chamber No. 3, the difference being that chamber No. 5 was 11 mm shorter in length than chamber No. 3. As was the case with chamber No. 3, better drainage from the waste drainage tube was observed with the spray chamber body positioned at 30° to the horizontal, so that the waste drainage tube was 15° off the vertical. During operation large droplet collection was visible in all parts of the chamber, except for the aerosol exit tube.

3.2.6 Chamber No. 6 (Fig. 3-6)

Chamber No. 6 was an 11 mℓ double-barrel design with a TOI type tangential outlet, and was similar in shape to chamber No. 3, the difference being that chamber No. 6 was narrower than chamber No. 3. During operation, liquid rapidly accumulated near the end of the inner cylinder of chamber No. 6, until the inner cylinder was occluded with liquid, the argon gas flow thereafter intermittently forcing its way through the liquid plug. This drainage problem made this chamber totally unsuitable, and it was abandoned.

This chamber showed that there is a limitation to the diameter of the inner cylinder, in the double-barrel type design, into which the primary aerosol from the nebulizer may be discharged without severe drainage problems being experienced. The internal diameter (i.d.) of 9 mm of the inner cylinder of chamber No. 6 was clearly too small for adequate drainage.

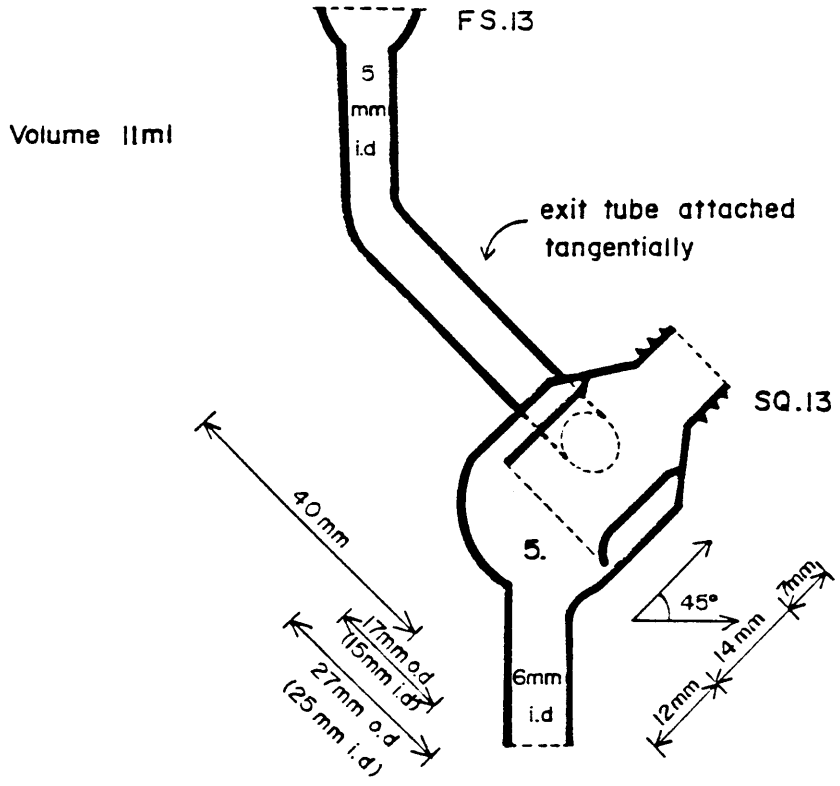

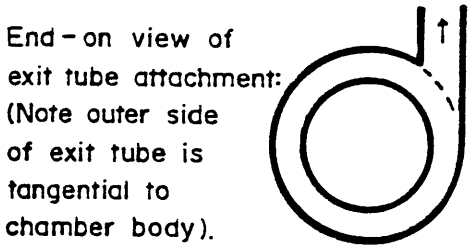

Fig. 3-5: Spray chamber No. 5, a 11 mℓ double-barrel design, with a tangential aerosol exit tube. A cross section of the manner of attachment of the aerosol exit tube is also shown, this type of attachment also being used in chambers 2, 3 and 6.

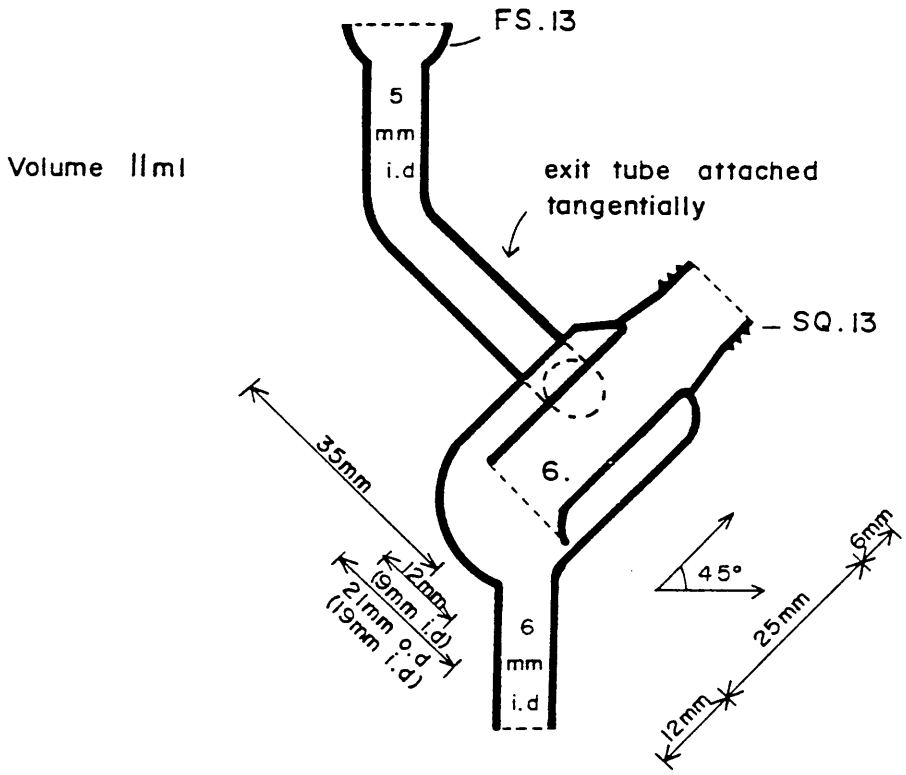

Fig. 3-6: Spray chamber No. 6, a 11 mℓ narrow double-barrel design, with a tangential aerosol exit tube.

3.2.7 Chamber No. 7 (Fig. 3-7)

This chamber was a conical, cyclone-type chamber with a tangential inlet, and an axial outlet for the aerosol. In an attempt to avoid the problem of large droplets bypassing the cyclone, as described for example by Ebdon and Cave (1982), the opening to the aerosol exit tube was placed well below the level of the tangential inlet tube to the cone (Fig. 3-7) as suggested by Vieira *et al* (1986). Further, a thin glass rod extended from the opening of the aerosol exit tube to the lower end of the cone, to assist the drainage of liquid droplets collecting on the aerosol exit tube to waste.

During operation, large liquid droplets rapidly collected in the first few mm of the aerosol exit tube, and tube plugging with obstruction to the aerosol flow was observed. This made chamber No. 7 unsuitable for further work.

Three other modifications of the conical type design (Fig. 3-7) were also tried. These were (i) the non-tangential placement of the aerosol inlet tube at right angles to the base of the cone instead of tangential as in chamber No. 7; (ii) a non-tangential right angle placement with a flared inlet tube; and (iii) a tangential placement of the aerosol inlet tube as in Fig. 3-7, but with the inlet tube 13 mm greater in length. In operation modifications (i) and (ii) showed the same severe accumulation of large liquid droplets in the lower end on the aerosol exit tube as chamber No. 7 showed. Modification (iii) showed severe accumulation of large liquid droplets in the aerosol inlet tube, with liquid plug formation, similar to the drainage problem observed with chamber No. 6.

The 11 mℓ conical type design was therefore abandoned.

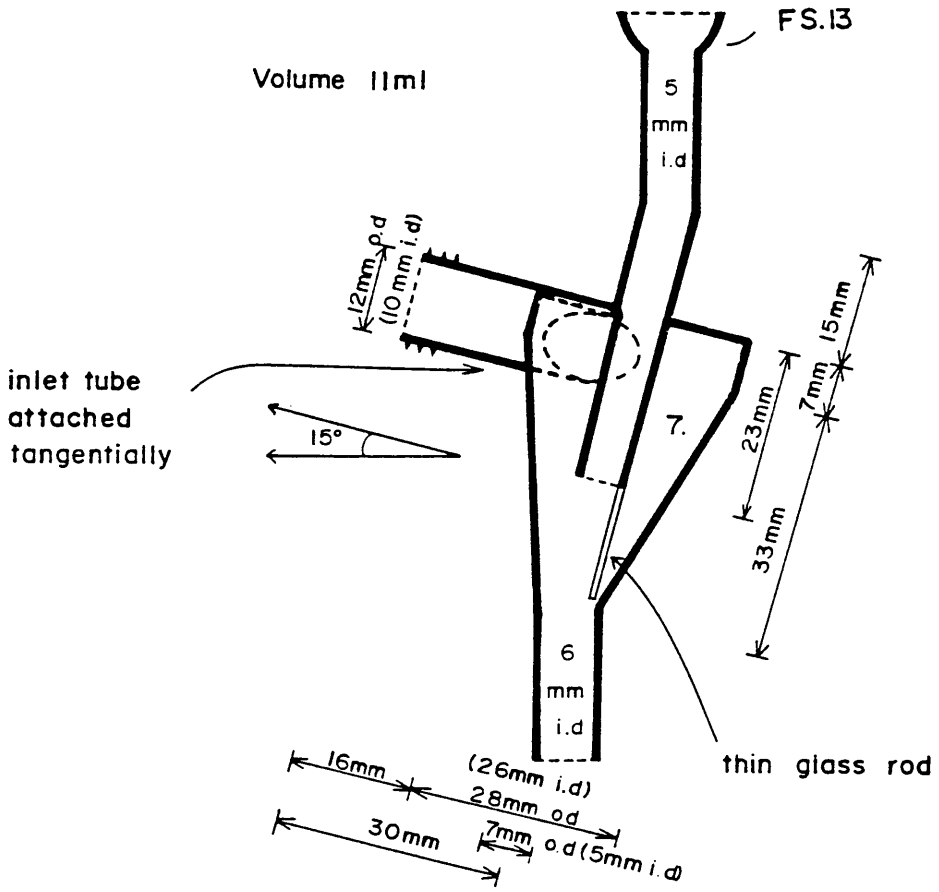

Fig. 3-7: Spray chamber No. 7, a conical design, with tangential introduction of the primary aerosol, and axial placement of the aerosol exit tube.

3.2.8 Chamber No. 8 (Fig. 3-8)

This chamber was a 17 mℓ double-barrel design similar to chamber No. 3, but with different attachment of the tangential aerosol exit tube. For chamber No. 8 the axis of the exit tube was tangential to the chamber body (Fig. 3-8). For purposes of further discussion this type of attachment is termed tangential outlet 2 (TO2). The spray chamber body was positioned at 30° to the horizontal during operation. Some droplet collection was observed on the distal side of the aerosol outlet tube as far as the elbow. Unlike chamber No. 3, this chamber did not show the desirable characteristic of limitation of most of the large droplet collection to the distal portion of the spray chamber body.

3.2.9 Chamber No. 9 (Fig. 3-9)

This chamber was a 12 mℓ double-barrel design, very similar to that used for chamber No. 5. For chamber No. 9, however, the aerosol exit tube was attached so that the inner side of the exit tube was tangential to the chamber body (Fig. 3-9). This type of tangential attachment, which is termed a tangential outlet 3 (TO3) for the purpose of further discussion, is similar to the attachment used for the inlet of a cyclone separator (Fig. 2-1). In operation chamber No. 9 showed good drainage, and the aerosol exit tube remained free of any visible large droplet collection. The body of the chamber was inclined at 30° to the horizontal during use.

3.3 The concentric pneumatic nebulizer

A commercial Meinhard concentric pneumatic nebulizer (Fig. 3-10) was used with chamber No. 1. A disadvantage of this nebulizer is the large dead volume of the rear end of the liquid uptake tube. The modified concentric glass

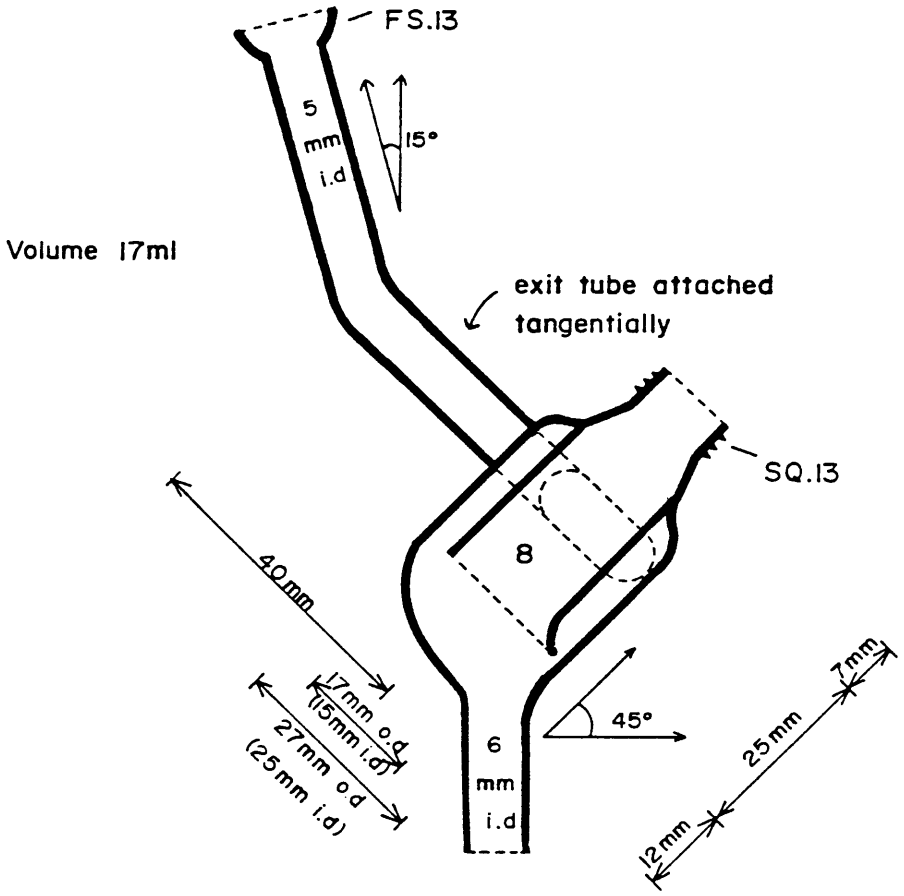

End-view of exit tube attachment: (Note axis of exit tube is tangential to chamber body).

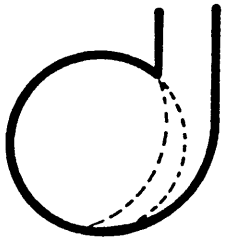

Fig. 3-8: Spray chamber No. 8, a 17 mℓ double-barrel design, with the axis of the aerosol exit tube placed tangential to the spray chamber body.

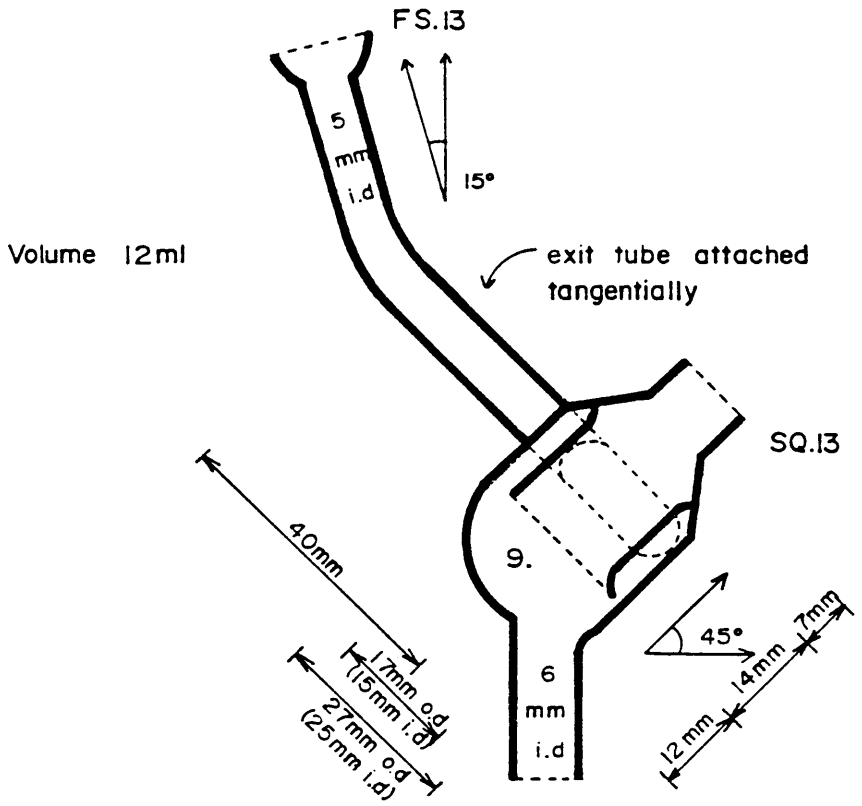

End-view of exit tube attachment: (Note inner side of exit tube is tangential to chamber body).

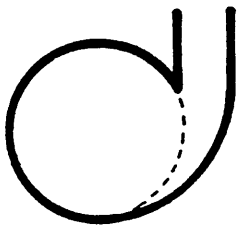

Fig. 3-9: Spray chamber No. 9, a 12 mℓ double-barrel design, with the tangential aerosol exit tube attached in a similar manner to that used for the gas inlet tube in a cyclone dust separator (vide Fig. 2-1).

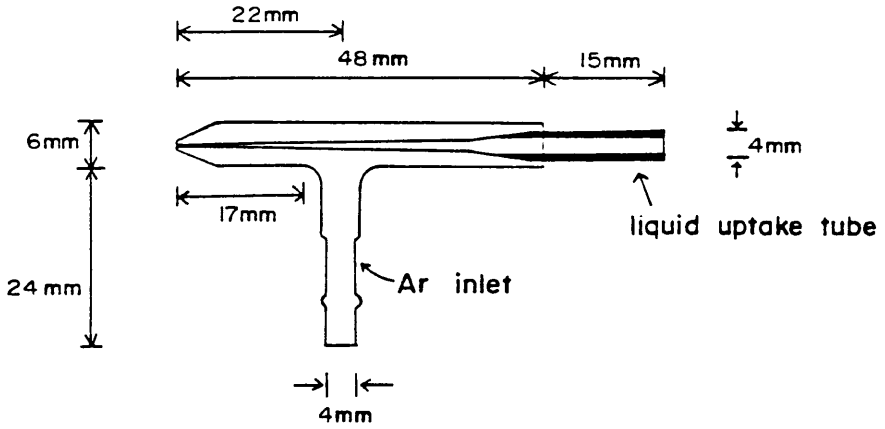

Fig. 3-10: The commercial Meinhard concentric nebulizer used with spray chamber No. 1.

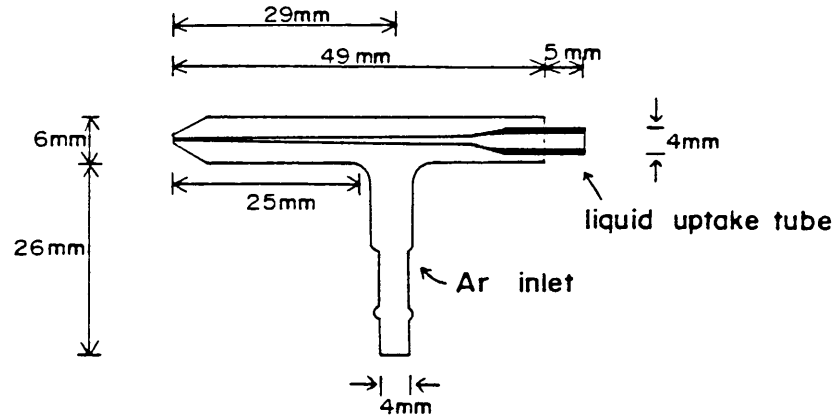

Fig. 3-11: The modified concentric glass nebulizer used with spray chambers Nos., 2 to 9.

pneumatic nebulizer constructed for use with the reduced volume spray chambers (No. 2 to 9) is shown in Fig. 3-11. The rear end of the liquid uptake tube of the modified nebulizer was made 10 mm shorter than the Meinhard nebulizer, thereby reducing the dead volume by about 65 µℓ. The argon inlet tube attachment in the modified nebulizer was 25 mm back from the nebulizer tip. During use the nebulizer was pushed forward into the screw cap fitting as far as it would go. The i.d. of the liquid capillary tip of the modified nebulizer was 0,32 mm.

3.4 Drainage arrangements

In order to keep the liquid level in the waste drainage tube close to the base of the reduced volume spray chamber, a water-trap was designed which was open at the top, to allow the trap to be placed physically close to the spray chamber body (Fig. 3-12). A 70 mm length of 6 mm i.d. tygon tubing was attached to the waste outlet tube of each reduced volume spray chamber, the tube being positioned in the 150 mm tube of the trap. A length of 6 mm i.d. tygon tubing was led from the drain tube of the trap to a waste bottle.

Further, the use of a 90 mm length of a 1 mm i.d. glass capillary tube, with the tip sealed in a flame, and the upper 7 mm bent by 45° to make an obtuse angle of 135°, was placed in the waste drainage tube of the reduced volume spray chambers, with the bent tip resting on the junction of the chamber body with the drainage tube. This procedure was found to assist in the drainage of liquid to waste. The capillary was held at the appropriate height using a suitable length of 0,8 mm i.d. tygon tubing, with its lower end resting in the base of the water-trap. As a further precaution, spray chambers were cleaned periodically when necessary with chromic acid. To avoid liquid plug formation in the waste drainage outlet from the chamber body, it was important to keep the chamber free of oil or grease.

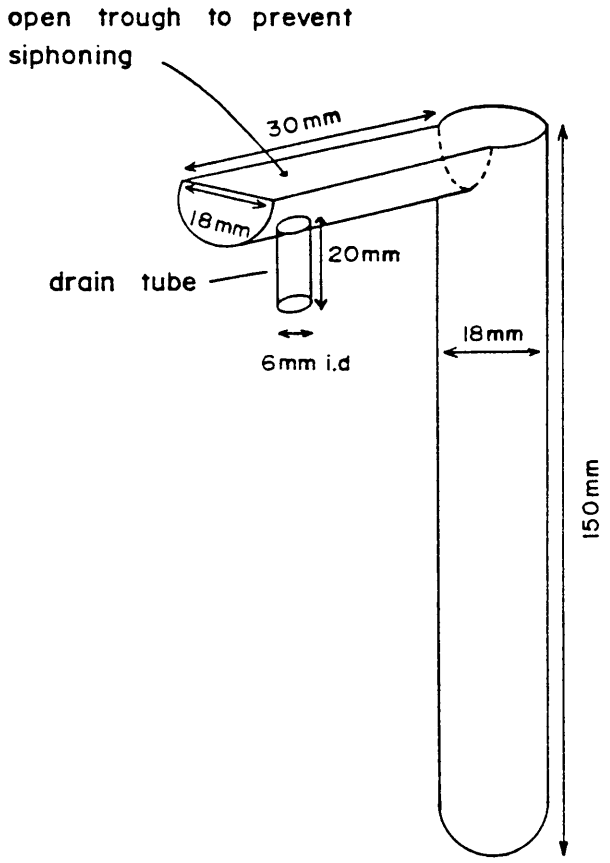

Fig. 3-12: The water drain trap used with spray chambers Nos., 2 to 9.

3.5 Nebulization efficiency

The procedure used for determining nebulization efficiency was based on the method described by Gustavsson (1984c), where liquid uptake and drainage to waste are measured gravimetrically. Glass sample cups of 12 mℓ capacity were used for containers for deionized water uptake and drainage vessels. The cups were covered with plastic laboratory film (Parafilm) to retard evaporation. For collecting waste drainage, the spray chamber was coupled to a pre-weighed glass cup with a cork stopper. Sample uptake was forced by means of a Gilson II Minipuls peristaltic pump, with a 0,57 mm i.d. Sterilin pump tube, and 0,4 mm i.d. polyethylene uptake tubing and a 70 mm length of glass capillary as a sample uptake tube. Sample uptake rate was adjusted to 1,3 $m\ell.min^{-1}$. Uptake and drainage were measured over 3 min periods. Ten replicate measurements were made for each chamber. The laboratory temperature was 20,0 $\pm$ 0,5°C, as was the temperature of the water used for aspiration. Nebulizer gas flow rate was 400 $m\ell.min^{-1}$ at 340 kPa.

The results of the nebulization efficiency measurement are shown in Table 3-1.

TABLE 3-1: Mean nebulization efficiency (%) and standard deviation (10 replicates) found for the various spray chambers[a]. Chamber volumes are also shown.

Chamber No.	Capacity/ mℓ	Nebulization efficiency/%[b] $\bar{n} \pm \sigma$
1	110	4,8 + 1,2
2	24	4,2 ± 1,3
3	15	3,8 ± 1,0
4	15	3,0 ± 0,5
5	11	3,2 ± 0,7
8	17	3,4 ± 1,0
9	12	2,5 ± 0,3

a Meinhard nebulizer used with chamber No. 1, while the modified concentric nebulizer (Fig. 3-11) was used with all other chambers.

b Mean ± standard deviation.

All the reduced volume spray chambers, with the modified concentric glass nebulizer showed smaller nebulization efficiency than the 4,8% efficiency found for chamber No. 1 with the Meinhard nebulizer. Therefore some loss of sensitivity may be expected. Also, there is a trend to decreased nebulization efficiency as the chamber volume is decreased. Further, the manner of attachment of the aerosol exit tube influences nebulization efficiency e.g., the lower efficiency of 2,5% for chamber No. 9 with a T03 attachment, is considerably lower than the 3,2% efficiency for chamber No. 5 with a T01 attachment of the aerosol exit tube.

3.6 Aerosol displacement time

The aerosol displacement time t_d, calculated from the ratio of spray chamber volume to inner gas flow rate, is shown in Table 3-2. Also shown in this table are the spray

chamber volume and chamber type, for the convenience of the reader. Note that the displacement time of chamber No. 1 of 4,9 s makes it unsuitable for FIA, whereas chambers 3 to 9 all have t_d values less than 1 s, a desirable characteristic for FIA sample introduction.

TABLE 3-2: Spray chamber types, showing the volume V, and the aerosol displacement time t_d.

Chamber No.[a]	Type[b]	V/mℓ.	t_d/s[c]
1	DB-RAO	110	4,9
2	DB-TO1	24	1,1
3	DB-TO1	15	0,67
4	DB-RAO	15	0,67
5	DB-TO1	11	0,49
6	DB-TO1	11	0,49
7	CON-TI	11	0,49
8	DB-TO2	17	0,76
9	DB-TO3	12	0,54

[a] Refer to Figures 3-1 to 3-9 for diagrams of the chambers.

[b] DB = Double barrel, CON = Conical,
RAO = Right angle outlet, TI = Tangential inlet,
TO1 = Tangential outlet type 1 with the outer side of the aerosol exit tube tangential to the spray chamber body (Fig. 3-5),
TO2 = Tangential outlet type 2 with the axis of the exit tube tangential to the spray chamber body (Fig. 3-8),
TO3 = Tangential outlet type 3 with the inner side of the exit tube tangential to the spray chamber body (Fig. 3-9).

[c] At an inner gas flow rate of 22,4 $m\ell.s^{-1}$ and a pressure of 101 kPa.

3.7 Particle exclusion diameters

An indication of the expected aerosol particle exclusion diameters for spray chambers incorporating centrifugal removal processes, through either a tangential inlet or outlet for the aerosol, can be obtained by applying the equations of Davies, Bosanquet or Fuks (Davies, 1952a and 1952b; Fuks, 1955). The use of Fuks (1955) formula (equation 35) is limited by the problem that the number of spiral turns is not known. The calculated particle exclusion diameters are shown in Table 3-3. Davies (1952a) and Fuks (1955) approaches give similar d_{min} values if three spiral turns are assumed in applying equation 35. Bosanquet's equation (2nd column of d_{min} values in Table 3-3) gives the lowest estimates for d_{min}. All the estimates of d_{min} for the double-barrel type chambers are less than 22 μm. The d_{min} values for the conical chamber No. 7 are, however, high and indicate poor large droplet exclusion for this chamber. The particle exclusion diameters of the small volume double-barrel chambers indicate that large droplets should be retained in the chamber and pass to waste, and indicates that the chambers should function satisfactorily as regards volatilization type interference occurrence.

TABLE 3-3: Calculated values for the aerosol particle exclusion diameter d_{min} of spray chambers using centrifugal droplet removal processes[a]. Also shown is the ratio of the inner to outer tube radii, R_1/R_2.

Chamber No.[b]	$d_{min}/\mu m$					R_1/R_2
	1[c]	2[d]	3[e]	4[f]	5[g]	
2[h]	8,4	6,9	20,5	14,5	11,9	0,62
3[h]	9,0	6,9	20,7	14,6	11,9	0,60
5[h]	10,7	6,9	20,7	14,6	11,9	0,60
6[h]	7,1	6,5	21,8	15,4	12,6	0,47
7[i]	19,2	17,4	75,7	53,5	43,7	0,19
8[h]	9,0	6,9	20,7	14,6	11,9	0,60
9[h]	10,7	6,9	20,7	14,6	11,9	0,60

a - With analytical conditions as given by Kempster (1986), and using values for the density of water ρ of 1 $g.m\ell^{-1}$; gravitational acceleration g = 980 $cm.s^{-2}$; viscosity of argon η = $221,7x10^{-6}$ $g.s^{-1}.cm^{-1}$ at 20°C and density of argon σ of $1,66x10^{-3}$ $g.cm^{-3}$ at 20°C and 101 kPa. Nebulizing gas flow rate of 22,4 $cm^3.s^{-1}$ at 101 kPa, and sample uptake rate by the nebulizer of 1,27 $m\ell.min^{-1}$, forced using a Gilson Minipuls II pump.

b - Refer to relevant Figures 3-2 to 3-9 for spray chamber diagrams.

c - d_{min} calculated using equation 33 (Davies, 1952a).

d - d_{min} calculated using equation 34 (Davies, 1952b).

e - d_{min} calculated using equation 35 (Fuks, 1955), and assuming that the number of spiral turns, of the aerosol, is s=1.

f - d_{min} calculated using equation 35 (Fuks, 1955) with s=2.

g - d_{min} calculated using equation 35 (Fuks, 1955) with s=3.

h - As the centrifugal motion is induced by a tangential aerosol outlet, V_0 in eqns., 33 to 35 is the tangential outlet velocity rather than inlet gas velocity. A value for V_0 of 114 $cm.s^{-1}$ was used.

i - V_0 is the inlet tangential velocity, in this case. A value for V_0 of 28,5 $cm.s^{-1}$ was used.

3.8 Summary and conclusion

Constructed small volume spray chambers, with volume reduction of as much as ten times less than the commercial 110 mℓ chamber, had aerosol displacement times of as little as 0,5 s which makes these chambers potentially useful for FIA application. The use of a tangential aerosol outlet tube attachment gave estimated aerosol droplet exclusion diameters of between 6,5 μm and 21,8 μm for the small double-barrel type chambers which indicates that volatilization type interferences should not be severe. The use of a conical design, with a tangential inlet based on the cyclone dust-separator design (Davies, 1952a) gave poor large droplet exclusion characteristics, both theoretically, (Table 3-3, chamber No. 7) as well as in practice, with large droplets depositing in the aerosol outlet tube.

The efficacy of tangential placement of the aerosol outlet tube in small volume double-barrel designs, as against conventional right-angle placement of the outlet tube was demonstrated with chambers No. 3 and 4. The former chamber, with a tangential outlet had no large droplets collecting in the outlet tube; whereas the latter chamber, with a conventional right-angle outlet, showed a marked deposition of liquid in the aerosol outlet tube.

In conclusion, the good drainage characteristics of 11 to 24 mℓ double-barrel type chambers including a tangentially placed aerosol outlet tube, and with the lip of the inner cylinder almost touching the outer tube, indicates their potential for analytical use. The evaluation of the chambers for analytical application, with conventional discrete sample presentation is given in the next chapter.

CHAPTER 4: ANALYTICAL CHARACTERISTICS OF THE SPRAY CHAMBERS

4.1 Introduction

In this chapter, the original spray chamber of the 34000 ICP spectrometer, as well as all the designed small volume chambers having adequate drainage i.e., chamber No's 2, 3, 4, 5, 8, and 9, are evaluated using conventional discrete sample presentation for the following analytical characteristics:

(i) Equilibration times: Both wash-in and wash-out times were determined for boron as well as for manganese.

(ii) Precision of analyte signal for 21 analyte elements at an analyte concentration of at least fifty times greater than the limit of detection.

(iii) Relative sensitivity of measurement for 21 analyte elements.

(iv) Detection limits for 21 analyte elements.

(v) Evaluation for the presence of volatilization type interference of phosphate and aluminium on calcium emission intensity, for both ionic and atomic calcium emission, as well as tests for the presence of sodium on calcium interference.

(vi) Evaluation of short term precision, as seen from the steady state signal for boron emission.

(vii) Performance of spray chamber No. 5 in the analysis of real samples.

4.2 Analytical conditions of measurement

The analytical conditions of measurement for the ARL 34000 ICP spectrometer are shown in Table 4-1, and the analytical lines of the 21 element channels used in this study shown in Table 4-2. For details of the spectrometer hardware, refer to Kempster (1986). For evaluation of precision and establishment of sensitivity, the upper concentration limit of the daily normalization standards* were used. These concentrations are shown in Table 4-3.

4.3 Equilibration times

Both wash-in and wash-out times were determined for the spray chambers for 10 $mg.\ell^{-1}$ boron in water, and for 10 $mg.\ell^{-1}$ manganese in **ϕ = 0,01 nitric acid, using the analogue output of the spectrometer and a potentiometric recorder to record the analyte signals.

---

* The standards were prepared from Titrisol stock solutions, as described by Kempster (1986).

** ϕ = volume fraction.

TABLE 4-1: Analytical operating conditions used for analysis on the ARL 34000 polychromator

1. Gas: Argon, spectrographic grade. Argon feed pressure to the source box 500 kPa, with the secondary regulator in the source box set at 340 kPa, this being the inlet pressure to the rotameters. Rotameter settings of 400 mℓ.min^{-1} for the inner (nebulizer) gas flow and intermediate (plasma) gas flow, and 11,0 ℓ.min^{-1} for the outer (coolant) argon.

2. Observation height: 18 mm above the load coil.

3. Sample delivery: Forced, with a Gilson Minipuls II peristaltic pump, using a 0,57 mm i.d. Sterilin pump tube and 0,4 mm i.d. polyethylene sample uptake tubing, with a 70 mm length glass capillary as sample uptake tube. The dead volume of the uptake tubing was 540 µℓ. Sample uptake rate was adjusted to 1,3 mℓ.min^{-1}.

4. rf power: Incident rf power was 1250 watt, with reflected rf power less than 5 watt.

5. A.C. mains: Separate Watford stabilizers were used on rf generator and spectrometer mains supplies, with the voltage to the rf generator set at 216 ± 1 volt, and that to the spectrometer electronics at 225 ± 1 volt.

6. Integration: Integration times of 10 s were used with 3 replicates, except for the tests for interference on calcium where 5 replicates were used.

7. Analogue output: The analogue output of the spectrometer was connected to a model 056-1002 Hitachi potentiometric recorder for readout of single channel instantaneous signals.

8. Spectrometer control: By means of a PDP11/04 compatible processor

9. Analytical wavelengths: Fixed, see Table 4-2.

10. Spectrometer profile: The profile setting of the movable entrance slit of the spectrometer was checked daily before use of the instrument, using a 10 mg.ℓ$^{-1}$ Y standard and the Y 360,07 nm line for profile alignment.

TABLE 4-2: Analytical element channels and wavelengths used on the ARL 34000 ICP spectrometer for evaluation of spray chamber characteristics.

Element[a]	λ/nm
Al (I)	396,15
B (I)	249,68
Ba (II)	455,40
Be (I)	234,86
Ca (II)	315,89
Cd (II)	226,50
Co (I)	340,51
Cr (II)	267,72
Cu (I)	327,39
Fe (II)	259,94
K (I)	766,49
Mg (I)	383,83
Mn (II)	257,61
Mo (II)	281,62
Na (I)	588,99
Ni (I)	352,45
Pb (I)	368,35
Sr (II)	421,55
Ti (II)	334,94
V (II)	311,07
Zn (I)	213,85

[a] (I) = atomic line; (II) = ion line.

TABLE 4-3: Concentrations of standards used for evaluation of precision, and establishment of sensitivity. These were the upper concentration limits used in daily calibration*.

Element	Concentration/mg.ℓ^{-1}
Al	50
B	10
Ba	30
Be	10
Ca	600
Cd	10
Co	50
Cr	10
Cu	10
Fe	10
K	600
Mg	600
Mn	10
Mo	10
Na	600
Ni	50
Pb	50
Sr	5
Ti	10
V	10
Zn	10

*Kempster (1986).

Wash-in and wash-out times were read off the recorder chart paper. Five replicate measurements were made. The mean and standard deviation of the wash-in and wash-out times are given in Tables 4-4 to 4-7.

There was a notable improvement in the wash-in times to 90% of steady state value for all the reduced volume spray chambers except No. 2, which had a similar wash-in time to chamber No. 1.

Wash-in times to 90% of steady state value for the other small volume chambers showed an approximate halving of the wash-in time, with $t_{90\%}^{in*}$ values of between 0,9s and 1,3s for boron, and 1,0s and 1,6s for manganese, compared to 2,1s for boron and 2,5s for manganese for chamber No.1 (Table 4-4 and 4-5).

Wash-out times to 10% of steady-state signal for manganese showed an improvement for all the small volume chambers, with the wash-out time $t_{10\%}^{out}$ between 0,7s and 1,6s compared to 3,2s for chamber No.1 (Table 4-7). In the case of boron, however, the shortening of wash-out time was generally only marginal, with $t_{10\%}^{out}$ values between 1,6s and 2,5s for chambers No. 3, 4, 5, 8 and 9, compared to 2,6s for chamber No. 1. Only chamber No. 2 showed a significant improvement with a $t_{10\%}^{out}$ value of 1,3s. A shortening of $t_{20\%}^{out}$ values for boron of between 0,3s and 0,7s was observed for the small volume spray chambers, however, (Table 4-6).

---

* Wash-in time to 90% of steady-state signal. For wash-out times analagous symbolism is used.

TABLE 4-4: Wash-in times (t^{in}/s) for the boron analyte signal for the various spray chambers, given as mean (five replicates) ± standard deviation (in seconds).

Chamber No:	1	2	3	4
% of steady state	$\bar{t}^{in} \pm \sigma$	$\bar{t}^{in} \pm \sigma$	$\bar{t}^{in} \pm \sigma$	$\bar{t}^{in} \pm \sigma$
50	0,4 ± 0,2	0,9 ± 0,2	0,4 ± 0,2	0,3 ± 0,1
80	1,2 ± 0,2	1,6 ± 0,2	0,6 ± 0,2	0,6 ± 0,1
90	2,1 ± 0,4	2,3 ± 0,3	1,1 ± 0,2	0,9 ± 0,1
95	3,5 ± 0,6	3,4 ± 0,5	1,9 ± 0,6	2,3 ± 0,7

Chamber No:	5	8	9
% of steady state	$\bar{t}^{in} \pm \sigma$	$\bar{t}^{in} \pm \sigma$	$\bar{t}^{in} \pm \sigma$
50	0,4 ± 0,2	0,3 ± 0,1	0,3 ± 0,1
80	0,8 ± 0,4	0,6 ± 0,1	0,6 ± 0,1
90	1,3 ± 0,6	1,0 ± 0,1	1,1 ± 0,3
95	1,8 ± 0,7	3,9 ± 1,2	3,3 ± 1,2

TABLE 4-5: Wash-in times (t^{in}/s) for the manganese analyte signal for the various spray chambers, given as mean (five replicates) ± standard deviation (in seconds).

Chamber No:	1	2	3	4
% of steady state	$\bar{t}^{in} \pm \sigma$	$\bar{t}^{in} \pm \sigma$	$\bar{t}^{in} \pm \sigma$	$\bar{t}^{in} \pm \sigma$
50	0,3 ± 0,1	0,6 ± 0,2	0,4 ± 0,2	0,3 ± 0,1
80	1,3 ± 0,2	1,3 ± 0,2	0,7 ± 0,4	0,7 ± 0,2
90	2,5 ± 0,3	2,0 ± 0,3	1,2 ± 0,5	1,1 ± 0,3
95	4,2 ± 0,8	2,7 ± 0,6	1,8 ± 0,6	2,1 ± 0,3

Chamber No:	5	8	9
% of steady state	$\bar{t}^{in} \pm \sigma$	$\bar{t}^{in} \pm \sigma$	$\bar{t}^{in} \pm \sigma$
50	0,5 ± 0,1	0,6 ± 0,3	0,3 ± 0,1
80	0,9 ± 0,2	1,0 ± 0,3	0,6 ± 0,1
90	1,3 ± 0,4	1,6 ± 0,5	1,0 ± 0,3
95	2,0 ± 0,6	3,4 ± 1,4	2,3 ± 1,1

TABLE 4-6: Wash-out times (t^{out}/s) for the boron analyte signal for the various spray chambers, given as mean (five replicates) ± standard deviation (in seconds).

Chamber No:	1	2	3	4
% of steady state	$\bar{t}^{out} \pm \sigma$	$\bar{t}^{out} \pm \sigma$	$\bar{t}^{out} \pm \sigma$	$\bar{t}^{out} \pm \sigma$
50	0,5 ± 0,1	0,2 ± 0,1	0,3 ± 0,1	0,3 ± 0,1
20	1,3 ± 0,1	0,8 ± 0,1	1,0 ± 0,4	0,8 ± 0,3
10	2,6 ± 0,3	1,3 ± 0,2	2,0 ± 0,3	2,5 ± 0,9
5	7,2 ± 2,2	3,8 ± 0,8	5,2 ± 1,0	6,0 ± 2,1

Chamber No:	5	8	9
% of steady state	$\bar{t}^{out} \pm \sigma$	$\bar{t}^{out} \pm \sigma$	$\bar{t}^{out} \pm \sigma$
50	0,4 ± 0,1	0,4 ± 0,1	0,3 ± 0,1
20	0,6 ± 0,2	0,7 ± 0,2	0,6 ± 0,2
10	2,3 ± 0,9	1,6 ± 0,3	2,0 ± 0,6
5	4,7 ± 0,7	4,7 ± 1,3	7,5 ± 4,0

TABLE 4-7: Wash-out times (t^{out}/s) for the manganese analyte signal for the various spray chambers, given as mean (five replicates) ± standard deviation (in seconds).

Chamber No:	1	2	3	4
% of steady state	$\bar{t}^{out} \pm \sigma$	$\bar{t}^{out} \pm \sigma$	$\bar{t}^{out} \pm \sigma$	$\bar{t}^{out} \pm \sigma$
50	0,6 ± 0,1	0,2 ± 0,1	0,4 ± 0,1	0,4 ± 0,1
20	1,6 ± 0,3	0,5 ± 0,3	0,7 ± 0,2	0,8 ± 0,2
10	3,2 ± 0,3	0,7 ± 0,3	1,5 ± 0,2	1,4 ± 0,4
5	7,0 ± 0,8	2,2 ± 0,6	4,2 ± 0,6	5,3 ± 1,4

Chamber No:	5	8	9
% of steady state	$\bar{t}^{out} \pm \sigma$	$\bar{t}^{out} \pm \sigma$	$\bar{t}^{out} \pm \sigma$
50	0,4 ± 0,2	0,4 ± 0,1	0,4 ± 0,1
20	0,9 ± 0,2	0,8 ± 0,1	0,9 ± 0,2
10	1,6 ± 0,3	1,4 ± 0,2	1,5 ± 0,4
5	4,0 ± 2,3	4,0 ± 2,4	4,0 ± 1,1

In interpretation of equilibration times it should be noted that these times include the wash-in and wash-out time delays contributed by the sample uptake tubing, which may have masked otherwise larger differences between the various chambers.

4.4 Precision of analyte signal

Precision of analyte signal, for the analyte concentrations given in Table 4-3, expressed as the percentage relative standard deviation (RSD%) of net analyte signal for 3 x 10s integrations is shown in Table 4-8, for the various chambers.

The mean precision of the net analyte signal for all the spray chambers tested was less than 1% with the exception of chamber No. 4, which showed a poor mean precision of 3,9%. This may be ascribed to the poor droplet exclusion characteristics of chamber No. 4, as reflected in the accumulation of large visible droplets in the aerosol exit tube, as mentioned in Chapter 3. Chamber No. 3, which was identical in all respects to chamber No. 4 except in the fact that chamber No. 3 had a tangential aerosol outlet, while chamber No. 4 had a conventional right-angle outlet, had in contrast, a mean precision of 0,37% i.e., an order of magnitude difference. This difference in precision between chambers 3 and 4 clearly shows the benefit of using a tangential aerosol exit tube attachment in small volume spray chambers.

TABLE 4-8: Precision of analyte signal, expressed as percentage relative standard deviation (RSD%) for 3x10s integrations, for the analyte concentrations given in Table 4-3, for various spray chambers.

Chamber No:	1	2	3	4	5	8	9
Al	0,63	0,59	0,12	2,14	0,98	0,55	0,25
B	0,04	0,25	0,10	2,74	0,91	0,96	0,74
Ba	0,33	0,22	0,17	3,91	1,18	0,21	0,05
Be	0,01	0,38	0,93	5,07	0,21	1,04	0,24
Ca	1,08	0,74	0,39	3,69	0,73	0,08	0,02
Cd	0,91	0,58	0,81	4,48	0,25	1,73	0,22
Co	0,16	0,31	0,51	2,08	0,65	0,10	0,14
Cr	0,03	0,99	0,17	4,25	0,65	0,60	0,42
Cu	0,28	0,06	0,18	5,03	0,73	0,28	0,50
Fe	0,73	0,92	0,28	4,45	0,53	0,47	0,49
K	0,22	0,44	0,34	7,79	2,29	0,66	1,35
Mg	0,28	0,22	0,24	5,07	0,99	0,28	0,001

.../continued.

TABLE 4-8 (continued): Precision of analyte signal, expressed as percentage relative standard deviation (RSD%) for 3x10s integrations, for the analyte concentrations given in Table 4-3, for various spray chambers. Also given is the mean precision for the 21 analyte elements tested.

Chamber No:	1	2	3	4	5	8	9
Mn	0,73	1,12	0,21	4,55	0,60	0,54	0,44
Mo	1,89	1,56	0,24	5,19	2,27	1,02	0,19
Na	0,48	0,31	0,09	3,49	1,81	0,15	0,61
Ni	0,39	0,22	0,47	2,05	0,67	0,18	0,19
Pb	0,70	1,21	0,70	2,09	1,39	0,70	0,76
Sr	0,45	0,28	0,35	1,20	0,81	0,04	0,05
Ti	1,13	0,79	0,76	5,29	0,45	0,86	0,18
V	1,10	0,56	0,52	3,82	0,38	0,50	0,22
Zn	0,004	0,67	0,27	4,34	0,67	0,56	0,47
Mean(n=21):	0,55	0,59	0,37	3,94	0,91	0,55	0,36

4.5 Relative sensitivity of measurement

The sensitivity of measurement for 21 analyte elements for the various small volume spray chambers, relative to the sensitivity for chamber No. 1, taken as unity, is given in Table 4-9. The slight loss of sensitivity is consistent with the smaller nebulization efficiency of the reduced volume spray chambers (Table 3-1). The changes in sensitivity tend, however, to be analyte element specific, as different excitation conditions in the plasma will affect each element differently. Mean sensitivity loss is greatest for the chambers with the smallest volumes e.g., chamber No. 5 with a volume of 11 mℓ, has a mean sensitivity of 0,47; and least for the small chamber with greatest volume e.g. chamber No. 2, with a volume of 24 mℓ has a mean sensitivity of 0,81. The linear correlation coefficient r, between spray chamber volume and mean relative sensitivity is 0,885 for the data for chambers 2, 3, 4, 5, 8 and 9, and indicates that there is an apparent relationship between mean relative sensitivity and spray chamber volume. This implies that there is a loss of some of the analytically useful small aerosol droplets in the primary aerosol occurring in the reduced volume spray chambers.

TABLE 4-9: Relative sensitivity for 21 analyte elements, for the small volume spray chambers, relative to the sensitivity for chamber No. 1, taken as unity. Also given is the mean sensitivity.

Chamber No:	2	3	4	5	8	9
Al	0,81	0,51	0,50	0,34	0,53	0,42
B	0,88	0,60	0,62	0,41	0,62	0,50
Ba	0,87	0,66	0,69	0,54	0,69	0,65
Be	0,94	0,79	0,77	0,52	0,83	0,69
Ca	0,80	0,90	0,92	0,62	1,04	0,87
Cd	0,76	0,83	0,81	0,56	0,89	0,78
Co	0,77	0,58	0,56	0,39	0,59	0,50
Cr	0,78	0,91	0,88	0,63	1,02	0,86
Cu	0,82	0,52	0,52	0,34	0,55	0,45
Fe	0,81	0,84	0,82	0,58	0,93	0,77
K	0,71	0,26	0,42	0,20	0,38	0,29
Mg	0,86	0,60	0,63	0,40	0,64	0,51
Mn	0,80	0,91	0,89	0,63	1,02	0,84
Mo	0,78	0,82	0,79	0,54	0,87	0,76
Na	0,76	0,49	0,51	0,30	0,50	0,42
Ni	0,78	0,53	0,51	0,36	0,54	0,43
Pb	0,73	0,45	0,44	0,29	0,45	0,38
Sr	0,85	0,73	0,73	0,60	0,76	0,70
Ti	0,82	0,78	0,76	0,52	0,83	0,70
V	0,87	0,86	0,84	0,58	0,90	0,78
Zn	0,82	0,81	0,76	0,54	0,84	0,65
Mean (n=21):	0,81	0,68	0,68	0,47	0,73	0,62

4.6 Detection limits

Detection limits, calculated from the twice-standard deviation background noise signal, for the various spray chambers, are shown in Table 4-10. For most elements, there was a deterioration in the detection limit for the small volume spray chambers. Some exceptions were Ba and Sr, where the small volume spray chambers all showed better detection limits than chamber No. 1. Boron showed similar detection limits with the various chambers, except with chamber No. 4, where a deterioration in detection limit was observed. Considering the poor precision shown by chamber No. 4 at high analyte concentrations (Table 4-8), it is interesting that this does not appear to be reflected in a deterioration of detection limit for most elements with chamber No. 4, compared for example to chamber No. 3 (Table 4-10).

4.7 Evaluation of volatilization and easily ionizable element interferences on calcium emission

The various spray chambers were evaluated for the presence of aluminium on calcium and phosphate on calcium volatilization type interferences, and for sodium on calcium interference, as a test for the presence of easily ionizable element (EIE) interferences by spiking 0,25 $mmol.\ell^{-1}$ Ca solutions with increasing concentrations of aluminium, phosphate and sodium respectively. Both calcium ionic emission, using the Ca(II) 315,89 nm ion line, and calcium atomic emission, using the Ca(I) 422,67 nm* line

---

* The ARL 34000 ICP spectrometer used did not have an atomic calcium line channel. To measure the Ca(I) 422,67nm emission, the Sr 421,55 nm channel was used, after shifting the entrance slit, with the profile dial setting by 1,12 nm, so that the Ca(I) 422,67 nm emission line coincided with the Sr channel exit slit.

were then recorded, and any change in net intensity expressed relative to that for the unspiked calcium standard, taken as 100%.

Molar ratios of interferant to calcium of up to 100 to 1 were used. All interferant solutions and the calcium standard were made up in ϕ = 0,01 nitric acid. For the testing of aluminium interference on calcium, aluminium chloride was used (Alkemade, 1966), while for phosphate interference on calcium, ammonium dihydrogen phosphate served as source of phosphate (Fukushima, 1959). Sodium chloride was used for making up the sodium interferant solutions. Calcium atomic and ionic emission intensities were recorded using 5x10s integrations.

The results of these matrix interference tests are shown in Tables 4-11 to 4-17 for the various spray chambers. Suppression of calcium atomic and ionic emission by aluminium, at an Al to Ca molar ratio of 100 to 1, was around 15% for chamber No. 1. and around 13,5% for chamber No. 2. Suppression was less than 3% for chamber Nos. 3, 5 and 8, with chamber No. 9 showing no suppression. Chamber No. 4 showed a 2,5% suppression for the atomic Ca line, and 6,7% suppression for the ionic Ca line. The small volume spray chambers showed thus less volatilization suppression interference than the 110 mℓ commercial chamber.

For the interference of phosphate on calcium emission chamber No. 1 showed an enhancement of Ca-ionic emission of 4% at a P to Ca molar ratio of 100 to 1. For chambers 2, 3, 4, 5, 8 and 9, there is almost no change in either Ca-atomic or Ca-ionic emission i.e., not more than 1%.

TABLE 4-10: Mean detection limits (9 replicates) in $\mu g.\ell^{-1}$ for 3 x 10s integrations, calculated as twice the standard deviation of the intensity readout, in concentration equivalent units, for a ϕ = 0,01 nitric acid blank solution, for various spray chambers.

Chamber No:	1	2	3	4	5	8	9
Al	22	40	119	45	90	60	88
B	6,1	2,8	7,4	15,3	5,7	4,8	8,1
Ba	3,0	1,0	2,2	1,4	0,8	1,3	2,0
Be	0,4	0,5	0,7	0,9	0,8	0,7	0,5
Ca	78	28	57	24	90	36	35
Cd	4,5	6,9	6,8	8,0	6,6	7,0	5,5
Co	25	21	38	80	30	34	28
Cr	4,9	7,0	5,6	10,1	4,9	6,9	3,7
Cu	2,3	2,7	5,5	7,8	7,4	4,8	7,9
Fe	4,7	5,5	20	6,7	4,9	6,0	13
K	214	600	810	690	2020	703	940
Mg	17	14	27	49	26	21	18
Mn	1,1	1,0	1,8	2,4	1,6	2,4	1,2
Mo	4,7	6,0	11	8,5	14	8,0	6,7
Na	42	38	63	68	126	63	114
Ni	23	16	38	82	25	30	29
Pb	154	258	316	364	601	355	376
Sr	0,5	0,1	0,4	0,4	0,2	0,2	0,4
Ti	0,6	0,8	1,5	1,5	1,4	1,1	1,0
V	2,0	2,4	4,7	3,7	3,9	3,4	2,0
Zn	2,9	5,5	4,4	7,3	7,1	5,4	4,9

TABLE 4-11: Interference tests for Al, P and Na on Ca-atomic line and Ca-ionic line emission, for spray chamber No. 1. Results given as mean net intensity* ± standard deviation, relative to the intensity in the absence of interferant, taken as 100%.

	Relative net Ca intensity ± std. deviation/%	
Molar ratio, Al to Ca	Ca-atomic line	Ca-ionic line
0	100,0 ± 0,8	100,0 ± 1,7
1	98,6 ± 1,0	99,6 ± 0,8
3	98,6 ± 0,7	96,2 ± 1,9
10	96,4 ± 1,0	95,7 ± 0,2
30	92,4 ± 0,9	88,3 ± 1,6
100	85,1 ± 0,8	84,7 ± 0,8
Molar ratio, P to Ca	Ca-atomic line	Ca-ionic line
0	100,0 ± 1,2	100,0 ± 1,3
1	99,8 ± 0,6	102,1 ± 1,5
3	98,2 ± 0,9	98,7 ± 0,4
10	99,5 ± 1,1	100,9 ± 0,6
30	99,9 ± 1,1	105,2 ± 1,2
100	99,8 ± 0,6	104,0 ± 0,8
Molar ratio, Na to Ca	Ca-atomic line	Ca-ionic line
0	100,0 ± 1,2	100,0 ± 1,2
1	98,3 ± 0,8	100,2 ± 0,8
3	101,8 ± 1,8	100,0 ± 0,6
10	103,1 ± 0,9	101,4 ± 1,0
30	100,4 ± 1,0	101,3 ± 1,3
100	100,6 ± 0,9	107,5 ± 0,7

* 5x10s integrations on the Ca(I) 422,67 nm atomic line, and Ca(II) 315,89 nm ionic line.

TABLE 4-12: Interference tests for Al, P and Na on Ca-atomic line and Ca-ionic line emission, for spray chamber No. 2. Results given as mean net intensity* ± standard deviation, relative to the intensity in the absence of interferant, taken as 100%.

	Relative net Ca intensity ± std. deviation/%	
Molar ratio, Al to Ca	Ca-atomic line	Ca-ionic line
0	100,0 ± 1,3	100,0 ± 0,5
1	100,9 ± 0,9	102,0 ± 1,8
3	99,3 ± 0,5	102,2 ± 0,8
10	96,2 ± 1,2	100,2 ± 0,6
30	92,0 ± 1,0	92,0 ± 1,3
100	86,3 ± 0,6	86,8 ± 0,6
Molar ratio, P to Ca	Ca-atomic line	Ca-ionic line
0	100,0 ± 1,0	100,0 ± 1,2
1	100,7 ± 1,3	99,5 ± 0,8
3	100,3 ± 1,2	100,0 ± 0,6
10	100,5 ± 1,2	100,6 ± 1,0
30	100,3 ± 1,4	99,7 ± 1,1
100	99,3 ± 1,5	99,2 ± 0,6
Molar ratio, Na to Ca	Ca-atomic line	Ca-ionic line
0	100,0 ± 1,1	100,0 ± 0,9
1	99,6 ± 1,0	101,1 ± 0,6
3	100,4 ± 0,9	100,6 ± 0,5
10	98,9 ± 0,6	101,0 ± 0,7
30	101,0 ± 1,6	97,4 ± 0,6
100	97,6 ± 1,3	100,6 ± 0,4

* 5x10s integrations on the Ca(I) 422,67 nm atomic line, and Ca(II) 315,89 nm ionic line.

TABLE 4-13: Interference tests for Al, P and Na on Ca-atomic line and Ca-ionic line emission, for spray chamber No. 3. Results given as mean net intensity* ± standard deviation, relative to the intensity in the absence of interferant, taken as 100%.

	Relative net Ca intensity ± std. deviation/%	
Molar ratio, Al to Ca	Ca-atomic line	Ca-ionic line
0	100,0 ± 0,3	100,0 ± 0,6
1	100,0 ± 0,4	99,8 ± 0,5
3	100,3 ± 0,4	99,9 ± 0,8
10	100,0 ± 0,3	99,2 ± 0,5
30	99,6 ± 0,5	99,0 ± 0,6
100	98,1 ± 0,5	97,8 ± 0,8
Molar ratio, P to Ca	Ca-atomic line	Ca-ionic line
0	100,0 ± 0,5	100,0 ± 0,4
1	100,2 ± 0,8	100,7 ± 0,8
3	100,6 ± 0,8	100,3 ± 0,4
10	100,6 ± 0,6	101,6 ± 0,7
30	101,3 ± 0,6	102,1 ± 0,3
100	100,1 ± 0,3	100,8 ± 0,2
Molar ratio, Na to Ca	Ca-atomic line	Ca-ionic line
0	100,0 ± 0,7	100,0 ± 0,9
1	100,6 ± 0,6	100,7 ± 0,6
3	100,6 ± 0,8	100,3 ± 0,6
10	100,5 ± 0,6	99,2 ± 0,4
30	99,2 ± 0,2	99,8 ± 0,7
100	99,8 ± 0,7	99,4 ± 0,9

* 5x10s integrations on the Ca(I) 422,67 nm atomic line, and Ca(II) 315,89 nm ionic line.

TABLE 4-14: Interference tests for Al, P and Na on Ca-atomic line and Ca-ionic line emission, for spray chamber No. 4. Results given as mean net intensity* ± standard deviation, relative to the intensity in the absence of interferant, taken as 100%.

	Relative net Ca intensity ± std. deviation/%	
Molar ratio, Al to Ca	Ca-atomic line	Ca-ionic line
0	100,0 ± 1,9	100,0 ± 0,9
1	99,4 ± 1,2	100,3 ± 0,9
3	99,2 ± 3,6	101,7 ± 1,5
10	100,0 ± 4,0	98,6 ± 2,4
30	100,0 ± 1,8	100,0 ± 0,8
100	97,5 ± 1,2	93,3 ± 1,4
Molar ratio, P to Ca	Ca-atomic line	Ca-ionic line
0	100,0 ± 1,4	100,0 ± 2,8
1	103,4 ± 3,8	100,1 ± 1,0
3	99,4 ± 2,4	100,0 ± 2,1
10	102,3 ± 1,5	98,1 ± 0,9
30	104,2 ± 4,4	101,5 ± 3,4
100	101,0 ± 1,7	100,7 ± 3,4
Molar ratio, Na to Ca	Ca-atomic line	Ca-ionic line
0	100,0 ± 0,9	100,0 ± 1,4
1	98,4 ± 0,8	97,5 ± 0,9
3	99,3 ± 1,1	99,3 ± 3,8
10	99,1 ± 1,6	98,6 ± 1,0
30	97,1 ± 2,4	96,8 ± 2,0
100	98,2 ± 1,2	97,6 ± 1,0

* 5x10s integrations on the Ca(I) 422,67 nm atomic line, and Ca(II) 315,89 nm ionic line.

TABLE 4-15: Interference tests for Al, P and Na on Ca-atomic line and Ca-ionic line emission, for spray chamber No. 5. Results given as mean net intensity* ± standard deviation, relative to the intensity in the absence of interferant, taken as 100%.

	Relative net Ca intensity ± std. deviation/%	
Molar ratio, Al to Ca	Ca-atomic line	Ca-ionic line
0	100,0 ± 1,0	100,0 ± 1,9
1	98,9 ± 1,2	99,5 ± 2,3
3	97,2 ± 1,4	99,7 ± 1,5
10	97,2 ± 1,6	100,5 ± 0,9
30	99,7 ± 0,5	97,9 ± 1,0
100	99,9 ± 1,1	98,8 ± 2,3
Molar ratio, P to Ca	Ca-atomic line	Ca-ionic line
0	100,0 ± 1,4	100,0 ± 1,4
1	99,2 ± 1,9	101,0 ± 1,0
3	99,6 ± 1,7	99,1 ± 1,1
10	100,9 ± 1,3	99,4 ± 1,3
30	102,7 ± 1,9	100,8 ± 0,6
100	100,6 ± 1,2	100,0 ± 1,1
Molar ratio, Na to Ca	Ca-atomic line	Ca-ionic line
0	100,0 ± 1,5	100,0 ± 1,0
1	99,6 ± 1,0	99,8 ± 2,2
3	100,0 ± 0,8	102,3 ± 0,5
10	99,5 ± 1,0	102,5 ± 0,8
30	100,0 ± 1,0	99,9 ± 1,0
100	99,2 ± 1,3	98,3 ± 0,6

* 5x10s integrations on the Ca(I) 422,67 nm atomic line, and Ca(II) 315,89 nm ionic line.

TABLE 4-16: Interference tests for Al, P and Na on Ca-atomic line and Ca-ionic line emission, for spray chamber No. 8. Results given as mean net intensity* ± standard deviation, relative to the intensity in the absence of interferant, taken as 100%.

	Relative net Ca intensity ± std. deviation/%	
Molar ratio, Al to Ca	Ca-atomic line	Ca-ionic line
0	100,0 ± 0,3	100,0 ± 0,3
1	99,9 ± 0,4	100,1 ± 0,4
3	100,2 ± 0,4	101,2 ± 0,3
10	100,3 ± 0,5	100,1 ± 0,2
30	99,4 ± 0,3	99,3 ± 0,3
100	98,6 ± 0,4	97,5 ± 0,2
Molar ratio, P to Ca	Ca-atomic line	Ca-ionic line
0	100,0 ± 0,1	100,0 ± 0,2
1	100,0 ± 0,3	99,8 ± 0,3
3	100,3 ± 0,2	100,5 ± 0,3
10	100,4 ± 0,4	100,3 ± 0,2
30	100,9 ± 0,3	100,6 ± 0,3
100	100,6 ± 0,5	100,3 ± 0,2
Molar ratio, Na to Ca	Ca-atomic line	Ca-ionic line
0	100,0 ± 0,3	100,0 ± 0,3
1	99,9 ± 0,2	100,2 ± 0,3
3	100,4 ± 0,4	99,7 ± 0,4
10	100,1 ± 0,3	100,1 ± 0,2
30	100,1 ± 0,4	98,1 ± 0,3
100	100,6 ± 0,2	98,3 ± 0,1

* 5x10s integrations on the Ca(I) 422,67 nm atomic line, and Ca(II) 315,89 nm ionic line.

TABLE 4-17: Interference tests for Al, P and Na on Ca-atomic line and Ca-ionic line emission, for spray chamber No. 9. Results given as mean net intensity* ± standard deviation, relative to the intensity in the absence of interferant, taken as 100%.

	Relative net Ca intensity ± std. deviation/%	
Molar ratio, Al to Ca	Ca-atomic line	Ca-ionic line
0	100,0 ± 0,3	100,0 ± 0,4
1	100,1 ± 0,3	100,0 ± 0,4
3	99,8 ± 0,2	100,2 ± 0,5
10	100,2 ± 0,2	100,0 ± 0,3
30	100,0 ± 0,2	100,1 ± 0,2
100	100,5 ± 0,2	100,4 ± 0,3
Molar ratio, P to Ca	Ca-atomic line	Ca-ionic line
0	100,0 ± 0,4	100,0 ± 0,2
1	100,2 ± 0,4	100,7 ± 0,2
3	100,5 ± 0,2	100,2 ± 0,5
10	100,0 ± 0,1	99,8 ± 0,2
30	100,2 ± 0,4	100,0 ± 0,1
100	100,0 ± 0,4	99,6 ± 0,2
Molar ratio, Na to Ca	Ca-atomic line	Ca-ionic line
0	100,0 ± 0,2	100,0 ± 0,4
1	100,6 ± 0,2	100,4 ± 0,3
3	100,2 ± 0,1	100,1 ± 0,2
10	100,5 ± 0,1	100,1 ± 0,3
30	99,8 ± 0,2	98,5 ± 0,4
100	100,6 ± 0,2	98,1 ± 0,4

* 5x10s integrations on the Ca(I) 422,67 nm atomic line, and Ca(II) 315,89 nm ionic line.

In the case of sodium on calcium interference, chamber No. 1 showed an enhancement of Ca-ionic emission of 7,5% at a Na to Ca molar ratio of 100 to 1. For chambers 2, 3, 4, 5, 8 and 9, there is very little evidence of either interference of Na on Ca-atomic or Ca-ionic emission i.e., less than 3%.

During these tests for matrix interferences, the poor precision of chamber No. 4, as mentioned previously (section 4.4 and Table 4-8) was again noted (vide the standard deviations, Table 4-14, and compare with those for chamber No. 3 in Table 4-13).

4.8 Short term precision

In section 4.4 the precision over a 10s integration period, as used in conventional discrete sample analysis, was evaluated, and it was noted that the mean precision for all chambers tested, except No. 4, was less than 1% (Table 4-8), indicating acceptability for this manner of analysis. In FIA analysis, however, where the analytical signal is transient, short term precision of direct readout, without integration, is important.

As this study is directed in particular towards the FIA analysis of boron by ICP emission spectrometry, the short term signal noise, for the steady state emission signal of the B(I) 249,68 nm emission line, on aspiration of a 10 $mg.\ell^{-1}$ B standard is shown in Fig. 4-1. This figure clearly shows that chamber Nos. 1 and 4 have a poorer short term precision, making them less suitable for FIA use. The two chambers with the least noise in the steady state signals were chamber Nos. 5 and 9 (Fig. 4-1), indicating their suitability for FIA work.

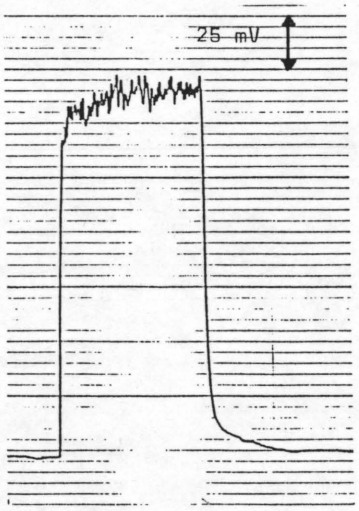

chamber No. 1.

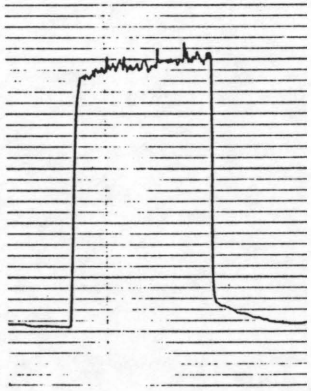

chamber No. 2.

chamber No. 3.

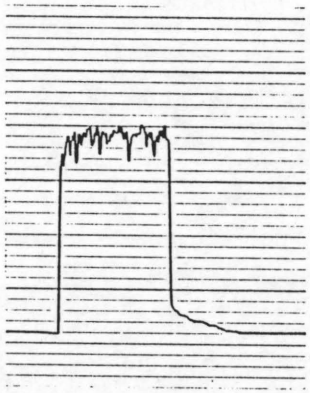

chamber No. 4.

chamber No. 5.

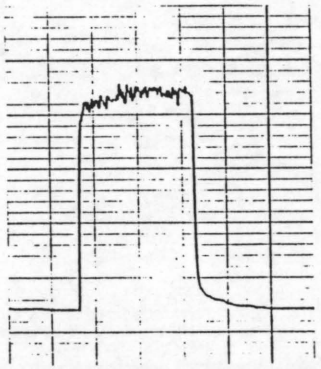

chamber No. 8.

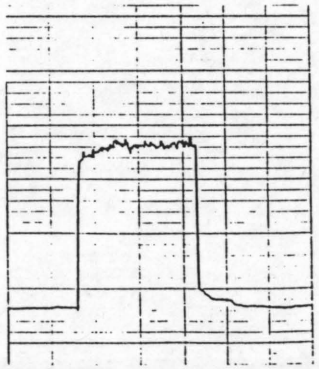

chamber No. 9.

Fig. 4-1: Steady state emission signals for 10 mg.ℓ^{-1} boron, found for the various spray chambers. The same recorder sensitivity was used in each case.

4.9 Performance of spray chamber No. 5 in the analysis of real samples

The 11 mℓ capacity spray chamber with a type T01 tangential aerosol outlet, i.e., chamber No. 5 (Fig. 3-5) gave good performance when used for the analysis of real samples, as shown by Kempster *et al* (1987). A comparison between the analyte concentration values found using the 110 mℓ commercial chamber (chamber No. 1) and chamber No. 5 is given in Table 4-18, and shows reasonable agreement between the two chambers. This indicates that chamber No. 5 is usable for discrete sample analysis, using the conventional discrete sample introduction procedure (Kempster, 1986; Kempster *et al*, 1987).

TABLE 4-18: Comparison of analyte concentrations found using the 110 mℓ chamber (a) and the short 11 mℓ chamber (b), for ten surface water samples in routine analysis, using the calibration procedure described by Kempster (1986). Each concentration value given is the mean of two determinations of concentration.

Sample Nos.	Spray Chamber*	Concentration/mg.ℓ$^{-1}$			Concentration/µg.ℓ$^{-1}$				
		Ca	Mg	Na	B	Fe	Mn	Sr	Zn
1	a	28,1	18,1	36,8	24	14	2	117	5
1	b	27,6	16,6	32,6	24	35	<2	104	<7
2	a	29,4	20,1	39,6	24	14	125	118	6
2	b	29,1	19,0	36,3	28	16	123	108	10
3	a	12,9	4,9	11,0	14	206	22	57	109
3	b	12,7	4,6	11,3	16	174	20	54	114
4	a	7,3	2,4	5,1	<6	674	264	36	<3
4	b	7,2	2,2	5,5	10	696	260	34	<7
5	a	3,3	1,6	3,2	<6	28	6	20	6
5	b	3,0	1,4	3,6	8	32	8	18	<7
6	a	11,9	5,0	6,2	10	109	4	84	20
6	b	11,5	4,6	6,5	16	95	4	76	24
7	a	44,3	15,9	29,7	142	4240	604	182	35
7	b	42,7	14,7	27,1	133	4140	567	164	35
8	a	30,4	30,7	58,2	196	44	4	216	<3
8	b	29,9	28,2	50,0	179	45	<2	196	<7
9	a	36,8	39,9	79,5	198	22	1	268	<3
9	b	36,6	37,4	70,6	184	23	<2	250	<7
10	a	16,2	5,8	6,7	<6	102	14	99	5
10	b	16,2	5,4	6,7	9	78	11	93	<7

* a = 110 mℓ chamber, No. 1 (Fig. 3-1).
b = 11 mℓ chamber, No. 5, with a TOI outlet (Fig. 3-5).

4.10 Summary and conclusion

An evaluation of the spray chambers showed that wash-in time to 90% of steady state signal was approximately halved for the small volume spray chambers, with volume of 17 mℓ and less. Mean precision of analyte signal, over a 10s integration period for the 21 analyte elements tested, was less than 1% except for chamber No. 4, showing the unsuitability of a conventional right-angle outlet positioning of the aerosol exit tube in small volume double-barrel spray chambers. The short term precision of chamber Nos. 5 and 9 (Fig. 4-1) was superior to that of the other chambers, and indicated the potential of these two chambers for FIA work.

While some loss of sensitivity for boron was observed for the small spray chambers, the detection limits for boron were comparable with that of chamber No. 1, except in the case of chamber No. 4. A boron detection limit of less that 10 $\mu g.\ell^{-1}$ is quite adequate for environmental water sample analysis.

Whereas the commercial 110 mℓ spray chamber showed the presence of aluminium on calcium volatilization interference, the reduced volume spray chambers were less susceptible to this interference, with this type of interference being almost absent in the case of chamber Nos. 5 and 9. Very little interference was observed from either P or Na on Ca for any of the chambers.

The two chambers showing the best overall characteristics for FIA use were the 11 mℓ double-barrel design with a T01 type tangential outlet tube (chamber No. 5, Fig. 3-5) and the 12 mℓ double-barrel design with a T03 type tangential outlet tube (chamber No. 9, Fig. 3-9).

The evaluation of chamber Nos. 1, 5 and 9 in FIA determination of boron by ICP emission spectrometry will be given in the next chapter.

CHAPTER 5: DETERMINATION OF BORON BY FIA-ICP

5.1 Introduction

This chapter describes the use of the FIA technique to introduce samples to the ICP source, and the establishment of those conditions allowing RFA (rapid flow analysis). Initially two small volume chambers were tested *viz.*, chamber No. 5 and No. 9, but the precision of the latter was inferior to that of chamber No. 5. RFA was thus only investigated for chamber No. 1 and chamber No. 5.

During the investigation of the FIA-ICP method, a major limitation was found to be the instability of the analogue output signal of the particular spectrometer used, the electronics of the analogue output being designed for profile centering purposes only, and not intended to be used for analytical purposes.

In this chapter the following subjects are discussed:

(i) The instrument setup used for the FIA-ICP measurements.

(ii) Precision of the FIA signal for chamber Nos. 1, 5 and 9.

(iii) Effect of injection volume on precision and on peak width.

(iv) Effect of carrier flow rate on peak width, and on sensitivity for chamber Nos. 1 and 5.

(v) Analytical characteristics of the FIA-ICP combination for the determination of boron at a sampling rate of 320 samples per hour.

All boron signals were recorded using the 249,68 nm boron analytical line on the ICP spectrometer.

5.2 Instrumental setup

The following instrumentation was used for FIA-ICP analysis:

(i) A Carle sampling valve, catalogue No. 2013, with a groove dead volume of 11 µℓ, with two sampling loops, and actuator. For sample loops, Tygon tubing was used. Four different loop volumes were used viz., 408 µℓ, 300 µℓ, 200 µℓ and 100 µℓ. The loop volumes given include the internal volume of the valve and stainless steel connnecting tubes to the valve. The internal diameter (i.d.) of the tygon sample loop tubes were 1,14 mm; 1,02 mm; 0,88 mm; and 0,64 mm for the 408 µℓ, 300 µℓ, 200 µℓ and 100 µℓ loops respectively.

(ii) A Cenco sampler, catalogue No. 345.17.700, which was actuated by a laboratory built electronic timer. The timer also served to actuate the Carle sampling valve. The logic switches of the Cenco sampler were set on zero, and the sampler activated by wires from the electronic timer, which were attached to the sample/wash switches of the Cenco sampler.

(iii) A 34000 ICP emission spectrometer, the basic characteristics of which were given in Chapter 4 (Table 4-1). The carrier stream tube from the Carle sampling valve was attached to the concentric pneumatic nebulizer of the spectrometer. This being either the Meinhard nebulizer with chamber No. 1 or the modified concentric nebulizer with chamber No. 5 or 9.

(iv) The analogue output of the spectrometer was connected to the input of a model 056-1002 Hitachi potentiometric chart recorder to record FIA peaks.

(v) A single channel Gilson Minipuls II peristaltic pump (P1, Fig. 5-1) to control the carrier stream flow (deionised water* or ϕ=0,01 volume fraction nitric acid) through the sampling valve to the nebulizer.

(vi) A dual channel Gilson Minipuls II peristaltic pump (P2, Fig. 5-1) to aspirate the sample from a sample cup and fill the sample loop of the sampling valve. To provide a sufficiently fast uptake rate, to fill the sample loops between injections into the carrier stream, it was necessary to use two 1,42 mm i.d. tygon tubes in parallel in the pump. At a pump digital setting of 900 this provided a sample loop filling flow rate of 6,3 $m\ell.min^{-1}$.

The experimental setup is indicated schematically in Fig. 5-1.

---

* Deionised water was used as carrier for all boron determinations, except in the tests for interferences from other metals, where ϕ=0,01 nitric acid was used. For other analyte elements (Chapters 6 & 7), ϕ=0,01 nitric acid was used as carrier.

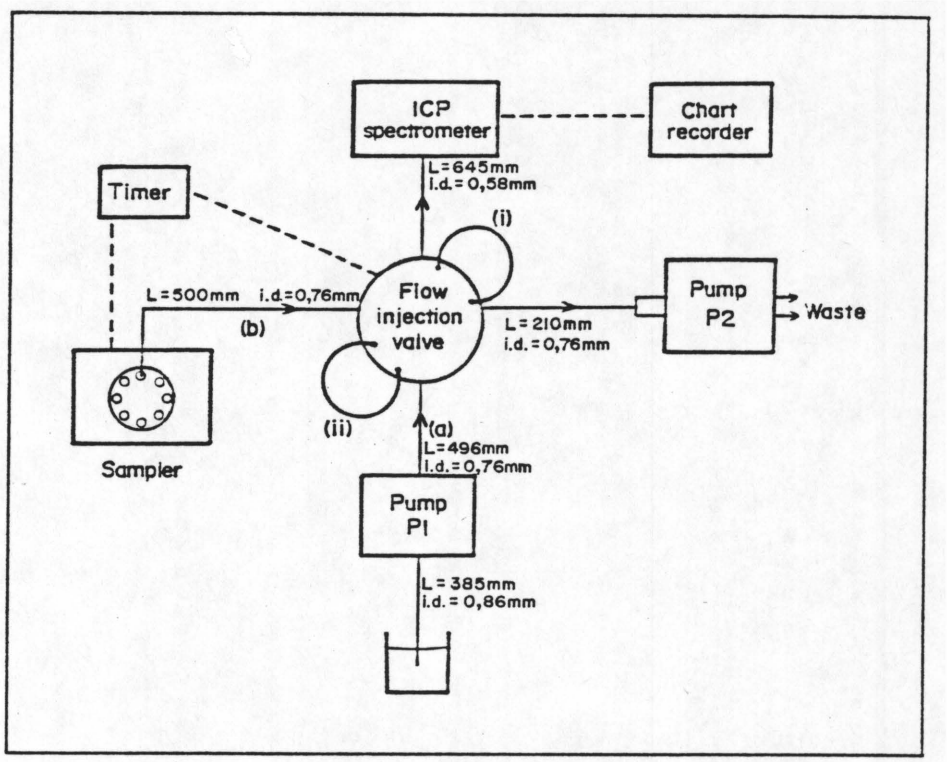

Fig. 5-1: Schematic diagram of FIA-ICP instrumental arrangement. The carrier-stream (a) is propelled under positive pressure, from pump P1, through each of the sample loops (i or ii) of the flow injection valve in turn, to the nebulizer of the ICP spectrometer; while the opposite sample loop is, in its turn, filled by negative pressure from pump P2, the loop being filled with the sample through the sample stream (b).

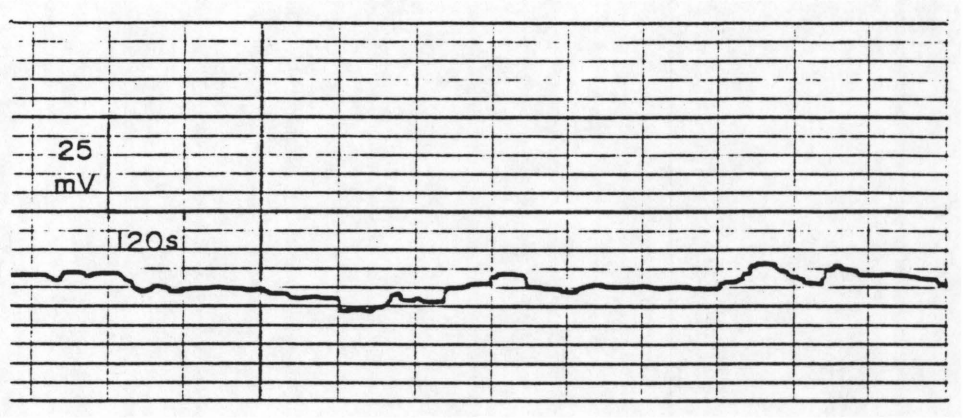

Fig. 5-2: The baseline instability; consequent to the instability in the analogue signal from the spectrometer's electronics, occurred irrespective of whether the plasma was on or off.

The detail on the dimensions of the connecting flow lines is as follows:

(a) A 496 mm length of 0,76 mm i.d. tygon tubing to transport the carrier stream from the pump P1 (Fig. 5-1) to the carrier inlet port of the sampling valve. The carrier uptake tube to pump P1 was a 385 mm length of 0,86 mm i.d. polyethylene tubing. For the initial experiments, a carrier flow rate* of 1,3 $m\ell.min^{-1}$ with a 1,14 mm i.d. Sterilin pump tube was used. For the subsequent experiments at higher carrier flow rates, however, a 1,42 mm i.d. Sterilin pump tube was used.

(b) A 645 mm length of 0,58 mm i.d. polyethylene tubing to transport the carrier stream from the carrier outlet port of the sampling valve to the nebulizer and spray chamber of the ICP source.

(c) To transport the sample from the sampler to the sample inlet port of the sampling valve, a 653 mm length of 0,58 mm i.d. polyethylene tubing was initially used, but due to the appearance of air bubbles as a consequence of the negative pressure exerted by pump P2 (Fig. 5-1), this was replaced by a 500 mm length of 0,76 mm i.d. tygon tubing. Using the latter tubing, degassing of the sample was not a problem. A 110 mm length of 1 mm i.d. stainless steel tubing was connected to the end of the sample uptake tubing for aspiration of samples on the Cenco sampler.

---

* A carrier flow rate of 1,3 $m\ell.min^{-1}$ was chosen initially as this was found to be the optimum uptake rate with conventional ICP sample introduction (Kempster, 1986).

(d) To conduct excess sample to waste, a 210 mm length of 0,76 mm i.d. tygon tubing transported the excess sample from the waste port of the sampling valve to pump P2 (Fig. 5-1). Just before pump P2, the waste stream was split into two streams, using a Y-glass fitting connected to two 1,42 mm i.d. Sterilin pump tubes.

The electronic timer, which had independent adjustment controls for the sampling rate, and the wash time, was adjusted for a wash time between samples of 2,6 s. The probe on the Cenco sampler took 1,4 s to move from wash receptacle to sample cup, or vice versa. The time spent by the probe in each sample cup depended on the sampling rate. This time was for instance 5,8 s at 320 samples per hour, and 30,6 s at 100 samples per hour. The actuation of the sampling valve occurred just before the rear end of the aspirated sample plug reached the sample inlet port of the sampling valve.

5.3 Limitation imposed by spectrometer electronics on detection limit

To record FIA signal peaks, the analogue output of the spectrometer was connected to a potentiometric chart recorder, as mentioned in Section 5.2. As the analogue output of the spectrometer was only intended for use in checking or aligning exit slit central profile positions, it did unfortunately not have the stability required for analytical purposes, especially for the purpose of recording the transient FIA signals.

The analogue output of the spectrometer had a baseline instability of around 10 mV (Fig. 5-2). This instability occurred irrespective of whether the plasma was on or off, thus indicating that the source of the erratic baseline was not the emission source. Further, the instability remained unchanged when the recorder was connected to the same stabilized power source and same earth as the spectrometer.

The baseline instability of the spectrometer's analogue output had the unfortunate consequence that the detection limit for boron was degraded about 2 orders of magnitude from that achieved by conventional analysis using 10 s integrations. Attempts to filter out the baseline noise using a capacitor and resistor, without also filtering out the FIA signal peaks was not successful.

5.4 Noise limitation at high concentrations of analyte element

A limitation of another sort, occurring at high concentrations of analyte element, was the noise in steady state signals found at the upper limit of the analytical range. This noise may, of course have contributions from both source noise and spectrometer electronics noise. In Fig. 5-3, the steady state signals for chamber No. 1, at a carrier rate of 1,3 $m\ell.min^{-1}$, are shown for boron concentrations from 0,5 $mg.\ell^{-1}$ to 25 $mg.\ell^{-1}$ B. The 25 $mg.\ell^{-1}$ B signal shows a noisy steady state signal, while little or no noise is visible at boron concentrations of 5 $mg.\ell^{-1}$ or lower. As the analogue signal from the spectrometer was unfiltered, the signal noise may be expected to affect the precision of FIA analytical measurements.*

5.5 Precision of FIA peak height

A comparison of the precision of measurement for the FIA signal given with a 10 $mg.\ell^{-1}$ B standard, for chamber Nos. 1, 5 and 9 is shown in Fig. 5-4 and Table 5-1. For this comparison, a sample volume of 408 $\mu\ell$ was injected into a deionised water stream flowing at 1,3 $m\ell.min^{-1}$, at a sampling rate of 100 per hour.

---

* The steady state noise (Fig. 5-3 for example) has a very important implication where FIA is used for sample introduction, particularly for low dispersion ratios. Depending on where the FIA signal peak falls, in relation to the noise, outliers will occur.

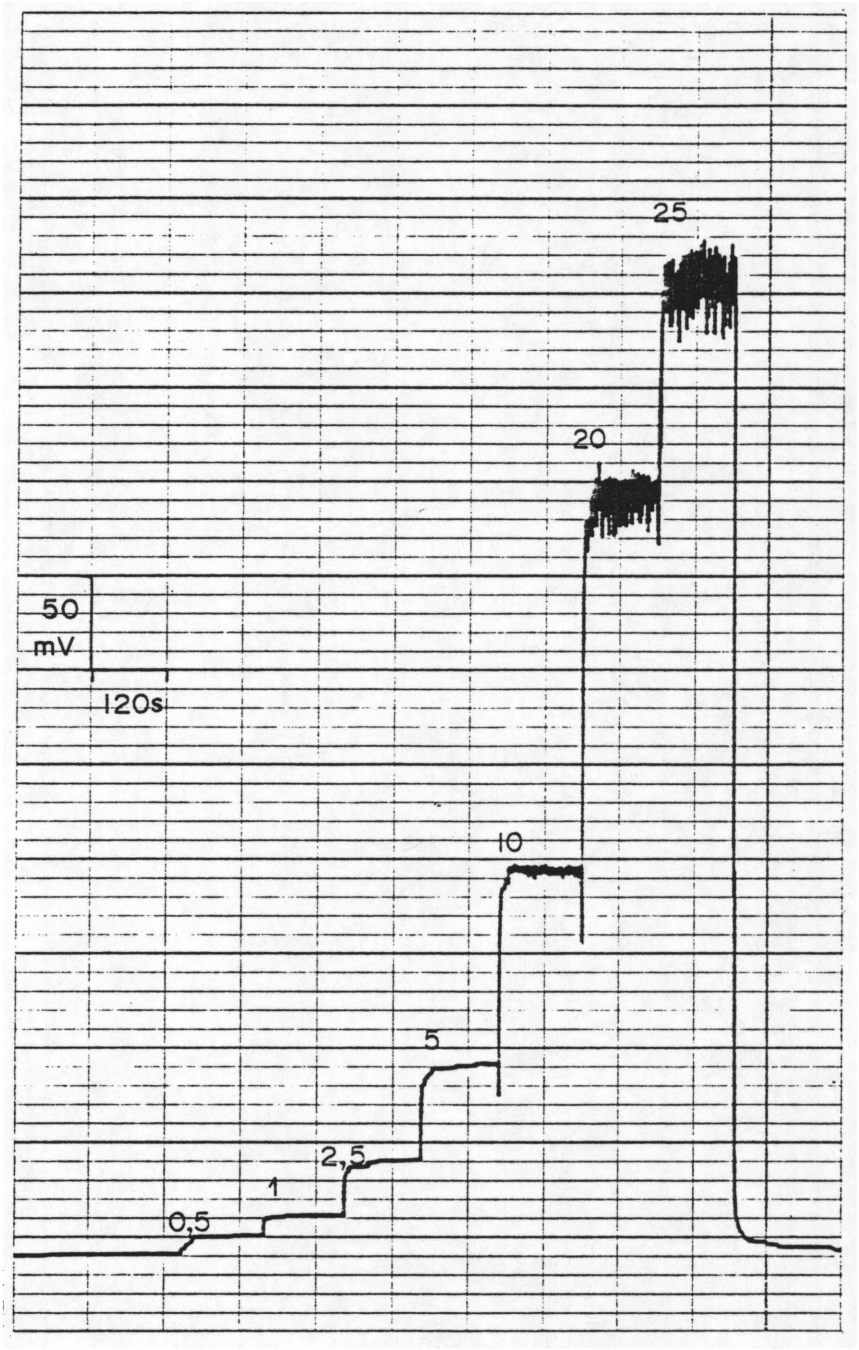

Fig. 5-3: Steady state signals for boron concentrations from 0,5 to 25 mg.ℓ$^{-1}$ B, using chamber No. 1, at a carrier flow rate of 1,3 mℓ.min^{-1}, at 1V FSD and 5 mm.min^{-1} chart speed, showing the noise in the steady state signals, particularly at the higher concentrations.

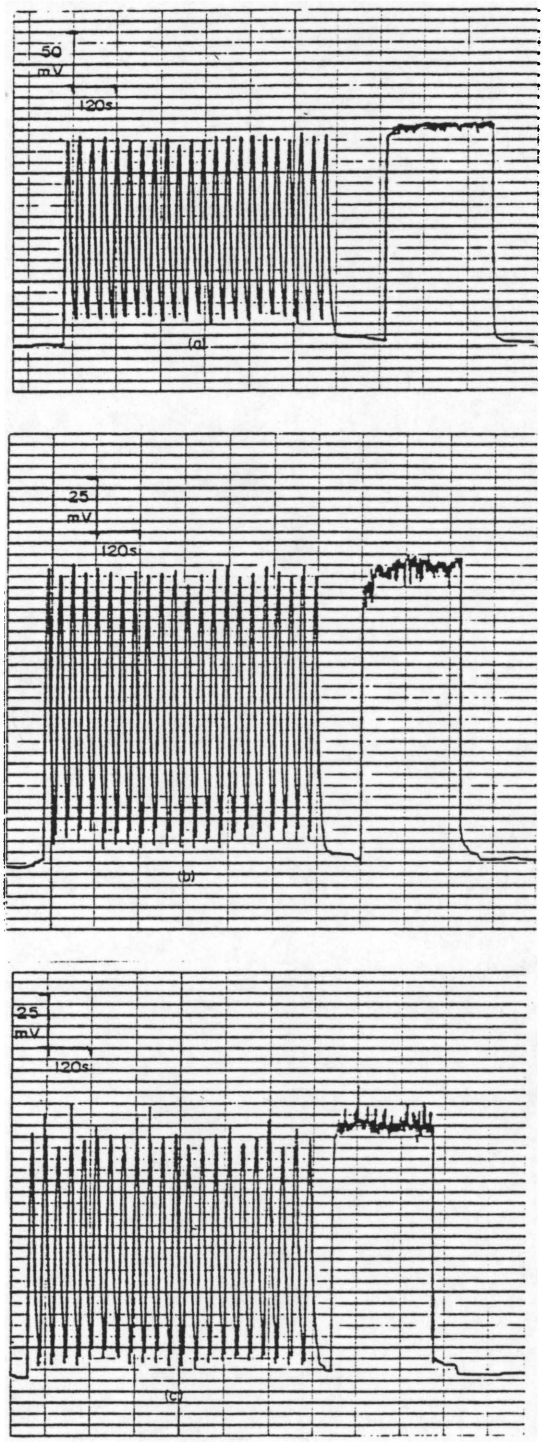

Fig. 5-4: Comparison of reproducibility of FIA signals and steady state, for chamber Nos. 1, 5 and 9, shown in (a), (b) and (c) respectively, for a 10 $mg.\ell^{-1}$ boron standard. Injection volume was 408 $\mu\ell$, sampling rate 100 per hour, and carrier flow rate 1,3 $m\ell.min^{-1}$.

Both chamber Nos. 1 and 5 gave good precision, with a RSD of less than 2% (Table 5-1). Chamber No. 9, on the other hand had a poor precision, giving a RSD of 5,2%. Chamber No. 9 was consequently excluded in further experiments.

Also shown in Table 5-1 is the dispersion ratio D. The D-value with chamber No. 1 corresponded to an FIA signal of 95% of the steady state signal; while the D-value using chamber No. 5 corresponded to an FIA signal of 98% of the steady state signal.

TABLE 5-1: Relative standard deviation (RSD) of peak height for 22 replicates of a 408 µℓ sample containing 10 $mg.ℓ^{-1}$ B, at a sampling rate of 100 per hour*, found using spray chambers 1, 5 and 9. Also given is the dispersion ratio D.

Chamber No.	RSD/%	D
1	1,4 %	1,05
5	1,6 %	1,02
9	5,2 %	1,02

* Carrier flow rate of 1,3 $mℓ.min^{-1}$.

While a FIA sampling rate of only 100 per hour** cannot really be considered as RFA (rapid flow analysis), it is of interest from a historical viewpoint. For instance, Greenfield (1983) used a FIA sampling rate of 90 samples per hour for calcium determination and obtained a precision of less than 2% RSD for a 40 $mg.ℓ^{-1}$ calcium concentration.

** If samples are analyzed in triplicate, then a FIA sampling rate of 100 per hour gives an actual analysis rate of approximately 33 per hour, which is similar to the analytical rate of conventional sample introduction by ICP emission spectrometry, and thus cannot be considered as rapid flow analysis.

The precision of boron determination by FIA-ICP, at a sampling rate of 100 per hour, with 408 µℓ injected sample at a carrier flow rate of 1,3 mℓ.min^{-1} is given in Table 5-2 for chamber No. 1, and in Table 5-3 for chamber No. 5. These tables show that the precision of boron determination, at 100 samples per hour was around 1 to 2% RSD, for both chambers, for a boron concentration of from 10 to 25 mg.ℓ$^{-1}$ B.

In order to speed up the analytical rate, and achieve rapid flow analysis, sample volume was decreased and carrier flow rate increased. This led to a slight deterioration in precision.

TABLE 5-2: Reproducibility (RSD%) of FIA peak height ($\bar{H} \pm \sigma$/mm) signals, for 10 replicate measurements for boron concentrations (C) between 0,5 and 25 mg.ℓ$^{-1}$ B for chamber No. 1; using a carrier flow rate of 1,3 mℓ.min^{-1}, an injected sample volume of 408 µℓ, and a sampling rate of 100 per hour.*

C/mg.ℓ$^{-1}$B	$\bar{H} \pm \sigma$/mm	RSD%
0,5	2,4 ± 0,4	17%
1,0	4,9 ± 0,3	6,1%
2,5	13,7 ± 0,4	2,9%
5,0	28,3 ± 1,1	3,9%
10,0	57,2 ± 1,0	1,7%
20,0	120,6 ± 1,5	1,2%
25,0	152,5 ± 1,1	0,7%

* Recorder range setting of 1,0V FSD.

TABLE 5-3: Reproducibility (RSD%) of FIA peak height ($\bar{H} \pm \sigma$/mm) signals, for 10 replicate measurements for boron concentrations (C) between 0,5 and 25 mg.ℓ$^{-1}$B for chamber No. 5; using a carrier flow rate of 1,3 mℓ.min^{-1}, an injected sample volume of 408 µℓ, and a sampling rate of 100 per hour.*

C/mg.ℓ$^{-1}$B	$\bar{H} \pm \sigma$/mm	RSD%
0,5	2,2 ± 0,8	36%
1,0	4,7 ± 0,7	15,1%
2,5	13,6 ± 0,8	5,9%
5,0	30,3 ± 0,5	1,6%
10,0	64,4 ± 1,5	2,3%
20,0	131,2 ± 2,1	1,6%
25,0	164,6 ± 3,5	2,1%

* Recorder range setting of 0,5V FSD.

5.6 Effect of injected sample volume on precision and on peak width

An investigation of the influence of injected sample volume on precision, for chamber Nos. 1 and 5 is shown in Table 5-4, for injected sample volumes of 408; 300; 200; and 100 µℓ. There was little difference in precision for the former two sample volumes, but a deterioration in precision was observed in the case of the latter two sample volumes, particularly for the 100 µℓ sample volume, where precision was poor.

The effect of injected sample volume on peak width at half height ($w_{0,5}$) is shown in Table 5-5. This showed that peak width decreases as the sample volume decreases. This result is to be expected, as for a given carrier tube radius, the length of the sample plug will decrease as the

volume injected is decreased. The transit time of the plug through the nebulizer is thereby shortened, and a narrower peak width is consequently observed. That the volume of a sample plug influences peak width can also be inferred if equations 8 and 9 (chapter 2) are inspected, while considering that the volume occupied by the sample plug is $\pi r^2 L^*$. Van Staden and Van Vliet (1984) have also referred to this influence of the length of the sample plug when studying the relationship between precision and injected volume. A narrow peak width is desirable to minimize peak overlap and consequently allow a rapid rate of analysis. As shown in Table 5-4, however, a deterioration in precision occurs particularly at an injected sample volume of 200 µℓ and less. As a compromise, a sample volume of 300 µℓ was chosen for further work.

TABLE 5-4: Effect of injected sample volume (V_i) on precision (10 measurements of peak height) given as RSD for a 10 $mg.ℓ^{-1}$ B standard, at a carrier flow rate of 1,3 $mℓ.min^{-1}$, for chamber Nos. 1 and 5.

V_i/µℓ	RSD%	
	Chamber 1	Chamber 5
100	7,4%	9,4%
200	2,9%	4,7%
300	1,3%	2,8%
408	1,5%	2,3%

* r = radius, and L = length of sample plug.

TABLE 5-5: Effect of injected sample volume (V_i) on peak width at half height ($w_{0,5}$), for a 10 mg.ℓ$^{-1}$ B standard, at a carrier flow rate of 1,3 mℓ.min^{-1}, for chamber Nos. 1 and 5.

V_i/µℓ	$w_{0,5}$/s*	
	Chamber 1	Chamber 5
100	9,2 ± 0,3	7,6 ± 0,4
200	9,8 ± 0,8	9,0 ± 0,4
300	13,1 ± 1,0	12,3 ± 0,2
408	17,2 ± 0,6	15,8 ± 0,3

* mean ± standard deviation for 4 measurements.

TABLE 5-6: Effect of injected sample volume (V_i) on dispersion ratio (D) for a 10 mg.ℓ$^{-1}$ B standard, at a carrier flow rate of 1,3 mℓ.min^{-1}, for chamber Nos. 1 and 5.

V_i/µℓ	D	
	Chamber 1	Chamber 5
100	2,23	2,04
200	1,24	1,24
300	1,12	1,15
408	1,05	1,02

A decrease in the sample volume injected is also associated with an increase in the dispersion ratio D (Table 5-6). The FIA peak almost reaches the steady state height in the case of an injected volume of 408 µℓ, the FIA peak reaching 95% (D = 1,05) of the steady state value with chamber No. 1, and 98% (D = 1,02) for the steady state value with chamber No. 5. For an injected volume of 100 µℓ, the analagous values are 45% of steady state (D = 2,23) for chamber No. 1, and 49% (D=2,04) of steady state height for chamber No. 5.

The deterioration in precision, and decrease in peak height as the sample volume is decreased from 300 µℓ to 100 µℓ is illustrated by the FIA and steady state recordings in Fig. 5-5.

5.7 Effect of carrier stream flow rate on peak width

From the equation of Vanderslice (equation 10, chapter 2, section 2.2) it is apparent that increasing the carrier flow rate should result in a decrease in peak width. While the baseline-to-baseline width is given by equation 10, this is not easily measured due to the peak tailing and consequent uncertainty about when the tail end of the peak actually coincides with the baseline (Fig. 5-6). Thus, in this study the width at one fiftieth of peak height was measured as an approximation of the baseline width. In addition, the peak width at one tenth of peak height and at half peak height was also measured.

Peak widths were determined for a 300 µℓ injected sample volume of 10 $mg.\ell^{-1}$ B, for chamber No. 1 and chamber No. 5, from a carrier flow rate of 0,5 $m\ell.min^{-1}$ to a carrier flow rate of 3,5 $m\ell.min^{-1}$.

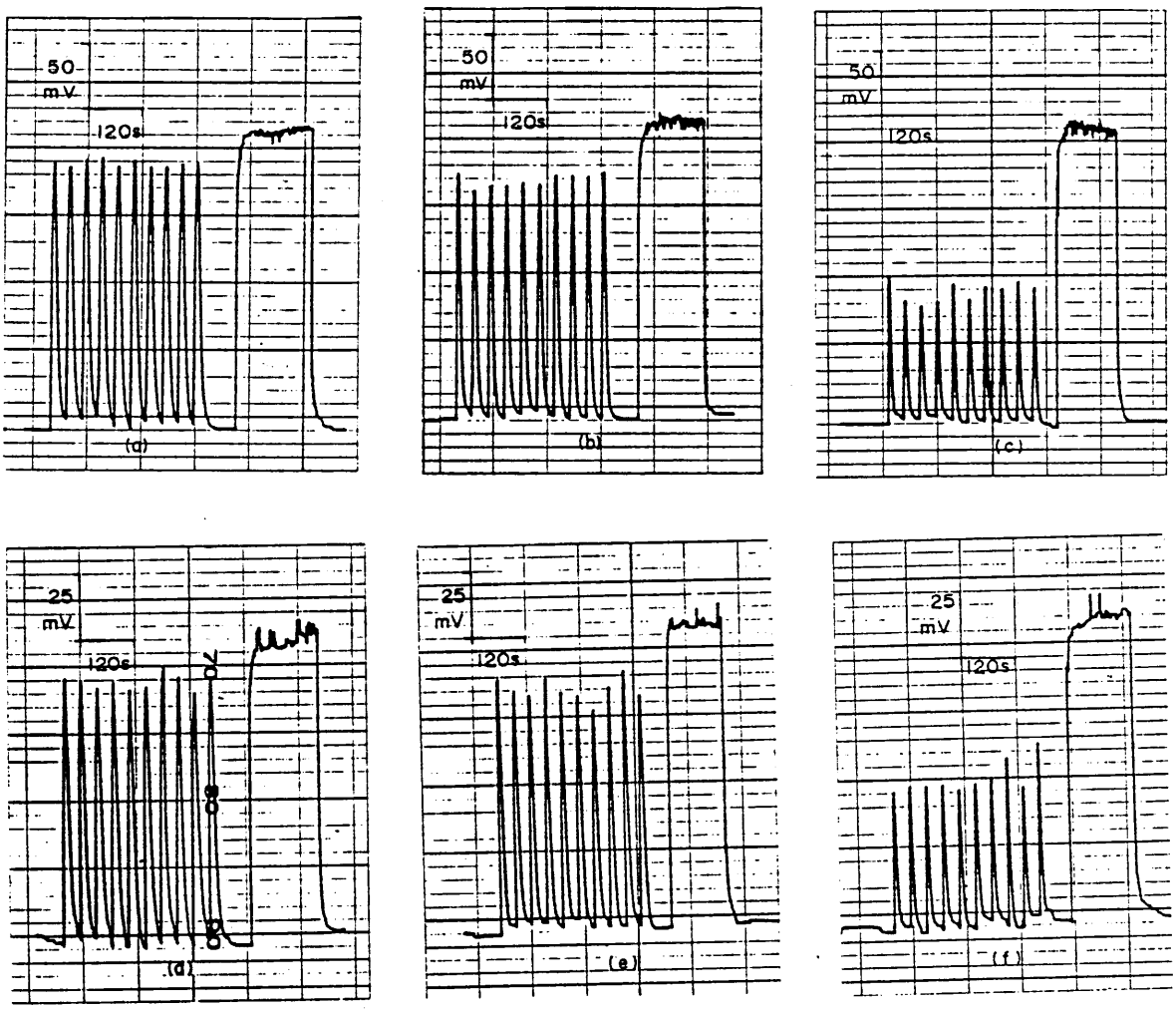

Fig. 5-5: Effect of injected sample volume on reproducibility, for 10 replicate injections of a 10 mg.ℓ^{-1} B standard, for chamber No. 1 (a to c), and chamber No. 5 (d to f). Injected sample volumes were 300 µℓ (a and d); 200 µℓ (b and e); and 100 µℓ (c and f). Note how the FIA peak height decreases with respect to the steady state signal as the injected volume is decreased.

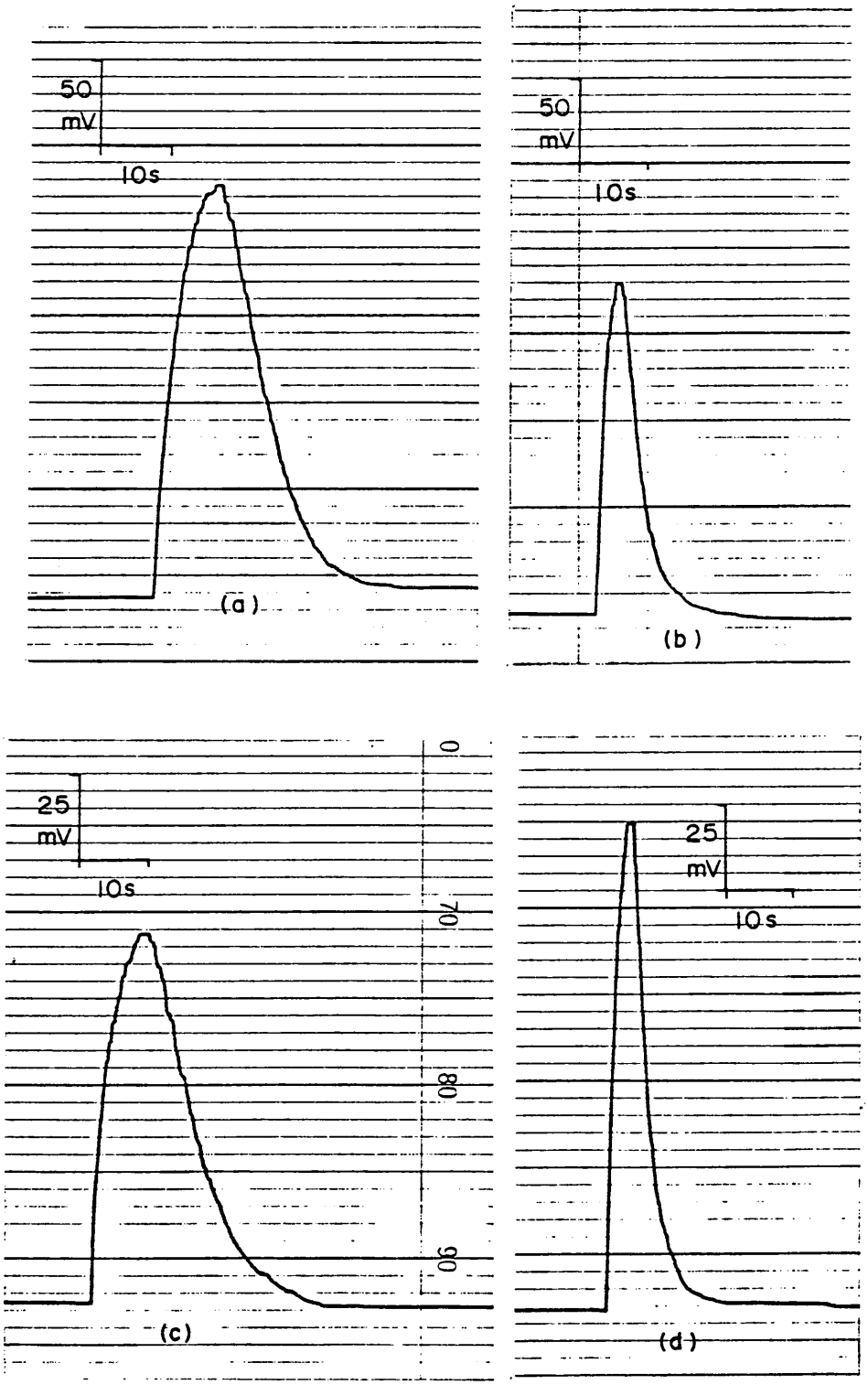

Fig. 5-6: Effect of carrier flow rate on peak width for chamber No. 1 (a and b), and chamber No. 5 (c and d) for a 300 µℓ injected sample of a 10 $mg.ℓ^{-1}$ B standard. Increasing the carrier flow rate from 1,3 (a and c) to 3,5 (b and d) $mℓ.min^{-1}$ results in a decrease in peak width. Note also the tailing of the rear end of the peaks.

The peak widths found are given in Tables 5-7 to 5-9, which give the peak widths at half height, one tenth height and one fiftieth height respectively. Note how peak width decreases with increasing flow rate, and also how the peak widths for chamber No. 5 tend to be smaller than those found for chamber No. 1, particularly at the more rapid carrier flow rates. This width difference is apparent at half height (Table 5-7) and one tenth height (Table 5-8). At one fiftieth height (Table 5-9) the difference is hidden by the uncertainty of measurement.

TABLE 5-7: Effect of carrier flow rate (F_c) on mean peak width, at half height ($\bar{w}_{0,5}$) given in seconds, of the FIA peak produced by a 300 µℓ injected sample of 10 mg.ℓ$^{-1}$B, for chamber Nos. 1 and 5.

F_c/mℓ.min^{-1}	Chamber No. 1 $\bar{w}^*_{0,5}$/s ± σ	Chamber No. 5 $\bar{w}^*_{0,5}$/s ± σ
0,5	31,4 ± 0,8	32,1 ± 1,2
0,8	22,4 ± 0,4	21,1 ± 0,9
1,1	16,7 ± 0,3	15,9 ± 0,4
1,3	13,7 ± 0,5	12,9 ± 0,2
1,55	11,5 ± 0,4	10,8 ± 0,4
1,85	10,1 ± 0,2	9,0 ± 0,9
2,1	9,2 ± 0,1	7,9 ± 0,2
2,4	8,0 ± 0,2	6,8 ± 0,4
2,8	6,6 ± 0,2	6,0 ± 0,2
3,1	6,1 ± 0,2	5,2 ± 0,1
3,5	5,1 ± 0,1	4,7 ± 0,2

* mean ± std. deviation for 4 measurements.

TABLE 5-8: Effect of carrier flow rate (F_c) on mean peak width, at one tenth height ($\bar{w}_{0,1}$) given in seconds, of the FIA peak produced by a 300 µℓ injected sample of 10 mg.ℓ$^{-1}$B, for chamber Nos. 1 and 5.

F_c/mℓ.min^{-1}	Chamber No. 1 $\bar{w}^*_{0,1}$/s ± σ	Chamber No. 5 $\bar{w}^*_{0,1}$/s ± σ
0,5	57,8 ± 1,4	61,6 ± 4,2
0,8	40,5 ± 1,3	38,4 ± 2,5
1,1	29,8 ± 0,3	30,3 ± 1,4
1,3	24,8 ± 0,7	24,1 ± 1,4
1,55	20,8 ± 0,5	19,9 ± 1,6
1,85	18,2 ± 0,2	17,5 ± 1,6
2,1	16,3 ± 0,4	14,8 ± 0,6
2,4	14,4 ± 0,3	13,4 ± 0,6
2,8	12,3 ± 0,4	10,7 ± 0,3
3,1	11,2 ± 0,3	10,2 ± 0,5
3,5	10,0 ± 0,2	9,8 ± 0,1

* mean ± std. deviation for 4 measurements.

TABLE 5-9: Effect of carrier flow rate (F_c) on mean peak width, at one fiftieth height ($\bar{w}_{0,02}$) given in seconds, of the FIA peak produced by a 300 µℓ injected sample of 10 mg.ℓ$^{-1}$B, for chamber Nos. 1 and 5.

F_c/mℓ.min^{-1}	Chamber No. 1 $\bar{w}^*_{0,02}$/s ± σ	Chamber No. 5 $\bar{w}^*_{0,02}$/s ± σ
0,5	79,5 ± 3,4	74,0 ± 10,5
0,8	58,9 ± 5,6	58,0 ± 9,8
1,1	39,5 ± 1,7	48,3 ± 9,8
1,3	35,2 ± 2,5	34,0 ± 3,8
1,55	28,4 ± 1,4	30,5 ± 3,1
1,85	23,4 ± 1,3	26,2 ± 5,8
2,1	21,6 ± 1,1	21,6 ± 2,2
2,4	20,1 ± 0,7	23,4 ± 2,7
2,8	16,5 ± 0,7	14,9 ± 1,6
3,1	17,0 ± 0,9	15,5 ± 1,5
3,5	16,0 ± 1,9	16,5 ± 2,5

* mean ± std. deviation for 4 measurements.

TABLE 5-10: The linear correlation coefficients (r) firstly between carrier flow rate (F_c) and the logarithm of peak width (ln w); and secondly, between the logarithm of carrier flow rate (ln F_c) and the logarithm of peak width (ln w). Widths were measured at 0,5; 0,1; and 0,02 of peak maximum height, for chamber Nos. 1 and 5, for FIA peaks on injecting 300 µℓ 10 mg.ℓ$^{-1}$ B into the carrier stream.*

r(x, y)**		Chamber No. 1	Chamber No. 5
$r(F_c, \ln w_{0,5})$	=	-0,975	-0,968
$r(F_c, \ln w_{0,1})$	=	-0,966	-0,958
$r(F_c, \ln w_{0,02})$	=	-0,940	-0,953
$r(\ln F_c, \ln w_{0,5})$	=	-0,998	-0,999
$r(\ln F_c, \ln w_{0,1})$	=	-0,999	-0,998
$r(\ln F_c, \ln w_{0,02})$	=	-0,993	-0,980

* data taken from Tables 5-7 to 5-9
** linear correlation coefficient between x and y.

A highly linear correlation, negative in sign, was found to exist between the natural logarithm of carrier flow rate F_c, and the natural logarithm of peak width. The linear correlation coefficients found are given in the lower half of Table 5-10. Thus, the natural logarithm of peak width may be expressed as a linear function of the logarithm of carrier flow rate:

$$\ln w_k = b.\ln F_c + i \quad \ldots \quad (37)$$

Where w_k = the full width in seconds, measured at the kth proportion of full peak height,

F_c = the carrier flow rate in mℓ.min^{-1},

b = the slope term,

and i = the intercept term.

The value of b, for chamber No. 1, is -0,933; -0,915; and -0,883, for a k value of 0,5; 0,1; and 0,02 respectively. The corresponding value of i is 2,865; 3,458; and 3,777 for a k value of 0,5; 0,1; and 0,02 respectively.

The value of b, for chamber No. 5 is -1,006; -0,980; and -0,882, for a k value of 0,5; 0,1; and 0,02 respectively. The corresponding value of i is 2,813; 3,445; and 3,800 for a k value of 0,5; 0,1; and 0,02 respectively.

It is readily shown that the slope term b, in equation 37 corresponds to the negative of the exponent of the L/q term in the Vanderslice equation for baseline-to-baseline width (equation 10, chapter 2). Using the assumption that the full width at one fiftieth peak maximum height $w_{0,02}$ may be used as an approximation of the baseline width Δt, the Vanderslice equation (10) may be written as:

$$\ln w_{0,02} = -0,64 \ln q + i \qquad \ldots \quad (38)$$

Where q is the flow rate in $m\ell.min^{-1}$,

and i is given by;

$$i = \ln\left(\frac{35,4.\ r^2.f.\ L^{0,64}}{D^{0,36}}\right)$$

where the variables are as given for equation 10.

Equation 38 is identical in form to equation 37. The experimental values for b found here were -0,883 for chamber No. 1, and -0,882 for chamber No. 5, implying values for the L/q exponent in the Vanderslice equation of +0,883 and +0,882 respectively. A value of 0,64 for the exponent is given by Vanderslice et al (1984).

As shown in the upper half of Table 5-10, the alternative assumption of a linear relationship between F_c and $\ln w_k$, rather than between $\ln F_c$ and $\ln w_k$ is also a reasonable one. If we consider this alternative assumption as the valid one, then the relationship between peak width and carrier flow rate is given by:

$$\ln w_k = b.F_c + i \qquad \ldots \qquad (39)$$

Where the variables are as given for equation 37.

The value of b for chamber No. 1 is -0,566; -0,550; and -0,519, for a k value of 0,5; 0,1; and 0,02 respectively. The corresponding value of i is 3,478; 4,049; and 4,324 for a k value of 0,5; 0,1; and 0,02 respectively.

The value of b for chamber No. 5 is -0,606; -0,585; and -0,533, for a k value of 0,5; 0,1; and 0,02 respectively. The corresponding value of i is 3,465; 4,070; and 4,374 for a k value of 0,5; 0,1; and 0,02 respectively.

Equation 39 may be written as*:

$$\ln w_k = b.\ \ln (e^{F_c}) + i \qquad \ldots \qquad (40)$$

As F_c and q are the same variable (carrier flow rate), equation 40 becomes:

$$\ln w_k = b.\ \ln e^{q} + i \qquad \ldots \qquad (41)$$

---

* Since $x = \ln e^{x}$

A comparison with equation 38 implies that the variable q in the Vanderslice equation should be replaced by e^q, with a value for the $L/(e^q)$ exponent of +0,53 (the negative of the b value for chamber No. 5 for a k value of 0,02) or +0,61 (the negative of the b value for chamber No. 5 for a k value of 0,5). These values for the exponent agree more closely with that of 0,64 given by Vanderslice et al (1984) in equation 10, than the value of 0,88 obtained when a relationship between peak width and carrier flow rate of the form given by equation 37 was assumed.

5.8 Effect of carrier stream flow rate on the magnitude of the boron steady state signal

The effect of variation in carrier stream flow rate on the magnitude of the boron steady state signal is shown in Table 5-11. Note how chamber No. 1, with the Meinhard nebulizer showed little change in signal magnitude except for a decrease in signal at very low flow rates, less than 0,5 $m\ell.min^{-1}$ (Fig. 5-7(a)). The behaviour of chamber No. 5, with the modified concentric nebulizer was, however, quite different, with the steady state signal increasing in magnitude, as the flow rate of liquid to the nebulizer increased (Fig. 5-7(b)).

5.9 Conditions for rapid flow analysis (RFA)

Rapid flow analysis (RFA) implies that the condition must be met that each signal peak must be narrow, i.e., of short duration, so that samples may be injected and analyzed in rapid succession. This condition follows from the expression for the maximum sampling rate S_{max}, given by equation 6 (chapter 2, section 2.2), which showed that the peak standard deviation σ_t should be small in order to achieve large values of S_{max}.

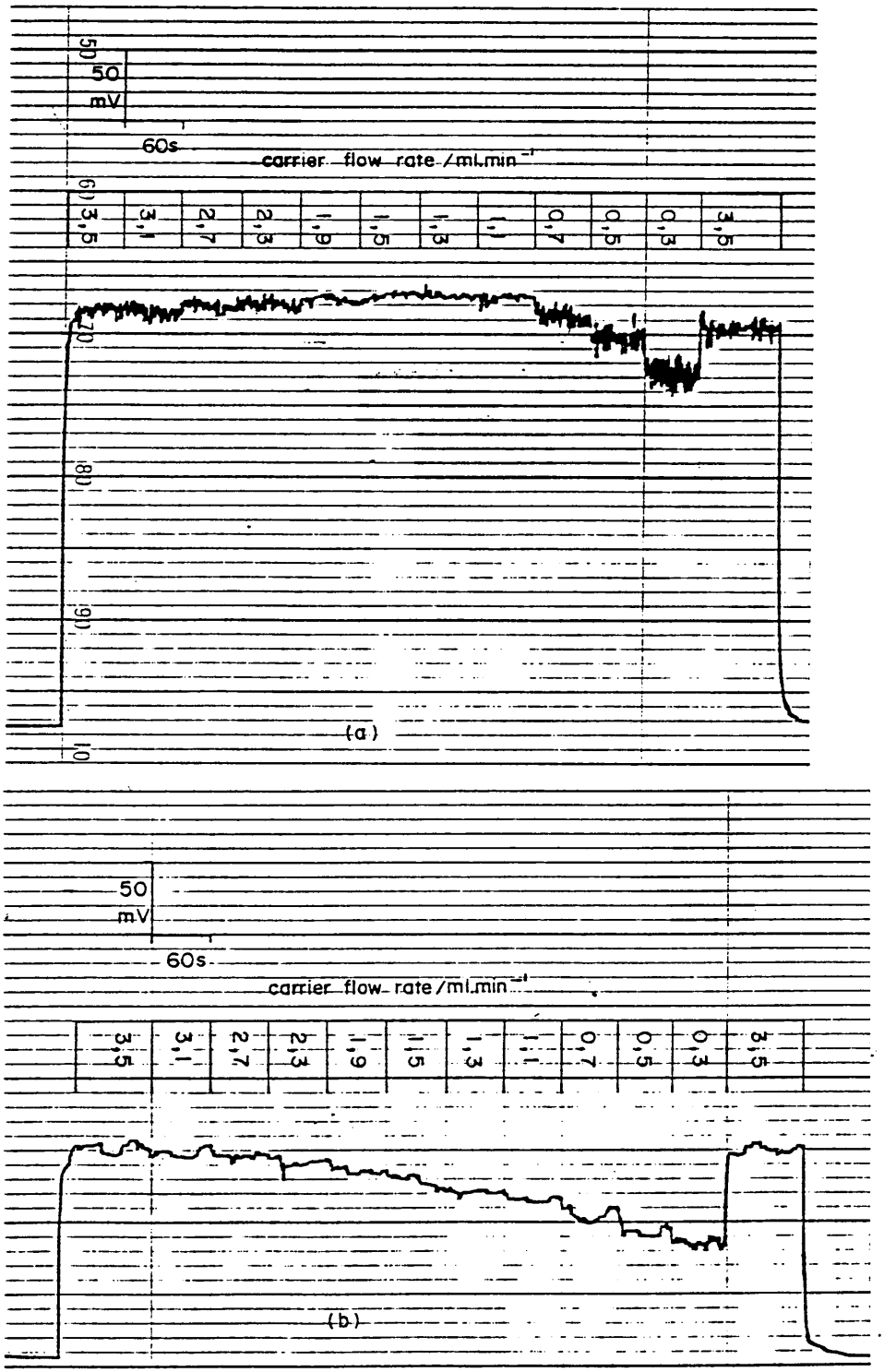

Fig. 5-7(a & b): Influence of carrier flow rate (F_C) on the steady state signal for a 10 mg.ℓ^{-1} B standard, for chamber No. 1 (a) and chamber No. 5 (b).

TABLE 5-11: Effect of carrier flow rate (F_c) on peak height (H) for the steady state signal produced by 10 mg.ℓ$^{-1}$B for chamber Nos. 1 and 5.

F_c/mℓ.min^{-1}	relative peak height/H%*	
	Chamber 1	Chamber 5
0,3	82%	69%
0,5	91%	74%
0,7	96%	86%
1,1	100%	95%
1,3	100%	100%
1,5	100%	107%
1,9	99%	112%
2,3	99%	117%
2,7	98%	122%
3,1	97%	124%
3,5	97%	128%

* relative to the peak height, at a flow rate of 1,3 mℓ.min^{-1}, taken as 100%.

Assuming that the shape of the FIA signal peak may be approximated by a Gaussian distribution, it is readily shown from the properties of the Gaussian function, that the peak standard deviation σ_t may be calculated from the full width at half height $w_{0,5}$ as follows:

$$\sigma_t = \left(\frac{w_{0,5}}{2\sqrt{2 \ln 2}} \right)$$

i.e. $\sigma_t = 0,4247\ w_{0,5}$ ... (42)

where σ_t and $w_{0,5}$ are given in seconds.

Substituting for σ_t from equation 42 into equation 6, the latter becomes;

$$S_{max} = \left(\frac{8477}{\kappa . \ w_{0,5}} \right) \quad \ldots \quad (43)$$

where S_{max} = maximum sampling rate per hour.

$w_{0,5}$ = full width at half height (s).

and κ = number of standard deviation units for acceptable resolution.

For a κ value of 4, equation 43 becomes:

$$S_{max} = \left(\frac{2119}{w_{0,5}} \right) \quad \ldots \quad (44)$$

At a carrier rate of 3,5 $m\ell.min^{-1}$, and an injected sample volume of 300 $\mu\ell$, the S_{max} value for chamber 1 is 415 samples per hour, and for chamber 5 S_{max} is 451 samples per hour, using the peak width values from Table 5-7. In practice, with the instrumentation used in this study, it was not possible to reach a sampling rate much over 320 samples per hour, and the latter rate was thus chosen for the evaluation of RFA-FIA on chamber Nos. 1 and 5. At a sampling rate of 320 samples per hour, the κ value of equation 43 is 5,2 for chamber No. 1, and 5,6 for chamber No. 5, indicating that good peak resolution should be obtained with both chambers, with the latter chamber giving slightly better resolution.

In view of the fact that the aerosol displacement time t_d of chamber No. 5 is a factor 10 smaller than that for chamber No. 1, i.e., 0,49s and 4,9s respectively (Table 3-2, chapter 3, section 3.6), it may seem strange that there is only a small difference between the S_{max} values for the two chambers. The reason is readily apparent if assuming plug-like flow, we consider the time taken for a 300 $\mu\ell$ injected sample to pass through the nebulizer at a carrier flow rate of 3,5 $m\ell.min^{-1}$. This time is 5,1s which is of the same magnitude as the aerosol displacement time (t_d) of the large chamber (No. 1), but much greater than the t_d value of 0,49s for chamber No. 5.

5.10 RFA-FIA determination of boron using chamber No. 1

The characteristics of chamber No. 1 for boron determination at a sampling rate of 320 samples per hour, with an injected volume of 300 µℓ and at a carrier flow rate of 3,5 mℓ.min^{-1} are given in this section.

The steady state signals are shown in Fig. 5-7(c). Note the noise present at the higher concentrations. The reproducibility of the FIA signals is shown in Fig. 5-8, the relative standard deviation being shown in Table 5-12. The reproducibility was better than 5% RSD between 2,5 and 25 mg.ℓ$^{-1}$ B, for 10 replicates. The mean wash-out between successive FIA peaks for the 25 mg.ℓ$^{-1}$B standard was to within 8,8% of the mean peak height. This can be seen in Fig. 5-8, where the valleys between peaks do not reach the baseline.

The reproducibility of 22 replicate injections of a 10 mg.ℓ$^{-1}$ B standard was 3,1% RSD (Fig. 5-9). The dispersion ratio D was 1,17 corresponding to a FIA peak height of 85% of the steady state signal.

The memory effect following a high concentration standard is shown in Fig. 5-10, the peak height of a 2,5 mg.ℓ$^{-1}$ B standard immediately following a 25,0 mg.ℓ$^{-1}$ B standard showed a mean increase in peak height of 15%.

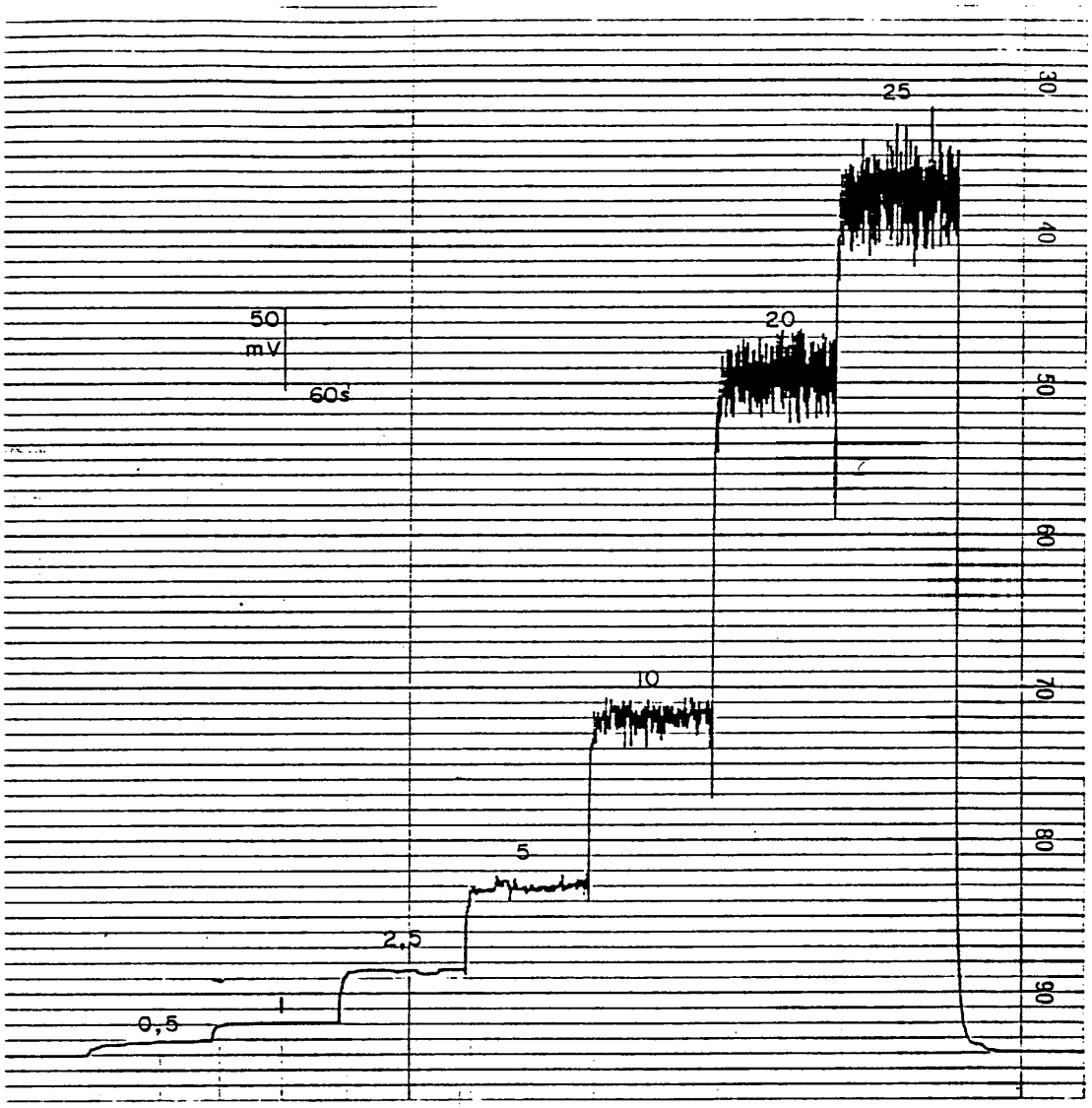

Fig. 5-7(c): Steady state signals for boron concentrations from 0,5 to 25 mg.ℓ^{-1} B, using chamber No. 1, at a carrier flow rate of 3,5 mℓ.min^{-1}, at 1V FSD and 10 mm.min^{-1} chart speed.

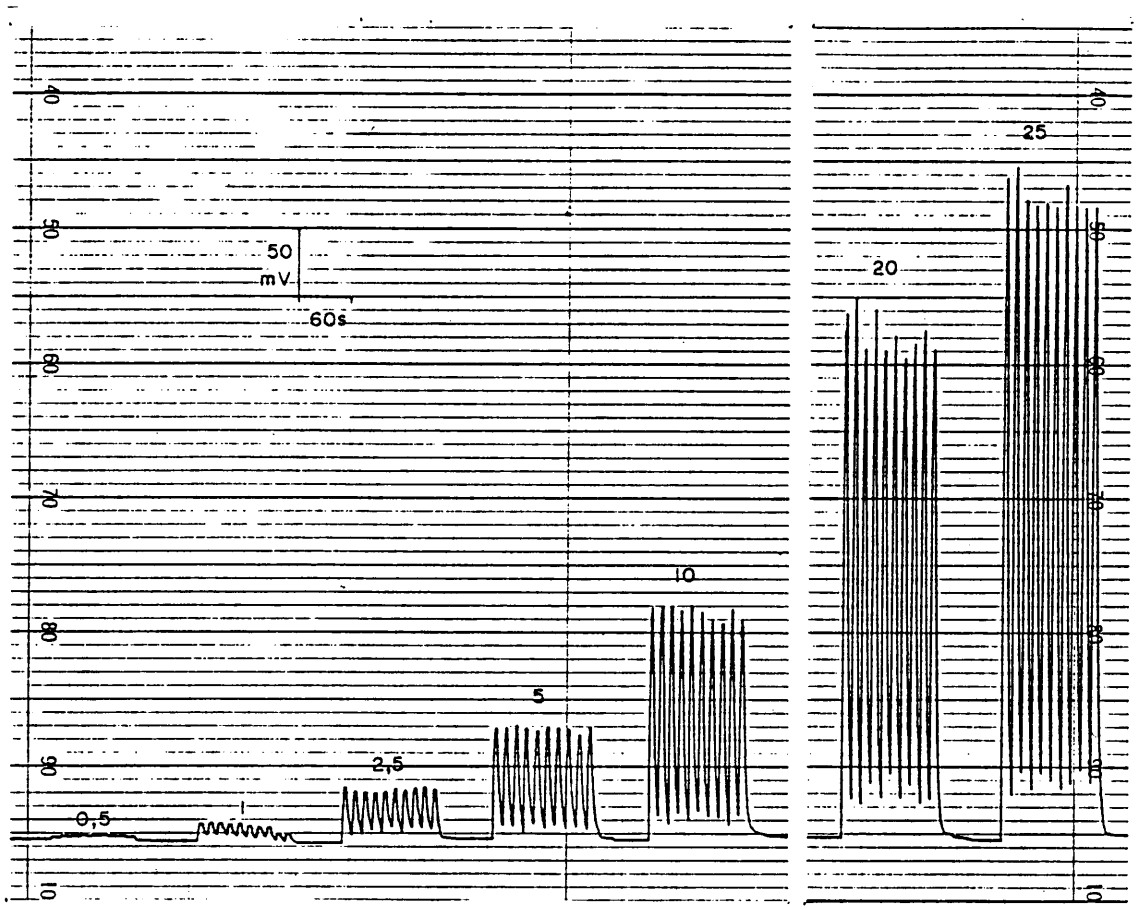

Fig. 5-8: Reproducibility of FIA signal peaks, for chamber No. 1, at a sample injection rate of 320 per hour, for boron standards of 0,5; 1,0; 2,5; 5; 10; 20; and 25 mg.ℓ^{-1} B. Injection volume was 300 µℓ, and carrier flow rate 3,5 mℓ.min^{-1}.

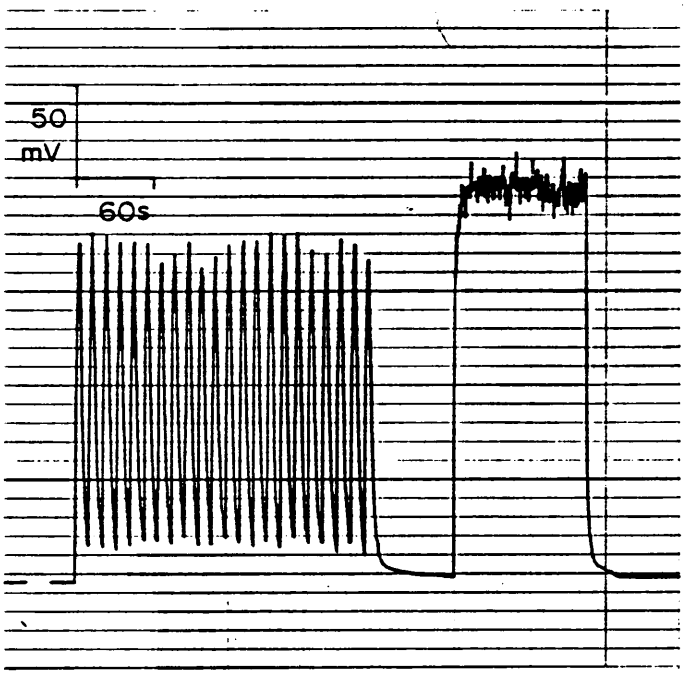

Fig. 5-9: Reproducibility of FIA signals, and steady state for a 10 mg.ℓ^{-1} B standard. Injection volume of 300 $\mu\ell$, at an injection rate of 320 per hour. Chamber No. 1 used, with a carrier flow rate of 3,5 mℓ.min^{-1}.

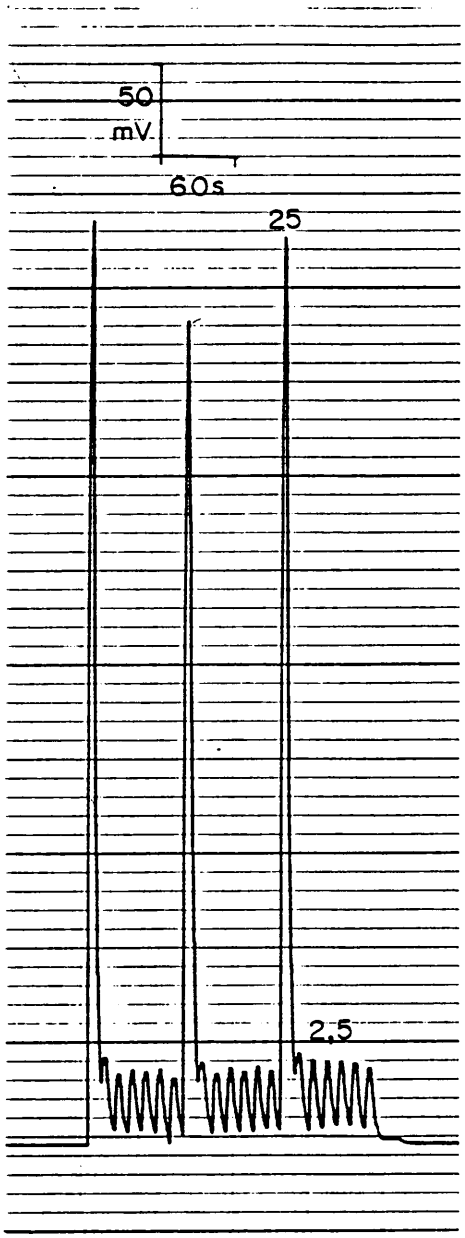

Fig. 5-10: Carry over of FIA signals for 25 mg.ℓ$^{-1}$ B followed by 6 replicates of a 2,5 mg.ℓ$^{-1}$ B standard, for chamber No. 1. Sampling rate 320 per hour.

TABLE 5-12: Reproducibility (RSD%) of FIA peak height ($\bar{H} \pm \sigma$/mm) signals, for 10 replicate measurements, for boron concentrations (C) between 0,5 and 25 mg.ℓ$^{-1}$ B for chamber No. 1.*

C/mg.ℓ$^{-1}$B	$\bar{H} \pm \sigma$/mm	RSD%
0,5	0,9 ± 0,2	22%
1,0	3,0 ± 0,7	23%
2,5	9,6 ± 0,4	4,2%
5,0	20,7 ± 0,5	2,4%
10,0	42,2 ± 1,3	3,1%
20,0	94,4 ± 4,1	4,3%
25,0	119,0 ± 2,9	2,4%

* Carrier flow rate 3,5 mℓ.min^{-1}; injected sample volume 300 µℓ; sampling rate 320 samples per hour. Recorder range adjustment set at 1V FSD.

TABLE 5-13: Calibration data for boron, for chamber No. 1, showing mean peak height ($\bar{H}$) and standard deviation (σ) for boron concentrations (C) between 0,5 and 25 mg.ℓ$^{-1}$ B. The linear correlation coefficient between C and $\bar{H}$ was 0,9997.*

C/mg.ℓ$^{-1}$B	$\bar{H} \pm \sigma$/mm
0,5	1,2 ± 0,2
1,0	2,4 ± 0,2
2,5	9,7 ± 0,4
5,0	22,3 ± 0,5
10,0	44,7 ± 0,8
20,0	94,5 ± 3,6
25,0	121,4 ± 0,9

* Sampling rate 320 per hour. Carrier flow rate 3,5 mℓ.min^{-1}. Injected sample volume 300 µℓ. Recorder range adjustment set at 1V FSD.

A calibration consisting of three replicates each of boron standards with concentrations of 0,5; 1,0; 2,5; 5,0; 10,0; 20,0 and 25,0 $mg.\ell^{-1}$ B is shown in Fig. 5-11. The calibration data is shown in Table 5-13, and plotted in Fig. 5-12, which shows the calibration graph. Note how the regression line intercepts the concentration axis at a boron concentration of 0,5 $mg.\ell^{-1}$ B, which thus constitutes the limit of detection when using this regression line. The regression has the equation:

$$H = 4,897\ C - 2,455 \qquad \ldots\ (45)$$

where H is the peak height in mm (at 1V FSD on the recorder, corresponding to 4 mV per mm) and C is the boron concentration in $mg.\ell^{-1}$ B.

In reality of course, the 0,5 $mg.\ell^{-1}$ B standard gave a small positive deflection above the baseline of 1,2 mm, and thus the calibration line should deviate slightly from the least squares regression line to pass through the origin, as shown by the dotted curve at the extreme lower left in Fig. 5-12. Alternatively, if we consider the two sigma value given by ten replicate measurements of the 1,0 $mg.\ell^{-1}$ boron standard (Table 5-12) as the detection limit, then a value of 0,8 $mg.\ell^{-1}$B is obtained for the limit of detection.

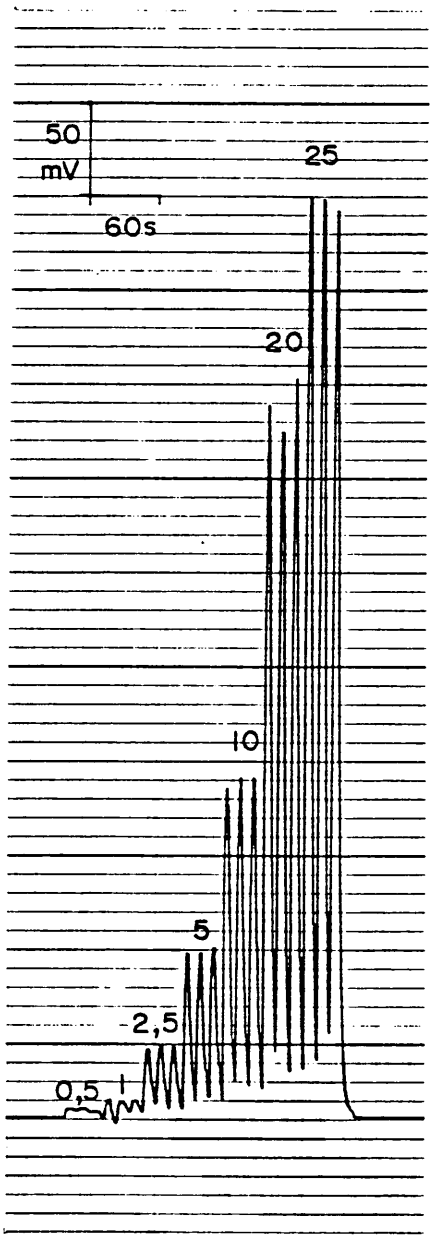

Fig. 5-11: Calibration data set for boron concentrations of 0,5; 1,0; 2,5; 5; 10; 20; and 25 mg.ℓ$^{-1}$ B, for chamber No. 1. Sampling rate 320 per hour. Volume injected 300 µℓ. Carrier flow rate 3,5 mℓ.min^{-1}.

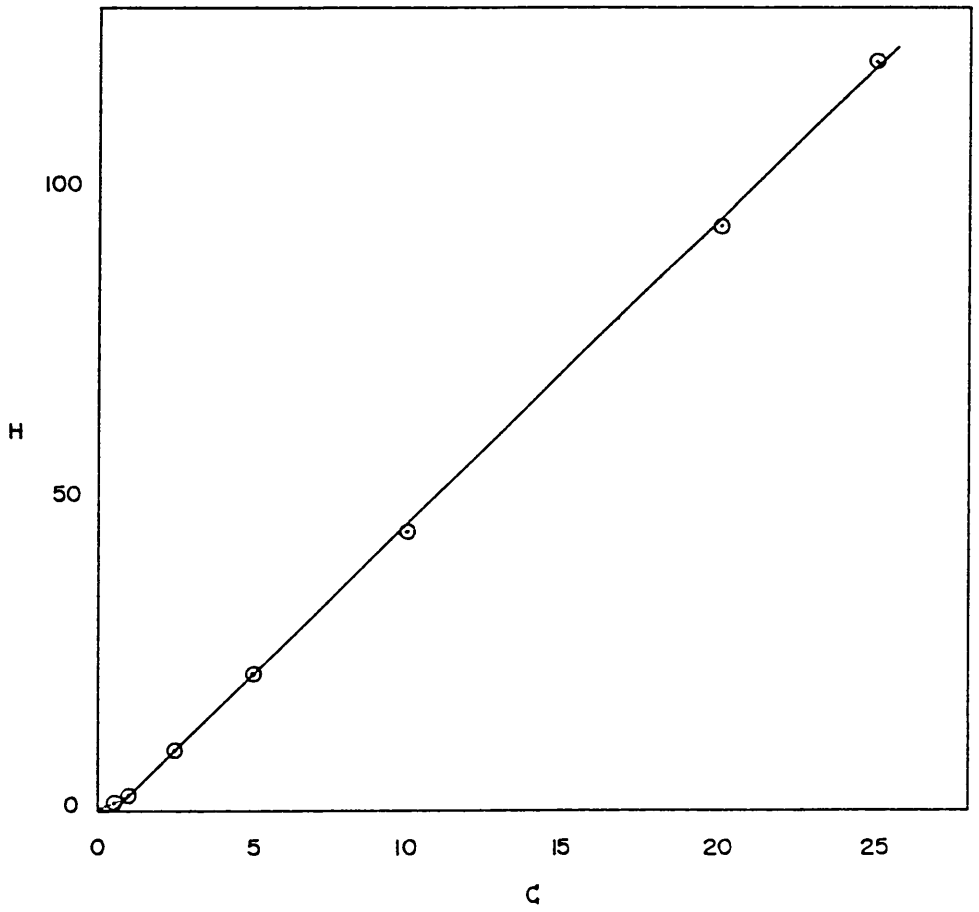

Fig. 5-12: Calibration graph for boron using chamber No. 1, showing the linear correlation (r = 0,9997) between the FIA peak height H (mm) and the boron concentration C (mg.ℓ$^{-1}$ B), with the regression equation: H = 4,897 C - 2,455. Analytical conditions were: Sampling rate 320 per hour, with a carrier flow rate of 3,5 mℓ.min^{-1} and an injected sample volume of 300 µℓ. The range adjustment of the potentiometric recorder was set at 1V FSD.

5.11 RFA-FIA determination of boron using chamber No. 5

The characteristics of chamber No. 5 for boron determination at a sampling rate of 320 samples per hour, with an injected volume of 300 µℓ and at a carrier flow rate of 3,5 mℓ.min^{-1} are given in this section. The recorder sensitivity was set at 0,5 V FSD for the chamber No. 5 measurements, and thus the instability of the baseline arising from the spectrometer electronics is more apparent than with the measurements on chamber No. 1 in section 5.10, which were made at 1,0 V FSD.

The steady state signals are shown in Fig. 5-13, which shows how the noise increases at the higher concentration. The reproducibility of the FIA signals is shown in Fig. 5-14, the relative standard deviation being shown in Table 5-14. The reproducibility was better than 4% RSD between 5,0 and 25 mg.ℓ$^{-1}$ B, for 10 replicates.

TABLE 5-14: Reproducibility (RSD%) of FIA peak height ($\bar{H} \pm \sigma$/mm) signals, for 10 replicate measurements, for boron concentrations (C) between 0,5 and 25 mg.ℓ$^{-1}$ B for chamber No 5.*

C/mg.ℓ$^{-1}$B	$\bar{H} \pm \sigma$/mm	RSD%
0,5	1,7 ± 0,8	47%
1,0	5,8 ± 0,8	14%
2,5	14,8 ± 0,8	5,4%
5,0	30,7 ± 0,9	2,9%
10,0	65,3 ± 2,1	3,2%
20,0	131,9 ± 2,6	2,0%
25,0	160,8 ± 5,0	3,1%

* Carrier flow rate 3,5 mℓ.min^{-1}; injected sample volume 300 µℓ; sampling rate 320 samples per hour. Recorder set at 0,5 V FSD.

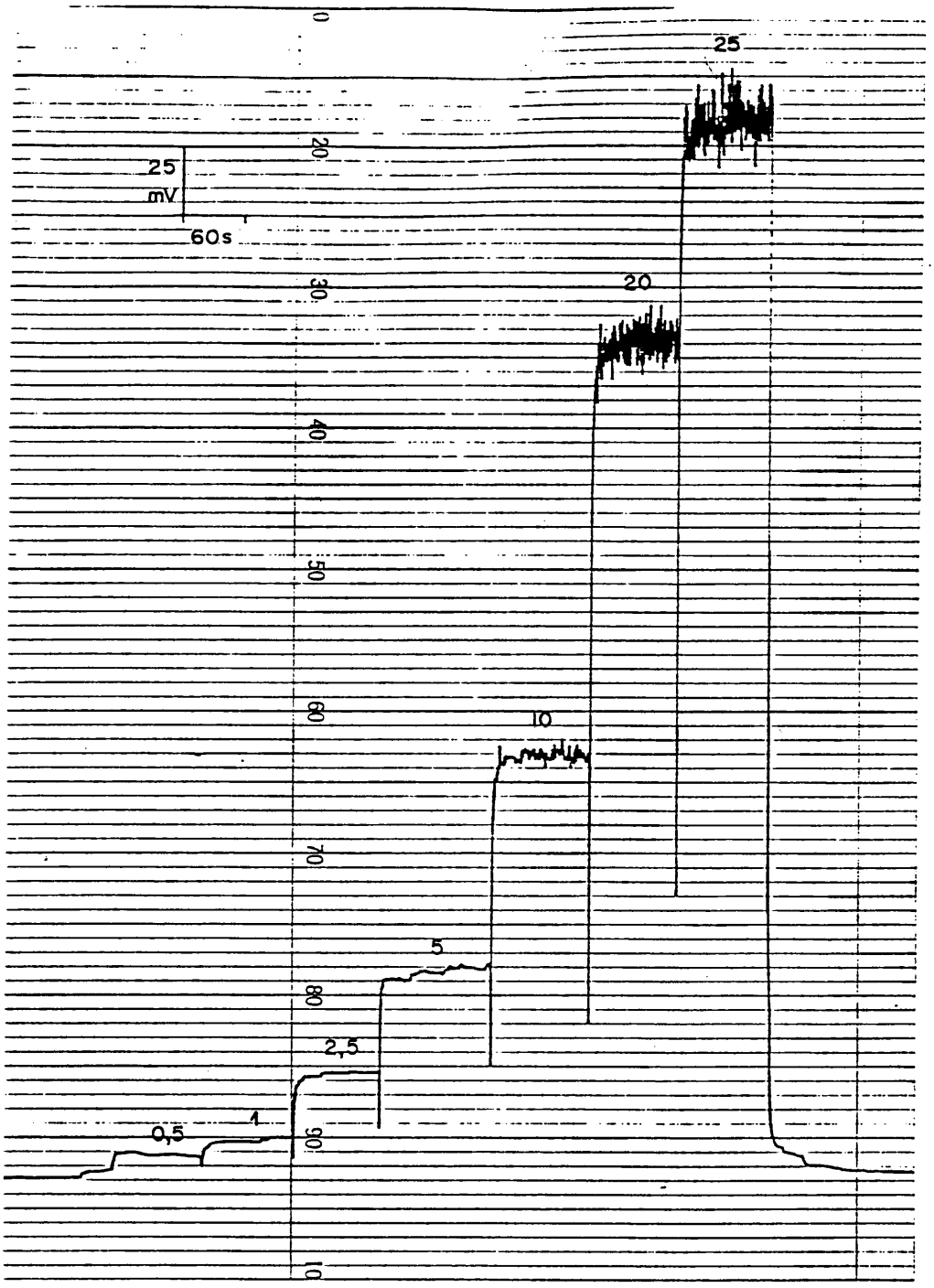

Fig. 5-13: Steady state signals, using chamber No. 5, for boron concentrations between 0,5 and 25 mg.ℓ$^{-1}$ B. Carrier flow rate was 3,5 mℓ.min^{-1}.

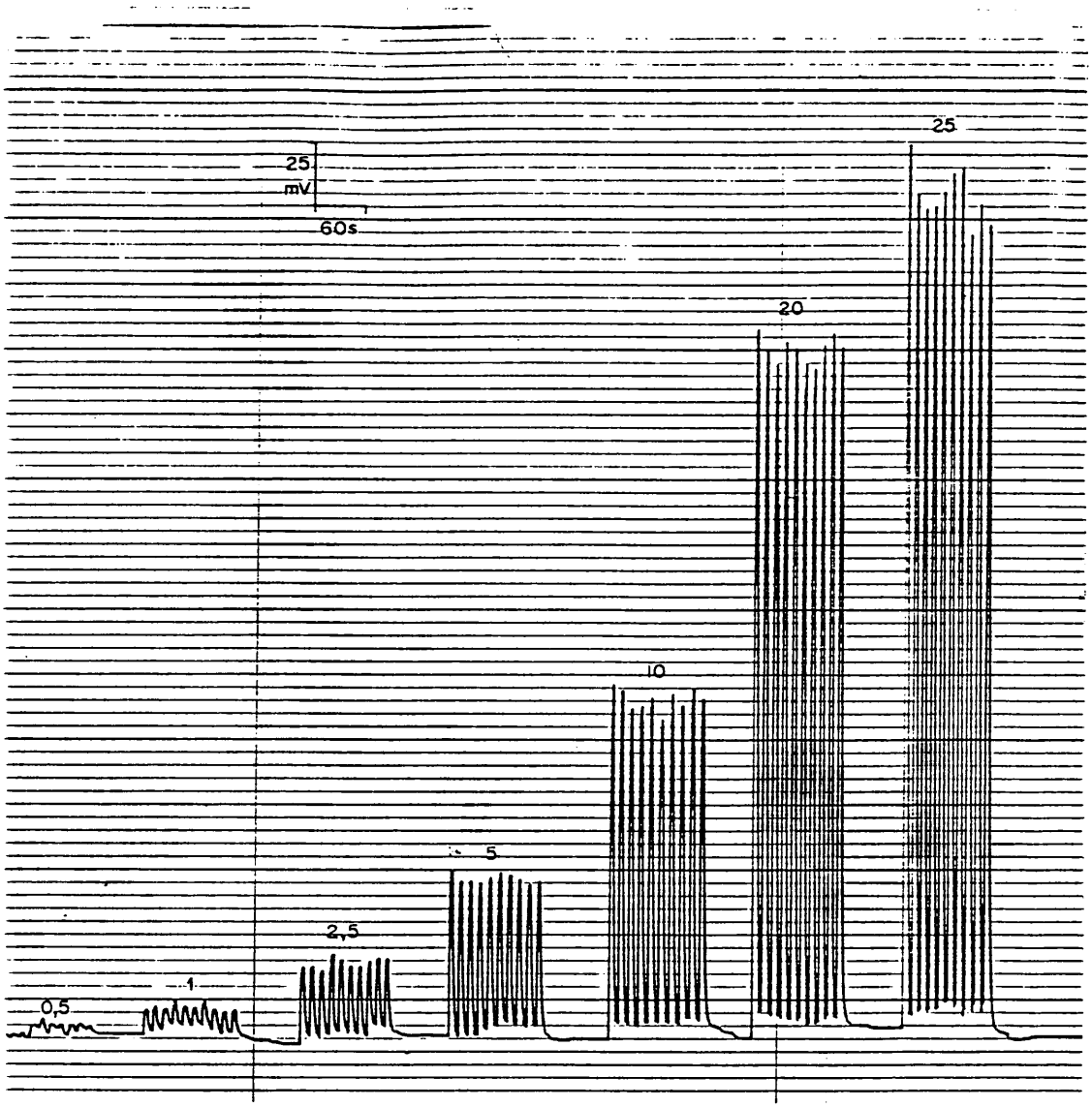

Fig. 5-14: Reproducibility of FIA signals for boron concentrations of 0,5; 1,0; 2,5; 5; 10; 20; and 25 mg.ℓ$^{-1}$ B, using chamber No. 5. The sampling rate was 320 per hour, with an injected sample volume of 300 µℓ, and a carrier flow rate of 3,5 mℓ.min^{-1}.

The mean wash-out between successive FIA peaks for the 25 $mg.\ell^{-1}$ B standard was to within 2,6% of the mean peak height. This can be seen in Fig. 5-14, where the valleys between peaks almost reach the baseline.

The reproducibility of 22 replicate injections of a 10 $mg.\ell^{-1}$ B standard was 2,4% RSD (Fig. 5-15). The dispersion ratio D was 1,12 corresponding to an FIA peak height of 89% of the steady state signal.

The memory effect following a high concentration standard is shown in Fig. 5-16, the peak height of a 2,5 $mg.\ell^{-1}$ B standard immediately following a 25,0 $mg.\ell^{-1}$ B standard showed a mean increase in peak height of 3%, i.e., very little carry-over was observed. The excellent wash-out of chamber No. 5 in comparison to chamber No. 1 is also clearly shown in Fig. 5-17, which shows how the valleys between the peaks almost reach the baseline for chamber No. 5, while for chamber No. 1 the valleys between the central 25 $mg.\ell^{-1}$ B standards are considerably elevated above the baseline.

A calibration consisting of three replicates each of boron standards with concentrations of 0,5; 1,0; 2,5; 5,0; 10,0; 20,0 and 25,0 $mg.\ell^{-1}$ B is shown in Fig. 5-18. The calibration data is shown in Table 5-15, and plotted in Fig. 5-19, which shows the calibration graph. Note how the regression line intercepts the concentration axis at a boron concentration of 0,25 $mg.\ell^{-1}$ B, which thus constitutes the limit of detection when using this regression line. The regression has the equation:

$$H = 6,7691\ C - 1,7318 \qquad \ldots\ (46)$$

Where H is the peak height in mm (at 0,5 V FSD on the recorder, corresponding to 2 mV per mm) and C is the boron concentration in $mg.\ell^{-1}$ B.

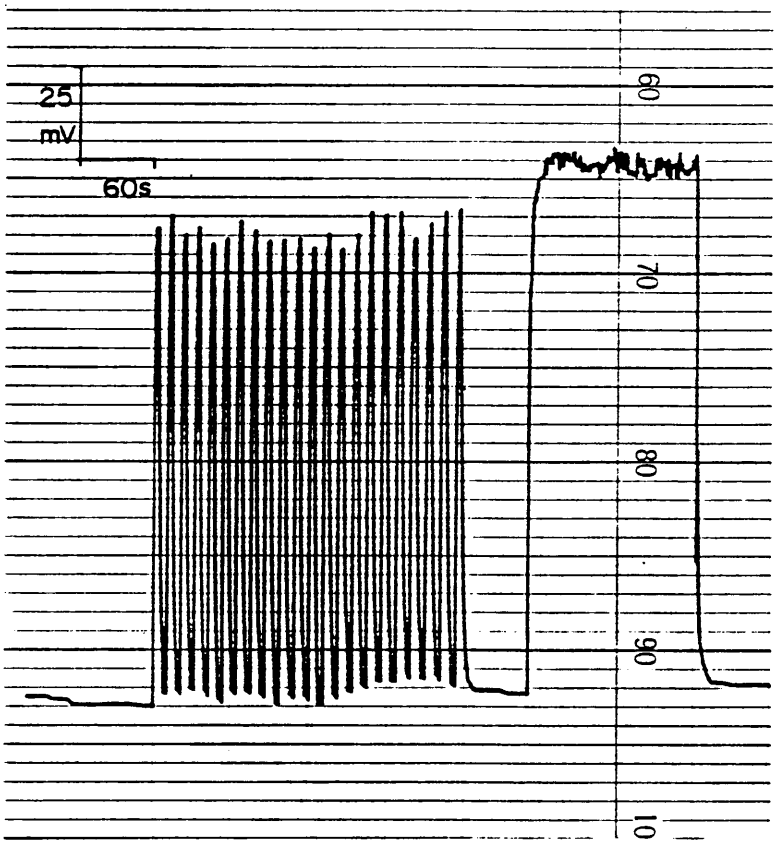

Fig. 5-15: Reproducibility of FIA signals, and steady state, for a 10 $mg.\ell^{-1}$ B standard. Injection volume of 300 $\mu\ell$, at an injection rate of 320 per hour. Chamber No. 5 used, with a carrier flow rate of 3,5 $m\ell.min^{-1}$.

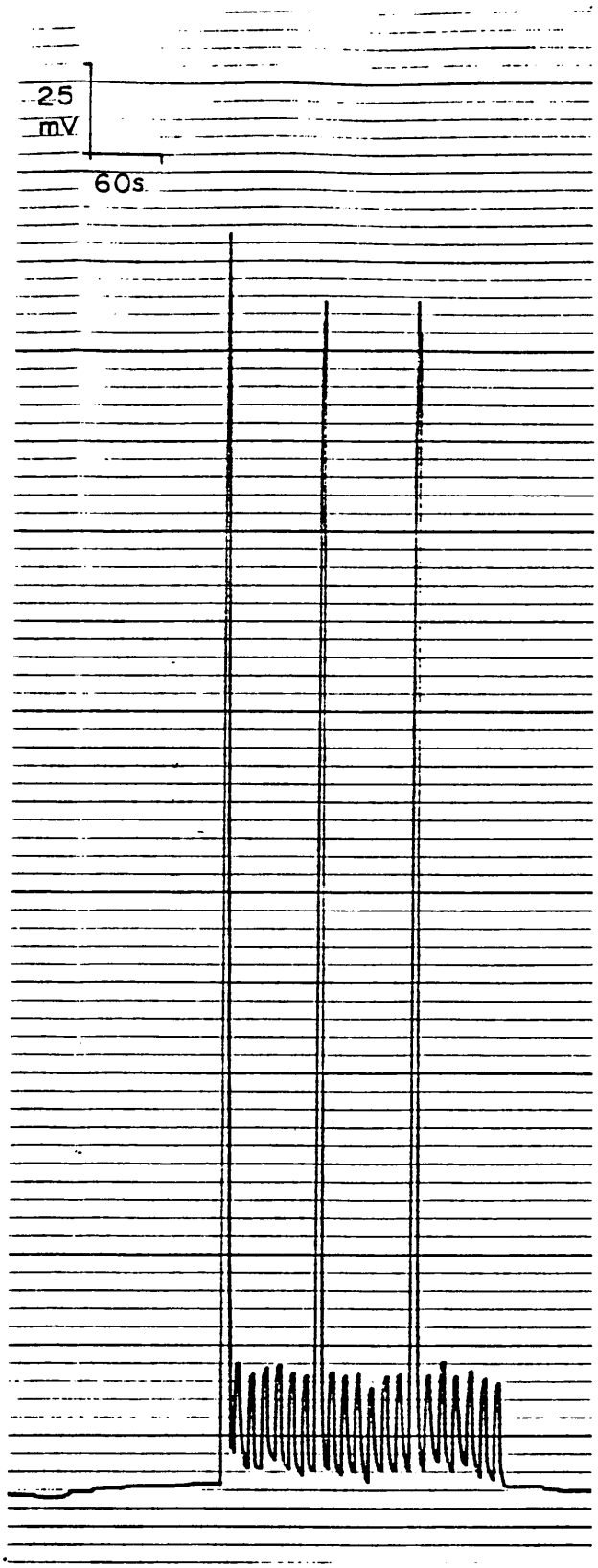

Fig. 5-16: Carry over of FIA signals for 25 mg.ℓ^{-1} B, followed by 6 replicates of a 2,5 mg.ℓ^{-1} B standard, for chamber No. 5. Sampling rate 320 per hour.

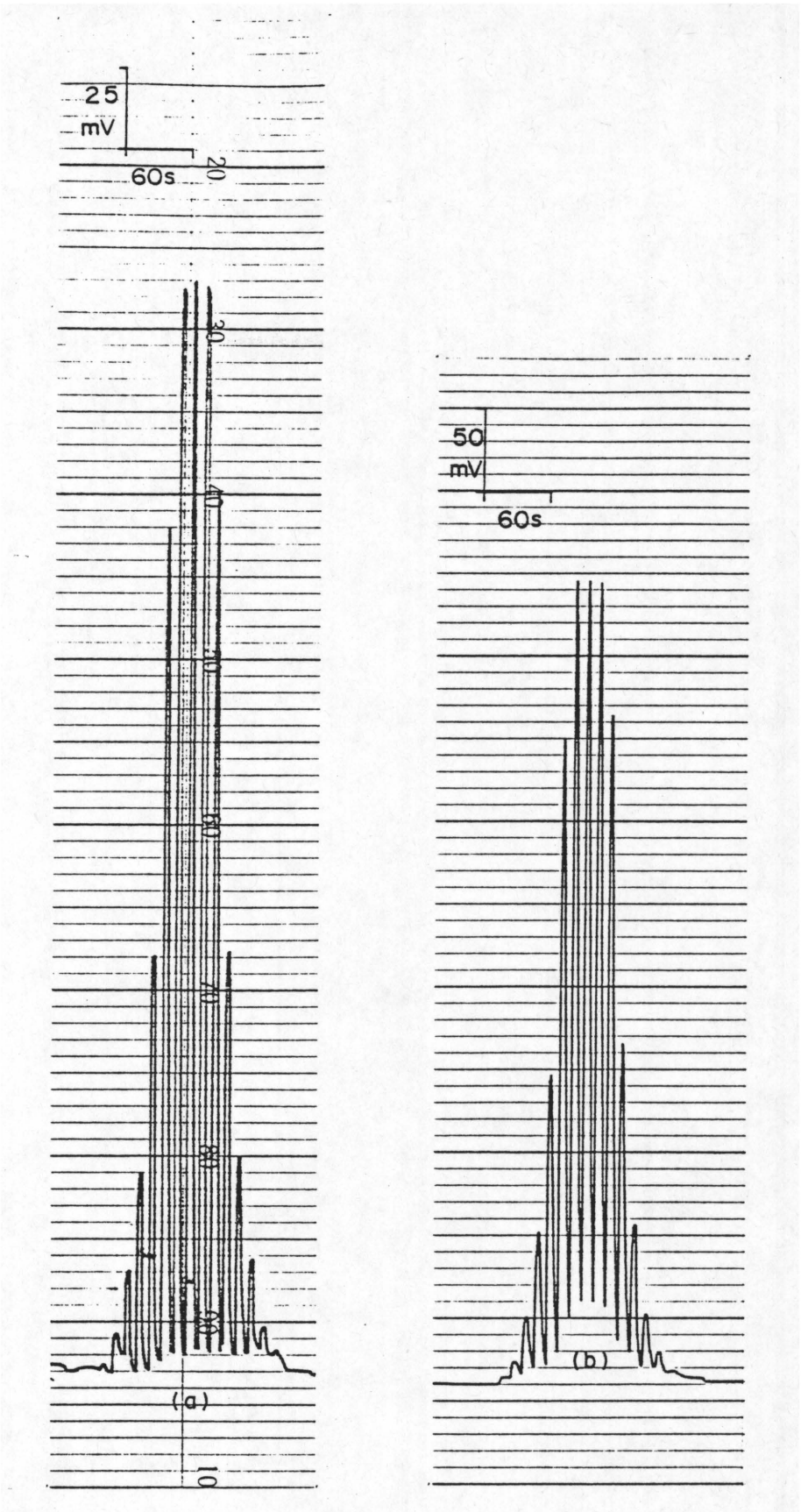

Fig. 5-17: FIA signals for (a) chamber No. 5; and (b) chamber No. 1, for boron calibration standards in ascending order followed by descending order. Note the good wash-out for chamber No. 5, compared to chamber No. 1.

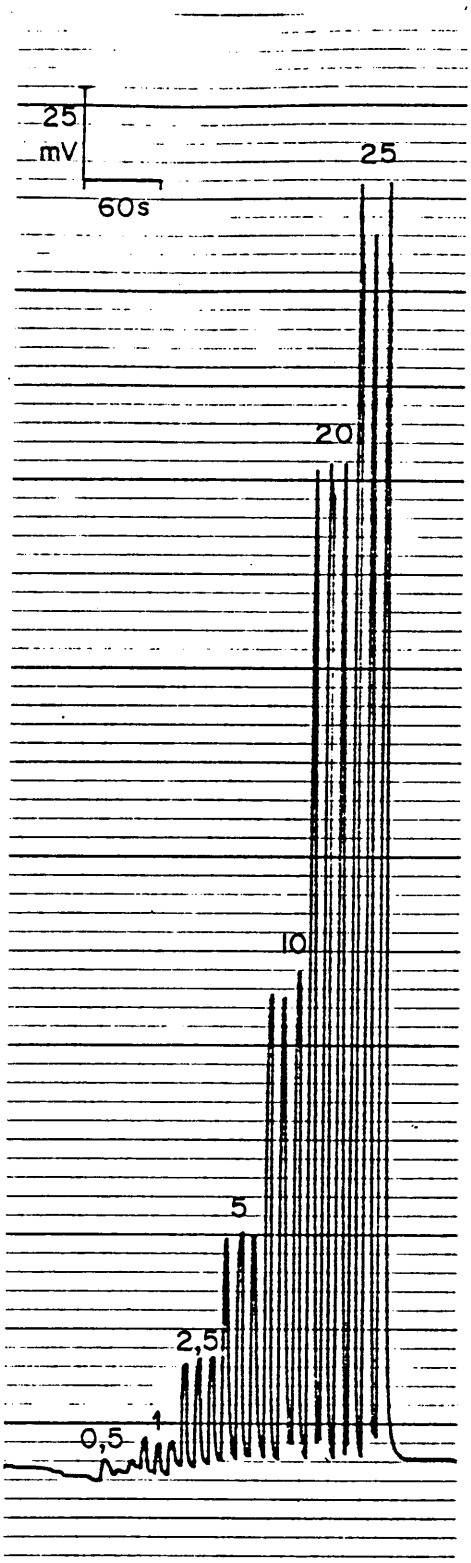

Fig. 5-18: Calibration data set for boron concentrations of 0,5; 1,0; 2,5; 5; 10; 20; and 25 mg.ℓ$^{-1}$ B, for chamber No. 5. Sampling rate 320 per hour. Volume injected 300 µℓ. Carrier flow rate 3,5 mℓ.min^{-1}.

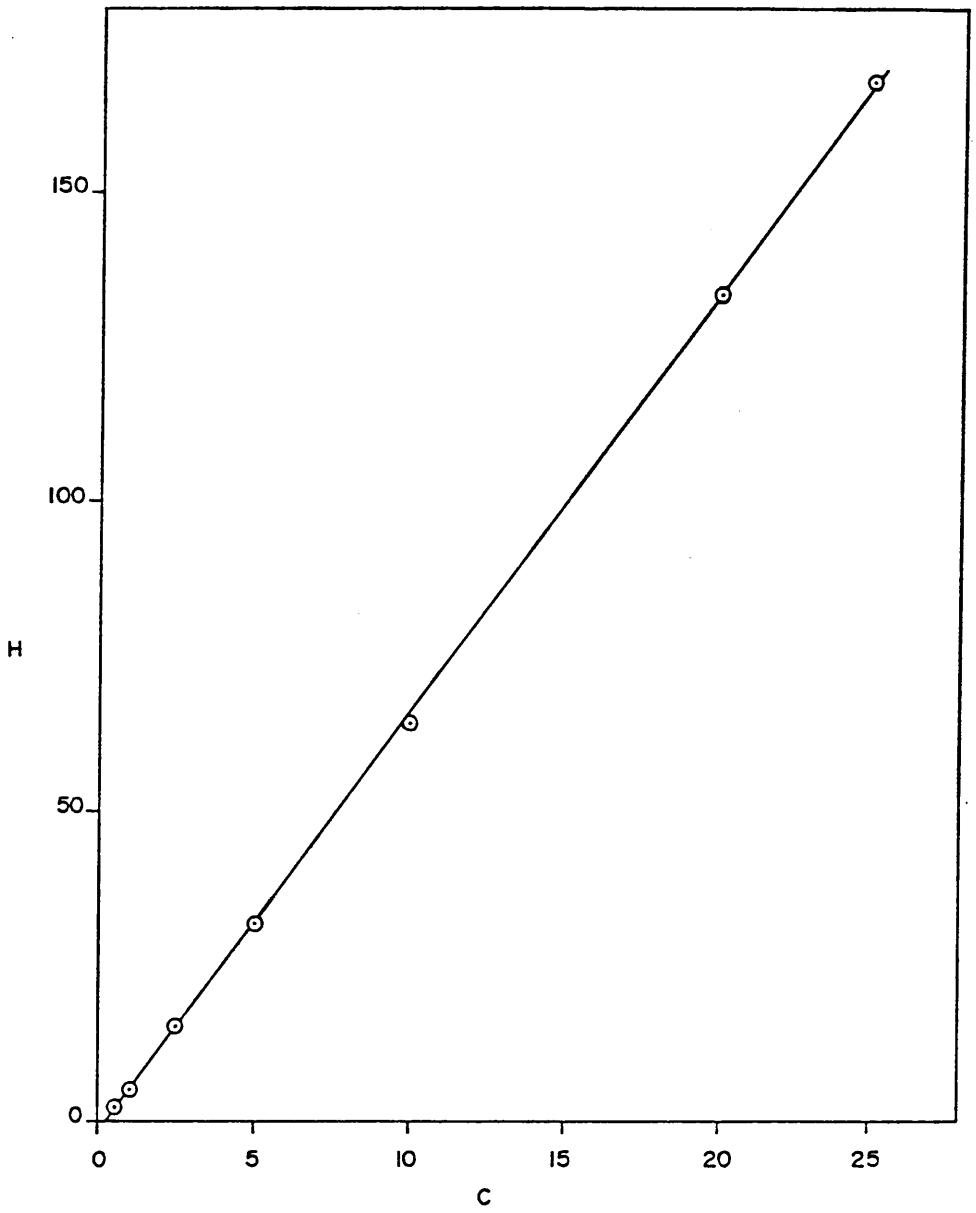

Fig. 5-19: Calibration graph for boron, for chamber No. 5, showing the linear correlation (r = 0,9999) between FIA peak height H (mm) and boron concentration C (mg.ℓ$^{-1}$ B), with the regression equation H = 6,7691C - 1,7318. Analytical conditions were: Sampling rate 320 per hour, with a carrier flow rate of 3,5 mℓ.min^{-1} and injected sample volume of 300 µℓ. The range adjustment on the potentiometric recorder was set at 0,5 V FSD.

TABLE 5-15: Calibration data for boron, for chamber No. 5, showing mean peak height ($\bar{H}$) and standard deviation (σ) for boron concentrations (C) between 0,5 and 25 mg.ℓ$^{-1}$ B. The linear correlation coefficient between C and $\bar{H}$ was 0,9999.*

C/mg.ℓ$^{-1}$B	$\bar{H} \pm \sigma$/mm
0,5	2,4 ± 0,9
1,0	5,2 ± 0,5
2,5	15,6 ± 0,5
5,0	31,9 ± 0,3
10,0	64,2 ± 1,8
20,0	133,5 ± 0,5
25,0	168,3 ± 4,0

* Sampling rate 320 per hour. Carrier flow rate 3,5 mℓ.min^{-1}. Injected sample volume 300 µℓ. Recorder range adjustment set at 0,5 V FSD.

If we consider the two sigma value given by ten replicate measurements of the 1,0 mg.ℓ$^{-1}$ boron standard (Table 5-14) as the detection limit, then a value of 0,5 mg.ℓ$^{-1}$ B is obtained for the limit of detection.

5.12 Tests for interferences

Possible interferences on the determination of boron by FIA-ICP using the B 249,68 nm analytical line were evaluated for six elements *viz.*, Al, Ca, Cr, Fe, Na and P. Calcium and iron are common interferants in ICP work, the former because of very bright resonance lines, and the latter because of a very rich line spectrum (Kempster, 1986). Phosphorus was evaluated as a potential interferant because of two phosphorus emission lines within 0,1 nm of the B 249,68 nm analytical line, while chromium was evaluated as it has an arc line at 249,63 nm (Parsons *et al*, 1980). Sodium was added to the list of potential

interferants, as an example of an easily ionizable element, while aluminium was added as aluminium salts are used as a flocculant in water purification, and may occur in elevated concentration in water. In addition, boron standards were made up in ϕ=0,01 nitric acid to see if any sensitivity difference occurred between a deionised water medium and dilute nitric acid medium.

Solutions were prepared* each containing 9,25 mmol.ℓ^{-1} Al, Ca, Cr, Fe, Na and P, in a ϕ=0,01 nitric acid medium. Aliquots of these solutions of potential interferants were spiked with 0,925 mmol.ℓ^{-1} B (i.e., 10 mg.ℓ^{-1} B) and then analyzed together with the unspiked solutions by FIA-ICP, under the following test conditions:

(a) Using chamber No. 1, at a sampling rate of 100 per hour, with an injection volume of 408 $\mu\ell$ and a carrier** flow rate of 1,3 mℓ.min^{-1}.

(b) Using chamber No. 5, at a sampling rate of 100 per hour, with an injection volume of 408 $\mu\ell$ and a carrier** flow rate of 1,3 mℓ.min^{-1}.

(c) Using chamber No. 5, at a sampling rate of 320 per hour, with an injection volume of 300 $\mu\ell$ and a carrier** flow rate of 3,5 mℓ.min^{-1}.

No difference was observed in sensitivity between boron standards made up in deionised water and made up in ϕ=0,01 nitric acid.

---

* Ca, Cr, Fe and Na solutions were prepared from Titrisol standards, and each metal was present as its chloride salt. Analytical grade aluminium chloride was used for Al, and analytical grade ammonium dihydrogen phosphate for the P standard.

** ϕ=0,01 nitric acid was used as carrier.

The unspiked solutions of Al, Ca, Cr, Fe, Na and P did not produce any detectable boron concentration readouts. The recovery of the 10 $mg.\ell^{-1}$ boron spikes are given in Table 5-16. The recoveries found lay between 95% and 101%, with Al, Ca, Na and P showing between 4 and 5% suppression in the case of chamber No. 1. In contrast, chamber No. 5 showed no suppression with Al, but still showed a 4% suppression with calcium at 100 samples per hour, and 5% suppression of the boron recovery at 320 samples per hour.

In conclusion, matrix effects on the boron calibration appear to be slight, with calcium showing a 5% suppression of the 10 $mg.\ell^{-1}$ B signal at a calcium concentration of 371 $mg.\ell^{-1}$ Ca (i.e., 9,25 $mmol.\ell^{-1}$ Ca).

TABLE 5-16: Recovery* of a 0,925 $mmol.\ell^{-1}$B spike added to solutions containing 9,25 $mmol.\ell^{-1}$ of Al, Ca, Cr, Fe, Na and P, for chamber No. 1 at 100 samples per hour, and chamber No. 5 at 100 (a) and 320 (b) samples per hour.

Potential matrix interferant	Recovery of boron spike/%		
	Chamber 1	Chamber 5 (a)	Chamber 5 (b)
Al	96%	102%	100%
Ca	96%	96%	95%
Cr	100%	95%	98%
Fe	101%	98%	97%
Na	95%	96%	97%
P	96%	97%	101%
mean recovery:	97%	97%	98%

* mean of three replicates.

5.13 Summary and conclusion

In the evaluation of the FIA-ICP emission spectrometric method for the determination of boron in water, as given in this chapter, the following was shown:

(a) Increasing the rate of delivery of liquid to the nebulizer from 1,3 mℓ.min^{-1} to 3,5 mℓ.min^{-1}, resulted in a decrease in peak width at half height by a factor of 2,7 which allowed sampling rates as high as 320 samples per hour to be achieved.

(b) Use of the small 11 mℓ volume spray chamber No. 5 produced better wash-out than given by the large 110 mℓ volume chamber No. 1. Wash-out between 25 mg.ℓ$^{-1}$ B FIA peaks occurred to within 8,8% of the baseline for chamber No. 1 and to within 2,6% of the baseline for chamber No. 5.

(c) Calibrations were highly linear with both chambers. The two sigma detection limit, based on the standard deviation of a 1 mg.ℓ$^{-1}$ B standard being 0,8 mg.ℓ$^{-1}$ for chamber No. 1 and 0,5 mg.ℓ$^{-1}$ for chamber No. 5, at 320 samples per hour. Precision of 22 replicates of a 10 mg.ℓ$^{-1}$ B standard was 3,1% RSD for chamber No. 1 and 2,4% RSD for chamber No. 5.

(d) Matrix interferences on a 10 mg.ℓ$^{-1}$ B concentration were less than 6% for a 10 molar excess of Al, Ca, Cr, Fe, Na and P, with mean recovery between 95% and 101% for chamber No. 5 at a carrier flow rate of 3,5 mℓ.min^{-1}.

Detection limits for FIA-ICP determination of boron were inferior, by about 2 orders of magnitude, than those found when using the conventional sample introduction and intensity integration method (chapter 4). The chief reason for this degradation in detection limit was believed to be the 10 mV instability of the analogue output signal from the spectrometer, which made measurements of small intensity signals impractical.

The FIA detection limit of around 0,5 $mg.\ell^{-1}$ B, found with chamber No. 1, using the present spectrometer, implies that the method is only suitable for the rapid determination of pollutant concentration levels of boron, in excess of 1 $mg.\ell^{-1}$, and is not suitable for background concentration levels of 0,01 to 0,1 $mg.\ell^{-1}$ B.

A sampling rate of 320 samples per hour, assuming samples are analyzed in triplicate, implies an analytical rate of just over 100 analyses per hour. This is at least three times faster than the conventional ICP sample introduction and integration method, and demonstrates the potential the FIA introduction procedure has in speeding up the rate of analysis.

The significance of this FIA-ICP work, in relation to that achieved by other workers, is that a rapid sampling rate of 320 injections per hour with good wash-out between peaks was achieved using a relatively large sample injection volume of 300 $\mu\ell$, so that the FIA peak height almost reached steady state. Alexander et al (1982) achieved a sampling rate for FIA-ICP of 240 per hour, but this only by using a small sample volume of 10 $\mu\ell$. When Alexander and co-workers used a 300 $\mu\ell$ injection volume, poor wash-out with carry-over between peaks was observed. These workers experimented with rapid sample throughput, at injection rates as high as 600 per hour, by injecting the sample just prior to the nebulizer. They experienced the

problem, however, of plasma instability, and even extinguishing occurring. FIA peaks close to steady state are desirable so that little sensitivity loss occurs as a consequence of dispersion. In the work of Greenfield (1983) on the FIA-ICP determination of calcium, the baseline-to-baseline peak width was 33s, using a 233 µℓ injected sample, a sampling rate of 90 per hour being achieved. The width at one fiftieth peak height (essentially baseline-to-baseline width) of 16 s, achieved in the study presented here with a carrier flow rate of 3,5 mℓ.min^{-1} and an injected sample volume of 300 µℓ, allowed an FIA-ICP sampling rate of 320 per hour.

CHAPTER 6: DETERMINATION OF CALCIUM BY FIA-ICP

6.1 Introduction

The determination of calcium in water samples by FIA-ICP is particularly interesting, as calcium concentrations in most surface waters are greater than 1 $mg.\ell^{-1}$ Ca, often by one or even two orders of magnitude, being considerably greater than the detection limit of the FIA-ICP technique. This element was also the one for which FIA-ICP determination at 90 sample injections per hour was described by Greenfield (1983).

In this chapter, the RFA determination of Ca by FIA-ICP, at a sample injection rate of 320 per hour is described, using the manifold setup delineated in chapter 5, section 5.2, with ϕ=0,01 nitric acid as the carrier. The use of both chamber No. 1 and chamber No. 5 was investigated.

For the FIA-ICP calcium determinations, the Ca-channel, profiled on the Ca 315,89 nm analytical line was used.

6.2 Precision of FIA peak height, carry-over and peak width

In Fig. 6-1 the reproducibility of peak height for 22 injections of an 80 $mg.\ell^{-1}$ Ca standard is shown, together with the steady state signal, for chamber No. 1. The reproducibility of peak height and steady state is analagously shown for chamber No. 5 in Fig. 6-2. Chamber No. 1 had a poor precision, with a RSD of 7,4%, while chamber No. 5 gave a precision of 3,4% RSD. The dispersion ratio was 1,13 for chamber No. 5, and approximately 1,2 for chamber No. 1.

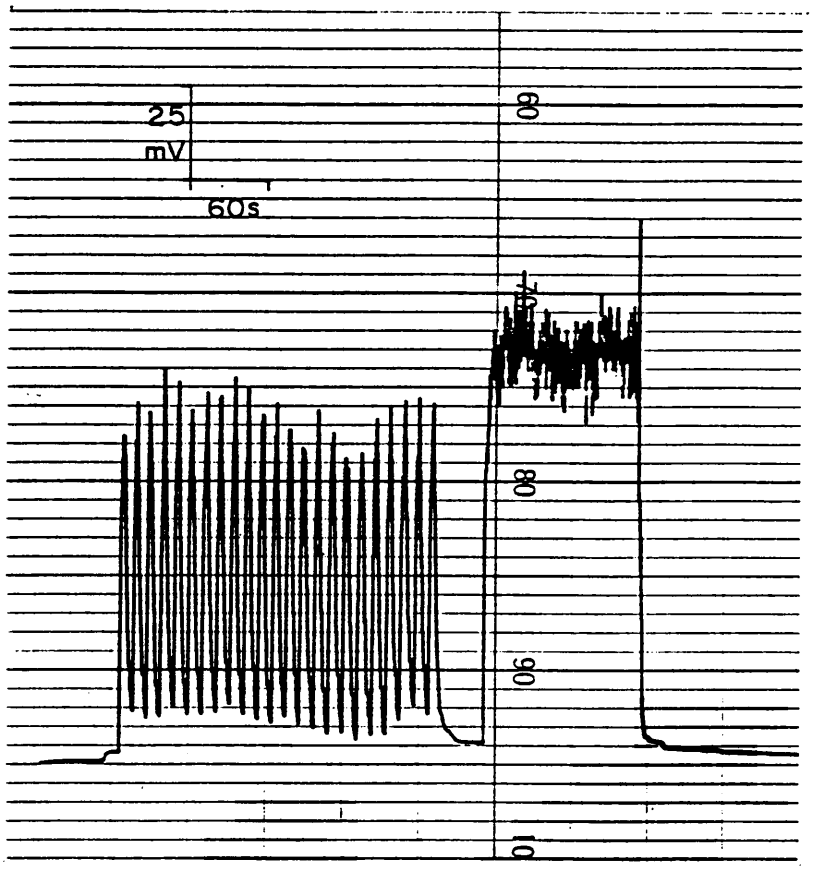

Fig. 6-1: Reproducibility of FIA signals for the Ca 315,89 nm analytical emission line, and steady state, for an 80 mg.ℓ$^{-1}$ calcium standard, using chamber No. 1. Injection volume 300 µℓ, at a sampling rate of 320 per hour. Carrier flow rate 3,5 mℓ.min^{-1}.

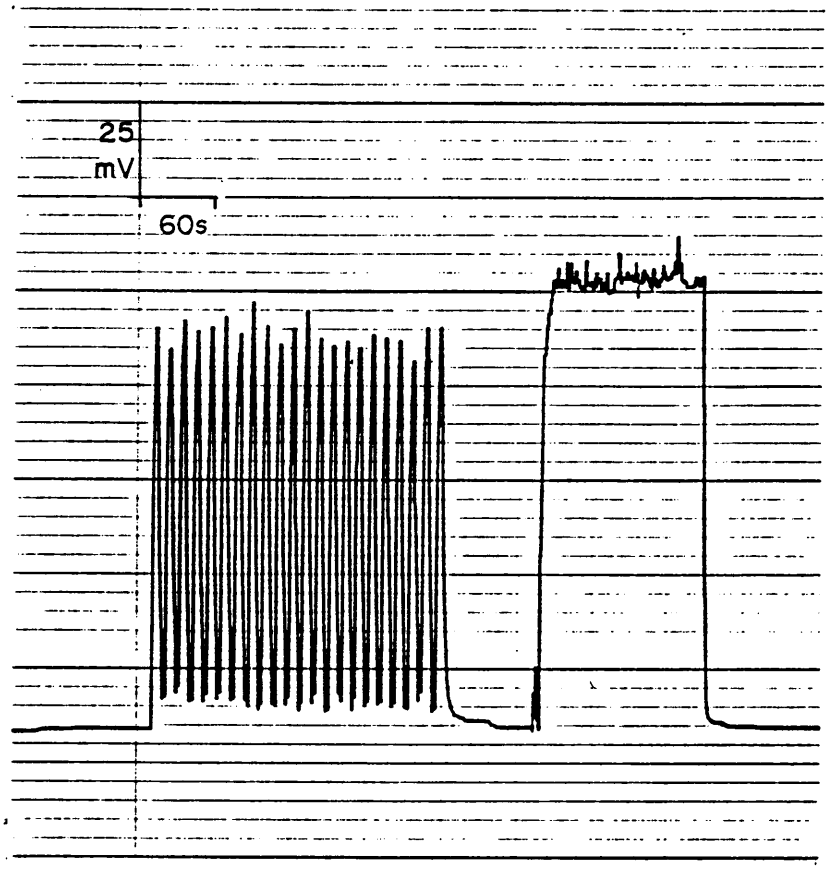

Fig. 6-2: Reproducibility of FIA signals for the Ca 315,89 nm analytical emission line, and steady state, for an 80 mg.ℓ^{-1} calcium standard, using chamber No. 5. Injection volume 300 µℓ, at a sampling rate of 320 per hour. Carrier flow rate 3,5 mℓ.min^{-1}.

To determine precision at different concentration levels, calcium standards between 4 $mg.\ell^{-1}$ and 200 $mg.\ell^{-1}$ Ca were injected, using ten injections at each concentration. The FIA peaks obtained are shown in Fig. 6-3 for chamber No. 1, and in Fig. 6-4 for chamber No. 5. The percentage RSD found is given in Table 6-1. From this table, the better precision of the small 11 mℓ chamber No. 5, compared to the 110 mℓ chamber No. 1 can be seen. The RSD was between 1,5 and 3,1% over the concentration range 40 to 200 $mg.\ell^{-1}$ for chamber No. 5, whereas the corresponding RSD values for chamber No. 1 were between 3,9 and 6,9%.

Wash-out between peaks was also superior for the small 11 mℓ chamber, the valley height between 200 $mg.\ell^{-1}$ Ca peaks reaching to within 3,8% of the baseline for this chamber. The large chamber No. 1, on the other hand showed wash-out between 200 $mg.\ell^{-1}$ Ca peaks only to within 8,0% of the baseline.

The better wash-out between peaks was also reflected in the carry-over of signal from a 200 $mg.\ell^{-1}$ Ca peak to a 20 $mg.\ell^{-1}$ Ca peak, chamber No. 1 showing a 14% carry-over, and chamber No. 5 a 3% carry-over.

Peak widths, for 300 µℓ of an 80 $mg.\ell^{-1}$ Ca standard injected into the carrier stream, are given in Table 6-2.

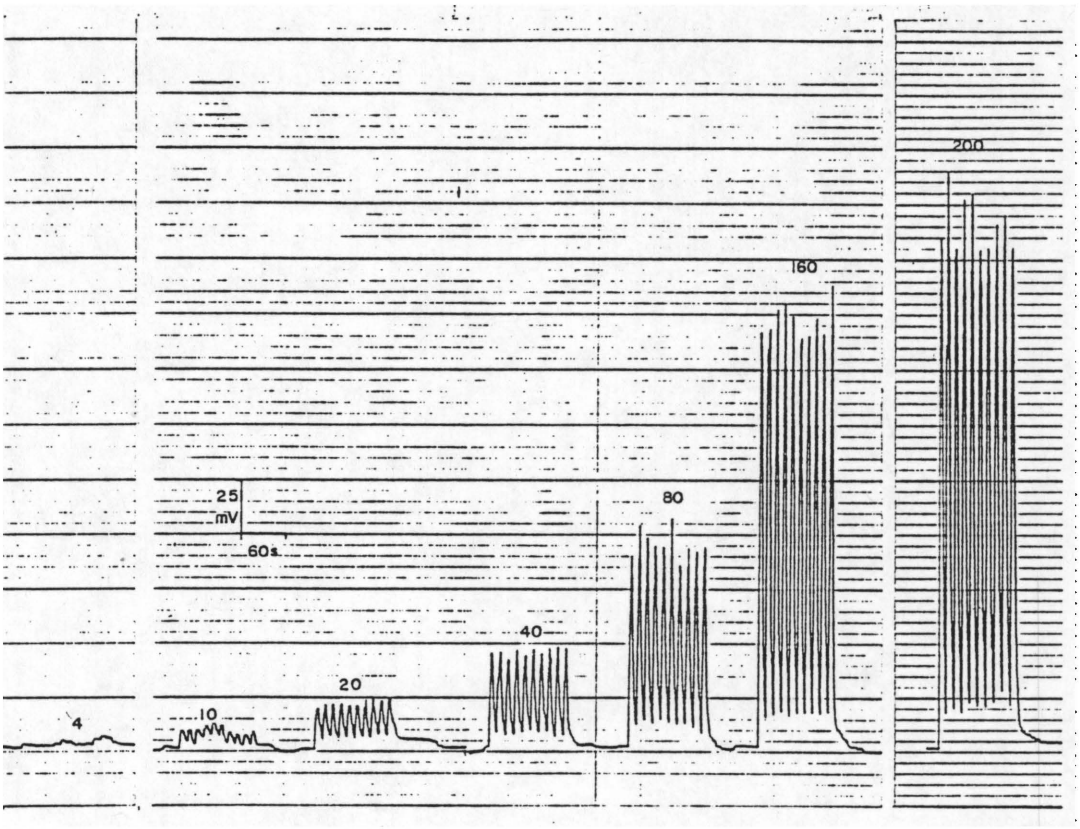

Fig. 6-3: Reproducibility of FIA signals, using chamber No. 1, for calcium concentrations of 4; 10; 20; 40; 80; 160; and 200 mg.ℓ$^{-1}$ Ca, at a sampling rate of 320 per hour, and an injection volume of 300 µℓ. Carrier flow rate 3,5 mℓ.min^{-1}.

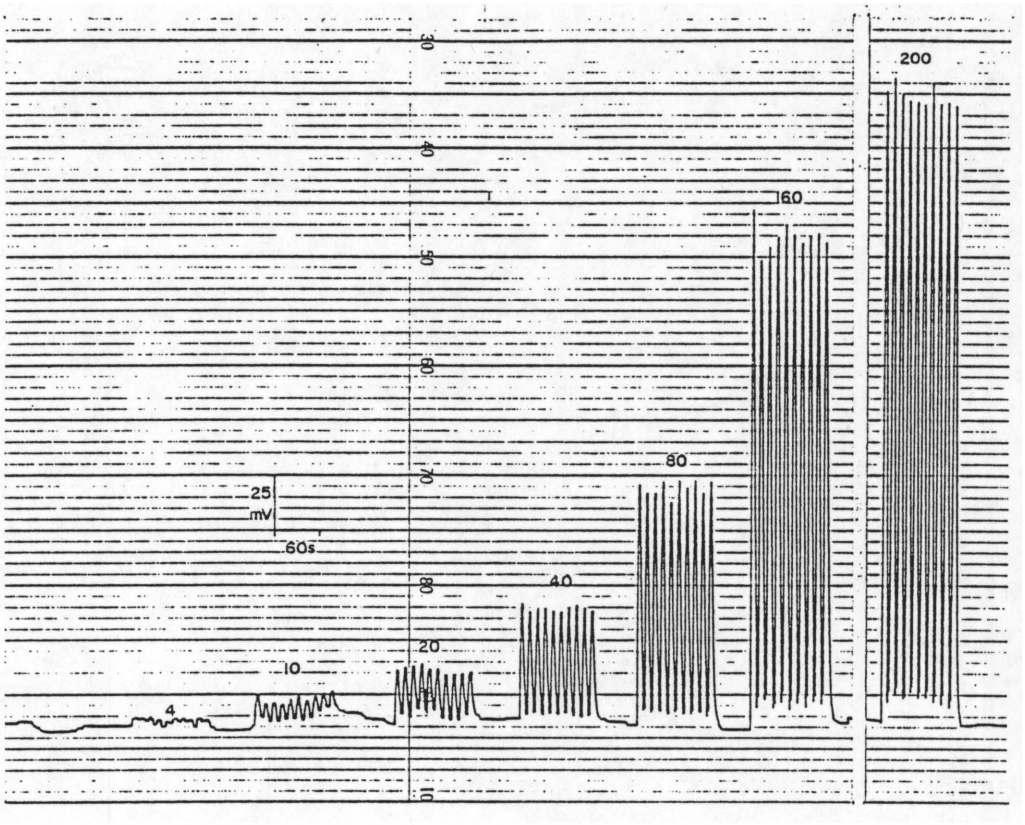

Fig. 6-4: Reproducibility of FIA signals, using chamber No. 5, for calcium concentrations of 4; 10; 20; 40; 80; 160; and 200 mg.ℓ$^{-1}$ Ca, at a sampling rate of 320 per hour, and an injection volume of 300 µℓ. Carrier flow rate 3,5 mℓ.min^{-1}.

TABLE 6-1: Reproducibility (RSD%) of FIA peak height ($\bar{H} \pm \sigma$/mm) signals, for 10 replicate measurements for calcium concentrations (C) between 4,0 and 200 mg.ℓ$^{-1}$ Ca, using a carrier flow rate of 3,5 mℓ.min^{-1}, an injected sample volume of 300 µℓ, and a sampling rate of 320 per hour.*

	Chamber No. 1		Chamber No. 5	
C/mg.ℓ$^{-1}$Ca	$\bar{H} \pm \sigma$/mm	RSD%	$\bar{H} \pm \sigma$/mm	RSD%
4,0	1,0±0,7	70%	2,0±0,3	15%
10,0	4,0±1,0	25%	5,3±0,8	15%
20,0	9,7±0,4	4,1%	12,0±1,0	**8,3%
40,0	21,8±0,9	4,1%	25,6±0,7	2,7%
80,0	46,6±3,2	6,9%	54,7±1,7	3,1%
160	97,6±3,8	3,9%	112,3±3,2	2,8%
200	119,4±6,3	5,3%	143,4±2,1	1,5%

* Recorder range setting 0,5 V FSD

** The RSD% obtained for the 10 replicates of the 20 mg.ℓ$^{-1}$ Ca standard with chamber No. 5 is unusually high, and is an outlier. The cause of this outlying value is readily apparent if one refers to Fig. 6-4, which shows how a baseline change has occurred during the recording of the FIA peaks of the 20 mg.ℓ$^{-1}$ Ca standard. A baseline shift may be inferred if one inspects the valleys between the FIA peaks. This observation is an example of how the poor baseline stability of the analogue signal of the spectrometer, refered to in chapter 5, influences the FIA analytical results. The baseline instability can also be seen on the extreme left of Fig. 6-4.

TABLE 6-2: Peak widths (w_k) at the kth proportion of maximum peak height, for a 300 µℓ volume of an 80 mg.ℓ$^{-1}$ Ca standard injected into the carrier stream flowing at 3,5 mℓ.min^{-1}, for chamber Nos. 1 and 5.

k	w_k/s*	
	Chamber No. 1	Chamber No. 5
0,5	4,6 ± 0,3	5,1 ± 0,1
0,1	10,4 ± 1,1	9,7 ± 0,4
0,02	24,6 ± 5,2	15,0 ± 2,8

* mean ± std. deviation for 4 measurements.

It is interesting that chamber No. 1 had a slightly narrower peak width than chamber No. 5 at half-height (k = 0,5), but that much larger peak widths occur near the baseline (k = 0,02) for chamber No. 1, consistent with the poorer peak resolution of chamber No. 1 compared to chamber No. 5.

6.3 Calibration

The FIA calibration data for chamber No. 1 is shown in Fig. 6-5a, and in Table 6-3. The calibration data for chamber No. 5 is given in Fig. 6-5b, and in Table 6-4. In both cases, the relationship between concentration and peak height was linear, the linear regression coefficient between calcium concentration and peak height being 0,9989 for chamber No. 1 and 0,9999 for chamber No. 5.

For chamber No. 1 the regression line has the equation:

$$H = 0,6325\ C - 1,467 \qquad \ldots\ (47)$$

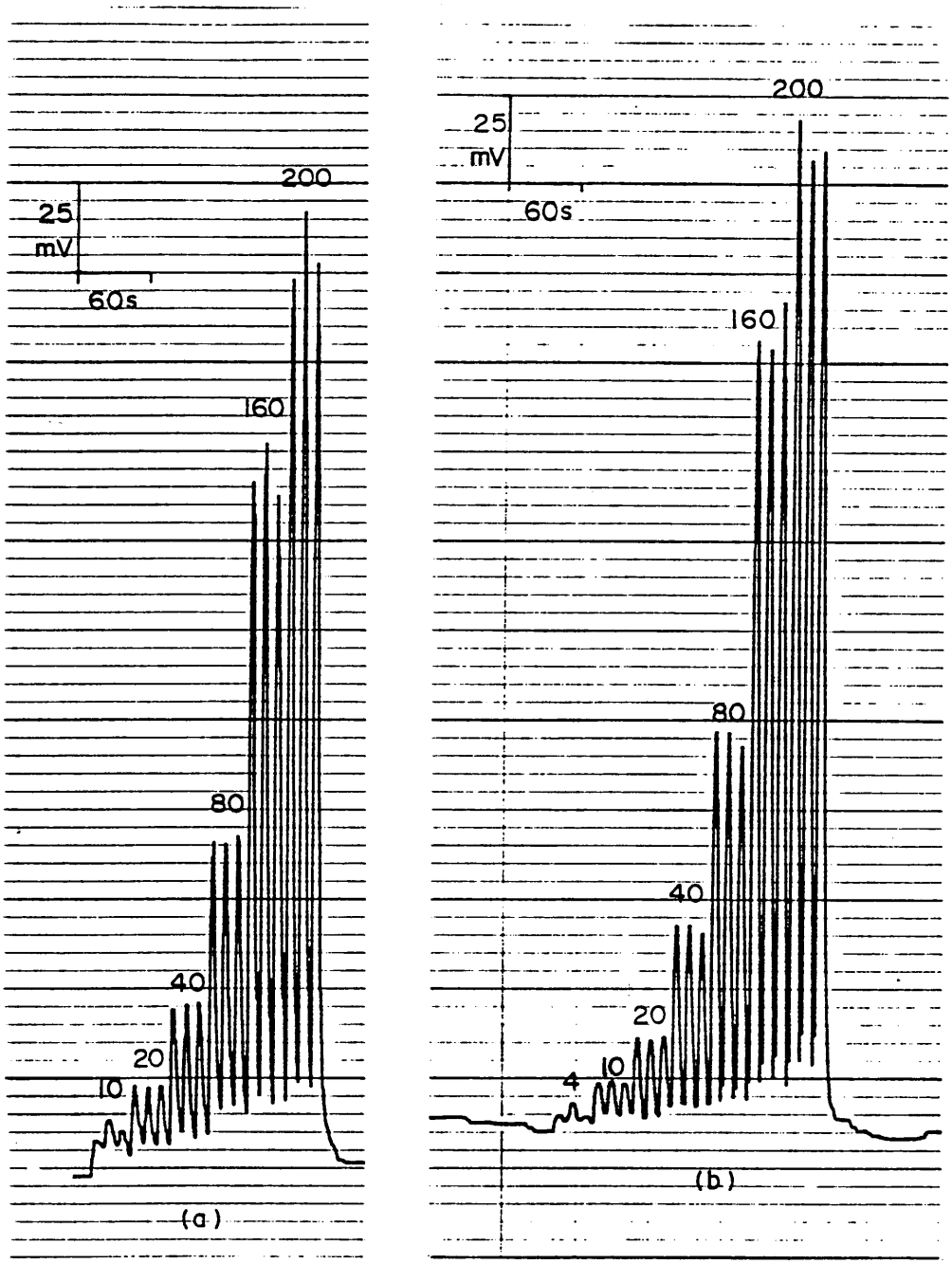

Fig. 6-5: Calibration data for (a) chamber No. 1, and (b) chamber No. 5. Sampling rate 320 per hour. Three injections of each calibration standard. Calcium concentrations, shown next to peaks, given as mg.ℓ^{-1} Ca.

Where H is the peak height in mm (at 0,5 V FSD on the recorder, corresponding to 2 mV per mm) and C is the calcium concentration in $mg.\ell^{-1}$ Ca.

For chamber No. 5 the regression line has the equation;

$$H = 0{,}6917\ C - 0{,}005 \qquad \ldots \quad (48)$$

where H and C are as defined for equation 47.

TABLE 6-3: Calibration data for calcium, for chamber No. 1, showing mean peak height ($\bar{H}$) and standard deviation (σ) for calcium concentrations (C) between 10 and 200 $mg.\ell^{-1}$ Ca. The linear correlation coefficient between C and H was 0,9989.*

$C/mg.\ell^{-1}Ca$	$\bar{H} \pm \sigma$/mm
10	6,4 ± 1,4
20	12,4 ± 0,2
40	23,4 ± 0,5
80	46,3 ± 0,6
160	97,2 ± 3,7
200	128,1 ± 5,0

* Sampling rate 320 per hour. Carrier flow rate 3,5 $m\ell.min^{-1}$. Injected sample volume 300 $\mu\ell$. Recorder range adjustment set at 0,5 V FSD.

TABLE 6-4: Calibration data for calcium, for chamber No. 5, showing mean peak height ($\bar{H}$) and standard deviation (σ) for calcium concentrations (C) between 4 and 200 mg.ℓ$^{-1}$ Ca. The linear correlation coefficient between C and $\bar{H}$ was 0,9999.*

C/mg.ℓ$^{-1}$ Ca	$\bar{H} \pm \sigma$/mm
4	2,9 ± 1,0
10	7,0 ± 0,2
20	13,1 ± 0,3
40	28,3 ± 0,7
80	54,9 ± 1,1
160	111,6 ± 3,5
200	137,7 ± 3,1

* Sampling rate 320 per hour. Carrier flow rate 3,5 mℓ.min^{-1}. Injected sample volume 300 µℓ. Recorder range adjustment set at 0,5 V FSD.

If we consider the two sigma value given by ten replicate measurements of the 40 mg.ℓ$^{-1}$ Ca standard (Table 6-1) as the detection limit, then a value of 5 mg.ℓ$^{-1}$ Ca is obtained for the detection limit using chamber No. 1, and a value of 2 mg.ℓ$^{-1}$ Ca is obtained for the detection limit for chamber No. 5, from equations 47 and 48 respectively.

6.4 Accuracy

As a test for accuracy of the FIA-ICP method, using chamber No. 5 at a sampling rate of 320 per hour, four river water samples were analyzed (a) by atomic absorption spectrometry, and (b) by FIA-ICP. In addition, aliquots of the samples were spiked with calcium, at a concentration of 30 mg.ℓ$^{-1}$ Ca, and then analyzed by FIA-ICP, and the

recovery of the added spike calculated. The results obtained are given in Table 6-5. Recoveries ranged from 93 to 102%, with a mean recovery of 97%. The FIA-ICP values were on average 6% lower than the AAS calcium values. This difference is, however, not significant as shown by a t-test (Table 6-5).

TABLE 6-5: Test of accuracy for FIA-ICP determination of calcium at a sampling rate of 320 per hour, using chamber No. 5, showing calcium concentration (C) as determined (a) by AAS*, (b) as determined by FIA-ICP, and (c) the recovery of a 30 $mg.\ell^{-1}$ Ca spike as determined by FIA-ICP**. The four samples used were river water samples. Ten replicate FIA-ICP measurements were made.

Sample No.	(a) AAS $C/mg.\ell^{-1}$	(b) FIA-ICP $\bar{C} \pm \sigma/mg.\ell^{-1}$	(c) % recovery
1	27,0	26,2 ± 1,6	102%
2	33,0	31,1 ± 0,8	95%
3	24,9	23,0 ± 1,2	93%
4	20,7	18,5 ± 0,8	97%
		Mean:	97%

* Atomic absorption spectroscopy (AAS) measurements were made on a Varian atomic absorption spectrometer model 1275, using an air-acetylene flame. Potassium and Lanthanum were added as ionization buffer and interferant suppressant respectively. Measurements were made at the Ca 422,7 nm line.

** The pooled mean of the FIA-ICP calcium concentration values is not significantly different from the pooled mean of the AAS calcium concentration values, at the 5% significance level, as shown by a two-tailed t-test (Green and Margerison, 1978). The calculated t-value was 0,461 which is less than the critical t value of 2,447 (5% two-tailed significance level for 6 degrees of freedom; Stoker, 1985).

Sample No. 1 (Table 6-5) was also analyzed by FIA-ICP using chamber No. 1. In this case the calcium concentration found was 26,6 ± 1,9 $mg.\ell^{-1}$ Ca, with the recovery of the added spike being 99%

6.5 Influence of carrier flow rate on the steady state signal

The influence of carrier flow rate variation on the steady state signal is shown in Fig. 6-6 for chamber No. 1 and in Fig. 6-7 for chamber No. 5, for the aspiration of an 80 $mg.\ell^{-1}$ Ca standard. Two differences in behaviour between the chambers are immediately apparent viz., firstly, the greater noise present in the steady state signal for chamber No. 1 as compared to the more stable signal from chamber No. 5, and secondly, signal magnitude decreases with increasing carrier flow rate for chamber No. 1, while the reverse holds for chamber No. 5. The latter variation of sensitivity with flow rate is summarized in Table 6-6. The first mentioned difference in noise levels parallels the observation that the FIA peak height signals mostly showed a smaller RSD% for chamber No. 5 than for chamber No. 1 (Table 6-1).

TABLE 6-6: Influence of carrier flow rate (F_C) variation on the sensitivity for calcium, expressed as the ratio of the signal net intensity to that found at a carrier flow rate of 1,3 $m\ell.min^{-1}$ taken as 100%.

$F_C/m\ell.min^{-1}$	Relative sensitivity %	
	Chamber No. 1	Chamber No. 5
0,7	121%	84%
1,1	106%	93%
1,3	100%	100%
1,5	96%	105%
1,9	88%	110%
2,3	81%	112%
2,7	79%	114%
3,1	78%	118%
3,5	76%	119%

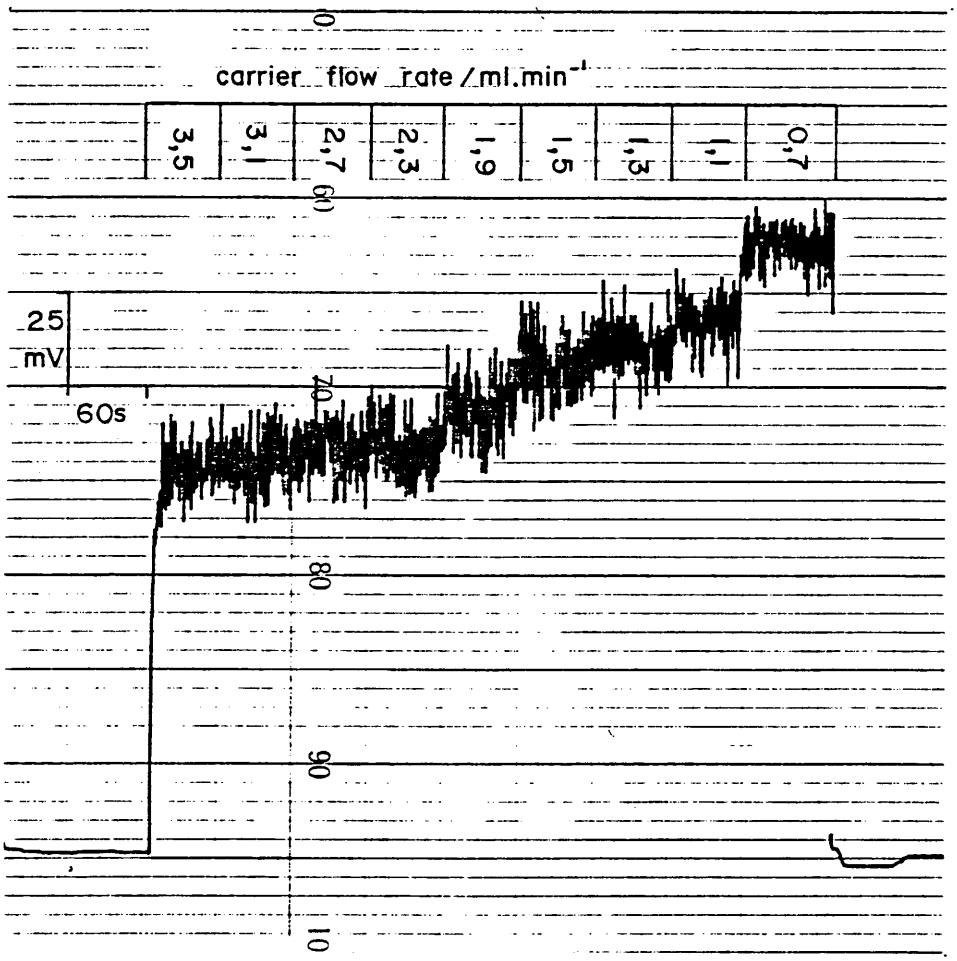

Fig. 6-6: Influence of carrier flow rate on the steady state signal of an 80 mg.ℓ$^{-1}$ calcium standard, for chamber No. 1, for a carrier flow rate from 3,5 mℓ.min^{-1} (left) to 0,7 mℓ.min^{-1} (right).

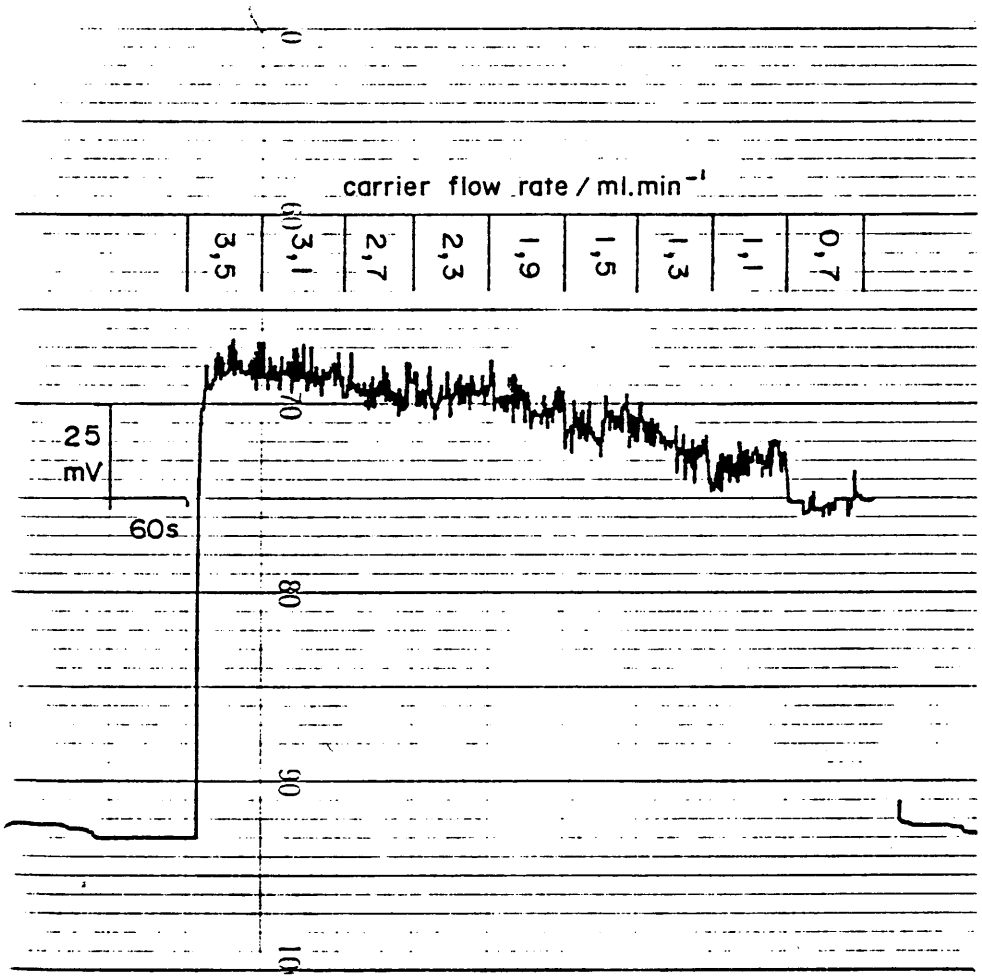

Fig. 6-7: Influence of carrier flow rate on the steady state signal of an 80 mg.ℓ$^{-1}$ calcium standard, for chamber No. 5, for a carrier flow rate from 3,5 mℓ.min^{-1} (left) to 0,7 mℓ.min^{-1} (right).

6.6 Steady state signals at different concentration levels

As was observed for boron in chapter 5, the steady state signal for calcium showed a progressive increase in noise amplitude at higher concentration levels. This is illustrated in Fig. 6-8, which shows the steady state signals between calcium concentrations of 4 $mg.\ell^{-1}$ Ca and 200 $mg.\ell^{-1}$ Ca, using chamber No. 5, at a carrier flow rate of 3,5 $m\ell.min^{-1}$. Chamber No. 1 showed similar behaviour. As was the case with boron, irregularity in the steady state signal at low concentration paralleled a similar irregularity in the baseline, consequent to the instability in the analogue signal output of the spectrometer used.

The analogue signal baseline instability, between 5 and 10 mV, has as a direct consequence, an expected effect on precision of measurement of peak height, as this instability constitutes a variation in the 200 $mg.\ell^{-1}$ Ca signal, at about 290 mV of 1,7% to 3,4%; while for the 80 $mg.\ell^{-1}$ Ca standard with a steady state signal at about 115 mV (Fig. 6-8), the 5 to 10 mV analogue baseline signal instability represents between 4,3% and 8,7% of the signal intensity.

It is thus to be expected that the FIA peak height precisions found (Table 6-1), are inferior to the oft better than 1% precision characteristic of conventional ICP emission spectrometry, with intensity integration over as much as 10 s (Kempster, 1986).

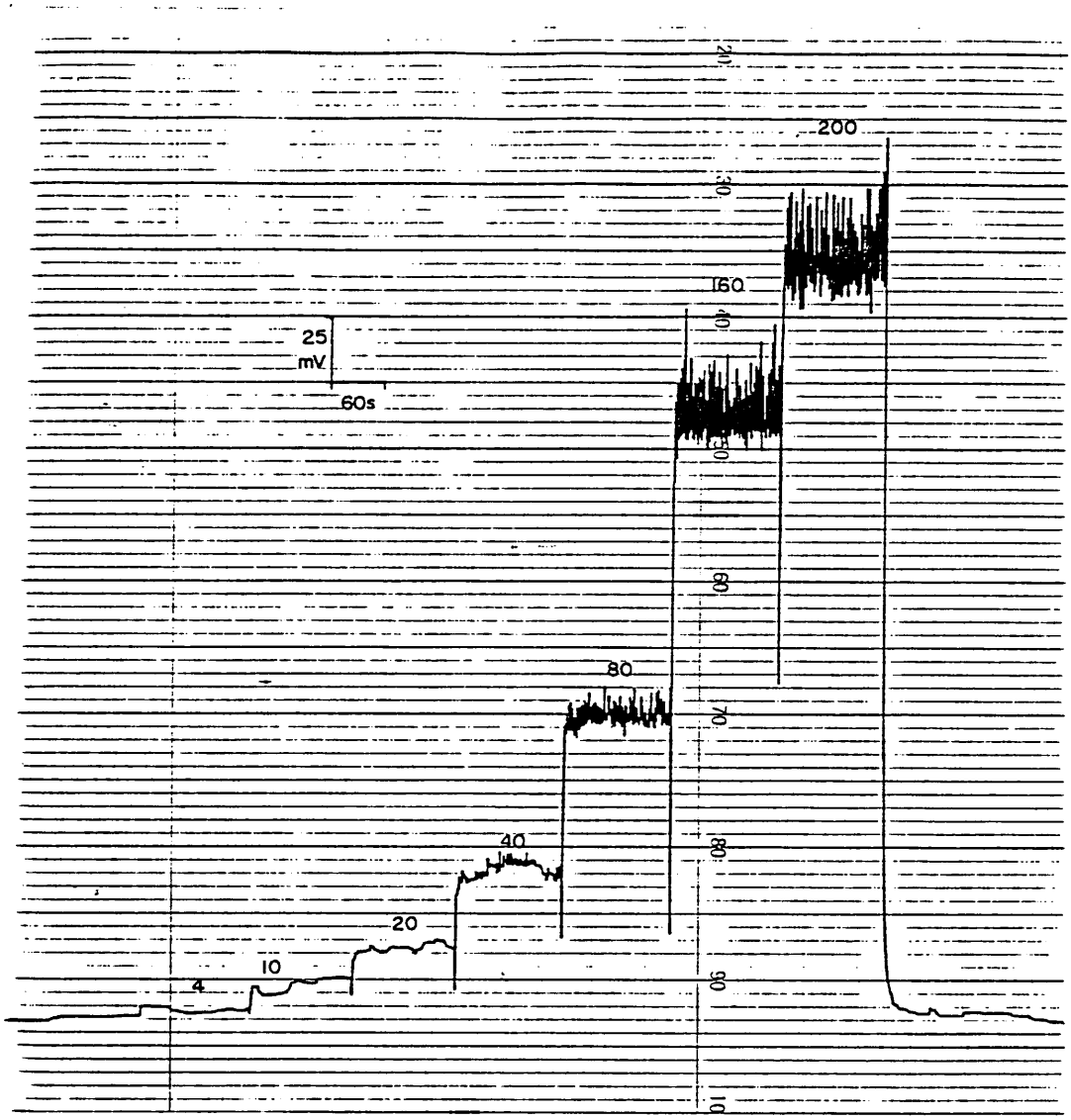

Fig. 6-8: Steady state signals, using chamber No. 5, for calcium concentrations from 4 mg.ℓ$^{-1}$ Ca to 200 mg.ℓ$^{-1}$ Ca.

6.7 Summary and conclusion

Rapid sample introduction, with a sample injection rate of 320 per hour, was tested using the FIA-ICP combination, as described in Chapter 5, for calcium using the conventional spray chamber No. 1, and the small 11 mℓ chamber No. 5.

The small chamber gave superior precision values of between 1,5% and 3,1% over the concentration range 40 to 200 $mg.\ell^{-1}$ Ca, whereas the conventional chamber No. 1 gave corresponding RSD values of 3,9% to 6,9%. Wash-out between peaks was excellent for chamber No. 5, with the valley between 200 $mg.\ell^{-1}$ Ca FIA peaks reaching to within 3,8% of the baseline. Chamber No. 1 by contrast only showed wash-out to within 8% of the baseline. The correlation between peak height and calcium concentration was highly linear, which facilitated calibration. The detection limit of the FIA-ICP method was 2 $mg.\ell^{-1}$ Ca for chamber No. 5, and 5 $mg.\ell^{-1}$ Ca for chamber No. 1.

Tests for accuracy of the FIA-ICP method, using chamber No. 5, showed mean recovery of 97% for the four river water samples evaluated. Comparison with calcium as determined by AAS showed the FIA-ICP values were around 6% lower than the AAS values, this difference was not significant, however (Table 6-5).

The base width of the FIA signal peaks of around 15 s for chamber No. 5, with a 300 µℓ injected sample volume and carrier flow rate of 3,5 $mℓ.min^{-1}$ were about 50% narrower than the base-width of around 30 s reported by Greenfield (1983). The conventional 110 mℓ chamber No. 1, by contrast gave FIA signal peaks with a base-width of around 25 s. Of the two chambers tested for the FIA-ICP determination of calcium, the 11 mℓ spray chamber clearly gave superior analytical characteristics, both with repsect to precision as well as wash-out between peaks, and the narrow peak base-widths facilitated rapid sample introduction.

As was the case for boron determination, a major limiting factor, both with respect to precision and detection limit was the instability in the analogue signal output of the particular spectrometer used.

CHAPTER 7: USE OF FIA-ICP FOR THE DETERMINATION OF MAGNESIUM, MANGANESE AND STRONTIUM

7.1 Introduction

In this chapter, the potential of the FIA-ICP method for the rapid determination of magnesium, manganese and strontium is described. The FIA-ICP instrumental setup as delineated in chapter 5, section 5.2 was used. The spray chamber employed was chamber No. 5. The carrier solution was ϕ=0,01 nitric acid. For a sample introduction rate of 320 per hour, a carrier flow rate of 3,5 $m\ell.min^{-1}$ was used, the sample volume injected being 300 $\mu\ell$. The analytical wavelengths of the magnesium, manganese and strontium channels of the ARL 34000 ICP emission spectrometer were 383,83 nm; 257,61 nm; and 421,55 nm respectively.

As was the case with boron (chapter 5) and calcium (chapter 6), detection limit and precision were limited by the instability in the analogue signal output from the spectrometer electronics (chapter 5, section 5.2).

7.2 Evaluation of the FIA-ICP method for magnesium determination

The reproducibility of peak height for 22 injections of a 100 $mg.\ell^{-1}$ Mg standard is shown, together with the steady state signal, using chamber No. 5, in Fig. 7-1.

The percentage relative standard deviation (RSD%) of the FIA peak height signals was 2,7%, the dispersion ratio being 1,16.

For evaluation of precision at different concentration levels over the analytical range, magnesium standards covering the concentration range from 5 $mg.\ell^{-1}$ to 300 $mg.\ell^{-1}$ Mg were injected, using ten injections at

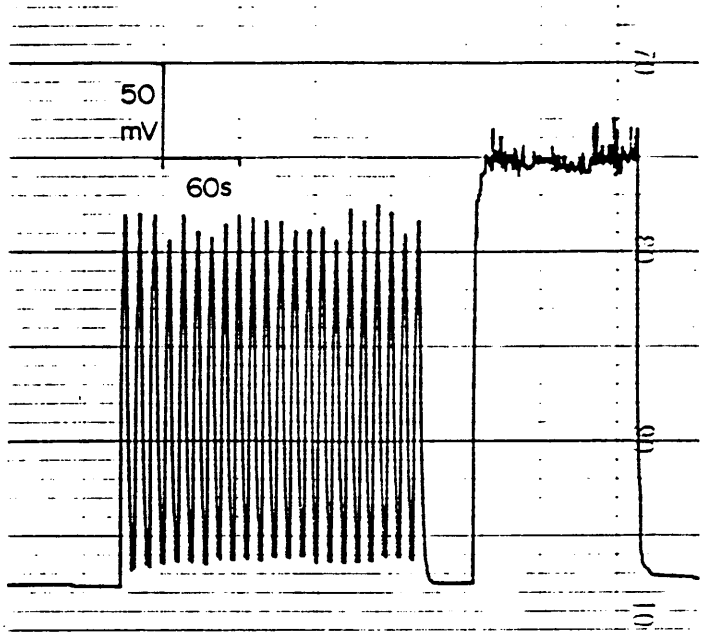

Fig. 7-1: Reproducibility of FIA signals for the Mg 383,83 nm analytical emission line, and steady state, for a 100 mg.ℓ$^{-1}$ magnesium standard, using chamber No. 5. Injection volume 300 µℓ, at a sampling rate of 320 per hour. Carrier flow rate 3,5 mℓ.min^{-1}.

each concentration. The FIA signals obtained are shown in Fig. 7-2. The percentage RSD found at each concentration level is given in Table 7-1. The RSD was between 2,8 and 6,0% over the concentration range 10 to 300 $mg.\ell^{-1}$ Mg.

Wash-out between peaks was good, the valley height above baseline between 300 $mg.\ell^{-1}$ Mg FIA signals reaching to within 3,2% of the baseline (Fig. 7-2). Carry-over of signal when a 200 $mg.\ell^{-1}$ Mg standard was immediately followed by a 20 $mg.\ell^{-1}$ Mg standard, showed an increase in the peak height of the 20 $mg.\ell^{-1}$ Mg standard of around 6%.

Peak widths, for a 300 $\mu\ell$ injection of a 100 $mg.\ell^{-1}$ Mg standard injected into the carrier stream, are given in Table 7-2.

TABLE 7-1: Reproducibility (RSD%) of FIA peak height ($\bar{H} \pm \sigma$/mm) signals, for 10 replicate measurements for magnesium concentrations (C) between 5,0 and 300 $mg.\ell^{-1}$ Mg, using a carrier flow rate of 3,5 $m\ell.min^{-1}$, an injected sample volume of 300 $\mu\ell$, and a sampling rate of 320 per hour.*

$C/mg.\ell^{-1}Mg$	$\bar{H} \pm \sigma$/mm	RDS%
5,0	**0,8 ± 0,2	25%
10,0	3,3 ± 0,2	6,0%
20,0	7,5 ± 0,4	5,3%
30,0	13,8 ± 0,6	4,3%
50,0	23,0 ± 0,8	3,5%
100	48,2 ± 1,2	2,5%
200	99,9 ± 2,4	2,4%
300	152,1 ± 4,2	2,8%

* Recorder range setting 1V FSD; chamber No. 5 used.

** Peak height at low concentration may be noticeably affected by analogue signal baseline instability.

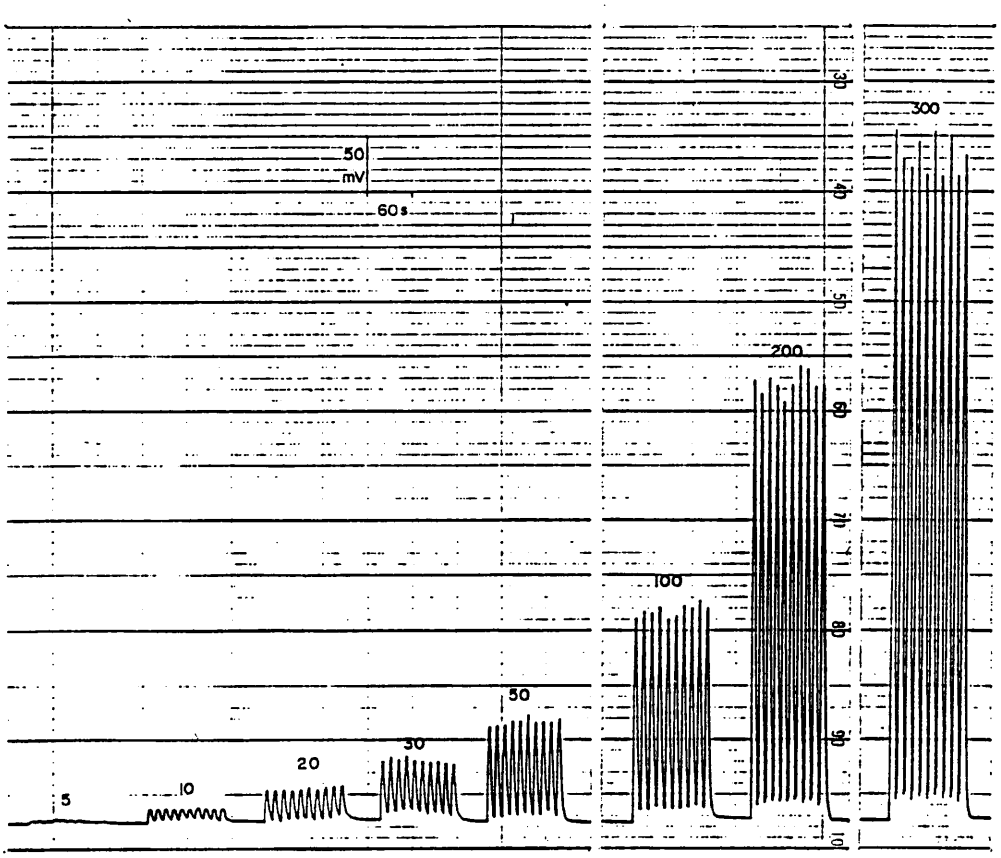

Fig. 7-2: Reproducibility of FIA signals, using chamber No. 5, for magnesium concentrations of 5; 10; 20; 30; 50; 100; 200; and 300 mg.ℓ$^{-1}$ Mg, at a sampling rate of 320 per hour, and an injection volume of 300 µℓ. Carrier flow rate 3,5 mℓ.min^{-1}.

TABLE 7-2: Peak width (w_k) at the kth proportion of maximum peak height, for a 300 µℓ volume of a 100 mg.ℓ$^{-1}$ Mg standard injected into the carrier stream flowing at 3,5 mℓ.min^{-1}, for chamber No. 5.

k	w_k/s*
0,5	5,1 ± 0,1
0,1	9,4 ± 0,4
0,02	13,9 ± 0,9

* mean ± std. deviation for 4 measurements.

TABLE 7-3: Calibration data for magnesium, for chamber No. 5, showing mean peak height ($\bar{H}$) and standard deviation (σ) for magnesium concentrations (C) between 5,0 and 300 mg.ℓ$^{-1}$ Mg. The linear correlation coefficient between C and $\bar{H}$ was 0,9998.*

C/mg.ℓ$^{-1}$Mg	$\bar{H}$ ± σ/mm
5,0	**1,5 ± 0,3
10,0	3,3 ± 0,3
20,0	8,6 ± 0,4
30,0	13,2 ± 0,8
50,0	23,5 ± 0,7
100	46,7 ± 0,5
200	96,1 ± 2,2
300	149,0 ± 2,2

* Sampling rate 320 per hour. Carrier flow rate 3,5 mℓ.min^{-1}. Injected sample volume 300 µℓ. Recorder range adjustment set a 1V FSD.

** Peak height at low concentration may be noticeably affected by analogue signal baseline instability.

The peak widths found for Mg, using chamber No. 5, were similar to those found for calcium in the previous chapter (Table 6-2).

FIA calibration data for magnesium is shown in Fig. 7-3, and in Table 7-3. The relationship between concentration and peak height was linear, the linear regression coefficient between magnesium concentration and peak height being 0,9998. The regression line has the equation:

$$H = 0,4976\ C - 1,732 \qquad (49)$$

where H is the peak height in mm (at 1V FSD on the recorder, corresponding to 4 mV per mm) and C is the magnesium concentration in $mg.\ell^{-1}$ Mg. If we consider the two sigma value given by ten replicate measurements of the 20 $mg.\ell^{-1}$ Mg standard (Table 7-1) as the detection limit; then a value for the detection limit of 5 $mg.\ell^{-1}$ Mg is obtained by substitution of the two sigma height value in equation 49.

As a test for accuracy of the FIA-ICP method for magnesium determination, at a sampling rate of 320 per hour, six river water samples were analyzed (a) by atomic absorption spectrometry, and (b) by FIA-ICP. In addition, aliquots of the samples were spiked with magnesium, at a concentration of 20 $mg.\ell^{-1}$ Mg, and then analyzed by FIA-ICP, and the recovery of the added spike calculated. The results obtained are given in Table 7-4. Recoveries ranged from 91% to 107%, with a mean recovery of 101%. The FIA-ICP values were on average 6% lower than the AAS magnesium values. This difference in means was not significant, however, as shown by a t-test (Table 7-4).

As shown in Fig. 7-1, noise is present in the steady state signal of a 100 $mg.\ell^{-1}$ Mg standard. The noise in the steady state signal is particularly marked at higher concentration levels, and becomes less marked at lower concentration levels (Fig. 7-4).

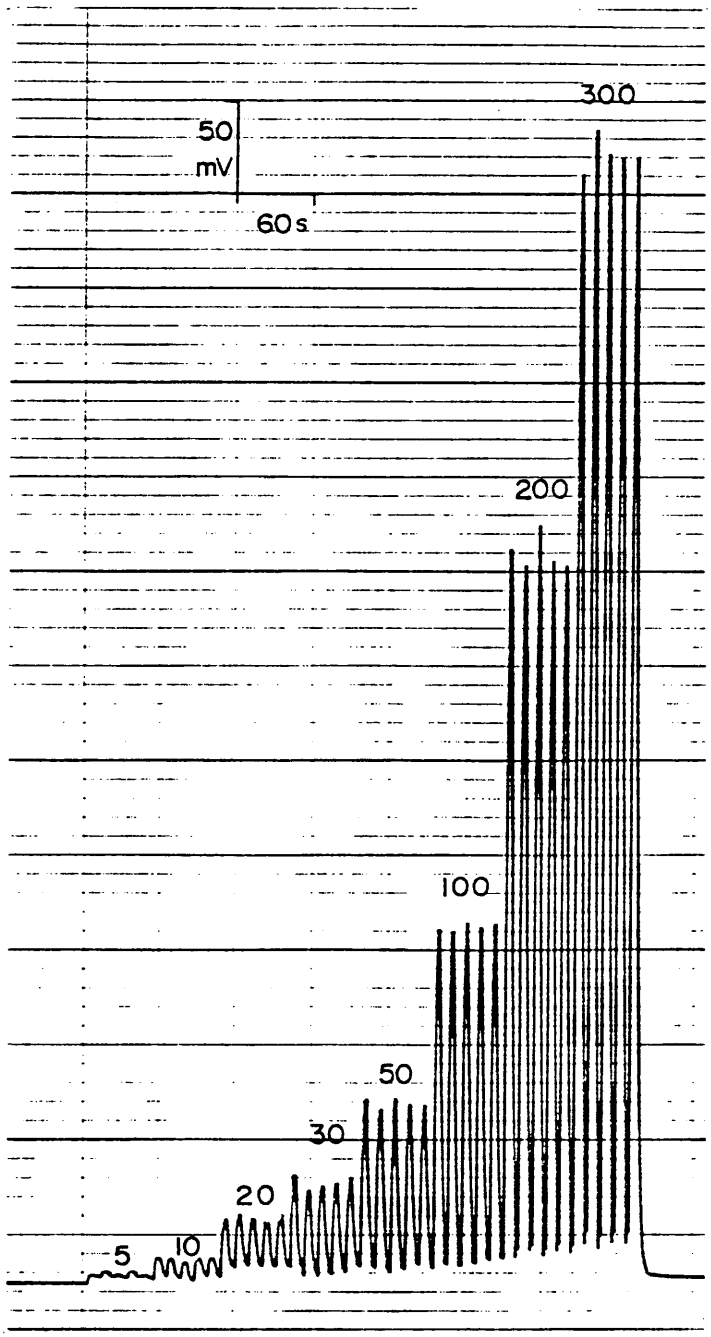

Fig. 7-3: Calibration data for magnesium, using chamber No. 5. Sampling rate 320 per hour. Five injections of each calibration standard. Injection volume 300 µℓ. Magnesium concentrations, shown next to the peaks, given as $mg.\ell^{-1}$.

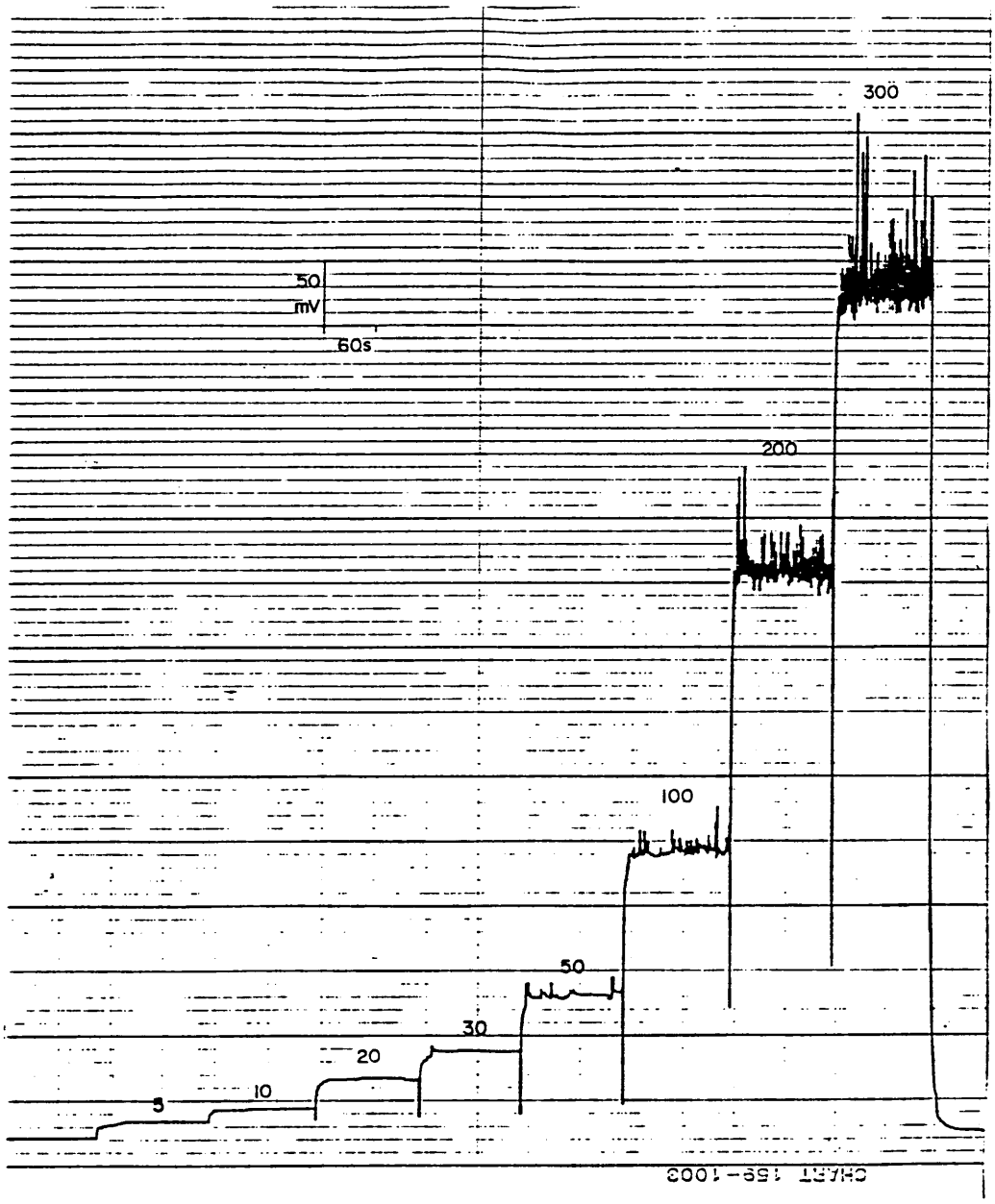

Fig. 7-4: Steady state signals, using chamber No. 5, for magnesium concentrations from 5 mg.ℓ$^{-1}$ Mg to 300 mg.ℓ$^{-1}$ Mg. Concentrations in mg.ℓ$^{-1}$ shown next to the steady state plateaus. Carrier flow rate was 3,5 mℓ.min^{-1}.

TABLE 7-4: Test for accuracy for FIA-ICP determination of magnesium at a sampling rate of 320 per hour, using chamber No. 5, showing magnesium concentration (C) as determined (a) by AAS*, (b) as determined by FIA-ICP**, and (c) the recovery of a 20 $mg.\ell^{-1}$ Mg spike as determined by FIA-ICP. The six samples used were river samples. Ten replicate FIA-ICP measurements were made.

Sample No.	(a) AAS $C/mg.\ell^{-1}$	(b) FIA-ICP $\bar{C} \pm \sigma/mg.\ell^{-1}$	(c) % recovery
1	7,9	8,1 ± 0,4	91%
2	21,9	19,3 ± 0,8	102%
3	12,0	11,2 ± 1,4	99%
4	35,5	32,0 ± 0,8	107%
5	30,6	29,5 ± 1,4	107%
6	45,6	44,4 ± 1,4	99%
		Mean:	101%

* Atomic absorption spectroscopy (AAS) measurements were made on a Varian atomic absorption spectrometer model 1275, using an air-acetylene flame. Potassium and Lanthanum were added as ionization buffer and interference suppresant respectively. Absorption measurements were made at the Mg 285,2 nm line.

** The pooled mean of the FIA-ICP magnesium concentration values is not significantly different from the pooled mean of the AAS magnesium concentration values, at the 5% significance level, as shown by a two-tailed t-test (Green and Margerison, 1978). The calculated t value was 0,184 which is less than the critical t value of 2,228 (5% two-tailed significance level for 10 degrees of freedom; Stoker, 1985).

The influence of carrier flow rate variation on the magnesium steady state signal is shown in Fig. 7-5 for chamber No. 5, and in Fig. 7-6 for chamber No. 1, for magnesium concentrations of 100 $mg.\ell^{-1}$ and 50 $mg.\ell^{-1}$ respectively. The variation in sensitivity with flow rate is summarized in Table 7-5, which shows that

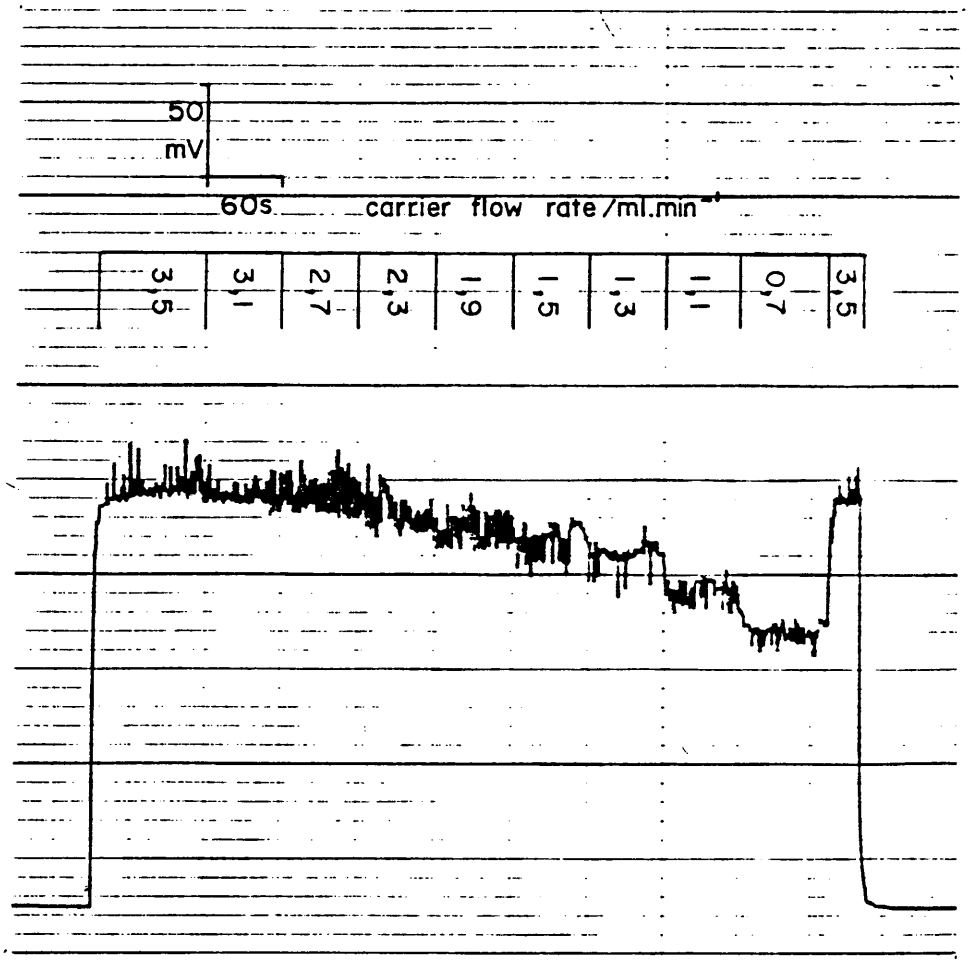

Fig. 7-5: Influence of carrier flow rate on the steady state signal of a 100 mg.ℓ$^{-1}$ magnesium standard, for chamber No. 5, for a carrier flow rate from 3,5 mℓ.min^{-1} to 0,7 mℓ.min^{-1}.

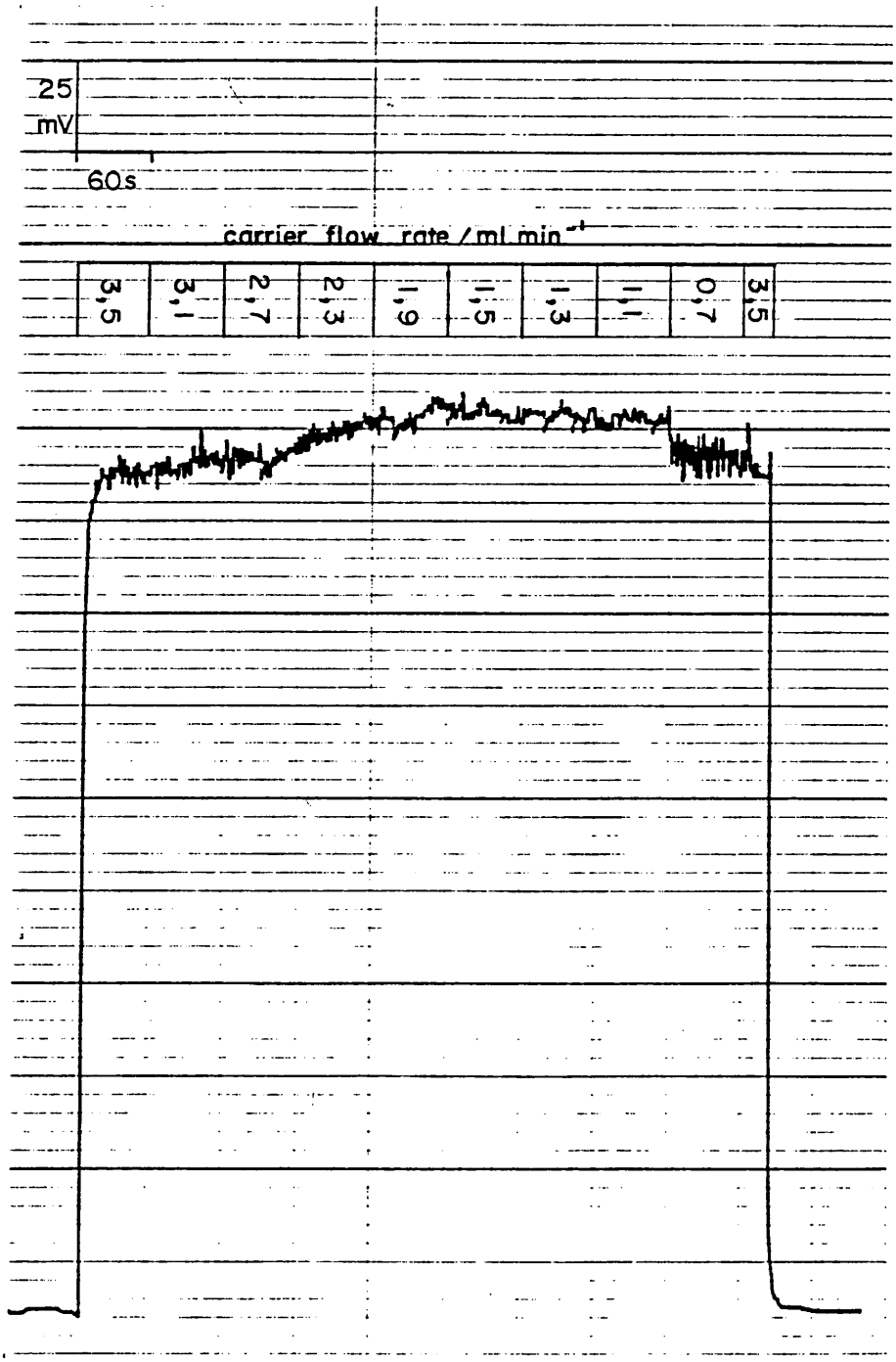

Fig. 7-6: Influence of carrier flow rate on the steady state signal of a 50 mg.ℓ$^{-1}$ magnesium standard, for chamber No. 1, for a carrier flow rate from 3,5 mℓ.min^{-1} to 0,7 mℓ.min^{-1}.

chamber No. 5 gave increased sensitivity at the higher carrier flow rates; while chamber No. 1 showed maximum sensitivity for magnesium at a carrier flow rate of around 1,5 mℓ.min^{-1}.

TABLE 7-5: Influence of carrier flow rate (F_c) variation on the sensitivity for magnesium, expressed as the ratio of the signal net intensity to that found at a carrier flow rate of 1,3 mℓ.min^{-1} taken as 100%.

F_c/mℓ.min^{-1}	Relative sensitivity %	
	Chamber No. 1	Chamber No. 5
0,7	95%	77%
1,1	99%	89%
1,3	100%	100%
1,5	100%	105%
1,9	100%	108%
2,3	98%	112%
2,7	96%	117%
3,1	95%	117%
3,5	93%	118%

7.3 Evaluation of the FIA-ICP method for manganese determination

The reproducibility of peak height for 22 injections of a 20 $mg.\ell^{-1}$ Mn standard is shown, together with a steady state signal, using chamber No. 5, in Fig. 7-7. The percentage relative standard deviation (RSD%) of the FIA peak height signals was 2,7%, the dispersion ratio being 1,11.

For evaluation of precision at different concentration levels over the analytical range, manganese standards covering the concentration range from 1,0 $mg.\ell^{-1}$ to 50 $mg.\ell^{-1}$ Mn were injected, using ten injections at each concentration. The FIA signals obtained are shown in Fig. 7-8. The percentage RSD found at each concentration level is given in Table 7-6. The RSD was between 1,5 and 4,8% over the concentration range 2,0 to 50 $mg.\ell^{-1}$ Mn.

Wash-out between peaks was good, the valley height above baseline between 50 $mg.\ell^{-1}$ Mn FIA signals reaching to within 3,4% of the baseline (Fig. 7-8). Carry-over of signal when a 50 $mg.\ell^{-1}$ Mn standard was immediately followed by a 5 $mg.\ell^{-1}$ Mn standard, showed an increase in the peak height of the 5 $mg.\ell^{-1}$ Mn standard of around 4%.

Peak widths, for a 300 $\mu\ell$ injection of a 25 $mg.\ell^{-1}$ Mn standard injected into the carrier stream, are given in Table 7-7.

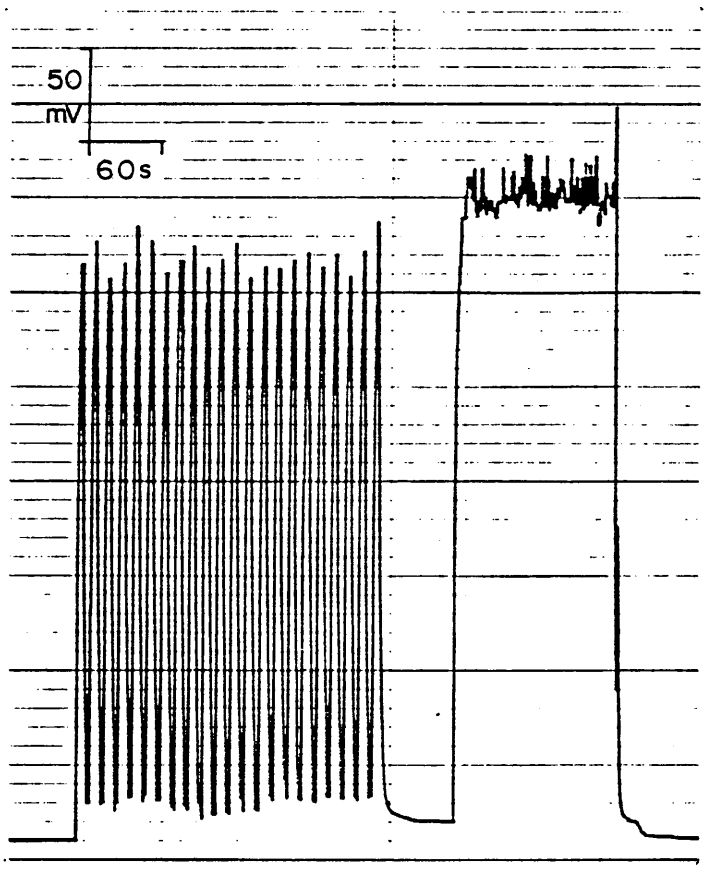

Fig. 7-7: Reproducibility of FIA signals for the Mn 257,61 nm analytical line, and steady state, for a 20 $mg.\ell^{-1}$ manganese standard, using chamber No. 5. Injection volume 300 µℓ, at a sampling rate of 320 per hour. Carrier flow rate 3,5 $m\ell.min^{-1}$.

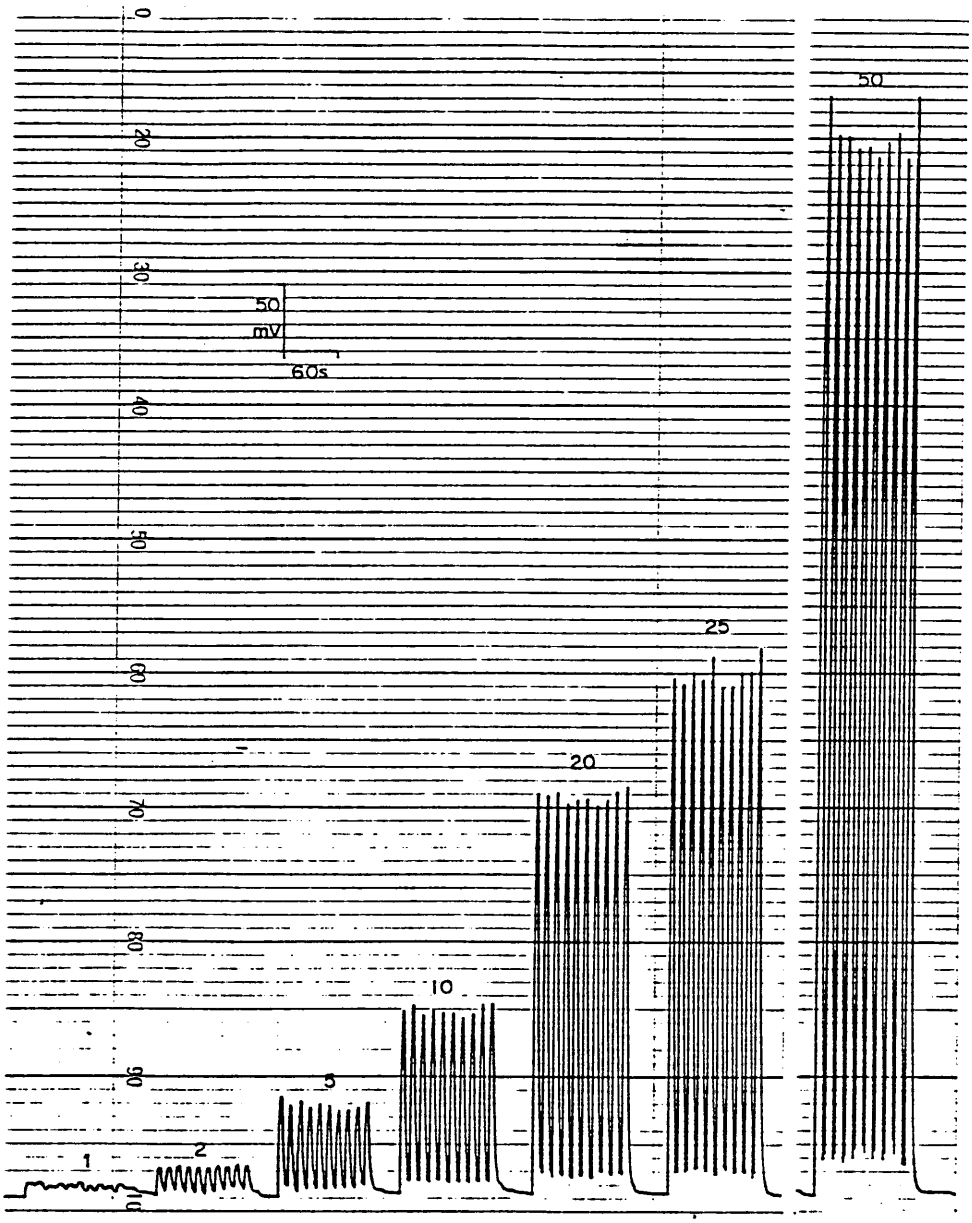

Fig. 7-8: Reproducibility of FIA signals, using chamber No. 5, for manganese concentrations of 1; 2; 5; 10; 20; 25; and 50 mg.ℓ$^{-1}$ Mn, at a sampling rate of 320 per hour, and an injection volume of 300 µℓ. Carrier flow rate 3,5 mℓ.min^{-1}.

TABLE 7-6: Reproducibility (RSD%) of FIA peak height ($\bar{H} \pm \sigma$/mm) signals, for 10 replicate measurements for manganese concentrations (C) between 1,0 and 50 mg.ℓ$^{-1}$ Mn, using a carrier flow rate of 3,5 mℓ.min^{-1}, an injected sample volume of 300 µℓ, and a sampling rate of 320 per hour.*

C/mg.ℓ$^{-1}$Mn	$\bar{H} \pm \sigma$/mm	RSD%
1,0	**2,5 ± 0,4	16%
2,0	5,4 ± 0,2	3,7%
5,0	16,6 ± 0,8	4,8%
10,0	33,7 ± 0,9	2,7%
20,0	73,7 ± 1,1	1,5%
25,0	96,7 ± 2,4	2,5%
50,0	197,2 ± 4,2	2,1%

* Recorder range setting 1V FSD; chamber No. 5 used.

** Peak height at low concentration may be noticeably affected by analogue signal baseline instability.

TABLE 7-7: Peak widths (w_k) at the kth proportion of maximum peak height, for a 300 µℓ volume of a 25 mg.ℓ$^{-1}$ Mn standard injected into the carrier stream flowing at 3,5 mℓ.min^{-1}, for chamber No. 5.

k	w_k/s*
0,5	4,9 ± 0,1
0,1	8,9 ± 0,4
0,02	13,1 ± 1,1

* mean ± std. deviation for 4 measurements.

FIA calibration data for manganese is shown in Fig. 7-9, and in Table 7-8. The relationship between manganese concentration and peak height was linear, the linear regression coefficient between manganese concentration and peak height being 0,99999. The regression line has the equation;

$$H = 3,7944\ C - 2,938 \qquad \ldots\ (50)$$

Where H is the peak height in mm (at 1V FSD on the recorder, corresponding to 4 mV per mm) and C is the manganese concentration in $mg.\ell^{-1}$ Mn. If we consider the two sigma value given by ten replicate measurements of the 1,0 $mg.\ell^{-1}$ Mn standard (Table 7-6) as the detection limit, then a value for the detection limit of 1 $mg.\ell^{-1}$ Mn is obtained by substitution of the two sigma height value in equation 50.

As a test for accuracy of the FIA-ICP method for manganese determination, at a sampling rate of 320 per hour, three stream samples contaminated by acid mine drainage and containing high manganese concentrations were analyzed (a) by atomic absorption spectrometry, and (b) by FIA-ICP. In addition, aliquots of the samples were spiked with manganese, at a concentration of 10 $mg.\ell^{-1}$ Mn, and then analyzed by FIA-ICP, and the recovery of the added spike calculated. The results obtained are given in Table 7-9. Recoveries ranged from 97 to 101%, with a mean recovery of 98%. The FIA-ICP values were on average 8% lower than the AAS manganese values. The near 100% recovery obtained by FIA-ICP suggests that matrix effects may possibly have been present in the AAS measurements.

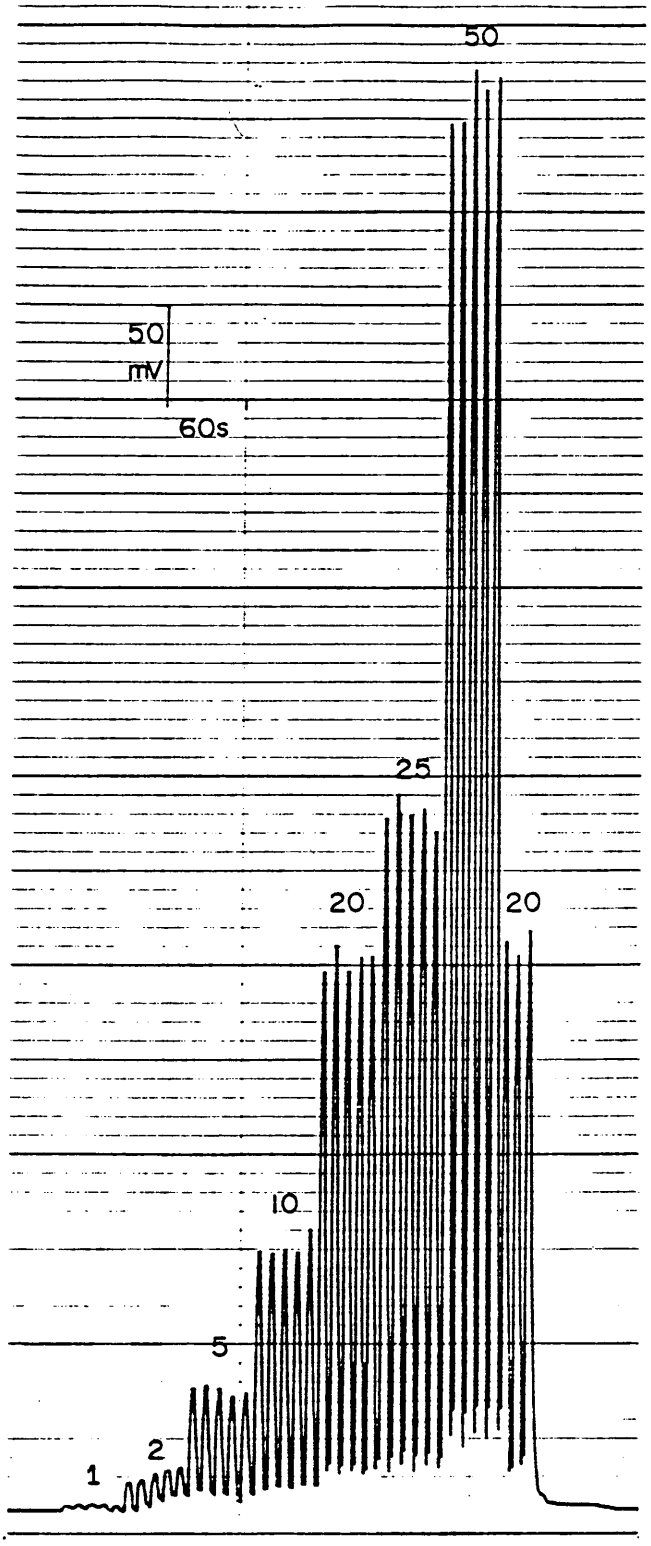

Fig. 7-9: Calibration data for manganese, using chamber No. 5. Sampling rate 320 per hour. Five injections of each calibration standard. Injection volume 300 µℓ. Manganese concentrations in $mg.\ell^{-1}$ shown next to the peaks. Carrier flow rate was 3,5 $m\ell.min^{-1}$.

TABLE 7-8: Calibration data for manganese, for chamber No. 5, showing mean peak height ($\bar{H}$) and standard deviation (σ) for manganese concentrations (C) between 1,0 $mg.\ell^{-1}$ and 50 $mg.\ell^{-1}$ Mn. The linear correlation coefficient between C and $\bar{H}$ was 0,99999.*

C/$mg.\ell^{-1}$ Mn	$\bar{H} \pm \sigma$/mm
1,0	**1,0 ± 0,1
2,0	5,0 ± 0,8
5,0	16,0 ± 0,5
10,0	34,8 ± 1,3
20,0	72,5 ± 1,4
25,0	91,9 ± 1,7
50,0	187,0 ± 3,3

* Sampling rate 320 per hour. Carrier flow rate 3,5 $m\ell.min^{-1}$. Injected sample volume 300 $\mu\ell$. Recorder range adjustment set at 1V FSD.

** Peak height at low concentration may be noticeably affected by analogue signal baseline instability.

As shown in Fig. 7-7, noise is present in the steady state signal of a 20 $mg.\ell^{-1}$ Mn standard. The noise in the steady state signal is particularly marked at higher concentration levels, and becomes less marked at lower concentration levels (Fig. 7-10).

The influence of carrier flow rate variation on the manganese steady state signal is shown in Fig. 7-11 for chamber No. 5, and in Fig. 7-12 for chamber No. 1, for manganese concentrations of 20 $mg.\ell^{-1}$ and 10 $mg.\ell^{-1}$ respectively. The variation in sensitivity with flow rate is summarized in Table 7-10 which shows that

chamber No. 5 has best sensitivity for manganese at high carrier flow rates, while chamber No. 1 shows the opposite, with best sensitivity at low carrier flow rates of the uptake solution to the nebulizer.

TABLE 7-9: Test for accuracy for FIA-ICP determination of manganese at a sampling rate of 320 per hour, using chamber No. 5, showing manganese concentration (C) as determined (a) by AAS*, (b) as determined by FIA-ICP**, and (c) the recovery of a 10 $mg.\ell^{-1}$ Mn spike as determined by FIA-ICP. The three samples used were stream samples contaminated by acid mine drainage. Ten replicate FIA-ICP measurements were made.

Sample No.	(a) AAS $\bar{C} \pm \sigma/mg.\ell^{-1}$	(b) FIA-ICP $\bar{C} \pm \sigma/mg.\ell^{-1}$	(c)% recovery
1	9,1 ± 0,1	8,5 ± 0,1	101%
2	9,3 ± 0,1	8,5 ± 0,1	97%
3	3,7 ± 0,1	3,4 ± 0,2	97%
		Mean:	98%

* Atomic absorption spectroscopy (AAS) measurements were made on a Philips Pye Unicam atomic absorption spectrophotometer model SP9, using an air-acetylene flame. Absorption measurements were made using the 279,5 nm absorption line. The AAS concentration mean given is based on three measurements.

** The pooled mean of the FIA-ICP manganese values is not significantly different from the pooled mean of the AAS manganese values, at the 5% significance level, as shown by a two-tailed t-test (Green and Margerison, 1978). The calculated t value was 0,228 which is less than the critical t value of 2,776 (5% two-tailed significance level for 4 degrees of freedom; Stoker, 1985).

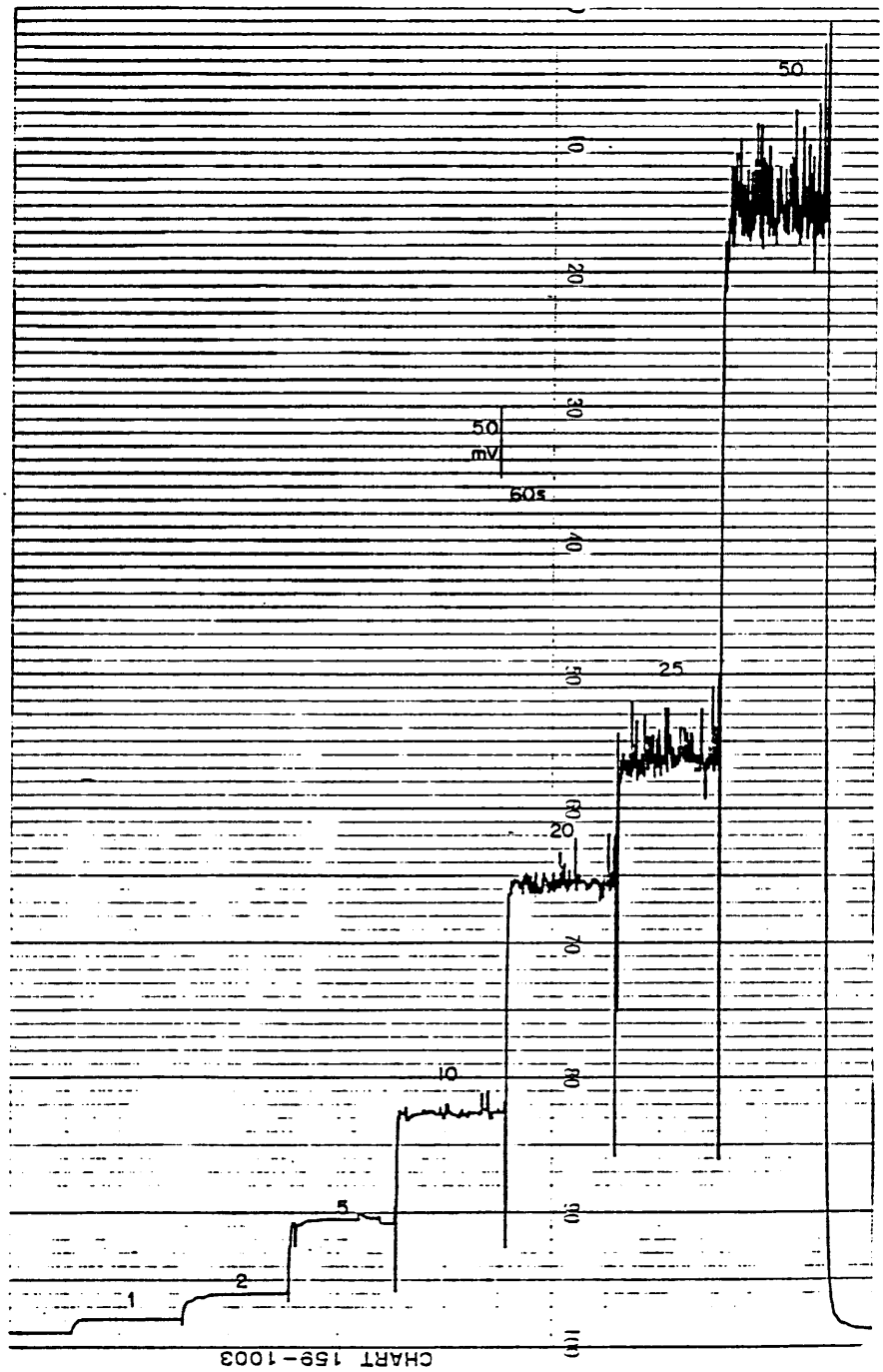

Fig. 7-10: Steady state signals, using chamber No. 5, for manganese concentrations from 1 $mg.\ell^{-1}$ Mn to 50 $mg.\ell^{-1}$ Mn. Concentrations in $mg.\ell^{-1}$ shown next to the steady state plateaus. Carrier flow rate was 3,5 $m\ell.min^{-1}$.

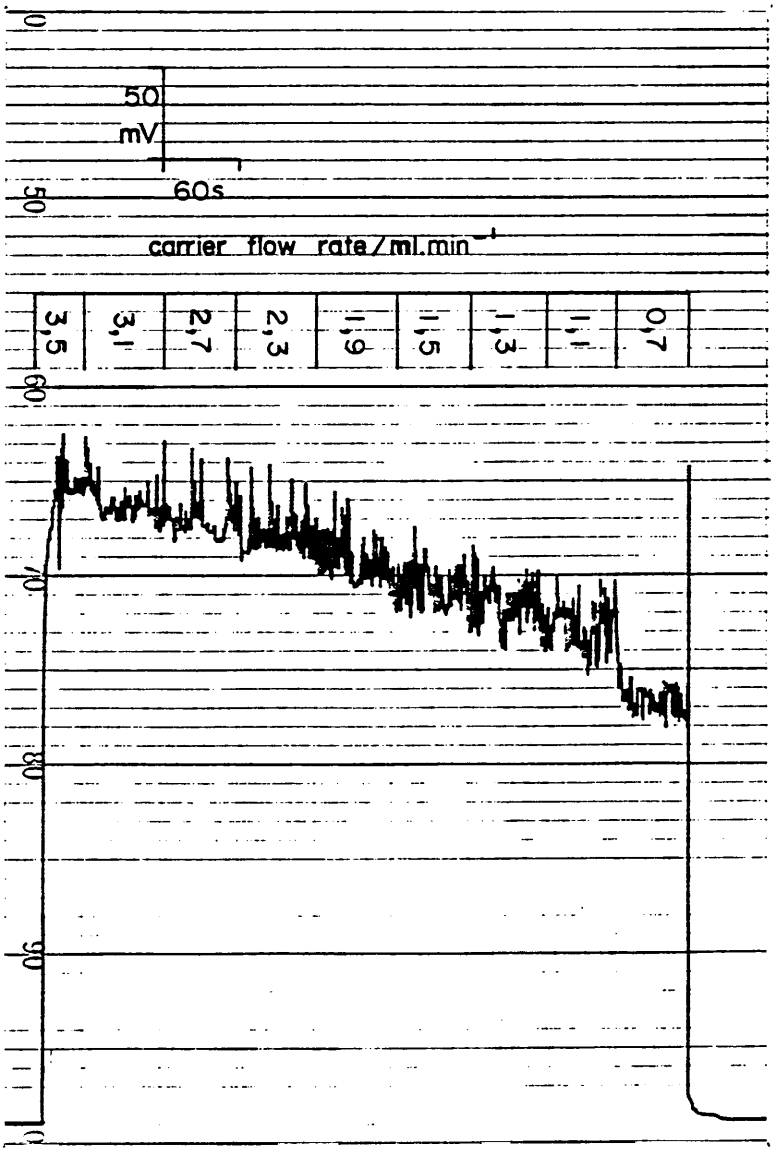

Fig. 7-11: Influence of carrier flow rate on the steady state signal of a 20 mg.ℓ$^{-1}$ manganese standard, for chamber No. 5, for a carrier flow rate from 3,5 mℓ.min^{-1} to 0,7 mℓ.min^{-1}.

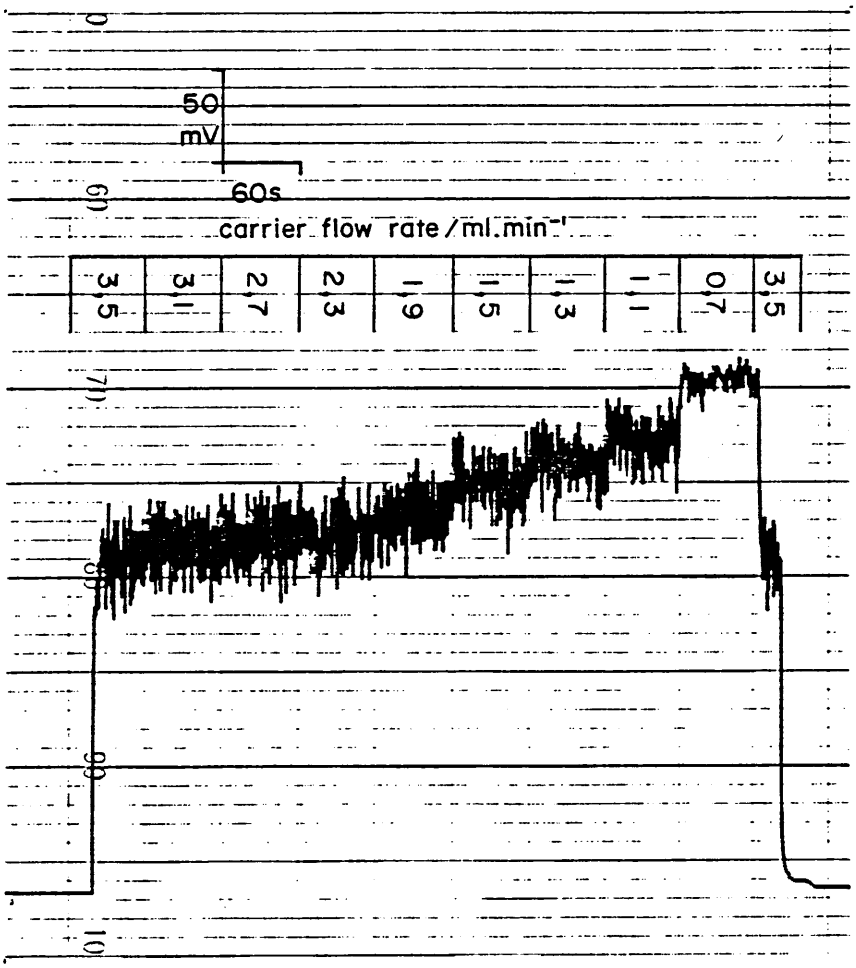

Fig. 7-12: Influence of carrier flow rate on the steady state signal of a 10 mg.ℓ$^{-1}$ manganese standard, for chamber No. 1, for a carrier flow rate from 3,5 mℓ.min^{-1} to 0,7 mℓ.min^{-1}.

TABLE 7-10: Influence of carrier flow rate (F_c) variation on the sensitivity for manganese, expressed as the ratio of the signal net intensity to that found at a carrier flow rate of 1,3 mℓ.min^{-1} taken as 100%.

F_c/mℓ.min^{-1}	Relative sensitivity %	
	Chamber No. 1	Chamber No. 5
0,7	118%	80%
1,1	105%	95%
1,3	100%	100%
1,5	95%	102%
1,9	88%	107%
2,3	83%	112%
2,7	82%	115%
3,1	81%	118%
3,5	79%	121%

7.4 Evaluation of the FIA-ICP method for strontium determination

The reproducibility of peak height for 22 injections of a 2,0 $mg.\ell^{-1}$ Sr standard is shown, together with the steady state signal, using chamber No. 5, in Fig. 7-13. The percentage relative standard deviation (RSD%) of the FIA peak height signal was 2,8%, the dispersion ratio being 1,20.

For evaluation of precision at different concentration levels over the analytical range, strontium standards covering the concentration range 0,1 $mg.\ell^{-1}$ to 5,0 $mg.\ell^{-1}$ Sr were injected, using ten injections at each concentration. The FIA signals obtained are shown in Fig. 7-14. The percentage RSD found at each concentration level is given in Table 7-11. The RSD was between 1,0 and 6,2% over the concentration range 0,5 to 5 $mg.\ell^{-1}$ Sr.

Wash-out between peaks was good, the valley height above baseline between 5 $mg.\ell^{-1}$ Sr FIA signals reaching to within 3,6% of the baseline (Fig. 7-14). Carry-over of signal when a 5 $mg.\ell^{-1}$ Sr standard was immediately followed by a 0,5 $mg.\ell^{-1}$ Sr standard, showed an increase in the peak height of the 0,5 $mg.\ell^{-1}$ Sr standard of around 5%.

Peak widths, for a 300 $\mu\ell$ injection of a 2,0 $mg.\ell^{-1}$ Sr standard injected into the carrier stream, are given in Table 7-12.

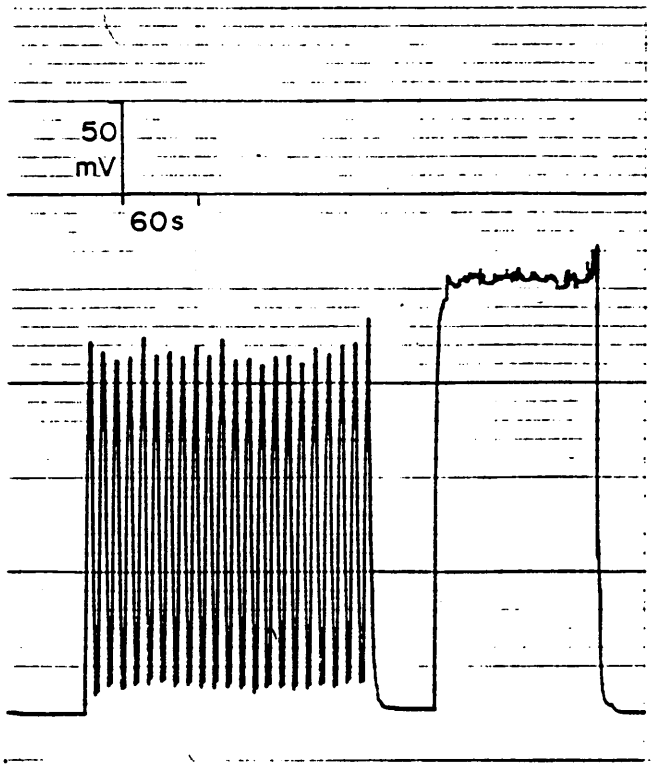

Fig. 7-13: Reproducibility of FIA signals for the Sr 421,55 nm analytical line, and steady state, for a 2 $mg.\ell^{-1}$ strontium standard, using chamber No. 5. Injection volume 300 $\mu\ell$, at a sampling rate of 320 per hour. Carrier flow rate 3,5 $m\ell.min^{-1}$.

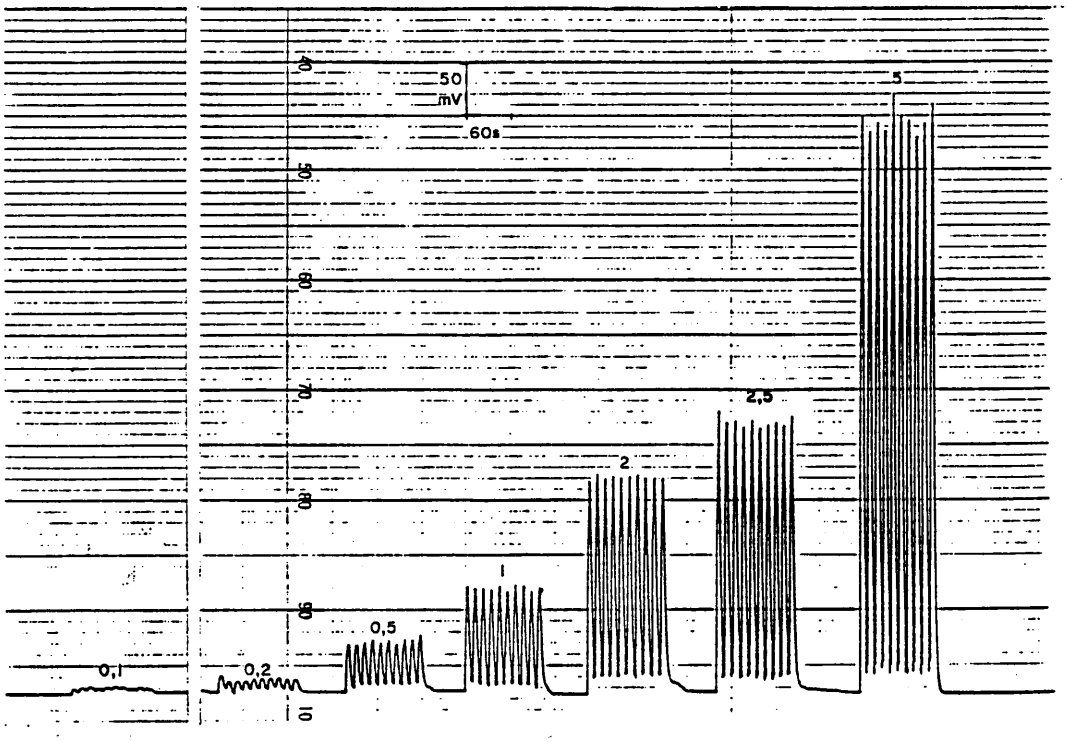

Fig. 7-14: Reproducibility of FIA signals, using chamber No. 5, for strontium concentrations of 0,1; 0,2; 0,5; 1; 2; 2,5; and 5 mg.ℓ^{-1} Sr, at a sampling rate of 320 per hour, and an injection volume of 300 $\mu\ell$. Carrier flow rate 3,5 mℓ.min^{-1}.

TABLE 7-11: Reproducibility (RSD%) of FIA peak height ($\bar{H} \pm \sigma$/mm) signals, for 10 replicate measurements for strontium concentrations (C) between 0,1 and 5,0 mg.ℓ$^{-1}$ Sr, using a carrier flow rate of 3,5 mℓ.min^{-1}, an injected sample volume of 300 µℓ, and a sampling rate of 320 per hour.*

C/mg.ℓ$^{-1}$Sr	$\bar{H} \pm \sigma$/mm	RSD%
0,1	1,7 ± 0,3	18%
0,2	3,2 ± 0,4	12%
0,5	11,3 ± 0,7	6,2%
1,0	23,7 ± 0,5	2,1%
2,0	49,2 ± 0,5	1,0%
2,5	61,4 ± 1,1	1,8%
5,0	130,9 ± 2,9	2,2%

* Recorder range setting 1V FSD; chamber No. 5 used.

TABLE 7-12: Peak widths (w_k) at the kth proportion of maximum peak height, for a 300 µℓ volume of a 2,0 mg.ℓ$^{-1}$ Sr standard injected into the carrier stream flowing at 3,5 mℓ.min^{-1}, for chamber No. 5.

k	w_k/s*
0,5	5,0 ± 0,1
0,1	9,3 ± 0,3
0,02	13,8 ± 0,8

* Mean ± std. deviation for 4 measurements.

FIA calibration data for strontium is shown in Fig. 7-15, and in Table 7-13. The relationship between strontium concentration and peak height was linear, the linear regression coefficient between strontium concentration and peak height being 0,99994. The regression line has the equation:

$$H = 25{,}607\ C - 1{,}137 \qquad \ldots\ (51)$$

where H is the peak height in mm (at 1V FSD on the recorder, corresponding to 4 mV per mm) and C is the strontium concentration in $mg.\ell^{-1}$ Sr. If we consider the two sigma value given by ten replicate measurements of the 0,1 $mg.\ell^{-1}$ Sr standard (Table 7-11) as the detection limit, then a value for the detection limit of 0,07 $mg.\ell^{-1}$ Sr is obtained by substitution of the two sigma height value in equation 51.

As a test for accuracy of the FIA-ICP method for strontium determination, at a sampling rate of 320 per hour, five samples were analyzed (a) by atomic absorption spectrometry, and (b) by FIA-ICP. In addition, aliquots of the samples were spiked with strontium, at a concentration of 1,00 $mg.\ell^{-1}$ Sr, and then analyzed by FIA-ICP, and the recovery of the added spike calculated. The results obtained are given in Table 7-14. Recoveries ranged from 100 to 122%, implying a tendency of the FIA-ICP strontium values to have a positive bias. Yet, despite this fact, the FIA-ICP strontium values were nevertheless lower than the strontium values obtained using atomic absorption spectroscopy.

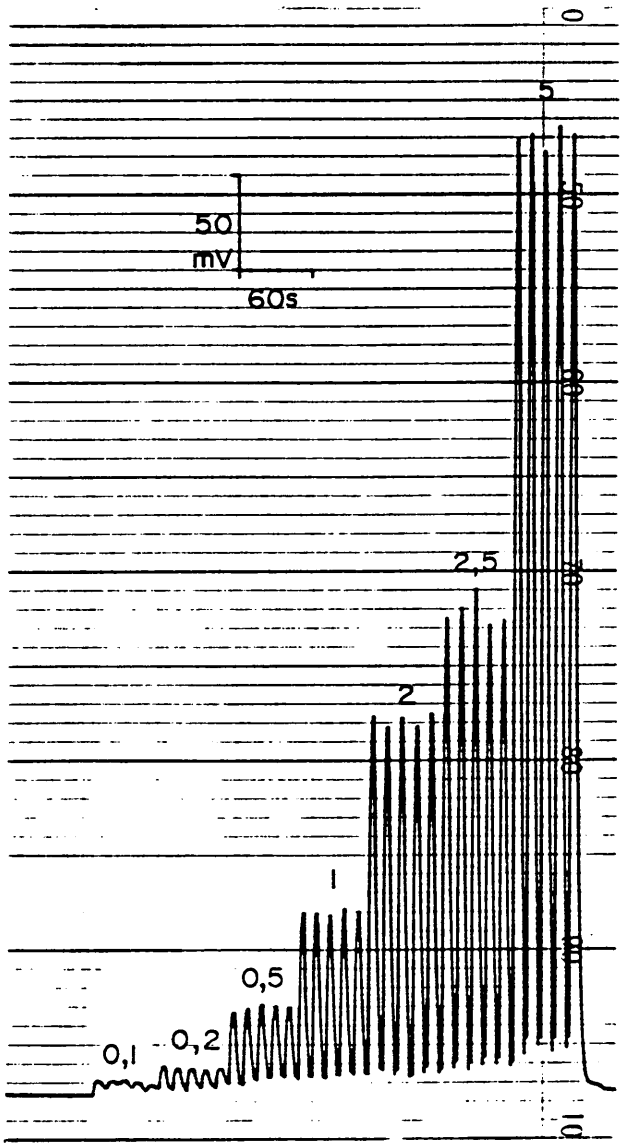

Fig. 7-15: Calibration data for strontium, using chamber No. 5. Sampling rate 320 per hour. Five injections of each calibration standard. Injection volume 300 µℓ. Strontium concentrations in $mg.\ell^{-1}$ shown next to the peaks. Carrier flow rate was 3,5 $m\ell.min^{-1}$.

TABLE 7-13: Calibration data for strontium, for chamber No. 5, showing mean peak height ($\bar{H}$) and standard deviation (σ) for strontium concentrations (C) between 0,1 $mg.\ell^{-1}$ and 5,0 $mg.\ell^{-1}$ Sr. The linear correlation coefficient between C and $\bar{H}$ was 0,99994.*

$C/mg.\ell^{-1}Sr$	$\bar{H} \pm \sigma$/mm
0,1	2,0 ± 0,3
0,2	3,7 ± 0,2
0,5	11,6 ± 0,4
1,0	24,1 ± 0,3
2,0	49,5 ± 0,8
2,5	63,7 ± 1,9
5,0	126,8 ± 1,2

* Sampling rate 320 per hour. Carrier flow rate 3,5 $m\ell.min^{-1}$. Injected sample volume 300 $\mu\ell$. Recorder range adjustment set at 1V FSD.

TABLE 7-14: Test of accuracy for FIA-ICP determination of strontium at a sampling rate of 320 per hour, using chamber No. 5, showing strontium concentration (C) as determined (a) by AAS*, (b) as determined by FIA-ICP**, and (c) the recovery of a 1,00 $mg.\ell^{-1}$ Sr spike as determined by FIA-ICP***.

Sample No.****	(c) AAS $\bar{C} \pm \sigma/mg.\ell^{-1}$	(b) FIA-ICP $\bar{C} \pm \sigma/mg.\ell^{-1}$	(c) % recovery
1	2,3 ± 0,1	2,05 ± 0,03	112%
2	2,2 ± 0,1	1,68 ± 0,03	122%
3	0,8 ± 0,1	0,56 ± 0,01	119%
4	<0,2	0,11 ± 0,01	100%
5	<0,2	0,14 ± 0,01	102%
		Mean:	111%

* Atomic absorption spectroscopy (AAS) measurements were made on a Philips Pye Unicam atomic absorption spectrophotometer model SP9, using an air-acetylene flame. Samples, standard and blank solutions were spiked with 2000 $mg.\ell^{-1}$ K as KNO_3, and 2000 $mg.\ell^{-1}$ La as $LaCl_3$. Absorption measurements were made using the 460,7 nm absorption line. The AAS concentration mean given is based on three measurements.

** The pooled mean of the FIA-ICP strontium concentration values is not significantly different from the pooled mean of the AAS strontium concentration values, at the 5% significance level, as shown by a two-tailed t-test (Green and Margerison, 1978). The calculated t value was 0,376 which is less than the critical t value of 2,306 (5% two-tailed significance level for 8 degrees of freedom; Stoker, 1985).

*** Ten replicate FIA-ICP measurements were used for samples 1 to 3, and five replicates for samples 4 and 5.

**** Samples 1 to 3 were from streams contaminated with acid mine drainage, and containing between 120 and 950 $mg.\ell^{-1}$ sulphate; while samples 4 and 5 were river water samples.

As shown in Fig. 7-13, noise is present in the steady state signal of a 2 $mg.\ell^{-1}$ Sr standard. The noise in the steady state signal is particularly marked at higher concentration levels, and becomes less marked at lower concentration levels (Fig. 7-16).

The influence of carrier flow rate variation on the strontium steady state signal is shown in Fig. 7-17 for chamber No. 5, and in Fig. 7-18 for chamber No. 1, for a strontium concentration of 2 $mg.\ell^{-1}$. The variation in sensitivity with flow rate is summarized in Table 7-15, which shows that chamber No. 5 has best sensitivity for strontium at high carrier flow rates, while chamber No. 1 shows the opposite, with best sensitivity at low carrier flow rates of the uptake solution to the nebulizer. Another interesting observation is that chamber No. 1 shows greater noise at the higher flow rates (Fig. 7-18), while chamber No. 5 shows less noise at 3,5 $m\ell.min^{-1}$ carrier flow rate than at 1,3 $m\ell.min^{-1}$ carrier flow rate.

TABLE 7-15: Influence of carrier flow rate (F_c) variation on the sensitivity for strontium, expressed as the ratio of the signal net intensity to that found at a carrier flow rate of 1,3 $m\ell.min^{-1}$ taken as 100%.

$F_c/m\ell.min^{-1}$	Relative sensitivity %	
	Chamber No. 1	Chamber No. 5
0,7	117%	81%
1,1	102%	95%
1,3	100%	100%
1,5	97%	108%
1,9	90%	112%
2,3	86%	114%
2,7	83%	116%
3,1	82%	119%
3,5	80%	120%

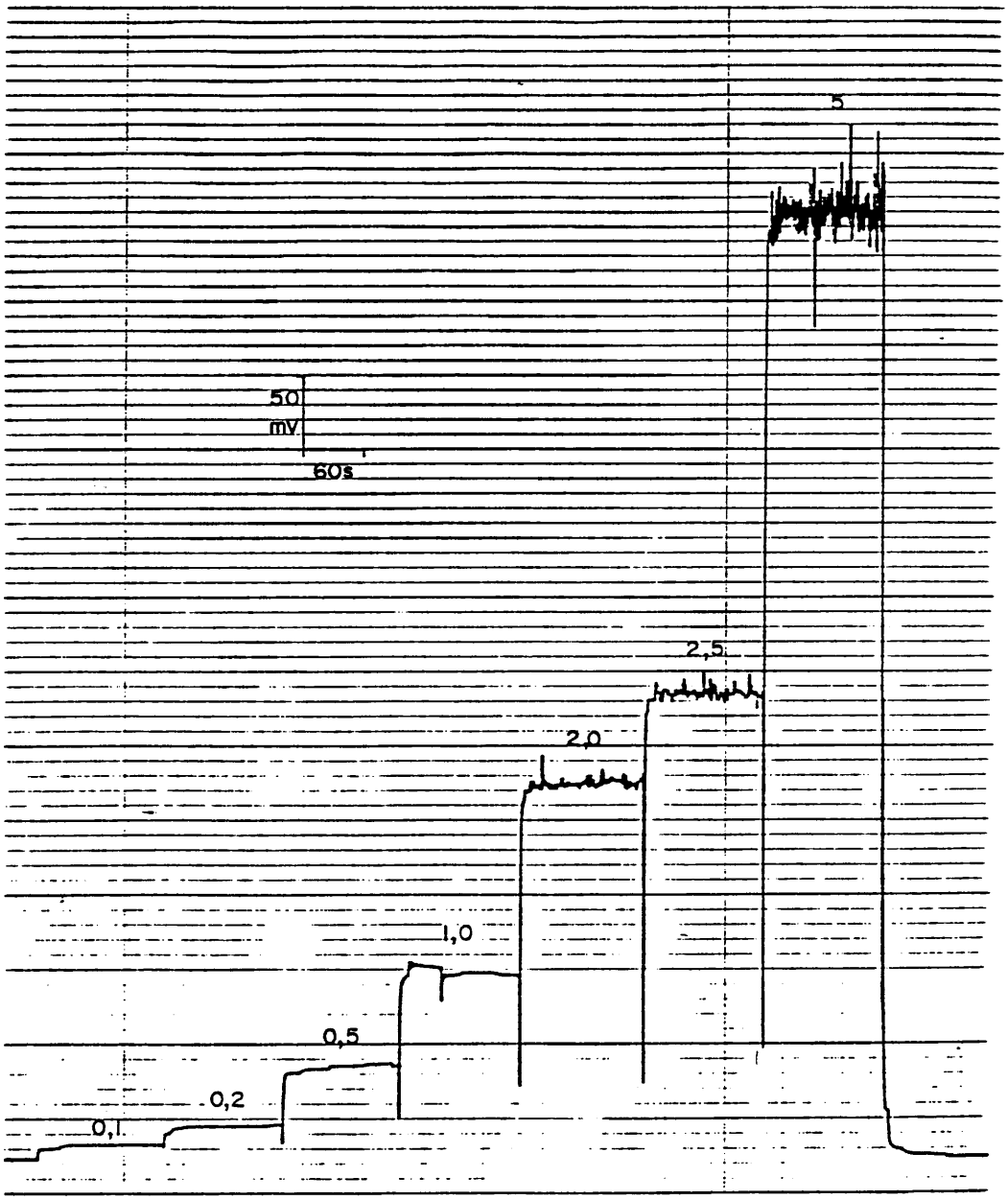

Fig. 7-16: Steady state signals, using chamber No. 5, for strontium concentrations from 0,1 mg.ℓ$^{-1}$ Sr to 5 mg.ℓ$^{-1}$ Sr. Concentrations in mg.ℓ$^{-1}$ shown next to the steady state plateaus. Carrier flow rate was 3,5 mℓ.min^{-1}.

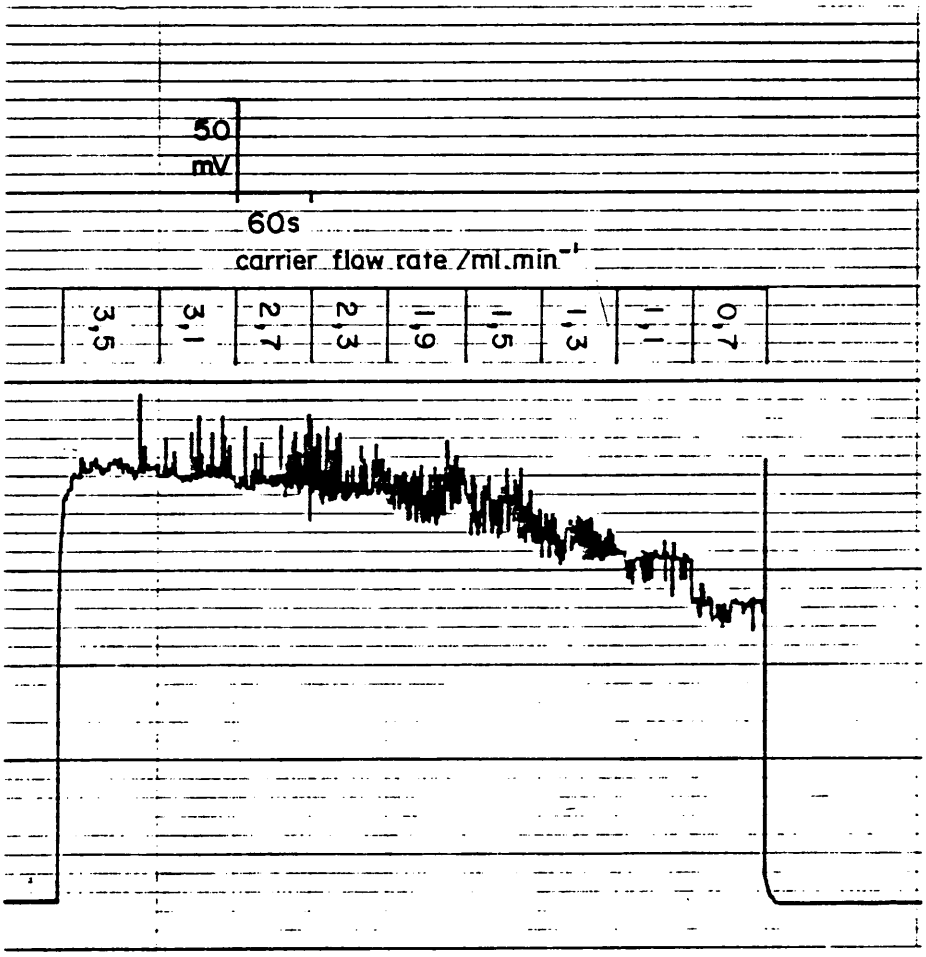

Fig. 7-17: Influence of carrier flow rate on the steady state signal of a 2 mg.ℓ$^{-1}$ strontium standard, for chamber No. 5, for a carrier flow rate from 3,5 mℓ.min^{-1} to 0,7 mℓ.min^{-1}.

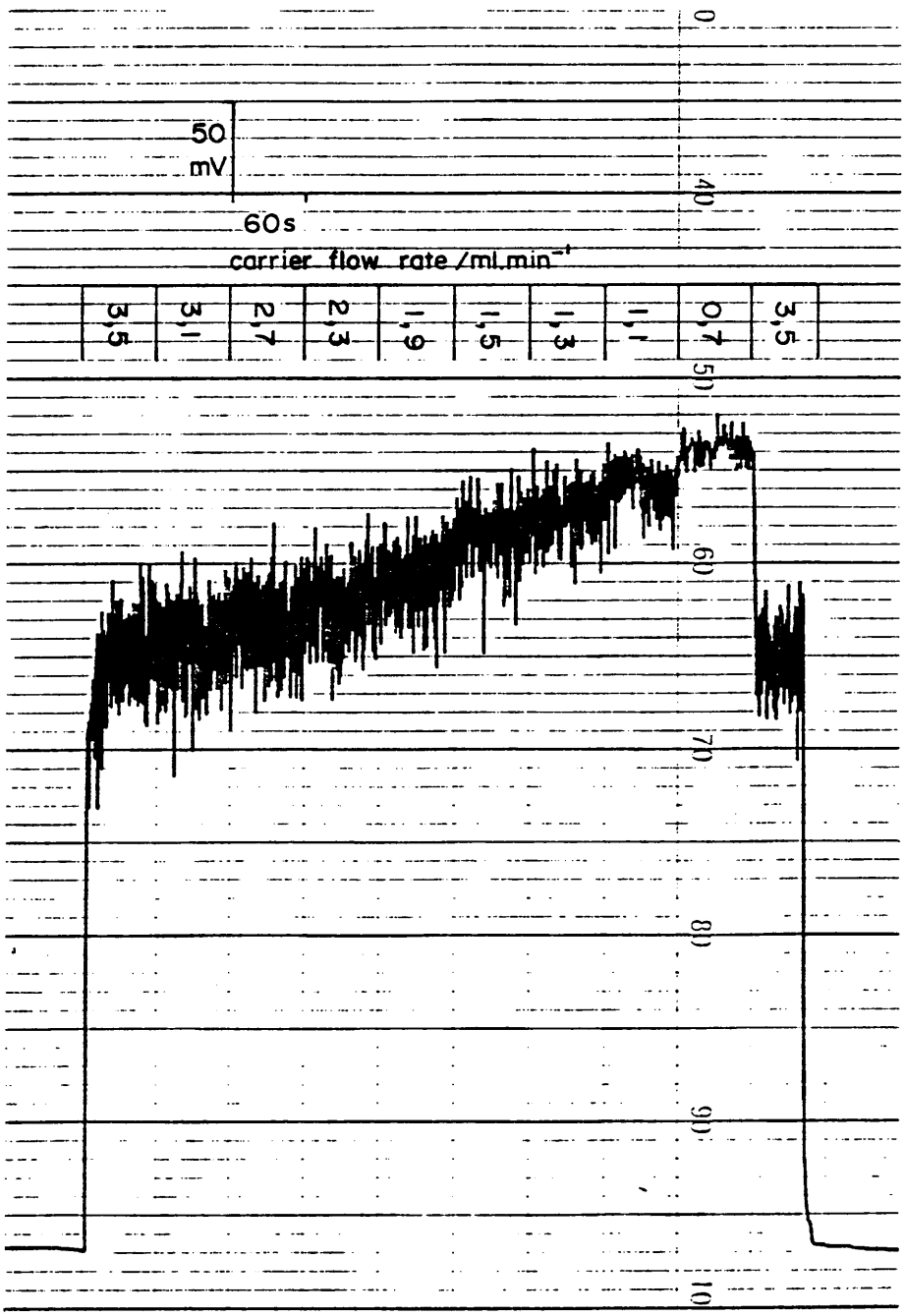

Fig. 7-18: Influence of carrier flow rate on the steady state signal of a 2 mg.ℓ$^{-1}$ strontium standard, for chamber No. 1, for a carrier flow rate from 3,5 mℓ.min^{-1} to 0,7 mℓ.min^{-1}.

7.5 Summary and Conclusion

The evaluation of the FIA-ICP method for the determination of magnesium, manganese and strontium, at a sample injection rate of 320 per hour showed that the peak resolution was good. Carry-over of 6% or less was observed when the peak from a high concentration of the analyte was immediately followed by a peak with the analyte present at one-tenth of the concentration of the first peak.

The relationship between peak height and concentration was highly linear for all three analyte elements tested. This made calibration a relatively simple procedure.

Detection limits for FIA-ICP determination of magnesium, manganese and strontium were 5 $mg.\ell^{-1}$ Mg, 1 $mg.\ell^{-1}$ Mn, and 0,07 $mg.\ell^{-1}$ Sr respectively, for a 300 $\mu\ell$ sample injection volume. Precision of peak height was 6% or better over the concentration range 10 to 300 $mg.\ell^{-1}$ Mg; 2 to 50 $mg.\ell^{-1}$ Mn and 0,5 to 5 $mg.\ell^{-1}$ Sr.

Accuracy was good for magnesium and manganese determination, with mean recoveries of 101% and 98% respectively. Strontium, however, showed a tendency for positive bias, with spikes on acid mine drainage samples giving recoveries as high as 122%. Two fresh water samples, nevertheless gave recoveries for strontium of 100 and 102%.

In conclusion, the determination of magnesium, manganese and strontium by FIA-ICP, at the rapid sample introduction rate of 320 per hour is clearly feasible. Using an injected sample volume of 300 $\mu\ell$, the dispersion ratio is close to unity i.e. around 1,1 to 1,2; and thus FIA peak heights are close to the steady state signal intensity. Little loss of sensitivity consequently occurs through using the FIA sample introduction method.

CHAPTER 8: CONCLUSIONS

8.1 Significance of findings

As indicated in the literature survey (chapter 2), the large dead volume of spray chambers conventionally used for conditioning a pneumatically nebulized sample aerosol before introduction into an ICP source, is associated with prolonged wash-in and wash-out times. This has been a limitation, not only in conventional discrete sample introduction, but is especially disadvantageous where FIA is used as a sample introduction technique. The peak broadening effect of the spray chamber dead volume has also been identified as a problem in liquid chromatography-ICP interfacing (Gardiner et al, 1987). Reduction of spray chamber volume, merely by scaling down existing designs based on the principle that sufficient time must elapse in the transit of the aerosol through the chamber to allow gravitational settling of large droplets to occur is self defeating, as decreased transit time allows less time for particles to settle. Gustavsson (1984b) suggested that the use of centrifugal principles may be a promising avenue to persue in the design of reduced volume spray chambers. Spray chamber designs using centrifugal principles, where the nebulized sample is introduced tangentially into the chamber, as in a cyclone separator (Davies 1952a) have the problem, however, that incomplete conditioning occurs, with a fraction of the aerosol bypassing the cyclone. An alternative approach to incorporating a centrifugal droplet removal process into a reduced volume spray chamber was used in this study, where the aerosol outlet from the chamber was attached tangentially, rather than the tangential inlet approach of inducing centrifugal flow as used by other researchers. The 11 mℓ capacity reduced volume chamber with such a tangential outlet (chamber No. 5, section 3.2.5) proved to effectively remove large

aerosol droplets, as evidenced by the absence of volatilization type interferences (Table 4-15, section 4.7). Indeed, this 11 mℓ capacity chamber had superior performance in this regard than the conventional 110 mℓ chamber, which showed a 15% suppression of calcium emission at a 100 to 1 molar ratio of aluminium to calcium (Table 4-11, section 4.7).

When used in conventional sample introduction, the small 11 mℓ spray chamber No. 5 (Fig. 3-5) gave comparable analytical results on real river water samples to the results obtained with the large 110 mℓ commercial spray chamber (Table 4-18, section 4.9). The two sigma detection limit for the determination of boron with conventional sample introduction was 5,7 $\mu g.\ell^{-1}$ B and 6,1 $\mu g.\ell^{-1}$ B for chamber Nos. 5 and 1 respectively (Table 4-10, section 4.6). As shown in chapter 4, the 11 mℓ capacity spray chamber No. 5 proved to be effective in conditioning the aerosol, despite a ten-fold smaller aerosol displacement time compared to the 110 mℓ commercial chamber No. 1.

In interfacing the FIA and ICP techniques, the 11 mℓ spray chamber No. 5 was shown to achieve better peak resolution at the rapid sample introduction rate of 320 sample injections per hour than when the 110 mℓ commercial spray chamber was used. Thus the carry-over, as reflected in the increase in peak height of a 2,5 $mg.\ell^{-1}$ B standard following immediately after a 25 $mg.\ell^{-1}$ B standard was 15% for the 110 mℓ commercial chamber No. 1 (section 5.10), but only 3% for chamber No. 5 (section 5.11). The calibration graph, for the relationship between peak height and concentration was highly linear for the FIA-ICP mode of operation, and in this respect the behaviour is analagous to the normal ICP spectrometric sample introduction and integration method.

This study demonstrated the potential that the FIA method of sample introduction has for the rapid determination of an element. A limitation encountered was the deterioration in the detection limit by about 2 orders of magnitude for the FIA mode when compared with the normal sample introduction mode. This was believed to be largely due to the instability of the analogue output signal of the particular spectrometer used in this study, this analogue output being designed only for profile centering purposes, and not intended for use for the measurement and recording of transient signals with high accuracy (section 5.3).

As far as the achievement of rapid sample introduction is concerned, it was found that increasing the rate of delivery of the carrier liquid to the nebulizer from 1,3 to 3,5 $m\ell.min^{-1}$ resulted in a decrease in peak width at half-height for boron by a factor of 2,7. This allowed the sampling rate to be increased from 100 to 320 samples per hour. Where samples are analyzed in triplicate, this gives an analytical rate of just over 100 per hour, which is more than three times faster than the conventional ICP sample introduction rate of only 30 per hour. Alexander *et al* (1982) found that when introducing a 300 $\mu\ell$ sample at 240 sample injections per hour in an FIA-ICP combination, that poor peak resolution occurred. The work in this thesis showed that excellent peak resolution may be achieved at a rapid sample introduction rate of 320 per hour, while still using a relatively large injected sample volume of 300 $\mu\ell$. The advantage of using a relatively large sample volume being that a dispersion ratio close to unity is found, which means that the FIA peak height is close to the steady state signal value in magnitude. Little loss of sensitivity thus occurs due to the FIA technique of sample introduction *per se*.

The beneficient effect of the small dead volume of the 11 mℓ spray chamber No. 5 was particularly apparent in the use of this chamber for calcium determination. The small 11 mℓ chamber gave a near-baseline peak width of 15 s, as compared to a value of around 25 s for the large 110 mℓ chamber No. 1, for a 300 µℓ injected sample volume of an 80 $mg.ℓ^{-1}$ calcium standard (section 6.2, Table 6-2). The baseline peak width for the FIA calcium peaks reported by Greenfield (1983) was 30 s. Precision of calcium determination was also better for the small 11 mℓ chamber than for the large 110 mℓ chamber, the former showing between 1,5 and 3,1% RSD values over the concentration range 40 to 200 $mg.ℓ^{-1}$ Ca, with the latter showing between 3,9 and 6,9% RSD values over the same concentration range.

Evaluation of the 11 mℓ spray chamber No. 5, with its tangential aerosol outlet, for the FIA-ICP determination of magnesium, manganese and strontium (chapter 7) showed that good peak resolution was obtained at an injection rate of 320 per hour for these elements as well. Carry-over of 6% or less being found when a peak from a high concentration of the analyte was immediately followed by a peak with an analyte concentration of one-tenth of that associated with the first peak. As was the case with boron and calcium, highly linear peak height to concentration calibration graphs were obtained.

Recovery tests showed that the accuracy of determination by FIA-ICP was good for boron, calcium, magnesium and manganese, with mean recoveries between 97% and 101%. Strontium recoveries, on the other hand, showed a tendency towards a positive bias in the case of acid mine drainage samples (Table 7-14).

As it was found in this study, that narrow peak width, with good resolution of FIA peaks, was favoured by increasing the sample uptake rate to the nebulizer from 1,3 to 3,5 mℓ.min^{-1}, the effect of this change in carrier rate on sensitivity was obviously of interest. For the 11 mℓ spray chamber No. 5, an increase in sensitivity was observed, at the higher nebulizer uptake rate, for all elements tested; while the large 110 mℓ chamber No. 1 showed either little change in sensitivity (boron and magnesium) or else a marked decrease in sensitivity at the higher nebulizer uptake rate (calcium, manganese and strontium).

8.2 Summary

In this study, on the design of a suitable small volume spray chamber, to facilitate the achievement of rapid sample introduction when interfacing the FIA and ICP techniques, two major findings of significance were:

Firstly, the demonstration that by appropriate spray chamber design, through incorporation of both aerosol flow reversal and centrifugal principles, the chamber volume could be reduced by an order of magnitude from that of the commercial chamber without the appearance of volatilization type interferences. Indeed, the 11 mℓ chamber No. 5 (Fig. 3-5), with its tangential aerosol outlet tube showed less evidence of volatilization interferences than the conventional 110 mℓ chamber No. 1 (Fig. 3-1). The reduction in spray chamber volume allowed a chamber dead volume displacement time of less than 1 s to be obtained, resulting in improved peak resolution between samples when employing the FIA method of sample introduction. Whereas other workers who have attempted using cyclone principles, through tangential introduction of the aerosol into a spray chamber, have experienced the problem that part of the

aerosol bypassed the cyclone (section 2-8); this problem was overcome in this study by incorporating both the flow reversal principle of the double-barrel design, as well as the centrifugal principle associated with spiral motion. The centrifugal action was induced by having the aerosol exit tube from the chamber attached tangentially instead of at a right angle.

Secondly, this work demonstrated that a rapid sample introduction rate of 320 per hour could be achieved, using the reduced volume spray chamber, with good FIA peak resolution. This was achieved, despite using a relatively large injection volume of 300 µℓ, so as to obtain a dispersion ratio near unity. The advantage of the latter was that little loss of sensitivity occurred consequent to the non-attainment of steady state conditions, which is characteristic of the FIA technique. Assuming that samples are analyzed in triplicate, the sample introduction rate of 320 per hour gives an analysis rate of over 100 per hour, which is more than three times faster than the conventional ICP sample introduction rate of at most 30 per hour. Use of the small 11 mℓ spray chamber in the FIA-ICP interface, allowed FIA peak widths to be decreased. Thus a near-baseline calcium peak width of 15 s was found for the 11 mℓ spray chamber No. 5, as compared firstly to a width of 25 s for the 110 mℓ chamber No. 1, and secondly to a baseline width of 30 s reported by Greenfield (1983). The FIA-ICP method showed highly linear peak height to concentration calibration graphs, and accuracy, as reflected by recovery tests, showed little evidence of matrix effects except in the case of strontium, where a positive bias was observed for acid mine drainage samples containing elevated sulphate concentrations. Mean recoveries of added spikes for boron, calcium, magnesium and manganese were 98%, 97%, 101% and 98% respectively.

A limitation of the method uncovered in this study was that the analogue output signal, which was used to record the FIA analyte signal peaks, showed a marked instability of around 10 mV. This had a degrading effect both on precision and detection limit, and the full potential of the FIA-ICP method could not be reached. Use of the FIA sample introduction method on a spectrometer with an analogue output signal designed for the recording of transient signals should give improved detection limits. A further recommendation for future work would be the automation of the recording and processing of FIA signals, so that the potential for rapid FIA-ICP analyses on routine samples might be realized in practical analysis.

In conclusion, this work demonstrated that rapid sample introduction and analysis of water samples for milligram per litre concentrations of boron, calcium, magnesium, manganese and strontium is quite feasible, using a reduced volume spray chamber in the FIA-ICP interface, so as to achieve aerosol displacement times of less than 1 s. The mini-volume spray chamber designed in this study (chamber No. 5, Fig. 3-5) also has potential application in conventional sample introduction to the ICP source, as shown in chapter 4. The unique aspect of the spray chamber designed in this work was that it included both centrifugal principles as well as the flow reversal principle of the conventional double-barrel ICP spray chamber design. The former principle allowed a reduction in spray chamber volume to be achieved without jeopardizing the large droplet removal function of the spray chamber, while the latter principle overcame the problem of incomplete aerosol conditioning found with conventional cyclone type separators.

REFERENCES

ALEXANDER, P.W., FINLAYSON, R.J., SMYTHE, L.E., and THALIB, A. (1982) Rapid flow analysis with inductively coupled plasma atomic-emission spectroscopy using a micro-injection technique, Analyst, 107, p1335-1342.

ALKEMADE, C. Th. J. (1966) On the interpretation of solute vaporization interference in flame photometry, Anal. Chem., 38(9), p1252-1253.

ALONSO, J., BARTROLI, J., LIMA, J.L.F.C., and MACHADO, A.A.S.C. (1986) Sequential flow-injection determinations of calcium and magnesium in waters, Anal. Chim. Acta, 179, p503-508.

ARMSTRONG LOWE, D. (1975) A guide to international recommendations on names and symbols for quantities and on units of measurement, World Health Organization, Geneva, p1-314.

ASTRÖM, O. (1982) Flow injection analysis for the determination of bismuth by atomic absorption spectrometry with hydride generation, Anal. Chem., 54, p190-193.

ATTIYAT, A.S., and CHRISTIAN, G.D. (1984) Flow injection analysis-atomic absorption determination of serum zinc, Clin. Chim. Acta, 137, p151-157.

BAGINSKI, B.R., and MEINHARD, J.E. (1984) Some effects of high solids matrices on the sample delivery system and the Meinhard concentric nebulizer during ICP emission analyses, Appl. Spectrosc., 38(4), p568-572.

BASSON, W.D., and VAN STADEN, J.F. (1980) Simultaneous determination of sodium, potassium, magnesium and calcium in surface, ground and domestic water by flow-injection analysis, Fresenius Z. Anal. Chem., 302, p370-374.

BERGAMIN F^{O}, H., ZAGATTO, E.A.G., KRUG, F.J., and REIS, B.F. (1978) Merging zones in flow injection analysis. Part 1. Double proportional injector and reagent consumption, Anal. Chim. Acta, 101, p17-23.

BERGMEYER, H.U., and HAGEN, A. (1972) Ein neues prinzip enzymatischer analyse, Fresenius Z. Anal. Chem., 261, p333-336.

BLAEDEL, W.J., and HICKS, G.P. (1962) Continuous analysis by measurement of the rate of enzyme catalyzed reactions, Anal. Chem., 34(3), p388-394.

BLAKLEY, C.R., and VESTAL, M.L. (1983) Thermospray interface for liquid chromatography/mass spectrometry, Anal. Chem., 55, p750-754.

BOROWIEC, J.A., BOORN, A.W., DILLARD, J.H., CRESSER, M.S., BROWNER, R.F., and MATTESON, M.J. (1980) Interference effects from aerosol ionic redistribution in analytical atomic spectrometry, Anal. Chem., 52, p1054-1059.

BROEKAERT, J.A.C., and LEIS, F. (1979) An injection method for the sequential determination of boron and several metals in waste-water samples by inductively-coupled plasma atomic emission spectrometry, Anal. Chim. Acta, 109, p73-83.

BROEKAERT, J.A.C., LEIS, F., and LAQUA, K. (1980) Investigation of an ICP-injection technique for the analysis of small-volume samples, Fresenius Z. Anal. Chem., 301, p105-106.

BROTHERTON, T., BARNES, B., VELA, N., and CARUSO, J. (1987) Evaluation of the grid-type nebuliser for organic solvent introduction into the inductively coupled plasma, J. Anal. At. Spectrom., 2, p389-396.

BROWN, M.W., and RUZICKA, J. (1984) Parameters affecting sensitivity and precision in the combination of flow injection analysis with flame atomic-absorption spectrophotometry, Analyst, 109, p1091-1095.

BROWNER, R.F. (1983) Sample introduction for inductively coupled plasma and flames, Trends in Anal. Chem., 2(5), p121-124.

BROWNER, R.F., and BOORN, A.W. (1984a) Sample introduction: The achilles' heel of atomic spectroscopy?, Anal. Chem., 56(7), p786A-798A.

BROWNER, R.F., and BOORN, A.W. (1984b) Sample introduction techniques for atomic spectroscopy, Anal. Chem., 56(7), p875A-888A.

BROWNER, R.F., BOORN, A.W., and SMITH, D.D. (1982) Aerosol transport model for atomic spectrometry, Anal. Chem., 54, p1411-1419.

BURGUERA, J.L., BURGUERA, M., GALLIGNANI, M., and ALARCON, O.M. (1983) More on flow injection/atomic absorption analysis for electrolytes, Clin. Chem., 29(3), p568-569.

BURGUERA, M., BURGUERA, J.L., CERGIO RIVAS, P., and ALARCON, O.M. (1986) Determination of copper, zinc, and iron in parotid saliva by flow injection with flame atomic absorption spectrophotometry, Atomic Spectrosc., 7(3), p79-81.

BUSHEE, D., KRULL, I.S., SAVAGE, R.N., and SMITH, S.B. (1982) Metal cation/anion speciation via paired-ion reversed phase HPLC with refractive index and/or inductively coupled plasma emission spectroscopic detection methods, J. Liq. Chromatogr., 5(3), p463-478.

BUTCHER, S.S., and CHARLSON, R.J. (1972) An introduction to air chemistry, Academic Press, N.Y., p157-210.

BYSOUTH, S.R., and TYSON, J.F. (1986) A microcomputer-based peak-width method of extended calibration for flow-injection atomic absorption spectrometry, Anal. Chim. Acta, 179, p481-486.

BYSOUTH, S.R., and TYSON, J.F. (1987) Flow manifold for automated on-line dilution of standards for flame atomic absorption spectrometry and its use in a null measurement method, J. Anal. At. Spectrom., 2, p217-220.

CHAN, C.C.Y. (1985) Semiautomated method for determination of selenium in geological materials using a flow injection analysis technique, Anal. Chem., 57, p1482-1485.

CHRISTIAN, G.D., and RUZICKA, J. (1987) Flow injection analysis: a novel tool for plasma spectroscopy, Spectrochim Acta, 42B (1/2), p157-167.

COBBOLD, D.G. (1986) Comments on the analysis of high-solids matrices using the Meinhard concentric nebulizer in ICP atomic emission spectroscopy, Appl. Spectrosc., 40(8), p1242-1244.

COOK, I.G., McLEOD, C.W., and WORSFOLD, P.J. (1986) Use of activated alumina as a column packing material for adsorption of oxyanions in flow injection analysis with ICP-AES detection, Analyt. Proc., 23, p5-6.

COX, A.G., COOK, I.G., and McLEOD, C.W. (1985) Rapid sequential determination of chromium (III)- chromium (VI) by flow injection analysis-inductively coupled plasma atomic emission spectrometry, Analyst, 110, p331-333.

COX, A.G., and McLEOD, C.W. (1986) Preconcentration and determination of trace chromium (III) by flow injection/inductively-coupled plasma/atomic emission spectrometry, Anal. Chim. Acta, 179, p487-490.

CRESSER, M.S., and BROWNER, R.F. (1980) Observations on the effects of impact beads, mixer paddles, and auxiliary oxidant on droplet distributions in analytical flame spectroscopy, Appl. Spectrosc., 34(3), p364-368.

DALE, L.S., and BUCHANAN, S.J. (1986) A comparison of cloud chambers for use in inductively coupled plasma nebulisation systems, J. Anal. At. Spectrom., 1(1), p59-62.

DAVIES, C.N. (1952a) The separation of airborne dust and particles, Proc. Inst. Mech. Eng., 1B, p185-198.

DAVIES, C.N. (1952b) Communications on the separation of airborne dust and particles, Proc. Inst. Mech. Eng., 1B, p209-212.

DUURSMA, R.P.J., SMIT, H.C., and MAESSEN, F.J.M.J. (1981) Characterization of noise in inductively-coupled plasma emission spectrometry, Anal. Chim. Acta, 133, p393-408.

EBDON, L., and CAVE, M.R. (1982) A study of pneumatic nebulisation systems for inductively coupled plasma emission spectrometry, Analyst, 107, p172-178.

ELGERSMA, J.W., MAESSEN, F.J.M.J., and NIESSEN, W.M.A. (1986) A low consumption thermospray nebulizer with a fused silica vaporizer for inductively coupled plasma atomic emission spectrometry, Spectrochim. Acta, 41B(11), p1217-1220.

FANG, Z., RUZICKA, J., and HANSEN, E.H. (1984) An efficient flow-injection system with on-line ion-exchange preconcentration for the determination of trace amounts of heavy metals by atomic absorption spectrometry, Anal. Chim. Acta, 164, p23-39.

FANG, Z., XU, S., WANG, X., and ZHANG, S. (1986) Combination of flow-injection techniques with atomic spectrometry in agricultural and environmental analysis, Anal. Chim. Acta, 179, p325-340.

FANG, Z., XU, S., and ZHANG, S. (1984) The determination of trace amounts of heavy metals in waters by a flow-injection system including ion-exchange preconcentration and flame atomic absorption spectrometric detection, Anal. Chim. Acta, 164, p41-50.

FARINO, J., and BROWNER, R.F. (1984) Surface tension effects on aerosol properties in atomic spectrometry, Anal. Chem., 56, p2709-2714.

FASKE, A.J., SNABLE, K.R., BOORN, A.W., and BROWNER, R.F. (1985) Microliter sample introduction for ICP-AES, Appl. Spectrosc., 39(3), p542-545.

FITTON, A. (1952) In "Communications on the separation of airborne dust and particles", Proc. Inst. Mech. Eng., 1B, p201-202.

FRALEY, D.M., YATES, D., and MANAHAN, S.E. (1979) Inductively coupled plasma emission spectrometric detection of simulated high performance liquid chromatographic peaks, Anal. Chem., 51(13), p2225-2229.

FRALEY, D.M., YATES, D.A., MANAHAN, S.E., STALLING, D., and PETTY, J. (1981) ICP-AES as a multiple element detector for metal chelates separated by HPLC, Appl. Spectrosc., 35, p525-531.

FUJISHIRO, Y., KUBOTO, M., and ISHIDA, R. (1984) A study of designs of a cross flow nebulizer for ICP atomic emission spectrometry, Spectrochim. Acta., 39B(4), p617-620.

FUKAMACHI, K., and ISHIBASHI, N. (1980) Flow injection-atomic absorption spectrometry with organic solvents, Anal. Chim. Acta, 119, p383-387.

FUKUSHIMA, S. (1959) Mechanism and elimination of interferences in flame photometry, Mikrochim. Acta, 4, p596-618.

FUKS, N.A. (1955) The mechanics of aerosols, Academy of Sciences of the U.S.S.R., translated from the Russian by E. Lachowicz, Technical Information Division, U.S. Army Chemical Warfare Laboratories, Maryland, p158-177.

GARBARINO, J.R., and TAYLOR, H.E. (1980) A Babington-type nebulizer for use in the analysis of natural water samples by inductively coupled plasma spectrometry, Appl. Spectrosc., 34(5), p584-590.

GARDINER, P.E., BRAETTER, P., GERKEN, B and TOMIAK, A. (1987) On-line sequential detection by inductively coupled plasma atomic emission spectrometry of trace elements after liquid chromatography of biological fluids, J. Anal. At. Spectrom., 2, p375-378.

GAST, C.H., KRAAK, J.C., POPPE, H., and MAESSEN, F.J.M.J. (1979) Capabilities of on-line element specific detection in high performance liquid chromatography using an inductively coupled argon plasma emission source detector, J. Chromatogr., 185, p549-561.

GERDING, J.J.T., KEMPEN, H.J.M., LAMERS, B.J.M., and GERDING, M.H. (1972) A new highly sensitive detection system for peptides in column effluents, J. Chromatogr., 66, p145-152.

GOMEZ-NIETO, M.A., DE CASTRO. M.D.L., MARTIN, A., and VALCAREL, M (1985) Prediction of the behaviour of a single flow-injection manifold, Talanta, 32(4), p319-324.

GRANCHI, M.P., BIGGERSTAFF, J.A., HILLIARD, L.J., and GREY, P. (1987) Use of a robot and flow injection for automated sample preparation and analysis of used oils by ICP emission spectrometry, Spectrochim. Acta, 42B (1/2), p169-180.

GREEN, J.R., and MARGERISON, D. (1978) Statistical treatment of experimental data, Elsevier, Amsterdam, p126-142.

GREENFIELD, S. (1981) FIA weds ICP - a marriage of convenience, Ind. Res. and Dev., 21(8), p140-145.

GREENFIELD, S. (1983) Inductively coupled plasma-atomic emission spectroscopy (ICP-AES) with flow injection analysis (FIA), Spectrochim. Acta, 38B(1/2), p93-105.

GREENFIELD, S., and SMITH, P.B. (1972) The determination of trace metals in microlitre samples by plasma torch excitation, Anal. Chim. Acta, 59, p341-348.

GUSTAVSSON, A. (1983) Mathematical model for concentric nebulizer systems, Anal. Chem., 55, p94-98.

GUSTAVSSON, A. (1984a) Prediction of nebulizer characteristics for concentric nebulizer systems with a mathematical model, Anal. Chem., 56, p815-817.

GUSTAVSSON, A. (1984b) A tutorial review of the basic theory for and practical aspects of aerosol chambers, Spectrochim. Acta, 39B(1), p85-94.

GUSTAVSSON, A. (1984c) The determination of some nebulizer characteristics, Spectrochim. Acta, 39B, p743-746.

GUSTAVSSON, A. (1986) Comparison of an indirect and a direct method for measuring the efficiency of nebulizer systems, Spectrochim. Acta, 41B(3), p291-294.

GUSTAVSSON, A. (1987) Characterization of an interface for sample introduction into an inductively coupled plasma, Spectrochim. Acta, 42B (1/2), p111-118.

HANSEN, E.H., and RUZICKA, J. (1979) The principles of flow injection analysis as demonstrated by three lab exercises, J. Chem. Educ., 56, p677-680.

HARNLY, J.M., and BEECHER, G.R. (1985) Two-valve injector to minimize nebulizer memory for flow injection atomic absorption spectrometry, Anal. Chem., 57, p2015-2016.

HARTENSTEIN, S.D., CHRISTIAN, G.D., and RUZICKA, J. (1985) Applications of an on-line preconcentrating flow injection analysis system for inductively coupled plasma atomic emission spectrometry, Can. J. Spectrosc., 30(6), p144-148.

HARTENSTEIN, S.D., RUZICKA, J.R., and CHRISTIAN, G.D. (1985) Sensitivity enhancements for flow injection analysis-inductively coupled plasma atomic emission spectrometry using an on-line preconcentrating ion-exchange column, Anal. Chem., 57, p21-25.

HAUSLER, D.W., and TAYLOR, L.T. (1981a) Nonaqueous on-line simultaneous determination of metals by size exclusion chromatography with inductively coupled plasma atomic emission spectrometric detection, Anal. Chem., 53, p1223-1227.

HAUSLER, D.W., and TAYLOR, L.T., (1981b) Size exclusion chromatography of organically bound metals and coal-derived materials with inductively coupled plasma atomic emission spectrometric detection, Anal. Chem., 53, p1227-1231.

IBRAHIM, M., GILBERT, T.W., and CARUSO, J.A. (1984) Determination of tetraalkyllead by high performance liquid chromatography with ICP detection, J. Chromatogr. Sci., 22, p111-115.

IBRAHIM, M., NISAMANEEPONG, W., and CARUSO, J. (1985) Microcolumn high pressure liquid chromatography with a glass-frit nebulizer interface for plasma emission detection, J. Chromatogr. Sci., 23(4), p144-150.

IBRAHIM, M., NISAMANEEPONG, W., HAAS, D.L., and CARUSO, J.A. (1985) Determination of alkyllead compounds by HPLC/ICP using a glass-frit nebulizer ICP interface, Spectrochim. Acta, 40B (1/2), p367-376.

ISRAEL, Y., and BARNES, R.M. (1984) Standard addition method in flow injection analysis with inductively coupled plasma atomic emission spectrometry, Anal. Chem., 56, p1188-1192.

ITO, T., NAKAGAWA, E., KAWAGUCHI, H., and MIZUIKE, A. (1982) Semi-automatic microliter sample injection into an inductively coupled plasma for simultaneous multielement analysis, Mikrochim. Acta, I/5-6, p423-431.

JACINTHO, A.O., ZAGATTO, E.A.G., BERGAMIN, F^{O}, H., KRUG, F.J., REIS, B.F., BRUNS, R.E., and KOWALSKI, B.R. (1981) Flow injection systems with inductively-coupled argon plasma atomic emission spectrometry, Part 1. Fundamental considerations, Anal. Chim. Acta, 130, p243-255.

JINNO, K., NAKANISHI, S., and FUJIMOTO, C. (1985) Direct sample introduction system for inductively coupled plasma emission spectrometric detection in microcolumn liquid chromatography, Anal. Chem., 57, p2229-2235.

KEMPSTER, P.L. (1986) Application of inductively coupled plasma emission spectrometry in the analysis of environmental samples, Technical Report TR 130, Department of Water Affairs, Pretoria, p1-209.

KEMPSTER, P.L., VAN STADEN, J.F., and VAN VLIET, H.R. (1987) Investigation of small volume cloud chambers for use in inductively coupled plasma nebulisation, J. Anal. At. Spectrom., in press.

KNISELEY, R.N., AMENSON, H., BUTLER, C.C., and FASSEL, V.A. (1974) An improved pneumatic nebulizer for use at low nebulizing gas flows, Appl. Spectrosc., 28(3), p285-286.

KNISELEY, R.N., FASSEL, V.A., and BUTLER, C.C. (1973) Application of inductively-coupled plasma excitation sources to the determination of trace metals in microliter volumes of biological fluids, Clin. Chem., 19(8), p807-812.

KRANZ, E. (1972) Untersuchungen über die optimale erzeugung und förderung von aerosolen für spektrochemische zwecke, Spectrochim. Acta, 27B, p327-343.

KRULL, I.S., BUSHEE, D., SAVAGE, R.N., SCHLEICHER, R.G., and SMITH, S.B. (1982) Speciation of Cr(III) and Cr(VI) via reversed phase HPLC with inductively coupled plasma emission spectroscopic detection, Anal. Lett., 15 (A3), p267-281.

KRULL, I.S., PANARO, K.W., and GERSHMAN, L.L. (1983) Trace analysis and speciation for Cr(VI) and Cr(III) via HPLC- direct current plasma emission spectroscopy (HPLC-DCP), J. Chromatogr. Sci., 21, p460-472.

LaFRENIERE, K.E. (1986) Evaluation of a direct injection nebulizer interface for flow injection analysis and high performance liquid chromatography with inductively coupled plasma-atomic emission spectroscopic detection, Ph.D., thesis, Iowa State University, p1-197.

LaFRENIERE, K.E., FASSEL, V.A., and ECKELS, D.E. (1987) Elemental speciation via high-performance liquid chromatography combined with inductively coupled plasma atomic emission spectroscopic detection: Application of a direct injection nebulizer, Anal. Chem., 59, p879-887.

LaFRENIERE, K.E., RICE, G.W., and FASSEL, V.A. (1985) Flow injection analysis with inductively coupled plasma-atomic emission spectroscopy: Critical comparison of conventional pneumatic, ultrasonic and direct injection nebulization, Spectrochim. Acta, 40B, (10-12), p1495-1504.

LAWRENCE, K.E., RICE, G.W., and FASSEL, V.A. (1984) Direct liquid sample introduction for flow injection analysis and liquid chromatography with inductively coupled argon plasma spectrometric detection, Anal. Chem., 56, p289-292.

LAYMAN, L.R., and LICHTE, F.E. (1982) Glass frit nebulizer for atomic spectrometry, Anal. Chem., 54(4), p638-642.

LINDSAY, W.N., (1981) Flow injection analysis, Anal. Chem., 53(3), p387A.

LIVERSAGE, R.R., VAN LOON, J.C., and DE ANDRADE, J.C. (1984) A flow injection/hydride generation system for the determination of arsenic by inductively-coupled plasma atomic emission spectrometry, Anal. Chim. Acta, 161, p275-283.

LUFFER, D.R., and SALIN, E.D. (1986) Rapid throughput nebulizer spray chamber system for inductively coupled plasma atomic emission spectrometry, Anal. Chem., 58, p654-656.

LYNCH, T.P., KERNOGHAN, N.J., and WILSON, J.N. (1984) Speciation of metals in solution by flow injection analysis. Part 1. Sequential spectrophotometric and atomic-absorption detectors, Analyst, 109, p839-842.

MAESSEN, F.M.J., COEVERT, P., and BALKE, J. (1984) Comparison of pneumatic nebulizers in current use for inductively coupled plasma atomic emission spectrometry, Anal. Chem., 56, p899-903.

MALAMAS, F., BENGTSSON, M., and JOHANSSON, G. (1984) On-line trace metal enrichment and matrix isolation in atomic absorption spectrometry by a column containing immobilized 8-quinolinol in a flow-injection system, Anal. Chim. Acta, 160, p1-10.

MALLOY, J.M., KELIHER, P.N., and CRESSER, M.S. (1980) Some studies of changes in efficiency of pneumatic nebulization on using small discrete samples, Spectrochim. Acta, 35B, p833-838.

MARINOV, M.I. (1984a) Dispersity of dry aerosol obtained from blood serum for analytical plasma spectrometry, Spectrosc. Lett., 17, p1-8.

MARINOV, M.I. (1984b) Dry aerosol producing system for direct plasma emission analysis of body fluids, Spectrosc. Lett., 17(1), p33-39.

MARINOV, M.I. (1984c) Dry aerosol producing system for direct plasma emission analysis of body fluids, Spectrosc. Lett., 17(2), p151-157.

MARTINEZ-JIMENEZ, P., GALLEGO, M., and VALCAREL, M. (1987) Indirect atomic absorption determination of chloride by continuous precipitation of silver chloride in a flow injection system, J. Anal. At. Spectrom., 2, p211-215.

McCARTHY, J.P., CARUSO, J.A., and FRICKE, F.L. (1983) Speciation of arsenic and selenium via anion-exchange HPLC with sequential plasma emission detection, J. Chromatogr. Sci., 21, p389-393.

McLEOD, C.W., COOK, I.G., WORSFOLD, P.J., DAVIES, J.E., and QUEAY, J. (1985) Analyte enrichment and matrix removal in flow injection analysis-inductively coupled plasma-atomic emission spectrometry: determination of phosphorus in steels, Spectrochim. Acta, 40B, p57-62.

McLEOD, C.W., WORSFOLD, P.J., and COX, A.G., (1984) Simultaneous multi-element analysis of blood serum by flow injection-inductively coupled plasma atomic-emission spectrometry, Analyst, 109, p327-332.

MICHAUD-POUSSEL, E., and MERMET, J.M. (1986) Comparison of nebulizers working below 0.8 $\ell.min^{-1}$ in inductively coupled plasma atomic emission spectrometry, Spectrochim. Acta, 41B (1/2), p49-61.

MITCHELL, P.G., SNEDDON, J., and RADZIEMSKI, L.J. (1987) Direct determination of copper in solids by direct current argon plasma emission spectrometry with sample introduction using laser ablation, Appl. Spectrosc., 41(1), p141-148.

MONTASER, A., CHAN, S-K., HUSE, G.R., VIEIRA, P.A., and VAN HOVEN, R.L. (1986) Prominent spectral lines for analytical atomic emission spectrometry with an Ar-N_2 inductively coupled plasma, Appl. Spectrosc., 40(4), p473-477.

MORITA, M., and UEHIRO, T. (1981) Determination of phosphates by liquid chromatography with inductively coupled argon plasma atomic emission spectrometric detection, Anal. Chem., 53, p1997-2000.

MOTTOLA, H.A. (1981) Continuous flow analyses revisited, Anal. Chem., 53(12), p1312A-1316A.

NAGY, G., FEHéR, ZS., and PUNGOR, E. (1970) Application of silicone rubber-based graphite electrodes for continuous flow measurements. Part II. Voltammetric study of active substances injected into electrolyte streams, Anal. Chim. Acta, 52, p47-54.

NIEMCZYK, T.M., and ESPINOSA, D.C. (1987) Evaluation of a glass frit nebulizer for use in atomic absorption spectrophotometry, Appl. Spectrosc., 41(1), p26-31.

NISAMANEEPONG, W., HAAS, D.L., and CARUSO, J.A. (1985) The use of organic solvents with a glass frit nebulizer for sample introduction in inductively coupled plasma emission spectrometry, Spectrochim. Acta, 40B (1/2), p3-10.

NISAMANEEPONG, W., IBRAHIM, M., GILBERT, T.W., and CARUSO, J.A. (1984) Speciation of arsenic and cadmium compounds by reverse-phase ion-pair LC with single-wavelength inductively coupled plasma detection, J. Chromatogr. Sci., 22(11), p473-477.

NORD, L., and KARLSBERG, B. (1981) An automated extraction system for flame atomic absorption spectrometry, Anal. Chim. Acta, 125, p199-202.

NOVAK, J.W., and BROWNER, R.F. (1980) Characterization of droplet sprays produced by pneumatic nebulizers, Anal. Chem., 52, p792-796.

NOVAK, J.W., LILLIE, D.E., BOORN, A.W., and BROWNER, R.F. (1980) Fixed crossflow nebulizer for use with inductively coupled plasmas and flames, Anal. Chem., 52, p576-579.

OLSEN, S., PESSENDA, L.C.R., RUZICKA, J., and HANSEN, E.H. (1983) Combination of flow injection analysis with flame atomic-absorption spectrophotometry: Determination of trace amounts of heavy metals in polluted seawater, Analyst, 108, p905-917.

OLSON, K.W., HAAS, W.J. Jr., and FASSEL, V.A. (1977) Multielement detection limits and sample nebulization efficiencies of an improved ultrasonic nebulizer and a conventional pneumatic nebulizer in inductively coupled plasma-atomic emission spectrometry, Anal. Chem., 49(4), p632-637.

PARSONS, M.L., FORSTER, A., and ANDERSON, D. (1980) An atlas of spectral interferences in ICP spectroscopy, Plenum Press, N.Y., p64-65.

RAMSEY, M.H., and THOMPSON, M. (1982) On-line diluter for atomic-absorption spectrophotometry, Analyst, 107, p232-234.

RAMSEY, M.H., THOMPSON, M., and COLES, B.J. (1983) Modified concentric glass nebulizer for reduction of memory effects in inductively coupled plasma spectrometry, Anal. Chem., 55, p1626-1629.

RANGER, C.B. (1981) Flow injection analysis-principles, techniques, applications, design, Anal. Chem., 53(1), p20A-32A.

REIJN, J.M., POPPE, H., and VAN DER LINDEN, W.E. (1983) A possible approach to the optimization of flow injection analysis, Anal. Chim. Acta, 145, p59-70.

REIJN, J.M., VAN DER LINDEN, W.E., and POPPE, H. (1980) Some theoretical aspects of flow injection analysis, Anal. Chim. Acta, 114, p105-118.

RENOE, B.W., SHIDELER, C.E., and SAVORY, J. (1981) Use of a flow-injection sample manipulator as an interface between a "high-performance" liquid chromatograph and an atomic absorption spectrophotometer, Clin. Chem., 27(9), p1546-1550.

ROCKS, B.F., SHERWOOD, R.A., BAYFORD, L.M., and RILEY, C. (1982a) Zinc and copper determination in microsamples of serum by flow injection and atomic absorption spectroscopy, Ann. Clin. Biochem., 19, p338-344.

ROCKS, B.F., SHERWOOD, R.A., and RILEY, C. (1982b) Direct determination of therapeutic concentrations of lithium in serum by flow-injection analysis with atomic absorption spectroscopic detection, Clin. Chem., 28(3), p440-443.

ROCKS, B.F., SHERWOOD, R.A., TURNER, Z.J., and RILEY, C. (1983a) Serum iron and total iron-binding capacity determination by flow-injection analysis with atomic absorption detection, Ann. Clin. Biochem., 20, p72-76.

ROCKS, B.F., SHERWOOD, R.A., and RILEY, C. (1983b) Rocks et al comment, Clin. Chem., 29(3), p569-570.

ROCKS, B.F., SHERWOOD, R.A., and RILEY, C. (1984) Direct determination of calcium and magnesium in serum using flow-injection analysis and atomic absorption spectroscopy, Ann. Clin. Biochem., 21, p51-56.

ROUTH, M.W. (1986) Characterization of ICP nebulizer aerosols using near-forward angle Fraunhofer diffraction, Spectrochim. Acta, 41B (1/2), p39-48.

RUZICKA, J. (1981) Theory and principles of flow injection analysis, Anal. Proc., 18, p267-269.

RUZICKA, J., and HANSEN, E.H. (1975) Flow injection analyses part 1. A new concept of fast continuous flow analysis, Anal. Chim. Acta, 78, p145-157.

RUZICKA, J., and HANSEN, E.H. (1978) Flow injection analysis. Part X. Theory, techniques and trends, Anal. Chim. Acta, 99, p37-76.

RUZICKA, J., and HANSEN, E.H. (1980) Flow injection analysis. Principles, applications and trends, Anal. Chim. Acta, 114, p19-44.

RUZICKA, J., and HANSEN, E.H. (1981) Flow injection analysis, Ch.3: Theoretical aspects of FIA, John Wiley and Sons, N.Y., p31-50.

RUZICKA, J., HANSEN, E.H., MOSBAEK, H., and KRUG, F.J. (1977) Exchange of comments: Pumping pressure and reagent consumption in flow injection analysis, Anal. Chem., 49(12), p 1858-1861.

SCHUTYSER, P., and JANSSENS, E. (1979) Evaluation of spray chambers for use in inductively coupled plasma-atomic emission spectrometry, Spectrochim. Acta., 34B, p443-449.

SCOTT, R.H., FASSEL, V.A., KNISELEY, R.N., and NIXON, D.E. (1974) Inductively coupled plasma-optical emission analytical spectrometry. A compact facility for trace analysis of solutions, Anal. Chem., 46(1), p75-80.

SHERWOOD, R.A., ROCKS, B.F., and RILEY, C. (1985) Controlled-dispersion flow analysis with atomic-absorption detection for the determination of clinically relevant elements, Analyst, 110, p493-496.

SIMONSEN, K.W., NIELSEN, B., JENSEN, A. and ANDERSEN, J.R. (1986) Direct microcomputer controlled determination of zinc in human serum by flow injection atomic absorption spectrometry, J. Anal. At. Spectrom., 1, p453-456.

SISLER, H.H., VANDERWERF, C.A., and DAVIDSON, A.W. (1949) General chemistry a systematic approach, Macmillan Co., N.Y., p35-36.

SKEGGS, L.T. (1957) An automated method for colorimetric analysis, Am. J. Clin. Pathol., 28, p311-322.

SKOGERBOE, R.K., and FREELAND, S.J. (1985a) Experimental characterization of aerosol production, transport, vaporization, and atomization systems. Part I: Factors controlling aspiration rates, Appl. Spectrosc., 39(6), p916-920.

SKOGERBOE, R.K., and FREELAND, S.J. (1985b) Experimental characterization of aerosol production, transport, vaporization, and atomization systems. Part II: Factors controlling aerosol size distributions produced, Appl. Spectrosc., 39(6), p920-925.

SKOGERBOE, R.K., and FREELAND, S.J. (1985c) Effects of solution composition on the physical characterization of aerosols produced by nebulization, Appl. Spectrosc., 39(6), p925-930.

SKOGERBOE, R.K., and OLSON, K.W. (1978) Aerosols, aerodynamics, and atomic analysis, Appl. Spectrosc., 32(2), p181-187.

SMITH, D.D., and BROWNER, R.F. (1982) Measurement of aerosol transport efficiency in atomic spectrometry, Anal. Chem., 54, p533-537.

SOMMER, D., and OHLS, K. (1979) Emissionsspektroskopie mit induktiv gekoppelter plasmaflamme als detektor zur elementanalyse nach gas-chromatographischer trennung, Fresenius Z. Anal. Chem., 295, p337-341.

SPACKMAN, D.H., STEIN, W.H., and MOORE, S. (1958) Automatic recording apparatus for use in the chromatography of amino acids, Anal. Chem., 30(7), p1190-1206.

STEWART, K.K. (1981) Flow injection analysis: A review of its early history, Talanta, 28, p789-797.

STEWART, K.K., BEECHER, G.R., and HARE, P.E. (1976) Rapid analysis of discrete samples: The use of nonsegmented, continuous flow, Anal. Biochem., 70, p167-173.

STOKER, D.J. (1985) Statistical tables, Academica, Pretoria, p8.

TANG, Y.Q., and TRASSY, C. (1986) Inductively coupled plasma: the role of water in axial excitation temperatures, Spectrochim. Acta, 41B (1/2), p143-150.

TAYLOR, G. (1954) The dispersion of matter in turbulent flow through a pipe, Proc. Royal Soc. (London), Ser. A., 223, p446-468.

TAYLOR, C.G., and TREVASKIS, J.M. (1986) Determination of lead in gasoline by a flow-injection technique with atomic absorption spectrometric detection, Anal. Chim. Acta, 179, p491-496.

THELIN, B. (1981) Nebuliser system for analysis of high salt content solutions with an inductively coupled plasma, Analyst, 106, p54-59.

TIJSSEN, R. (1980) Axial dispersion and flow phenomena in helically coiled tubular reactors for flow analysis and chromatography, Anal. Chim. Acta, 114, p71-89.

TYSON, J.F. (1981) Flow-injection techniques in atomic-absorption spectrometry, Anal. Proc., 18, p542-545.

TYSON, J.F. (1983) Flow injection methods and atomic-absorption spectrophotometry, Anal. Proc., 20, p488-491.

TYSON, J. (1984a) Flow injection analysis combined with atomic-absorption spectrometry, Anal. Proc., 21, p377-378.

TYSON, J.F. (1984b) Extended calibration of flame atomic-absorption instruments by a flow injection peak width method, Analyst, 109, p319-321.

TYSON, J.F. (1985) Flow injection analysis techniques for atomic absorption spectrometry. A review, Analyst, 110, p419-429.

TYSON, J.F., ADEEYINWO, C.E., APPLETON, J.M.H., BYSOUTH, S.R., IDRIS, A.B., and SARKISSIAN, L.L. (1985) Flow injection techniques of method development for flame atomic-absorption spectrometry, Analyst, 110, p487-492.

TYSON, J.F., and APPLETON, J.M.H. (1985) Concentration gradients for calibration purposes, Anal. Proc., 22, p17-19.

TYSON, J.F., APPLETON, J.M.H., and IDRIS, A.B. (1983a) Flow injection sample introduction methods for atomic-absorption spectrometry, Analyst, 108, p153-158.

TYSON, J.F., APPLETON, J.M.H., and IDRIS, A.B. (1983b) Flow injection calibration methods for atomic absorption spectrometry, Anal. Chim. Acta, 145, p159-168.

TYSON, J.F., and IDRIS, A.B. (1981) Flow injection sample introduction for atomic-absorption spectrometry: Applications of a simplified model for dispersion, Analyst, 106, p1125-1129.

TYSON, J.F., and IDRIS, A.B. (1984) Determination of chromium in steel by flame atomic-absorption spectrometry using a flow injection standard additions method, Analyst, 109, p23-26.

TYSON, J.F., MARIARA, J.R., and APPLETON, J.M.H. (1986) A variable dispersion flow injection manifold for calibration and sample dilution in flame atomic absorption spectrometry, J. Anal. At. Spectrom., 1, p273-276.

UCHIDA, H., NOJIRI, Y., HARAGUCHI, H., and FUWA, K. (1981) Simultaneous multi-element analysis by inductively-coupled plasma emission spectrometry utilizing micro-sampling techniques with internal standard, Anal. Chim. Acta, 123, p57-63.

UDEN, P.C., BARNES, R.M., and DISANZO, F.P. (1978) Determination of methylcyclopentadienylmanganesetricarbonyl in gasoline by gas chromatography with interfaced direct current argon plasma emission detection, Anal, Chem., 50(7), p852-855.

UNGER, S.E., McCORMICK, T.J., BOLGAR, M.S., and HUNT, J.B. (1987) Interchangeable insert thermospray probe, Anal. Chem., 59(8), p1242-1243.

VALCARCEL, M., and LUQUE DE CASTRO, M.D. (1987) Flow-injection analysis principles and applications, translated from Spanish by A. LOSADA, Ellis Horwood Ltd., Chichester, p354-377.

VALENTE, S.E., and SCHRENKE, W.G. (1970) The design and some emission characteristics of an economical dc arc plasmajet excitation source for solution analysis, Appl. Spectrosc., 24(2), p197-205.

VANDERSLICE, J.T., BEECHER, G.R., and ROSENFELD, A.G. (1984) Dispersion and diffusion coefficients in flow injection analysis, Anal. Chem., 56, p293-297.

VANDERSLICE, J.T., STEWART, K.K., ROSENFELD, A.G., and HIGGS, D.J. (1981) Laminar dispersion in flow-injection analysis, Talanta, 28, p11-18.

VAN STADEN, J.F. (1987) On-line sulphate monitoring by reversed flow injection analysis and alternating reagent injection, Fresenius Z. Anal. Chem., 326, p754-756.

VAN STADEN, J.F., and VAN VLIET, H.R. (1984) Vloei-inspuit analise vir die bepaling van die totale alkaliniteit in oppervlakte-, grond- en huishoudelike water volgens die geoutomatiseerde bromokresolgroen metode, Water S.A., 10(3), p168-174.

VERMEIREN, K.A., TAYLOR, P.D.P., and DAMS, R. (1987) Use of a thermospray nebulizer as a sample introduction system for inductively coupled plasma atomic emission spectrometry, J. Anal. At. Spectrom., 2, p383-387.

VESTAL, M.L., and FERGUSSON, G.J. (1985) Thermospray liquid chromography/mass spectrometer interface with direct electrical heating of the capillary, Anal. Chem., 57, p2373-2378.

VIEIRA, P.A., ZHIZHUANG, H., CHAN, S-K., and MONTASER, A. (1986) Evaluation of recycling cyclone spray chambers for ICP-AES, Appl. Spectrosc., 40(8), p1141-1146.

WEAST, R.C. (Ed.,) (1980) CRC Handbook of chemistry and physics, 60th edition, CRC Press, Boca Raton, Florida.

WHALEY, B.S., SNABLE, K.R., and BROWNER, R.F. (1982) Spray chamber placement and mobile phase flow rate effects in liquid chromatography/inductively coupled plasma atomic emission spectrometry, Anal. Chem., 54, p162-165.

WINDSOR, D.L., and DENTON, M.B. (1979) Empirical formula determination with an inductively coupled plasma gas chromatographic detector, Anal. Chem., 51(8), p1116-1119.

WOLCOTT, J.F., and SOBEL, C.B. (1982) Fabrication of a Babington-type nebulizer for ICP sources, Appl. Spectrosc., 36(6), p685-686.

WOLF, W.R., and STEWART, K.K. (1979) Automated multiple flow injection analysis for flame atomic absorption spectrometry, Anal. Chem., 51(8), p1201-1205.

YOZA, N., AOYAGI, Y., OHASHI, S., and TATEDA, A. (1979) Flow injection system for atomic absorption spectrometry, Anal. Chim. Acta, 111, p163-167.

ZAGATTO, E.A.G., BAHIA F°, O., GINE, M.F., and BERGAMIN, F°, H. (1986) A simple procedure for hydrodynamic injection in flow injection analysis applied to the atomic absorption spectrometry of chromium in steels, Anal. Chim. Acta, 181, p265-270.

ZAGATTO, E.A.G., JACINTHO, A.O., KRUG, F.J., REIS, B.F., BRUNS, R.E., and ARANJO, M.C.U. (1983) Flow injection systems with inductively coupled argon plasma atomic emission spectrometry. Part 2. The generalized standard addition method, Anal. Chim. Acta, 145, p169-178.

ZAGATTO, E.A.G., KRUG, F.J., BERGAMIN F°, H., JORGENSEN, S.S., and REIS, B.F. (1979) Merging zones in flow injection analysis. Part 2. Determination of calcium, magnesium and potassium in plant material by continuous flow injection atomic absorption and flame emission spectrometry, Anal. Chim. Acta, 104, p279-284.

ZHOU, N., FRECH, W., and LÜNDBERG, E. (1983) Rapid determination of lead, bismuth, antimony and silver in steels by flame atomic absorption spectrometry combined with flow injection analysis, Anal. Chim. Acta, 153, p23-31.

ZHUANG, H.Z., and BARNES, R.M. (1985) Recycling nebulizing system for milliliter volume samples with inductively coupled plasma spectrometry, Spectrochim. Acta, 40B (1/2), p11-19.